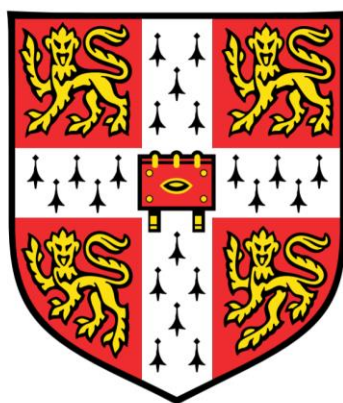


# Design of flow processes for C–H activation-type reactions



**Jacek Zakrzewski**

**Christ's College**

Department of Chemical Engineering and Biotechnology  
University of Cambridge

This dissertation is submitted for the degree of  
*Doctor of Philosophy*

December 2017



# Deposit & Copying of Dissertation Declaration



UNIVERSITY OF  
CAMBRIDGE

Board of Graduate Studies

Please note that you will also need to bind a copy of this Declaration into your final, hardbound copy of thesis - this has to be the very first page of the hardbound thesis.

1	Surname (Family Name)	Forenames(s)	Title
	Zakrzewski	Jacek	Mr
2	Title of Dissertation as approved by the Degree Committee		
	Design of flow processes for C–H activation-type reactions		

In accordance with the University Regulations in *Statutes and Ordinances* for the PhD, MSc and MLitt Degrees, I agree to deposit one print copy of my dissertation entitled above and one print copy of the summary with the Secretary of the Board of Graduate Studies who shall deposit the dissertation and summary in the University Library under the following terms and conditions:

## 1. Dissertation Author Declaration

I am the author of this dissertation and hereby give the University the right to make my dissertation available in print form as described in 2. below.

My dissertation is my original work and a product of my own research endeavours and includes nothing which is the outcome of work done in collaboration with others except as declared in the Preface and specified in the text. I hereby assert my moral right to be identified as the author of the dissertation.

The deposit and dissemination of my dissertation by the University does not constitute a breach of any other agreement, publishing or otherwise, including any confidentiality or publication restriction provisions in sponsorship or collaboration agreements governing my research or work at the University or elsewhere.

## 2. Access to Dissertation

I understand that one print copy of my dissertation will be deposited in the University Library for archival and preservation purposes, and that, unless upon my application restricted access to my dissertation for a specified period of time has been granted by the Board of Graduate Studies prior to this deposit, the dissertation will be made available by the University Library for consultation by readers in accordance with University Library Regulations and copies of my dissertation may be provided to readers in accordance with applicable legislation.

3	Signature	Date
		31.05.2018

## Corresponding Regulation

Before being admitted to a degree, a student shall deposit with the Secretary of the Board one copy of his or her hardbound dissertation and one copy of the summary (bearing student's name and thesis title), both the dissertation and the summary in a form approved by the Board. The Secretary shall deposit the copy of the dissertation together with the copy of the summary in the University Library where, subject to restricted access to the dissertation for a specified period of time having been granted by the Board of Graduate Studies, they shall be made available for consultation by readers in accordance with University Library Regulations and copies of the dissertation provided to readers in accordance with applicable legislation.



# Design of flow processes for C–H activation-type reactions

The last 15 years have seen tremendous advances in using different metal catalysts to functionalize traditionally unreactive C–H bonds. Given the high potential of these seemingly ideal strategic bond forming reactions, the uptake of C–H activation in fine chemical manufacture is slow. Part of the reason for this deficiency is limited mechanistic understanding of these complex reactions. This can preclude industrial applications of either batch or continuous C–H activation processes. Owing to the synthetic utility of C–H activation reactions, it is highly desirable to design intensified processes for this family of transformations, what can possibly facilitate industrialisation of C–H activation reactions.

Firstly, an *ab initio* process design of a novel C(sp<sup>3</sup>)–H activation reaction giving access to aziridines yielded a predictive mechanistic model that has been used in an *in silico* optimisation. The identified set of conditions was suitable for a scalable continuous process. A separation technique was developed, and the utility of the process was extended by a subsequent reaction, a nucleophilic ring opening. Secondly, a black-box optimisation of the investigated reaction was performed. The applied algorithm was able to identify a set of conditions fulfilling the set targets within few experimental trails.

The second project has set out to design a process for a C–H oxidative carbonylation. A kinetic study has shown that the reaction is CO-starved even at elevated pressures and that there is an optimal CO concentration. The turn-over number was increased from 8 to nearly 500. Two scalable processes were then developed. The first was a batch process, characterised by a very low catalyst loading. The second was, to the best of author's knowledge, the first continuous process for an oxidative carbonylation reaction. The continuous process was tested on several oxidative carbonylations yielding excellent results with virtually no optimisation performed. Finally, an environmental sustainability assessment was performed using both, simplified metrics and an LCI analysis.

The developed mechanistic understanding allowed identification of sources of inherent inefficiencies of C–H activation reactions. Appropriate solutions to these obstacles were suggested. Thus, it is believed that a step towards generic principles of design of intensified, scalable processes for C–H activation-type reactions has been made.



# Preface

This dissertation is the result of my own work and includes nothing which is the outcome of work done in collaboration except as declared in the Preface and specified in the text.

It is not substantially the same as any that I have submitted, or, is being concurrently submitted for a degree or diploma or other qualification at the University of Cambridge or any other University or similar institution except as declared in the Preface and specified in the text. I further state that no substantial part of my dissertation has already been submitted, or, is being concurrently submitted for any such degree, diploma or other qualification at the University of Cambridge or any other University or similar institution except as declared in the Preface and specified in the text.

The dissertation does not exceed the prescribed word limit for the relevant Degree Committee.

Jacek Zakrzewski

December 2017



## Acknowledgements

First and foremost, I would like to express my most profound gratitude to Prof. Alexei Lapkin for giving me the opportunity to work in his group and for his supervision throughout my time in Cambridge. Your encouragement in (and out of) the office has helped me to develop as a scientist and a person; I could not have asked for a better supervisor and mentor.

I am greatly indebted to Prof. Matthew Gaunt for his constant support and encouragement as well as for hosting me at the Chemistry Department. Without your invaluable advice and support, it would not be possible to conduct this research.

Sincere thank you to Alexander Echtermeyer and Yehia Amar for their assistance in the black-box optimisation project. Many thanks to Mikhail Kabeshov for his support in DFT calculations. I am particularly grateful to Adam Smalley for our fruitful discussions, his unlimited patience and guidance in the Chemistry Department.

Thank you to everyone in the Sustainable Engineering Group. Thank you, Philipp for your moral support. My experience in Cambridge would not be the same without you. Special appreciation to the Gaunt group for welcoming me into their community and help throughout last three years.

Last but not least, I would like to thank my family: my parents and my brothers for moral and emotional support throughout my doctoral studies and my life in general. I am also grateful to my other family members and friends who have supported me along the way. Finally, thank you, Julia. Without you, I would never have made it to where I am today, and for that, I am forever thankful.



# Abstract

## Design of flow processes for C–H activation-type reactions

The last 15 years have seen tremendous advances in using different metal catalysts to functionalize traditionally unreactive C–H bonds. Given the high potential of these seemingly ideal strategic bond forming reactions, the uptake of C–H activation in fine chemical manufacture is slow. Part of the reason for this deficiency is limited mechanistic understanding of these complex reactions. This can preclude industrial applications of either batch or continuous C–H activation processes. Owing to the synthetic utility of C–H activation reactions, it is highly desirable to design intensified processes for this family of transformations, what can possibly facilitate industrialisation of C–H activation reactions.

Firstly, an *ab initio* process design of a novel C(sp<sup>3</sup>)–H activation reaction giving access to aziridines yielded a predictive mechanistic model that has been used in an *in silico* optimisation. The identified set of conditions was suitable for a scalable continuous process. A separation technique was developed, and the utility of the process was extended by a subsequent reaction, a nucleophilic ring opening. Secondly, a black-box optimisation of the investigated reaction was performed. The applied algorithm was able to identify a set of conditions fulfilling the set targets within few experimental trials.

The second project has set out to design a process for a C–H oxidative carbonylation. A kinetic study has shown that the reaction is CO-starved even at elevated pressures and that there is an optimal CO concentration. The turn-over number was increased from 8 to nearly 500. Two scalable processes were then developed. The first was a batch process, characterised by a very low catalyst loading. The second was, to the best of author's knowledge, the first continuous process for an oxidative carbonylation reaction. The continuous process was tested on several oxidative carbonylations yielding excellent results with virtually no optimisation performed. Finally, an environmental sustainability assessment was performed using both, simplified metrics and an LCI analysis.

The developed mechanistic understanding allowed identification of sources of inherent inefficiencies of C–H activation reactions. Appropriate solutions to these obstacles were suggested. Thus, it is believed that a step towards generic principles of design of intensified, scalable processes for C–H activation-type reactions has been made.



# Table of contents

Preface.....	I
Acknowledgements.....	III
Abstract.....	V
Table of contents.....	VII
List of figures.....	X
List of schemes.....	XVI
List of tables.....	XVIII
Chapter 1. Introduction.....	1
Chapter 2. Literature review.....	4
2.1. Methods and tools of process design.....	4
2.1.1. Hierarchical process design.....	4
2.1.2. Describing process complexity.....	9
2.1.2.1. Self-optimisation.....	10
2.1.2.2. Initial deconvolution of the observed behaviour.....	13
2.1.2.3. True deconvolution of the observed behaviour.....	21
2.1.3. Summary.....	29
2.2. Continuous processing methods for fine chemical synthesis.....	30
2.2.1. Mass transfer.....	31
2.2.2. Residence time distribution.....	37
2.2.3. Heat transfer.....	41
2.2.4. Photons and electrons.....	43
2.2.5. Pressure, temperature and supercritical fluids.....	45

---

2.2.6.	Types of reactors.....	46
2.2.7.	Copper-tube flow reactors.....	48
2.2.8.	Integrated processes.....	48
2.2.9.	Scaling of continuous processes.....	50
2.2.10.	Summary.....	54
2.3.	Palladium catalysed C–H activation reactions.....	56
2.3.1.	C(sp <sup>3</sup> )–H activation of secondary aliphatic amines.....	57
2.3.2.	C–H oxidative carbonylation.....	58
2.3.3.	C–H activation in flow.....	62
2.3.4.	Carbonylation in flow.....	64
2.4.	Life-cycle assessment.....	70
2.5.	Conclusions.....	76
Chapter 3.	Experimental section.....	77
3.1.	Continuous-flow synthesis and derivatisation of aziridines through palladium-catalyzed C(sp <sup>3</sup> ) C–H activation.....	78
3.1.1.	Black-box optimisation.....	85
3.1.1.1.	Data processing.....	88
3.2.	β-C–H carbonylation of aliphatic amines to β-lactams.....	91
Chapter 4.	Results and data analysis.....	100
4.1.	Continuous-flow synthesis and derivatisation of aziridines through palladium-catalyzed C(sp <sup>3</sup> ) C–H activation.....	100
4.1.1.	Scope of the reaction.....	101
4.1.2.	Mechanistic understanding.....	102
4.1.3.	Detailed kinetic investigation.....	108
4.1.4.	Black box optimisation.....	116
4.1.5.	Design of the reactor and separation system for the aziridination reaction	119
4.1.6.	Nucleophilic ring opening reaction.....	122

---

4.1.7. Discussion.....	128
4.2. $\beta$ -C–H carbonylation of aliphatic amines to $\beta$ -lactams.....	131
4.2.1. Kinetic investigation .....	132
4.2.2. Process optimisation .....	146
4.2.3. Process design.....	148
4.2.4. Environmental sustainability analysis of the developed processes.....	157
4.2.4.1. Simplified metrics.....	157
4.2.4.2. LCI assessment .....	158
4.2.5. Discussion.....	169
Chapter 5. Conclusions.....	173
Chapter 6. Future work.....	177
Chapter 7. References.....	179
Chapter 8. Appendices.....	193
8.1. Appendix 1 .....	193
8.2. Appendix 2 .....	205
8.3. Appendix 3 .....	210
8.4. Appendix 4 .....	217
8.5. Appendix 5 .....	235

## List of figures

Figure 1.1-1. Sources of process complexity.....	1
Figure 2.1-1. Comparison of a classical sequential R&D model with the new parallel approach. Based on ref. 2.....	6
Figure 2.1-2. Representation of a motif in a general fine chemical reaction. Based on ref. 39.....	14
Figure 2.1-3. Possible motifs for a simple two-step reaction. Based on ref. 39. ....	15
Figure 2.1-4. The Michaelis-Menten model of a catalytic reaction. Based on ref. 40. ....	16
Figure 2.1-5. The mechanism for a simple catalytic reaction with two substrates and one intermediate species. Based on ref. 40.....	17
Figure 2.1-6. A flow chart for the Reaction Progress Kinetic Analysis. Reproduced from ref. 40. ....	20
Figure 2.1-7. Model validation procedure based on MBDoE. Based on ref. 53. ....	24
Figure 2.1-8. Geometrical interpretation of the most commonly implemented criteria for the experiment design. The grey area represents the confidence region of the model parameters, based on ref. 53. ....	28
Figure 2.2-1. The concentration profile of the gas reactant in the gas-liquid mass transfer in the quasi-equilibrium state of the reaction.....	35
Figure 2.2-2. Residence time distribution of a pulse experiment for the ideal (a) CSTR; (b) plug-flow reactor.....	38

---

Figure 2.2-3. Residence time distribution of a pulse experiment for non-ideal (a) CSTR; (b) plug-flow reactor.....	38
Figure 2.2-4 Transmittance as a function of the path length and concentration of the photoredox catalyst. The dashed vertical dashed line represents the inner diameter of a 0.02” tubing. Reproduced from ref. 71. ....	44
Figure 2.2-5. Commonly used types of flow reactors.....	46
Figure 2.2-6. Multi-step synthesis approaches. Based on ref. 113. ....	49
Figure 2.2-7. Decision diagram for continuous processing. Based on ref. 71.....	55
Figure 2.4-1. Twelve principles of green chemistry. Based on ref. 188.....	71
Figure 3.1-1. <sup>1</sup> H NMR (CDCl <sub>3</sub> , 400 MHz) 2,2,6-Trimethyl-4-oxa-1-azabicyclo[4.1.0]heptan-5-one.....	80
Figure 3.1-2. <sup>13</sup> C NMR (CDCl <sub>3</sub> , 100 MHz) 2,2,6-Trimethyl-4-oxa-1-azabicyclo[4.1.0]heptan-5-one.....	80
Figure 3.1-3. 3,3,5,5-Tetramethylmorpholin-2-one.....	81
Figure 3.1-4. <sup>1</sup> H NMR (CDCl <sub>3</sub> , 400 MHz) 3,3,5,5-Tetramethylmorpholin-2-one .....	82
Figure 3.1-5. <sup>13</sup> C NMR (CDCl <sub>3</sub> , 100 MHz) 3,3,5,5-Tetramethylmorpholin-2-one .....	82
Figure 3.1-6. An example of a GC analysis. Solv: toluene, IS: internal standard, Ox: PIDA, SM: Starting material, AZ: Product. ....	83
Figure 3.1-7. A calibration curve for the GC analysis, using an internal standard (IS), was established for the product (Az) in the upper and for the starting material (SA) in the lower plot. ....	84
Figure 3.1-8 Example of residence time distribution experiment. Theoretical result for ideal plug-flow is added in the figure. 2 ml reaction mixture segment was used. Concentration is represented by UV signal measured by in-line UV cell. ....	86
Figure 3.1-9 Calibration curve for the UV cell.....	86

---

Figure 3.1-10 Schematics of the semi-automated continuous-flow system used for the black box sequential optimisation. ....	87
Figure 3.1-11 An overview of the MOAL algorithm including the training feedback loop. ....	89
Figure 3.2-1. N-Ethyl-2-((6-(trifluoromethyl)pyridin-2-yl)oxy)ethan-amine .....	91
Figure 3.2-2. N-Ethyl-3-phenylpropan-1-amine.....	91
Figure 3.2-3. N-(2,6-Difluorobenzyl)propan-2-amine.....	92
Figure 3.2-4. N-(2-(Pyrimidin-2-yloxy)ethyl)propan-2-amine.....	93
Figure 3.2-5. N-isopropyltetrahydro-2H-thiopyran-4-amine.....	93
Figure 3.2-6. 2-Methyl-N-(2-(pyridin-2-yloxy)ethyl)propan-2-amine.....	94
Figure 3.2-7. 2-Methyl-N-(2-(phenylsulfonyl)ethyl)propan-2-amine .....	94
Figure 3.2-8. N-Isopropyladamantan-1-amine .....	95
Figure 3.2-9. <sup>1</sup> H NMR (CDCl <sub>3</sub> , 400 MHz) 1-Cyclohexyl-4-methylazetid-2-one .....	99
Figure 3.2-10. <sup>13</sup> C NMR (CDCl <sub>3</sub> , 100 MHz) 1-Cyclohexyl-4-methylazetid-2-one .....	99
Figure 4.1-1 C–H activation reaction leading towards the synthesis of aziridines substrate scope. Yields are given for the isolated compounds. Adapted from ref. 148. ....	101
Figure 4.1-2. Proposed mechanistic cycle. ....	104
Figure 4.1-3 Energy profile of cyclopalladation proceeding through a CMD mechanism. ....	106
Figure 4.1-4 Proposed mechanistic cycle including the influence of the acetic acid on the mechanistic cycle. ....	107
Figure 4.1-5 The influence of agitation on the product concentration as a function of time. ....	109
Figure 4.1-6 Comparison of the kinetic model with experimental results for semi-batch experiments. ....	115

Figure 4.1-7 Results of continuous-flow experiments under optimal conditions. ....	115
Figure 4.1-9 Results of the black box optimisation. Blue “dots” correspond to the cost function – left vertical axis; Orange “diamonds” correspond to the yield – right vertical axis. ....	117
Figure 4.1-10 Trajectory of the black box optimisation. The red star represents the final set of conditions. ....	118
Figure 4.1-11 Flow process for the aziridination C–H activation reaction. a) Flow reactor: silicon/glass microfluidic reactor or PFE tubular reactor. The first column separates the catalyst from the spent mixture; the second column separates the product. Reactants were delivered via: pump A (starting material, oxidant, acetic acid), pump B (catalyst, acetic acid, acetic anhydride). A 6 bar pressure regulator was fitted; b) Elution of the product from the “catch” column. ....	121
Figure 4.1-12 Tested scope of the nucleophilic ring opening of aziridine product. Yields are given for the isolated compounds. ....	123
Figure 4.1-13. <sup>1</sup> H NMR (CDCl <sub>3</sub> , 400 MHz) 3-(Azidomethyl)-3,5,5-trimethylmorpholin-2-one. ....	125
Figure 4.1-14. <sup>13</sup> C NMR (CDCl <sub>3</sub> , 100 MHz) 3-(Azidomethyl)-3,5,5-trimethylmorpholin-2-one. ....	125
Figure 4.1-15. <sup>1</sup> H NMR (CDCl <sub>3</sub> , 400 MHz) 3-(Hydroxymethyl)-3,5,5-trimethylmorpholin-2-one. ....	126
Figure 4.1-16. <sup>13</sup> C NMR (CDCl <sub>3</sub> , 100 MHz) 3-(Hydroxymethyl)-3,5,5-trimethylmorpholin-2-one. ....	126
Figure 4.1-17. <sup>1</sup> H NMR (CDCl <sub>3</sub> , 400 MHz) 3-(Methoxymethyl)-3,5,5-trimethylmorpholin-2-one. ....	127

---

Figure 4.1-18. $^{13}\text{C}$ NMR ( $\text{CDCl}_3$ , 100 MHz) 3-(Methoxymethyl)-3,5,5-trimethylmorpholin-2-one.....	127
Figure 4.1-19 Development of the continuous process for the aziridination reaction.....	129
Figure 4.2-1. Influence of the concentration of the starting material on the observed reaction rate for standard conditions. Trend lines added for the convenience of the eye. Csm0: initial concentration of starting material. p=7 bar(g). .....	134
Figure 4.2-2. Influence of the catalyst loading on the observed reaction rate for standard conditions. Trend lines added for the convenience of the eye. ....	134
Figure 4.2-3. Influence of the gauge pressure of 6.25% CO balanced by air v/v on the observed reaction rate for standard conditions. Trend lines added for the convenience of the eye. ....	135
Figure 4.2-4. Influence of the concentration of copper acetate on the observed reaction rate for standard conditions. Trend lines added for the convenience of the eye.....	136
Figure 4.2-5. Influence of the concentration of Li-quinoline on the observed reaction rate for standard conditions. Trend lines added for the convenience of the eye. p=7 bar(g)..	137
Figure 4.2-6. Influence of the concentration of p-benzoquinone on the observed reaction rate for standard conditions. Trend lines added for the convenience of the eye.....	137
Figure 4.2-7. Influence of the concentration of 1-adamantanecarboxylic acid on the observed reaction rate for standard conditions. Trend lines added for the convenience of the eye. ....	137
Figure 4.2-8 Proposed, simplified catalytic cycle. Ad- denotes adamantane. ....	138
Figure 4.2-9 By-product of the $\beta\text{-C-H}$ carbonylation reaction: N-cyclohexyl-N-isopropylacetamide. ....	140
Figure 4.2-10. Selected substrate scope. Yields are given for the isolated compounds. Yields in brackets are from the initial report of Gaunt and co-workers ref. 203.....	151

---

Figure 4.2-11 Selected scope of the process. Yields are given for the isolated compounds. Tests performed under 10 barg of 6.25 % v/v CO balanced by synthetic air. ....	152
Figure 4.2-12. Scale-up of the batch process. A represents reactions without an additional delivery of CO at the bottom of the reactor and using the small stirrer bar, B reactions with a constant CO delivery and for larger scale also enhanced mixing. ....	156
Figure 4.2-13. Comparison of impacts for the developed process options. Results were normalised against the original work. ....	160
Figure 4.2-14. Distribution of impacts between reactants. ....	162
Figure 4.2-15. Comparison of impacts for the developed process options, accounting for metal recovery. Results were normalised against the original work. ....	164
Figure 4.2-16. Distribution of impacts between reactants including metal recovery. ....	166
Figure 4.2-17. Sensitivity analysis of the developed LCI assessment. ....	168
Figure 4.2-18 $\beta$ -C–H oxidative carbonylation of aliphatic amines to $\beta$ -lactams. Yields are given for the isolated compounds. ....	169
Figure 8.1-1. Energy profile of cyclopalladation proceeding through a CMD mechanism. ....	193

## List of schemes

Scheme 2.3-1. Schematic representation of the directing group effect on a palladium catalysed C–H bond activation. ....	57
Scheme 2.3-2. C(sp <sup>3</sup> )-H functionalisation of a secondary amine. ....	58
Scheme 2.3-3. Schematic representation of carbonylation processes. Based on ref. 154. ....	59
Scheme 2.3-4. Examples of Orito carbonylation. ....	61
Scheme 2.3-5. Palladium-catalyzed oxidative carbonylation of N-allylamines for the synthesis of $\beta$ -lactams. ....	61
Scheme 2.3-6. Palladium-catalysed C–H carbonylation of sterically hindered aliphatic amines. ....	61
Scheme 2.3-7. C3-olefination of indoles in flow. TFA: trifluoroacetic acid, DMSO: dimethyl sulfoxide. ....	62
Scheme 2.3-8. C–H functionalisation/Cope rearrangement reaction in a hollow fibre reactor. ....	63
Scheme 2.3-9. Continuous palladium-catalysed aerobic oxidative coupling of o-xylene. TfOH is trifluoromethyl sulfonic acid, 2-F-py is 2-fluoro-pyridine. ....	63
Scheme 2.3-10. Meta-selective C-H arylation of anilines. Piv denotes pivalate. ....	64
Scheme 2.3-11. Synthesis of N-benzylamides and $\alpha$ -ketoamide via carbonylative cross-coupling. ....	66
Scheme 2.3-12. Palladium-catalyzed single/double carbonylation of aryl iodides. ....	66
Scheme 2.3-13. Palladium-catalyzed carbonylative Sonogashira cross-coupling. ....	66

---

Scheme 2.3-14. Radical carbonylation of aliphatic halides. ....	67
Scheme 2.3-15. Palladium catalysed methoxycarbonylation of aryl, heteroaromatic and vinyl iodides and an aryl bromide.....	68
Scheme 2.3-16. Palladium-catalysed alkoxy carbonylation of aryl iodides. ....	68
Scheme 2.3-17. Koch–Haaf reaction of adamantanols.....	69
Scheme 2.3-18. Heck carbonylation of 1-bromo-3,4-bis(trifluoromethyl)benzene. ....	69
Scheme 4.1-1 C–H activation reaction leading towards the synthesis of aziridines. Adapted from ref. 148; $\text{PhI}(\text{OAc})_2$ - (Diacetoxyiodo)benzene; $\text{Pd}(\text{OAc})_2$ – palladium (II) acetate; R – functional groups. ....	100
Scheme 4.1-2. KIE experiment.....	103
Scheme 4.2-1 $\beta$ -C–H carbonylation of aliphatic amines to $\beta$ -lactams. AdCOOH = 1-adamantanecarboxylic acid. Conditions: 10 mol% $\text{Pd}(\text{OAc})_2$ , 10 mol% $\text{Cu}(\text{OAc})_2$ , 1 eq p-benzoquinone, 30 mol% AdCOOH, 10 mol% Li-quinoline, PhMe, 120 °C, 12 h. ....	131
Scheme 4.2-2. Reaction conditions for a batch process for carbonylation reaction. Yield is given for the isolated compound.....	153

## List of tables

Table 2.1-1. Selected recent advanced in the field of self-optimisation.....	12
Table 2.2-1. Examples of scale-up criteria for stirred tank reactors. Based on ref. 88..	51
Table 2.2-2. Relative changes of reactors parameters in the scale-up procedure. Based on ref. 88.....	52
Table 2.4-1. Burdens, mid-point and end-point impact categories.....	74
Table 2.4-2. Impact categories outlined in ReCiPe 2008 based on ref. 196.....	75
Table 3.1-1 Constraints used in the black box optimisation.....	90
Table 4.1-1 Set of experiments used to estimate the kinetic parameters. ....	110
Table 4.1-2 Fit between energies obtained during the parameter estimation and DFT modelling. ....	112
Table 4.1-3 Correlation matrix .....	112
Table 4.1-4 Results of parameter estimation for 70 °C.....	113
Table 4.1-5 Design of the semi-batch experiments. ....	114
Table 4.1-10 Recipes for experiments in the initial training of the black box optimisation. ....	116
Table 4.1-11 Recipes for experiments suggested by the algorithm.....	118
Table 4.2-1 Standard conditions used for carbonylation experiments.....	132
Table 4.2-2 A summary of the influence of the substrates on the observed reaction rate and their use in setting up a kinetic model. ....	138

---

Table 4.2-3 Results of parameter estimation for 120 °C for the simplified mechanism of the carbonylation reaction.....	141
Table 4.2-4 Correlation matrix for experiments at 120 °C for the carbonylation reaction. .....	142
Table 4.2-5 Results of parameter estimation for 120 °C for the reduced model for simplified mechanism of the carbonylation reaction. ....	143
Table 4.2-6 Results of parameter estimation for the reduced model for simplified mechanism of the carbonylation reaction .....	143
Table 4.2-7 Correlation matrix for the simplified mechanism for the carbonylation reaction for 120 °C. ....	144
Table 4.2-8 Correlation matrix for the simplified mechanism for the carbonylation reaction. .....	144
Table 4.2-9 Henry's law coefficients predicted by COSMOtherm at 150 °C. ....	145
Table 4.2-10. Standard conditions used in process optimisation of the oxidative carbonylation reaction.....	146
Table 4.2-11. Selected results from the process optimisation. ....	148
Table 4.2-12. Development of the flow process for the oxidative carbonylation reaction. .....	150
Table 4.2-13. Estimation of the mass transfer coefficient. ....	154
Table 4.2-14. Comparable sustainability analysis of the available process options using simplified metrics.....	157
Table 4.2-15. Impact potentials used in the LCI assessment. ....	159
Table 4.2-16. Distribution of impacts between reactants. ....	161
Table 4.2-17. Distribution of impacts between reactants including metal recovery. ....	165



## Chapter 1. Introduction

The method of hierarchical process design based on flow sheets and case scenarios has gained significant interest in last decades. This method, pioneered by Douglas,<sup>1</sup> allows reduction of a complex process to a set of elementary operations and, based on *a priori* knowledge, choose the optimal solution to the problem. However, this approach requires a thorough understanding of the investigated process and, in case of an insufficient description of the process or large uncertainties of the process parameters, can lead to substantial inefficiencies. Hence, as a prerequisite to beginning a hierarchical process design, one must solve a problem of complexity of chemical and physical phenomena underpinning the process. This requires an adequate description of the influence of the mass and energy transfer on the system as well as providing enough data describing chemical reactions taking part in the process, Figure 1.1-1

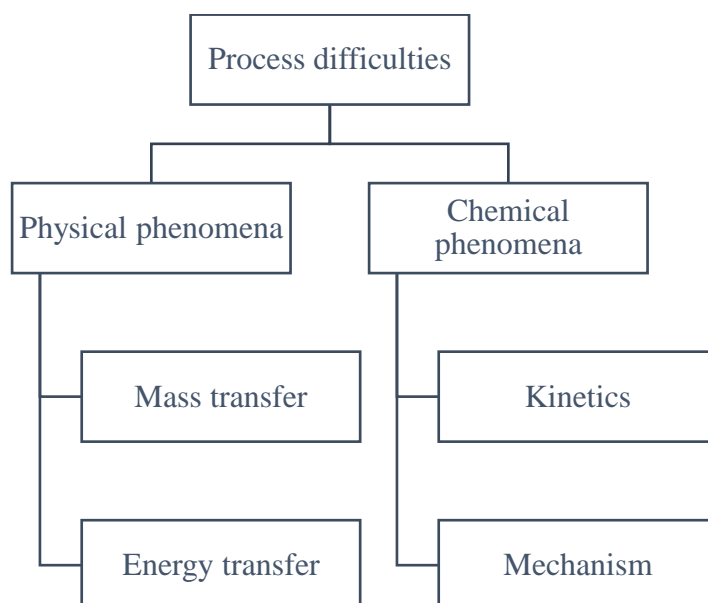


Figure 1.1-1. Sources of process complexity.

An attempt to solving the process difficulty quite often requires a significant amount of time and resources and still does not guarantee to obtain the information one aimed for. That is why a generic and robust “roadmap” towards solving process complexity could be of great help to engineers involved in process design. However, due to the large variety of chemical mechanisms and a substantial number of complex chemical transformations, forming a “one-size-fits-all” solution, although highly desirable, seems to be impossible.

Over last several decades a significant attention was paid to a field of process intensification. Particularly, the concept of flow chemistry gained an unprecedented interest. Flow chemistry can be defined as a general range of chemical processes that occur in a continuously flowing stream taking place in a flow reactor. A flow reactor can take a form of a tubular reactor, packed-bed reactor, series of continuously stirred tank reactors and many more. Arguably, the implementation of flow chemistry techniques results in superior mass and energy transfer being a consequence of smaller reactor dimensions. This leads to faster, cleaner and safer chemical reactions. Furthermore, the scalability and the integration of typically used PATs and separation techniques in flow systems can be significantly easier.

This work aims to develop intensified continuous processes for palladium catalysed C–H activation type reactions of secondary amines. These transformations, currently considered as not-scalable, should benefit from a holistic approach to the process design. Applying the hierarchical process design paradigm should allow a significant increase in efficiency of investigated processes. Furthermore, the developed mechanistic and kinetic understanding of investigated processes could potentially allow formulation of generic principles of design of scalable processes for C–H activation type reactions. This may potentially facilitate industrialisation of C–H activation-type reactions.

**Dissemination**

Results included in the thesis were partially published. The rest is included in the manuscripts under preparation.

Zakrzewski, J., Smalley, A. P., Kabeshov, M. A., Gaunt, M. J., & Lapkin, A. A. (2016). Continuous-Flow Synthesis and Derivatization of Aziridines through Palladium-Catalyzed C(sp<sup>3</sup>)-H Activation. *Angewandte Chemie International Edition*, 55(31), 8878-8883.

Echtermeyer, A., Amar, Y., Zakrzewski, J., & Lapkin, A. (2017). Self-optimisation and model-based design of experiments for developing a C-H activation flow process. *Beilstein Journal of Organic Chemistry*, 13, 150.

Zakrzewski, J. Gaunt, M. A., & Lapkin, A. A. (2018). A scalable palladium-copper catalysed C-H oxidative carbonylation. Manuscript under preparation.

Zakrzewski, J. Lapkin, A. A. (2018). Sustainability analysis of a C-H oxidative carbonylation. Manuscript under preparation.

## **Chapter 2. Literature review**

Owing to the interdisciplinary nature of the thesis there is a need for a theoretical introduction to several fields. The following literature review covers four themes: methods and tools of process design, continuous processing methods for fine chemical synthesis, palladium catalysed C–H activation reaction and life-cycle assessment.

### **2.1. Methods and tools of process design**

Design of chemical processes strongly depends on available process information. Without access to reliable models describing the physical and chemical complexity of the process, it is rarely possible to choose the optimal reactor and a set of conditions to run the process. Furthermore, in the absence of predictive models, previously unknown scale-up dependant phenomena can be observed upon re-sizing of the reactor. Hence, it is of utmost importance to build as thorough as economically feasible understanding of the process as possible before choosing the reactor system and the conditions to run the process. The following chapter focuses on tools and principles of chemical process design.

#### **2.1.1. Hierarchical process design**

The route from a molecular discovery to a plant scale synthesis is a time as well as capital demanding development process and requires an agile cooperation between numerous departments localised in separate units of a chemical company or a research institute. The classical, sequential research and development approach assumes that the work on the process is conducted as a set of discrete elements completed by separate functional units, i.e. results of molecular discovery, lab scale synthesis and product properties studies performed in a research laboratory are passed on to process chemists conducting synthesis scale-up and developing a process model that is implemented, or, if necessary, refined, by

process engineers at a pilot plant scale, Figure 2.1-1. This, finally, leads to a full production scale process development. Such methodology, being a very long and cost demanding process, is characterised by high risk factors. It is not uncommon to discover that the synthesis route designed in a research laboratory is not optimal or even not feasible at a larger scale. Failures at advanced stages of the process can bring significant burdens to the economic position of the department or the whole company, especially when a small unit is being considered. Thus, all possible actions must be taken to prevent it from happening. This may be done by nurturing cooperation and communication between separate cells within the whole company. However, this may be problematic and require dramatic changes in the way modern chemical companies function. An other, more drastic approach, is abandoning, or profound modification of, the classical R&D approach and following a new, parallel methodology, Figure 2.1-1. The parallel approach assumes that the operations preceding the process model formulation are performed within the same functional unit. This, in theory, should minimise the risk of failures on advanced levels of the project.

Despite its apparent advantages, the parallel approach to process flow sheet generation results in an increased number of degrees of freedom, which generates a heavily under-defined optimisation problem that can be difficult to solve. For the sequential process design, assumptions at every level reduce the number of degrees of freedom. Thus, even though the optimisation problem is still under-defined, the solution is usually possible to be found. On the other hand, a faulty assumption can lead towards a suboptimal global solution to the problem generating a significantly more capital-intensive solution. This can cause project failures, especially if the mistake was made at an early stage of the project and it is not economically feasible to repeat all the operations following changing the solution of the step. This is why the collaborative, parallel approach, even though difficult to solve, can prove to be much safer and more effective. Optimising of such complex systems and choosing the most appropriate technologies for every step of the process can be easier solved when a hierarchical process design is implemented, i.e. a structured technique for organisation and analysis of complex problems requiring multidimensional decisions.

A number of tools and methodologies aiding process flow sheet generation for complex, heavily under-defined problems has been published. Douglas<sup>1</sup> in his work presented a heuristic solution to the problem. Dividing process complexity into five decision levels

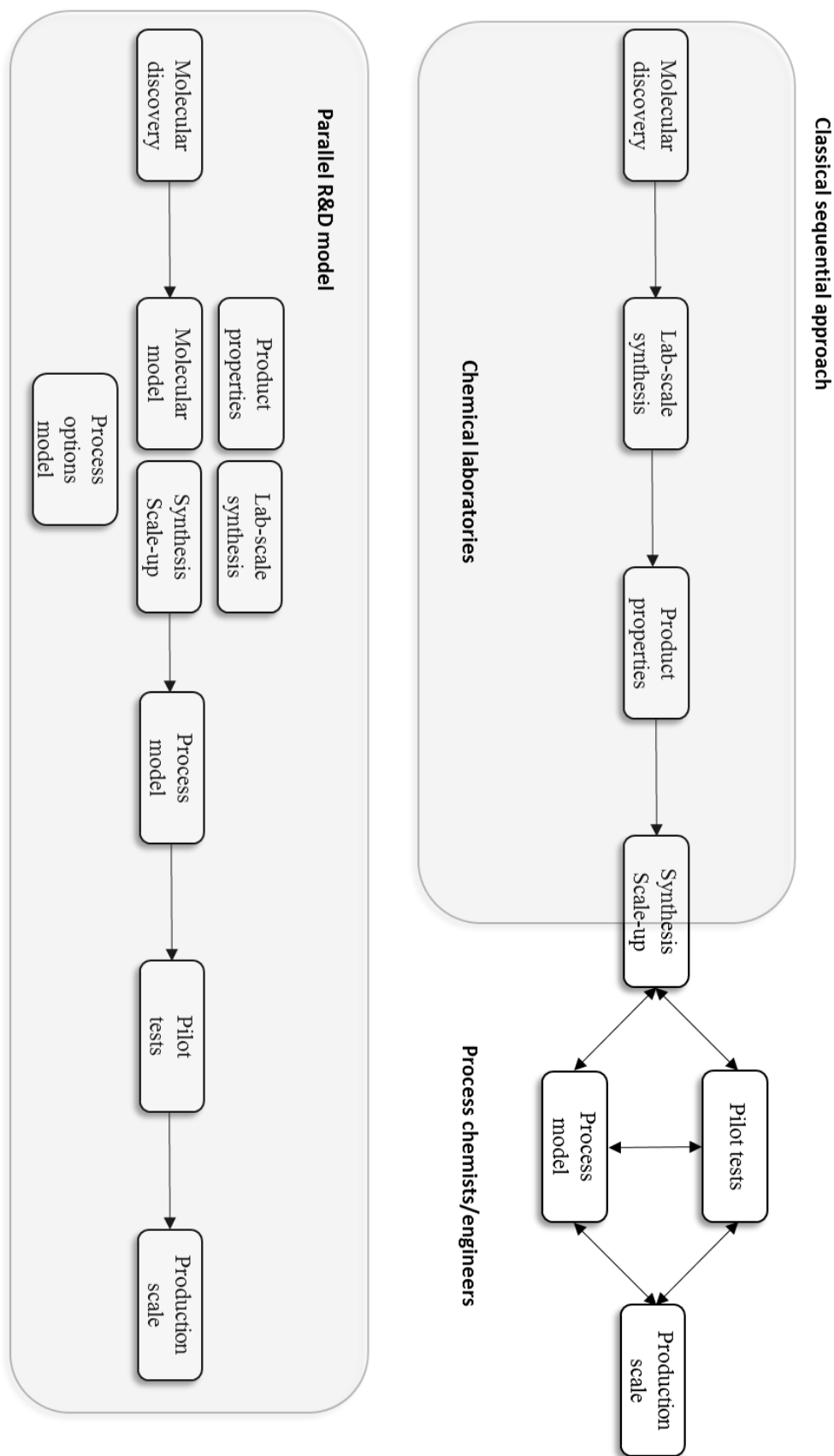


Figure 2.1-1. Comparison of a classical sequential R&D model with the new parallel approach. Based on ref. 2.

dramatically simplifies and unifies the places of making assumptions. The hierarchy of decisions is as follows:

1. Batch vs continuous
2. Input-output structure of the flow sheet
3. Recycle structure of the flow sheet and reactor considerations
4. Separation system specification
  - 4a,b. Vapour and liquid recovery system
5. Heat exchanger network

A complete process must be considered at each level and, if required, additional sublevels shall be created for more complex case studies. Ideally, for all levels and sublevels, multiple scenarios should be generated and, following feasibility studies, a multi-criteria optimisation should be performed to identify the optimal pathway.

Douglas also identified input information required to develop the flow sheet. He again divided it into groups:

- A. Reactions
  - A.1. Stoichiometry, temperature, pressure of each step
  - A.2. Correlation of product distribution vs conversion and temperature
  - A.3. Catalyst for each reaction
  - A.4. Desired phase condition of each reaction step
- B. Products
  - B.1. Desired production rate and product purity
  - B.2. Product price or price as a function of purity
  - B.3. Values of all by-products as chemical or fuel
- C. Raw materials
  - C.1. Composition, temperature and pressure of all raw material streams
  - C.2. Prices of all raw material streams or prices as functions of purities
- D. Constraints
  - D.1. Explosive limits and safety considerations
  - D.2. Coking limits, polymerisation or decomposition limits
- E. Plant and site data
  - E.1. Utilities; i.e. fuel, steam levels, cooling water, refrigeration
  - E.2. Waste disposal facilities and cost

Lapkin et al. in their work described a high-level conceptual framework for the description of complexity in intensive chemical processes.<sup>2</sup> The authors aimed to employ a hierarchical process design to develop a predictive methodology for building an understanding of the complexity of interactions between chemical species and facilitate reverse engineering of chemical process design from final products. Rejecting excessive simplifications and adding an additional dimension, i.e. time, a multilevel hierarchical conceptualisation was formed. Additionally, unlike other published structures, by adding a supplementary criterion describing the impact of chemical species on the environment, i.e. sustainability criterion, the framework equips users with a tool to predict any negative consequences of the developed processes to the environment.

Lapkin et al. based his hierarchy on a system operating tool developed for the description of real-life complex problems possessing a structural hierarchy and temporal dependences published by Mann.<sup>3</sup> The 9-windows design was modified to represent the life-cycle of a generic chemical process consisting of four steps: reactants, product mixture, isolated molecule or formulated product and, finally, use phase, end of life, recycling or regeneration, and four levels: subsystem, i.e. atomic level, system, i.e. molecular level, super system, i.e. phases or materials and finally chemical reactor and environment. For a detailed graphical representation see ref. 2.

Similarly to the work of Douglas,<sup>1</sup> the input information is unified and designed as a six-category descriptor.<sup>2</sup> It contains data on six parameters characterising the substance, its structure, space, time, energy and information. This data would accompany each component at every hierarchy level within the system.

Another conceptualisation framework is the one reported by Yang and Marquardt. Their framework is designed to define fundamental chemical concepts precisely.<sup>4</sup> The critical element of the work is the clarification of the nature of a scale in the multiscale modelling concept. The framework is being developed by following a three-step approach, i.e. conceptualisation of general systems, rigorous definitions for a precise characterisation of scales as well as inter-scale relationships and finally composition of a general multiscale model. The steps are made consecutively, by building upon previous ones. The developed framework is structured in the form of an ontology, reusing elements of the Bunge-Wand-Weber (BWW) ontology<sup>5</sup> upon some modifications (introduction of laws on intra-level

couplings, the environment and the structure of a level, the laws on inter-scale relations and a multiscale model and its clarification).

A number of other tools aiding process system engineering and flowsheet generation have been developed, a review on these was written by Vlachos.<sup>6</sup> To examples of such tools, one can include the work of Casola,<sup>7</sup> Morbach,<sup>8</sup> and Daichendt.<sup>9</sup> This list is not comprehensive since the primary aim of the thesis was not building of tools for the hierarchical process design, but it employed the philosophy of such approaches.

### **2.1.2. Describing process complexity**

Even a simple chemical reaction can be characterised by a complex and challenging to understand behaviour. Hence, unravelling all of the physical and chemical phenomena concealed behind a chemical transformation may prove to be challenging. That is why a number of tools aiding building of such understanding have been developed, and they are being employed by process chemists in academia and industry on a daily basis. Generally, the tools vary by the amount of information about the process they provide their users with; usually, the amount of information is directly proportional to the amount of resources the particular methodology requires. Rapid and experimentally inexpensive self-optimisation techniques provide users only with a minimum information about the process and, quite often, the results are difficult to interpret without additional mechanistic or kinetic studies. Power-law kinetics or more complex polynomials enable researchers to conduct an initial deconvolution of the observed behaviour. Finally, a true, full description of the process complexity can be built by detailed micro-kinetic studies yielding in predictive mechanistic models. This approach, being “Holy Grail” of process development requires sacrificing the most of resources and often can prove to be impossible to exercise.

The following chapters focus on the description of these three general approaches to unfolding the process complexity.

### 2.1.2.1. Self-optimisation

Self-optimisation is a technique in which the parameters of the system being optimised are autonomously and continuously changed until the output of the process reaches the predefined target. In chemical engineering, the target is usually associated with process characteristics such as, for example, yield, throughput, selectivity or qualities of the product such as, for instance, purity, particle-size or morphology. To achieve the predefined target, a feedback loop between the input and the output of the process must be generated, and the data must be processed using one of the available statistical approaches. The data is generated by conducting experiments performed in autonomously operated reactors equipped with suitable process analytical technologies (PAT) and is fed back to an algorithm in a closed loop until the target is reached. Upon reaching the target, i.e. completion of the optimisation, a set of parameters is identified. They may represent a local or a global optimum depending on the algorithm used and imposed on it restrictions.

Since an autonomous operation of batch processes is somewhat complicated, the flow chemistry methods emerged as ideal tools for such investigations. Easily implemented into flow setups PATs such as UV-vis,<sup>10</sup> IR,<sup>11-15</sup> Raman<sup>16-18</sup> and NMR<sup>19</sup> spectroscopies or gas<sup>20-22</sup> and liquid<sup>23</sup> chromatographies allow qualitative and, upon calibration, also quantitative analyses of complex reaction mixtures. Furthermore, usage of microreactors allows reduction of the amount of the material used in the optimisation effort what can significantly lower its cost.

Equally important to the choice of a suitable PAT is the choice of an algorithm to search for optima. Arguably, the most commonly used numerical method is the Simplex Method or its modifications.<sup>11,19,21,24,25</sup> Other algorithms employed in self-optimisations of chemical processes are Steepest Descent Method,<sup>23</sup> SNOBFIT (Stable Noisy Optimisation by Branch and Fit)<sup>10,11,22,26-28</sup> and MOAL (Multi-Objective Active Learner).<sup>20,29</sup> McMullen and Jensen in their work implemented three of the above-mentioned algorithms and compared their performance.<sup>23</sup> Even though all of them achieved similar final solutions, the amount of experimental work differed quite significantly between them. It is worth noticing that there is no universally superior algorithm and the performance of the algorithm depends on the optimisation problem. Furthermore, some of the algorithms offer additional steps aiming towards determination whether the identified solution is a global or a local optimum. These

steps require supplementary experimental efforts. However, they may result in finding a better solution.

Despite being very useful in adjusting continuous variables of the process, the main disadvantage of self-optimisation is its inability to handle discrete variables. Some work has been done on describing discrete variables with appropriate functions.<sup>30</sup> However, this field of optimisation is still a domain of high-throughput experiments (HTE), where multiple experiments are simultaneously performed on a micro-scale. HTE proved to be very useful in screening for optimal solvents, oxidants, bases, ligands, catalysts and more.<sup>31-33</sup>

Since self-optimisation is based solely on a statistical search for optimal conditions, it does not provide any process knowledge. This technique is used predominately in cases where a rapid and cost-effective search for conditions is needed. Additionally, the researcher is not provided with any information on the scale-dependant behaviour of the process, unless the optimisation is repeated for the desired scale, nor can predict the behaviour of the system outside the tested range of conditions. Thus, it is not possible to construct a predictive model based on a self-optimisation. Self-optimisation and other black box techniques are also employed in cases where the system is too complex for a more detailed description of the problem, for example, biological systems.<sup>34</sup> Despite its drawbacks, self-optimisation is perhaps the most cost-effective tool for optimisation of chemical processes and is often used in both academia and industry. Additionally, data generated using autonomous systems can serve as a starting point for more detailed mechanistic and kinetic studies, should building process knowledge be the aim of the researcher.

A selection of recent applications of automated self-optimisation of chemical processes in flow reactors is listed in Table 2.1-1.

Table 2.1-1. Selected recent advanced in the field of self-optimisation.

Reaction	Variables	PAT
CdSe nanoparticle synthesis <sup>10</sup>	temperature, residence time and stoichiometry	fluorescence
Knoevenagel condensation, benzyl alcohol oxidation <sup>23</sup>	temperature, residence time and concentration	HPLC
Diels–Alder <sup>24</sup>	temperature, residence time and concentration	HPLC
Heck coupling <sup>25</sup>	residence time and stoichiometry	HPLC
Alcohols etherification in supercritical CO <sub>2</sub> <sup>11,21,22,35</sup>	temperature, pressure, supercritical CO <sub>2</sub> flow rate and stoichiometry	GC, IR
Paal-Knorr reaction <sup>12</sup>	temperature and residence time	IR
Nucleophilic aromatic substitution <sup>36</sup>	temperature, residence time concentration and stoichiometry	HPLC
Monoalkylation of an amine <sup>30</sup>	temperature, residence time, stoichiometry and solvent	LC-MS
Imine formation <sup>19</sup>	residence time and volume fraction	NMR
Aminocarbonylation of aryl halides <sup>37</sup>	temperature, residence time stoichiometry and pressure	GC, IR
Amidation to AZD9291 EGFR kinase inhibitor <sup>27</sup>	temperature, residence time and stoichiometry	HPLC
Suzuki-Miyaura cross-coupling <sup>38</sup>	temperature, residence time and catalyst loading	HPLC
Amidation <sup>26</sup>	temperature, residence time and stoichiometry	MS
Pd-catalyzed aziridination <sup>20</sup>	temperature, residence time and stoichiometry	UV, GC

### **2.1.2.2. Initial deconvolution of the observed behaviour**

Designing of some chemical processes may require building a broader knowledge concerning the physical and chemical phenomena underpinning the reaction. This information cannot be easily obtained through a self-optimisation. Hence, a different approach must be implemented. That is why a set of flowcharts or “roadmaps” was designed to equip chemists and engineers with tools to quickly and efficiently gain sufficient information on the process and to be able to describe it using power law kinetic expressions or simplified mechanistic scaffolds. This chapter will present two of numerous approaches available in the literature, i.e. the Kinetic Motif Analysis and the Reaction Progress Kinetic Analysis.

#### **2.1.2.2.1. Kinetic Motifs Analysis**

According to the Oxford English Dictionary, motif is a “distinctive, significant, or salient theme or idea; a recurrent or prevalent characteristic”. Motifs are prevalently used in studies of biological processes to describe interactions and dynamics of such systems in a simplified manner. It is due to inherent complexity of biological systems and inability to describe them in more details. Such simplifications allow quantifications of investigated systems despite incapability to observe some, or even most of the characteristics of the system. Hone et al. proposed application of this paradigm to catalytic/enzymatic transformations that could be used in kinetic or mechanistic studies.<sup>39</sup> These studies would benefit greatly from reducing the complexity of a chemical reaction to a set of “prevalent characteristics” that can represent all time-dependant behaviours.

Hone et al. in his description of a generic motif of a chemical transformation included, besides the reaction itself, also the substrate and product decomposition as well as the reactant pre-equilibrium (Figure 2.1-2). Arguably, this representation should be sufficient to describe a vast majority of chemical processes available in the literature. According to the authors, the analysis of kinetic motifs can prove to be superior to a polynomial representation of kinetics since motifs can be further reduced to a number of elementary steps, each with its unique rate expression. An independent nature of these expressions can potentially represent the time-dependent behaviour of the process in much greater details than polynomials. Additionally, deriving a kinetic motif from its essential components can

prove to be a much faster exercise and require fewer resources than formulation of a complex polynomial. Such approach, and especially the analysis of time-dependent behaviours, may be particularly valuable for optimisation of targets represented by non-monotonic functions.

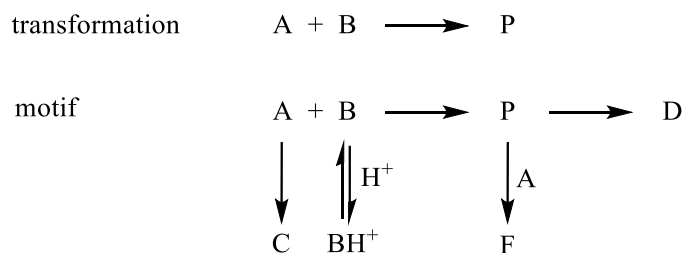


Figure 2.1-2. Representation of a motif in a general fine chemical reaction. Based on ref. 39.

To illustrate the process of development of kinetic motifs the authors assumed a multi-step reaction where A, in the presence of B, gives a product R and a by-product S (Figure 2.1-3a). From this general, fine chemical reaction motif, one can derive six possible options describing this simple process (Figure 2.1-3b). Performing a set of experiments and attempting to fit the values of the parameters of the rate expressions would reveal that only for two of the available options it was possible to find parameter values that fit the concentration profiles. Upon further experiments, it would be revealed that only the first option can describe all features of the process with sufficient precision.

The authors presented the utility of their methodology by applying it to two case studies: a nucleophilic aromatic substitution and the Paal-Knorr pyrrole synthesis.<sup>39</sup> For both examples, they were able to build a satisfactory kinetic understanding within a short period of time.

The Kinetic Motifs Analysis provides a simple and powerful methodology for the description of the kinetic behaviour of the investigated processes. Building upon a generic scaffold of a chemical reaction, the researcher can evolve the kinetic motif so that it will suit the specific reaction. In this way, a more detailed understanding of the investigated reaction can be developed. If required, this understanding can be expanded by the scale-dependent phenomena by addition of mass and energy transfer descriptions to the kinetic motif.

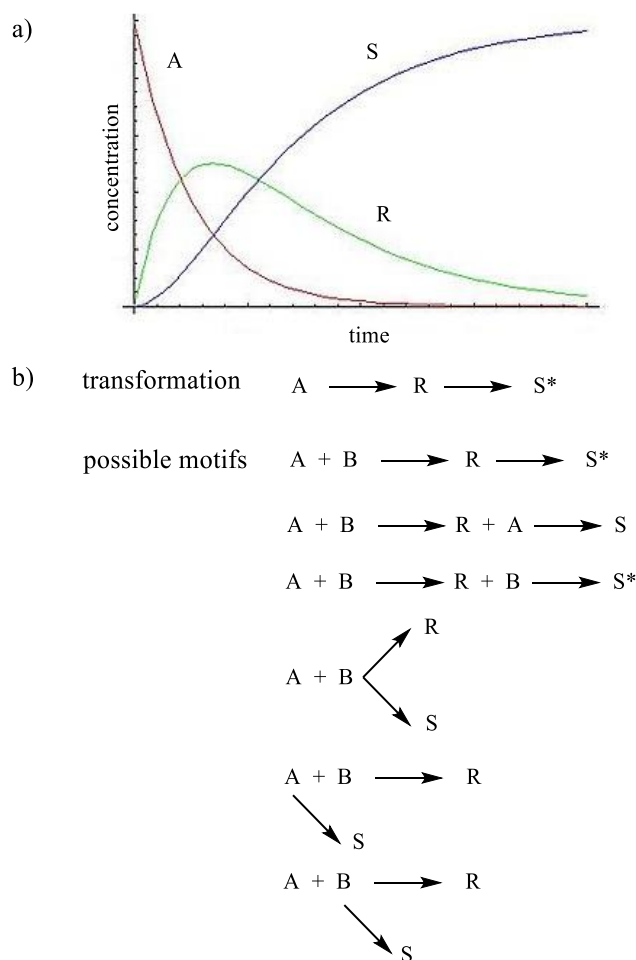


Figure 2.1-3. Possible motifs for a simple two-step reaction. Based on ref. 39.

### 2.1.2.2.2. Reaction Progress Kinetic Analysis

Donna Blackmond suggested a very concise methodology of analysing kinetic data that can be rapidly acquired via off-line, or ideally on-line measurements.<sup>40</sup> These measurements can be used to decide whether the process follows one of the mechanistic scaffolds or detect patterns, such as, for example, catalyst activation or deactivation, substrate and product inhibition or promotion.

For simple catalytic processes involving only one substrate, Blackmond suggests employing one of the available graph-representations of reaction mechanisms; such representations are prevalently used in biochemistry and organometallic catalysis. For example, the Michaelis-Menten model can be used, Figure 2.1-4.<sup>41</sup>

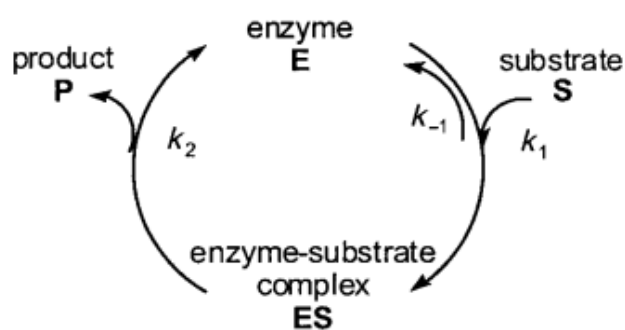


Figure 2.1-4. The Michaelis-Menten model of a catalytic reaction. Based on ref. 40.

The Michaelis-Menten model assumes formation of an enzyme-substrate complex, or more generally, a catalyst-substrate intermediate by coordination of a molecule of a substrate to a molecule of a catalyst. The second step of the reaction yields in a molecule of product and a molecule of a reformed catalyst. The rate of the whole process can be expressed by Equation ( 1 ):

$$r = \frac{r_{\max}[S]}{K_M + [S]} \quad (1)$$

where  $r_{\max}$  is the maximum reaction rate ( $\text{mol dm}^{-3} \text{min}^{-1}$ ),  $[S]$  is the concentration of a substrate ( $\text{mol dm}^{-3}$ ) and  $K_M$  is the Michaelis-Menten constant ( $\text{mol dm}^{-3}$ ).

Several simplified representations of the Michaelis-Menten model were proposed. Arguably, the most recognised one is the Lineweaver-Burk linearisation, Equation ( 2 ).<sup>42</sup> It is broadly applied to graphical determination of the parameters of the Michaelis-Menten model, i.e.  $r_{\max}$  and  $K_M$ .

$$\frac{1}{r} = \frac{1}{r_{\max}} + \frac{K_M}{r_{\max}} \frac{1}{[S]} \quad (2)$$

Other available linearisations of the Michaelis-Menten model include, among others the Hanes-Woolf plot<sup>43</sup> and the Eadie-Hofstee diagram.<sup>44</sup>

The Michaelis-Menten model, despite its enormous simplicity, was successfully applied to several families of chemical transformations such as decompositions, isomerisations and hydrogenations.<sup>40</sup>

For more complicated processes involving more than one substrate, Blackmond suggested modification of the Michaelis-Menten mechanism.

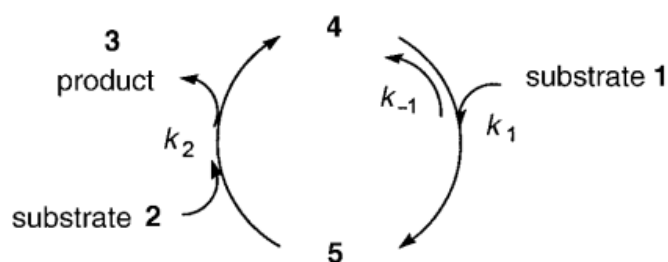


Figure 2.1-5. The mechanism for a simple catalytic reaction with two substrates and one intermediate species. Based on ref. 40.

The reaction rate expression can be presented in the form of Equation (3):

$$r = \frac{r_{max}[1]}{K_M + [1]} \quad (3)$$

where:

$$r_{max} = k_2[2][4]_{total} \quad (4)$$

$$K_M = \frac{k_{-1} + k_2[2]}{k_1} \quad (5)$$

Since, for a reaction with two substrates, the  $r_{max}$  and the  $K_M$  are no longer constant, linearisation of the model cannot be performed that easily; a set of experiments should be used to estimate the values of the parameters.

For the cases where the Michaelis-Menten model does not provide a sufficient fit of the experimental data to the model, Blackmond recommended a yet another, more generic,

representation of a reaction rate. This representation dismissed Michaelis-Menten model assumptions and is derived directly from elementary steps of the investigated process and can be represented in the form of Equation ( 6 ):

$$r = \frac{k_1 k_2 [1][2][4]_{total}}{k_{-1} + k_1 [1] + k_2 [2]} \quad (6)$$

alternatively, Equation ( 7 ):

$$r = \frac{a[1][2][4]_{total}}{1 + b[1] + c[2]} \quad (7)$$

where

$$a = \frac{k_1}{k_{-1}} k_2 \quad (8)$$

$$b = \frac{k_1}{k_{-1}} \quad (9)$$

$$c = \frac{k_2}{k_{-1}} \quad (10)$$

Similar expressions can be derived for even more complex cases, i.e. for three or more substrates. However, this should not be required most of the times since a vast majority of chemical reactions do not require more than two substrates. Should this be the case, they can presumably be reduced to a set of two-substrate reactions.

Blackmond also formulated a “road-map” for the Reaction Progress Kinetic Analysis allowing researchers to quickly and precisely determine the orders of the influence of separate reactants on the observed reaction rate and, based on them, derive a specific rate expression tailored for the investigated process. However, before drawing the “road-map”, Blackmond introduced a parameter called *[excess]*. She specified that the *[excess]* is a difference in the initial concentration of two substrates ( 11 ).<sup>40</sup>

$$[excess] = [2]_0 - [1]_0 \quad (11)$$

Assuming lack of side reactions, the *[excess]* parameter does not change as the reaction progresses, i.e. both substrates are consumed at the same rate, and the *[excess]* is not identical to either the number of equivalents or to the percentage excess concentration since both of them do change as the reaction progresses.

Using the definition of *[excess]* and following steps visualised in Figure 2.1-6, a researcher should be able to gather a sufficient understanding of the process and take a decision which scaffold of the mechanism to use, alternatively, if necessary, attempt more detailed kinetic studies. This choice, for ideal cases, should be made after as little as six experiments. Such a small amount of experimental work allows saving a significant amount of resources and accelerate kinetic and mechanistic studies of complex chemical transformations.

The Reaction Progress Kinetic analysis was successfully applied in numerous research reports providing easily accessible mechanistic and kinetic data aiding process development and optimisation of investigated processes.

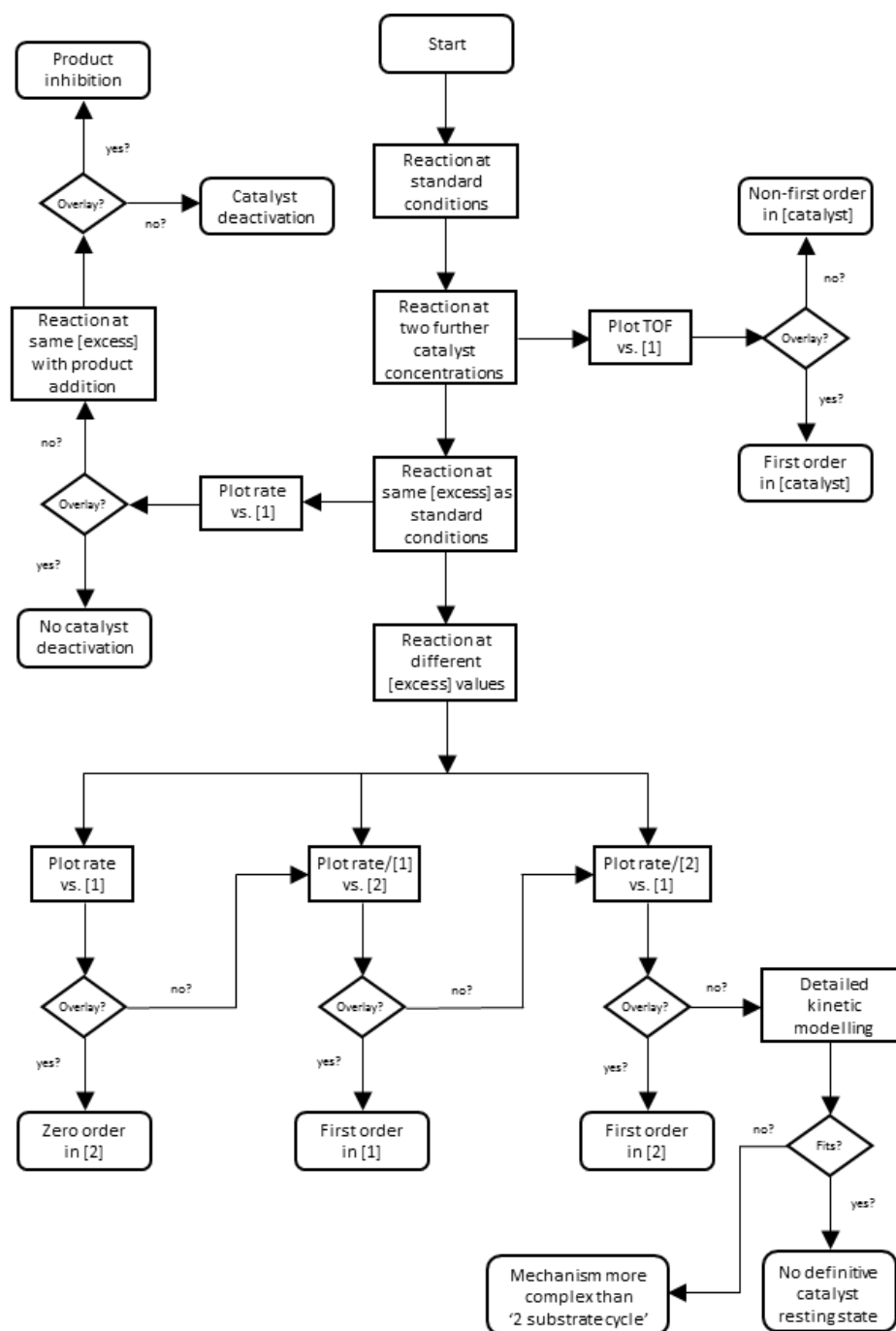


Figure 2.1-6. A flow chart for the Reaction Progress Kinetic Analysis. Reproduced from ref. 40.

### 2.1.2.3. True deconvolution of the observed behaviour

The “Holy Grail” of process development is obtaining all necessary information on the process and being able to describe it using elementary chemical reactions and *ab initio* mathematical descriptions of physical phenomena. Reducing a complex physiochemical behaviour of a chemical transformation to a set of basic equations and estimating values of all their parameters generates a predictive model that can be easily used to design an optimal setup for the reaction being under investigation and predict its behaviour at different scales. On the other hand, this type of process description is by far the most experimentally expensive and quite often cannot be performed due to excessively complex nature of the process or lack of suitable analytical techniques. Despite this, true deconvolution of the observed behaviour is being performed for some processes or parts of them. Mainly because of the amount of information about the process it provides its users with. This information delivers a predictive description of the process also outside of the investigated range of conditions. Hence, can be used in, for example, implementations of quality by design methodology, where manufactures of, for instance, pharmaceutical products, must obtain a sufficient amount of process knowledge to be able to predict how the quality of the product correlates with the change of process conditions. Other example where a full deconvolution of the observed behaviour is of utmost importance are large-scale industrial processes. In these cases, an increase of the yield by even 1% upon a knowledge-based process optimisation can bring a significant additional revenue.

An *ab initio* description of a process requires reducing the complexity of the chemical reaction to a set of elementary equations in the form of either equilibria or irreversible reactions. This, non-trivial exercise, especially for complex processes, must be followed by a description of all physical phenomena such as mass and energy transfer. The application of, among others, mixing models to the real systems requires estimation of the additional parameters and can prove to be a significant challenge, especially for heterogeneous systems. Even for a homogeneous process conducted in a tubular reactor under a laminar flow regime, the description of mass transfer requires measurements of the residence time distribution and construction of the dispersion model.

A true deconvolution of the observed behaviour involves estimation of a large number of parameters; for example, the microkinetic modelling of the Fischer-Tropsch process performed by Azadi et al. required estimation of 85 independent parameters.<sup>45</sup> This would

not be possible without a significant amount of experimental data. Well-designed experiments, ideally performed using *in-situ* analytical techniques characterised by high precision and resolution are ideal sources of data for parameter estimation. However, due to a large cost of high-quality experimental results, a number of computational tools, such as the Model-Based Design of Experiment, MBDoE, can be used to minimise the amount of resources used in building and parametrisation of the model. This is done by maximisation of the information obtained from the conducted experiments. However, even for ideally designed experiments, it may be challenging to separate the physical phenomena underpinning the behaviour of the system from the chemical properties of the process. A solution to this problem is provided by the microreactor technology. Reducing the dimensions of the reactor system to micro, or even nanometres provides excellent mass and energy transfer. Thus, ideal physical models can be applied. Following construction of the chemical model, experiments at different scales can be performed to complete the model by the scale-dependent phenomena.

In addition to experimental tools for identifying reaction mechanisms, quantum chemical calculations methodologies for mechanistic studies have gained a significant attention. Especially, the density functional theory (DFT) modelling has been used extensively for investigations of the energy profiles of chemical transformations.<sup>46–48</sup> Implementation of DFT can potentially result in an easier description of the chemical complexity of the process by identification of the possible elementary steps involved in the reaction. Additionally, upon the transition state analysis, it is possible to estimate the energetic barrier between the intermediates forming the elementary step. The energetic barrier obtained via DFT studies provides a valuable initial guess for the parameter estimation. The quality and the experimental cost of the parameter estimation is strongly correlated with the quality of the initial guess for the parameters. Thus, an approximation of these values obtained via DFT studies can prove to accelerate the work significantly.

Similarly to unravelling the chemical complexity of a process, the work on the physical intricacy of the process can be significantly accelerated by using appropriate modelling techniques. For example, the description of mixing can be based not only on the experimental results but also on the computational fluid dynamics (CFD) modelling. This very comprehensive technique is capable of providing detailed information on the flow of fluids thus, can be used in defining of mixing models.

A large number of computational techniques allowing theoretical description of the investigated processes, namely the computer-aided process design, is available.<sup>49</sup> The choice of suitable techniques can potentially not only accelerate the work on the project, but in some cases, where the amount of information obtained from the experimental data is limited owing to technical difficulties, such as an inability to detect intermediates on a quantitative level, can allow building the detailed kinetic and mechanistic models for the processes where such description would not be possible in the absence of these computational techniques.

The full deconvolution of the observed behaviour was developed, among others, for some variations of the Fischer-Tropsch process, i.e. collection of reactions converting a mixture of carbon monoxide and hydrogen into liquid hydrocarbons. Azadi et al.<sup>45</sup> derived 128 elementary reactions with 85 free parameters and attempted the parameter estimation of all of them. Employing DFT modelling and the transition state theory, they were able to identify a set of parameters that provided a sufficient fit to the experimental data despite the relatively small amount of experimental data available. Other approaches to the description of the Fischer-Tropsch process utilising different catalysts are available in the literature.<sup>50-52</sup> All of them required extensive experimental work and usage of computational modelling tools.

### **2.1.2.3.1. Model-Based Design of Experiments**

As previously mentioned, generating the high-quality experimental data required to build and validate the model can be time and resource intensive. Additionally, poorly designed experiments can bring very little useful information about the investigated process. Therefore, it is essential to develop tools and methodologies designed to maximise the information obtained from the conducted experiments, thus, to minimise the amount of the necessary experimental work.

The Model-Based Design of Experiments (MBDoE) is a tool aiming to obtain as much information as possible from the experimental work being performed by precise planning and exclusive execution of experiments that should yield the most informative data. The generated data can be used in the model discrimination or the parameter estimation.

A validation of a mechanistic model based on the model-based experimental design consists of several steps: generating a proposal of a model, preliminary tests aiming towards identification whether it is possible to obtain required experimental data to quantify the model, model discrimination performed to validate if the proposed model is capable of predicting the behaviour the reaction in sufficient details. Should the proposed model fail at any of the initial steps, a different model should be suggested and the procedure ought to be repeated. Following the identification of a suitable model, the estimation of the model parameters should be exercised. Improved values of the parameters shall yield the final, validated model being able to describe all features of the investigated process and, ideally, predict its behaviour outside of the tested range of conditions, Figure 2.1-7.

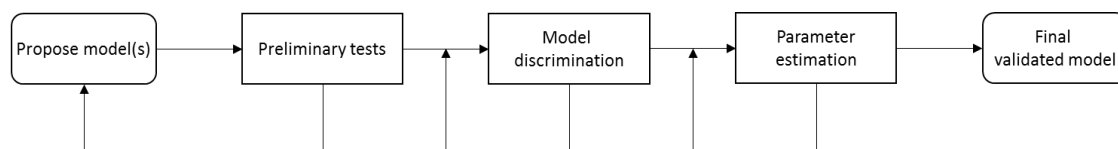


Figure 2.1-7. Model validation procedure based on MBDoe. Based on ref. 53.

In the present work, MBDoe was primarily used in the final step of model validation, i.e. parameter estimation. Thus, this chapter will focus on this part of the cycle.

The estimation of the process parameters aims towards increasing the precision of the model parameters and can be expressed in mathematical terms by operations done to reduce the size of the inference regions of the model parameters. Thus, operations performed to minimise the elements of the variance-covariance matrix,  $\mathbf{V}$ , of the parameters ( 12 ).

$$optimum = \min \arg(\mathbf{V}) \quad ( 12 )$$

Adopting the Bayesian approach,<sup>54</sup> it is possible to estimate the variance-covariance matrix that will be obtained after the experiment is conducted. Therefore, the design of experiments problem, namely maximisation of the information obtained from the performed experiments, reduces to the minimisation of ( 13 ) by optimally choosing the set of experiment decision variables.<sup>53</sup>

$$\mathbf{V}(\hat{\theta}, \varphi) = \left[ \sum_r^{n_{resp}} \sum_s^{n_{resp}} \widetilde{\sigma}_{rs} \mathbf{Q}_r^T \mathbf{Q}_s + \sum_{\theta} \hat{\theta}^{-1} \right]^{-1} \quad (13)$$

where  $\hat{\theta}$  is the best currently available estimate of the set of the model parameters,  $\varphi$  are the experiment design variables,  $n_{resp}$  represents the number of the model responses with regards to the parameters,  $\widetilde{\sigma}_{rs}$  denotes the (r,s) element of the inverse of the  $\sum_y$  – variance-covariance matrix of the experimental measurements, ( 14 ),  $\mathbf{Q}_r$  and  $\mathbf{Q}_s$  are the dynamic sensitivity of the respectively  $r^{\text{th}}$  and  $s^{\text{th}}$  response, defined as ( 15 ). Following the suggestion made by Box and Lucas, the prior information on the parameter uncertainty,  $\sum_{\theta} \hat{\theta}^{-1}$ , can be neglected.<sup>55</sup>

$$\sum_y = \begin{bmatrix} \sigma_{y_1}^2 & \sigma_{y_1 y_2}^2 & \cdots & \sigma_{y_1 y_{n_{resp}}}^2 \\ \sigma_{y_2 y_1}^2 & \sigma_{y_2}^2 & \cdots & \vdots \\ \vdots & \vdots & \ddots & \vdots \\ \sigma_{y_{n_{resp}} y_2}^2 & \cdots & \cdots & \sigma_{y_{n_{resp}}}^2 \end{bmatrix} \quad (14)$$

$$\mathbf{Q}_r = \begin{bmatrix} \left. \frac{\partial \hat{y}_r}{\partial \theta_1} \right|_{t_1} & \cdots & \left. \frac{\partial \hat{y}_r}{\partial \theta_p} \right|_{t_1} \\ \cdots & \cdots & \cdots \\ \left. \frac{\partial \hat{y}_r}{\partial \theta_1} \right|_{t_{n_{sp}}} & \cdots & \left. \frac{\partial \hat{y}_r}{\partial \theta_p} \right|_{t_{n_{sp}}} \end{bmatrix} \quad (15)$$

Zullo defined the inverse version of the parameter variance-covariance matrix ( $\mathbf{V}$ ) as the discrete version of the information matrix  $\mathbf{M}$ , suitable for the optimal design of dynamic experiments in non-linear multi-response systems.<sup>56</sup>

$$\mathbf{V}(\hat{\theta}, \varphi) = \mathbf{M}(\hat{\theta}, \varphi)^{-1} \quad (16)$$

The information matrix, similarly to the parameter variance-covariance matrix,  $\mathbf{V}$ , depends on the sensitivity matrices,  $\mathbf{Q}$  and the inverse of the variance-covariance matrix of the experimental measurements,  $\widetilde{\boldsymbol{\sigma}}_{rs}$ . However, unlike the variance-covariance matrix,  $\mathbf{V}$ , the information matrix,  $\mathbf{M}$ , allows evaluation of the information content from a number of experiments,  $n_j$ , ( 17 ).

$$\mathbf{M}(\hat{\boldsymbol{\theta}}, \boldsymbol{\varphi}) \equiv \sum_{j=1}^{n_{resp}} \sum_{r=1}^{n_{resp}} \sum_{s=1}^{n_{resp}} \widetilde{\boldsymbol{\sigma}}_{rs,j} \mathbf{Q}_{r,j}^T \mathbf{Q}_{s,j} + \mathbf{M}^0 \quad (17)$$

Similarly to ( 13 ), the preliminary information on the parameter uncertainty,  $\mathbf{M}^0$ , can often be neglected.<sup>53</sup>

When implementing ( 13 ) or ( 17 ), one should remember that, due to the local first-order approximation of the parameter variance function, the expression is not valid for highly non-linear problems.<sup>57</sup> Despite the possibility of obtaining significant errors due to a large non-linearity of the optimisation problem, this MBDoe technique is commonly used in scientific publications.

From the definitions of  $\mathbf{V}$ , ( 13 ), and  $\mathbf{M}$ , ( 17 ), the algorithm of designing experiments can accordingly maximise some metric of  $\mathbf{M}$  or minimise some metric of  $\mathbf{V}$  by varying an element or elements of  $\boldsymbol{\varphi}$ , the experiment control variables.

A number of possible metrics to measure and compare  $\mathbf{V}$  or  $\mathbf{M}$  can be found in the literature.<sup>53,58</sup> Here only four, the most commonly applied, will be presented.

Arguably, the most commonly used metric is the D-optimality criterion ( 18 ),<sup>58</sup> which aims to maximise the determinant of the information matrix,  $\mathbf{M}$ , or to minimise that of the variance-covariance matrix,  $\mathbf{V}$ , Figure 2.1-8.<sup>53</sup>

$$D_{opt}: \min\{\det\mathbf{V}\} \vee \max\{\det\mathbf{M}\} \quad (18)$$

The D-optimal design gained a significant interest due to a straightforward geometrical interpretation, Figure 2.1-8, invariance with respect to, for example, parameter rescaling or other numerical transformations and good results for systems described by multiple parameters.<sup>53</sup> However, the D-optimality criterion has some significant drawbacks. According to Zullo, the D-optimal design aims towards improving the precision of the parameter characterised by the highest sensitivity, while leaving the less sensitive parameters unchanged. Even though this approach results in a reduced variance of the model, the uncertainties of some of the model parameters may remain significantly large.<sup>53,56</sup>

The A-optimal criterion aims to reduce the size of the box enclosing the confidence region, Figure 2.1-8. Thus, the A-optimality aims to maximise the trace of the information matrix,  $\mathbf{M}$ , or minimise that of the variance-covariance matrix,  $\mathbf{V}$ , ( 19 ).

$$A_{opt}: \min\{\text{trace}\mathbf{V}\} \vee \max\{\text{trace}\mathbf{M}\} \quad ( 19 )$$

The main advantage of the A-optimality is minimisation of the arithmetic mean of the parameter error as well as reduction of the parameter correlation.<sup>6,53</sup> The main drawback of the A-optimality criterion are, arguably, unreliable results for systems characterised by high correlations.<sup>53,56,59</sup>

The E-optimal criterion aims to maximise the smallest eigenvalue of the information matrix,  $\mathbf{M}$ , or minimise that of the variance-covariance matrix,  $\mathbf{V}$ , ( 20 ). Meaning that it tries to minimise the major axis of the confidence ellipsoid, Figure 2.1-8.

$$E_{opt}: \min\{\lambda_{max} \mathbf{V}\} \vee \max\{\lambda_{min} \mathbf{M}\} \quad ( 20 )$$

The E-optimality can result in a minimisation of the largest parameter uncertainty. Notwithstanding, this approach focuses on improving only the values of the parameters characterised by the largest eigenvalue, hence little attention is being paid to the rest of the parameters.<sup>53,60,61</sup>

Finally, the modified E-optimality criterion was developed to work with systems characterised by a high correlation between parameters. However, application of the modified E-optimality criterion is possible exclusively for models described by only two parameters, Figure 2.1-8, ( 21 ). Another significant drawback of the modified E-optimality is its discrete nature. The discrete nature may potentially lead to convergence issues or result in large, spherical confidence ellipsoids, not improving precision of the model.<sup>53</sup>

$$modE_{opt}: \max \left\{ \frac{\lambda_{max} \mathbf{V}}{\lambda_{min} \mathbf{V}} \right\} \vee \min \left\{ \frac{\lambda_{max} \mathbf{M}}{\lambda_{min} \mathbf{M}} \right\} \quad (21)$$

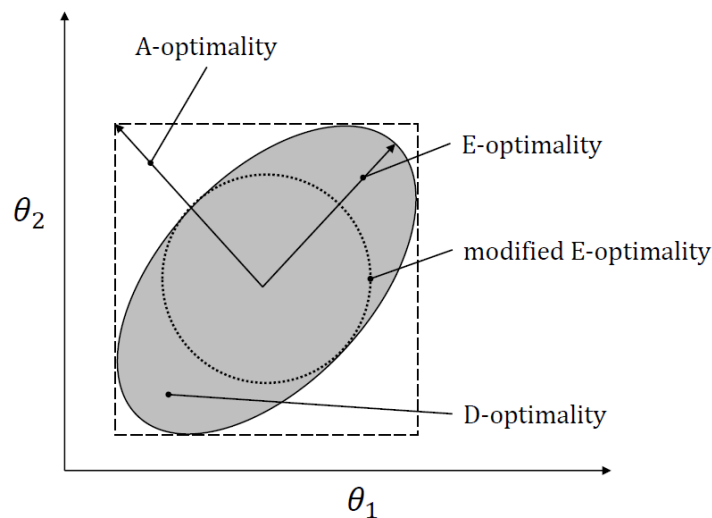


Figure 2.1-8. Geometrical interpretation of the most commonly implemented criteria for the experiment design. The grey area represents the confidence region of the model parameters, based on ref. 53.

A detailed discussion and presentation of other optimisation criteria can be found in the literature.<sup>58,62</sup>

Recent attention paid to the development of MBDoe resulted in implementation of some of the most commonly used techniques in commercially available software packages. gPROMS Model Builder 4.0.0 used in the present work provides user-friendly access to A-, D- and E-optimality criteria.

### 2.1.3. Summary

The chapter provided an overview of tools and methods of building process knowledge. The discussed tools and methodologies offer their users a different depth of process information that usually is directly proportional to the amount of resources necessary to build the model. Despite numerous tools designed for the computer-aided process design or statistical tools, such as MBDoE, process engineers still need to weight the cost of building the knowledge due to limited resources. That is why it is crucial to understand which tool is the best suited and the most cost-effective for the specific case.

Full mechanistic predictive models provide a vast amount of information on the process including a description of scale-dependent phenomena. Due to a significant cost of development, this type of process understanding is being used for challenging processes generating a large added value. Furthermore, these models are ideally suited for *in silico* optimisation, process intensification and for scaling. When a limited, scale-dependent information is sufficient, an initial deconvolution of the observed behaviour can be applied. Using methods such as the Reaction Progress Kinetic Analysis or the Kinetic Motif Analysis allows building polynomials describing the behaviour of the process under the tested range of conditions. When a rapid search for optimal conditions is required, a black-box optimisation, ideally performed autonomously, is the method of choice. Unfortunately, it provides its users with virtually no process knowledge. Thus, it cannot be used for scaling without repeating the procedure at the desired scale.

## 2.2. Continuous processing methods for fine chemical synthesis

The round-bottom flask has been the most commonly used piece of equipment in synthetic laboratories for centuries. Its versatility, chemical as well as thermal resistance, availability and low cost facilitated a significant advancement of the field of organic chemistry. Despite its unparalleled usefulness, a typical round-bottom flask can generate only a limited range of operating conditions. This restriction precludes implementation of, for example, high-pressure, highly exothermic or endothermic processes or severely lowers the efficiency of, for instance, multiphase reactions. Circumventing this issue by broadening the range of the available process conditions or opening of new, previously unexplored process options should result in a significant acceleration of further development of organic chemistry.

A possible solution to the narrow range of available process conditions can be delivered by a re-evaluation of the way reactions are conducted. The adaptation of continuous flow technologies developed over last two decades enables chemists and chemical engineers to utilise conditions that were previously a domain of a large-scale bulk chemicals production; for instance high temperature and high pressure reactions. Furthermore, much smaller dimensions of the new type of flow reactors allow practitioners of flow chemistry to benefit from the previously inaccessible, even for well-designed large-scale continuous systems, range of conditions. For example, a much greater and uniform penetration of light allows efficient and selective implementation of photochemical transformations; positioning of electrodes in a very close proximity to each other allows electrochemists to reduce the amount of used electrolytes, or even abandon adding them at all. Furthermore, for a flow process, a much lower voltage must be applied to achieve comparable results. This may reduce the risk of Joule heating and may increase the selectivity of electrochemical processes.

The following chapters will focus on the description of some of the new possibilities brought by the “flow revolution” in organic synthesis. Detailed reviews on tools and methods of flow chemistry are available in the literature.<sup>63–75</sup>

### 2.2.1. Mass transfer

Arguably, the most important result of the implementation of the flow chemistry technology is an enhanced and controlled mass transfer. The mass transfer within the reactor depends on the length scale of the reactor. The importance of mass transfer for reaction engineering originates from a fact that if diffusion or thermal conduction is potentially slower than the reaction rate in a given reaction system, then the mass transport may be controlling the outcome of the process, i.e. its overall rate and selectivity.

In a typical reaction system, the mass-transfer occurs between two or more homogeneous fluids, two or more heterogeneous fluids, otherwise, between solids and fluids. These cases can be reduced to three model examples, namely homogeneous and miscible liquid-liquid, liquid-gas and liquid-solid mass transfer. The description of all other systems can be derived from these three model examples.

For two homogeneous, miscible liquid phases, the mass transfer, namely mixing, shall be considered at two levels, micromixing, i.e. mixing at the molecular level, and macromixing, i.e. mixing at the macro-scale.

Liquid-liquid flow chemical processes, commonly run in microfluidic chips or tubular reactors, are characterised by a laminar flow regime owing to low Reynolds numbers,<sup>76</sup>  $Re$ , often below one,

$$Re = \frac{\rho ul}{\mu} \quad (22)$$

where  $\rho$  is the density of the liquid ( $\text{kg m}^{-3}$ ),  $\mu$  is the dynamic viscosity of the liquid ( $\text{kg m}^{-1} \text{s}^{-1}$ ),  $u$  is the velocity of the liquid with respect to the object ( $\text{m s}^{-1}$ ), and  $l$  is the characteristic linear dimension (m).

The ideal laminar flow regime is characterised by a “lamination” of the contact of homogeneous miscible liquid streams, resulting in mixing being predominantly by diffusion of molecules across the neighbouring streams. The diffusion can be quantified by the 2<sup>nd</sup> Fick’s law, Equation ( 23 ),<sup>77</sup>

$$\frac{\partial c}{\partial t} = D \frac{\partial^2 c}{\partial x^2} \quad (23)$$

where  $c$  is the concentration ( $\text{mol m}^{-3}$ ),  $t$  is the time (s), and  $x$  (m), is the position and  $D$  is the diffusion coefficient ( $\text{m}^2 \text{s}^{-1}$ ).

Thus, for binary systems, the characteristic mixing time,  $t$ , is directly proportional to the square of the diffusion length,  $x$ , and inversely proportional to the diffusion coefficient,  $D$ , Equation ( 24 ).

$$t = \frac{x^2}{D} \quad (24)$$

Mixing on the macro-scale in simple flow reactors, namely where no additional power utilised for mixing is delivered, is governed largely by axial dispersion. While the ideal plug-flow regime is characterised by a constant velocity of the fluid at every cross-section of the pipe perpendicular to the axis of the pipe, non-ideal laminar flow regime results in a parabolic velocity profile across the pipe. The parabolic velocity profile is caused by friction effects. Thus, material moving along the centre of the reactor channel flows faster than the material in a close proximity to the walls. The variation in the axial velocity across the channel translates to the variation in the residence time distribution between different fluid laminae. The degree of axial dispersion can be measured using the tracer injection methods<sup>78,79</sup> and characterised using the Bodenstein number,  $Bo$ , which represents a relation between the axial convective forces from flow to the back-mixing caused by the axial dispersion, Equation ( 25 ),

$$Bo = \frac{uL}{D^*} \quad (25)$$

where  $u$  ( $\text{m s}^{-1}$ ), is the average velocity of the reaction stream,  $L$  (m), is the length of the reactor and  $D^*$  ( $\text{m}^2 \text{s}^{-1}$ ), is the effective axial diffusivity.

Generally, a small value of the Bo number suggests large deviations from the ideal plug-flow regime, thus a highly dispersive flow.

More complex flow systems equipped with mixing zones and additional mixing systems such as magnetic micro impellers, unsteady injection of fluids, namely oscillations, or peristaltic pumps have been developed.<sup>71</sup> The description of micro and macromixing in these is complex and requires implementation of appropriate mixing models.<sup>80,81</sup>

In the laboratory scale batch reactors, mixing is usually realised by a mechanical agitation using magnetic or overhead stirrers. The theoretical description of the mass transfer in these cases also requires implementation of appropriate mixing models. Alternatively, the computational fluid dynamics methods (CFD) can be used, or micro and macromixing can be investigated heuristically. While macromixing is often expressed in terms of the fluid segregation and measured experimentally using, for example, observation of the evolution of the degree of segregation using fluorescent dye,<sup>82</sup> micromixing is investigated by employing tools such as systems of competitive reactions, namely Bourne<sup>81</sup> or Villermaux-Dushman methods.<sup>83</sup> These methods exploit differences in intrinsic reaction rates of two parallel reactions conducted in the same system. Assuming an ideally micromixed reactor, only the reaction characterised by a greater reaction rate should occur; for the non-ideally mixed systems the products of both, the slower and the faster reaction would be detected. Based on the ratio of the concentrations of the products and the intrinsic kinetics of both reactions, one can calculate the time of micromixing of the system. The same tools have been successfully applied in the experimental determination of micromixing in flow reactors.<sup>84,85</sup>

Generally, the time to achieve 99% mixing in microreactors not equipped with an active nor passive mixers varies between 1 and 0.2 s depending on the channel width. For reactors equipped with mixing zones these values are much lower, sometimes less than 1 ms.<sup>85,86</sup> When a batch reactor is considered, it may be difficult to achieve 99% mixing faster than within 10 s. Even turbulent systems equipped with well-designed impellers and baffles cannot achieve a similar mixing performance to the well-designed continuous flow systems.<sup>63</sup> For a detailed consideration of mixing in chemical reactors see refs 81 and 80.

It is worth mentioning that an essential factor in choice of a mixer in an industrial environment is energy dissipation rate  $\varepsilon$ ,  $\text{W kg}^{-1}$ , that can be understood as the amount of energy utilised for mixing. When comparing two mixers characterised by a similar time to

99% mixing, the choice of a suitable technology is based on the amount of energy that must be delivered to achieve it. Thus, mixers characterised by a lower energy dissipation rate are preferred.<sup>81</sup>

To quantify the influence of mixing on the measured kinetics the Damköhler number,  $Da$ , can be used.<sup>87</sup> The Damköhler number is defined as a ratio of the reaction rate relative to the mass transport rate, Equation ( 26 ),

$$Da = \frac{r}{\frac{1}{t_{99\%}}} \quad (26)$$

where  $r$  represents the reaction rate ( $s^{-1}$ ), and  $t_{99\%}$  (s) denotes the time required for 99% mixing.

Generally, for the  $Da$  numbers lower than one, the process is reaction rate limited. When the  $Da$  number is greater than one, experimentally measured reaction rates are controlled by the mass transport.

The liquid-gas mass transfer at the molecular level, similarly to the liquid-liquid systems, is governed by diffusion. The flux of the gas stream to the liquid,  $N_g$ , in the quasi-equilibrium state can be expressed using, for example, the two-film theory, Equation ( 27 ),

$$N_g = k_g(c_g - c_{gi}) = k_l(c_{Li} - c_L) \quad (27)$$

where,  $k_g$  and  $k_L$  are the mass transfer coefficients respectively for the gas and the liquid side,  $c_g$  and  $c_L$  are respectively the concentration of the gas reactant in bulk of the gas and the liquid phase and  $c_{gi}$  and  $c_{Li}$  are respectively the concentration of the gas reactant at the interfacial layer at the gas and the liquid side.

The two-film model assumes: operation in a steady state, that the interface between the gas and the liquid phase is a sharp boundary, that the laminar film exists at the interface on both sides of the interface, that there is a negligible resistance to mass transfer across the

interface and that bulk of the gas and the liquid is ideally mixed. It is worth mentioning that  $c_{Li}$  represents a saturated solution of the liquid phase. The ratio between  $c_{gi}$  and  $c_{Li}$  is equal to Henry's law coefficient for the investigated system, Equation ( 28 ).<sup>88,89</sup>

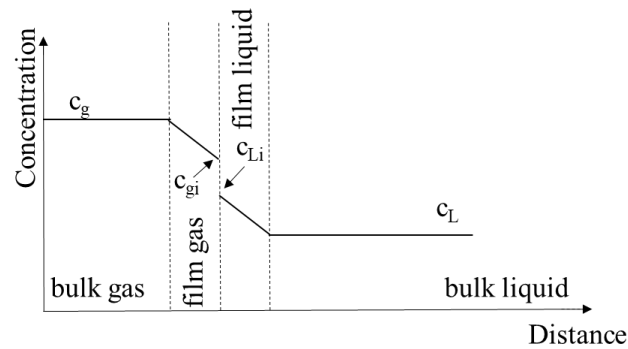


Figure 2.2-1. The concentration profile of the gas reactant in the gas-liquid mass transfer in the quasi-equilibrium state of the reaction.

$$k_H = \frac{c_{gi}}{c_{Li}} \quad (28)$$

For non-equilibrium systems, the change of concentration of a gaseous reactant in the liquid phase can be expressed as Equation ( 29 ) or Equation ( 30 ),

$$\frac{dc}{dt} = -k_g a (c_g - c_{gi}) \quad (29)$$

$$\frac{dc}{dt} = k_l a (c_{li} - c_l) \quad (30)$$

where  $a$  ( $\text{m}^2$ ) is the interfacial area.

The volumetric mass transfer coefficient,  $k_L a$  ( $\text{s}^{-1}$ ), is a convenient metric to compare reactor systems in terms of the gas-liquid mass transfer. For a gas-liquid microreactor operating in the slug-flow regime,  $k_L a$  varies between 0.3 and 21  $\text{s}^{-1}$ . Conventional stirred tanks are characterised by  $k_L a$  between 0.03 and 0.4  $\text{s}^{-1}$ .<sup>90</sup>

Clearly, the main factors governing the mass transfer between gasses and liquids are interfacial area, gradient of concentrations and equilibrium solubility. According to Henry's law, equilibrium concentration of the gaseous reactant in the liquid phase is directly proportional to partial pressure of the reactant in gaseous phase and to Henry's law coefficient, being a unique function of temperature for the solvent-solute system. Thus, without changing the solvent, one can influence solubility of the gaseous reactant by lowering the temperature of the system or increasing the partial pressure of the gaseous reactant. While the temperature often cannot be lowered without slowing down the reaction significantly, an increase in pressure, especially for flow systems, is feasible. To enhance the rate of mass transfer, thus, to reach the equilibrium faster, the interfacial area should be increased. For continuous systems, the interfacial area is a complex function of flow-rates of the gas and the liquid phase.<sup>91</sup> The commonly used in small-scale flow processes annular and slug-flow regimes generate an interfacial area in the range of  $700 \text{ m}^2 \text{ m}^{-3}$  for annular flow and up to  $18\,000 \text{ m}^2 \text{ m}^{-3}$  for slug flow regime.<sup>65</sup> These values are usually sufficient to operate within concentrations of gaseous reactants in the liquid phase close to saturation.

Operation in round-bottom flasks often precludes applying high pressures. Thus a solubility of gasses in liquids is severely lowered. Additionally, the interfacial area varies between  $107 \text{ m}^2 \text{ m}^{-3}$  for a typical 5 ml flask when the liquid is static and only  $35 \text{ m}^2 \text{ m}^{-3}$  for a 250 ml assuming static liquid phase.<sup>65</sup> This results in a slow mass-transfer and can cause operation far from the equilibrium concentration. To address the low surface area, an additional delivery of gasses is often introduced. Gas injectors located at bottoms of reactors generate bubbles travelling vertically through the liquid phase increasing the contact area between the gas and the liquid phase.

An another disadvantage of batch reactors is a significant head-space where toxic or explosive gasses can accumulate causing safety concerns. In flow reactors, the head-space hardly exists. Thus no accumulation of dangerous gaseous reactants occurs.

Owing to the fact that liquid-solid systems were not a focus of the thesis, a detailed theoretical consideration of this aspect is omitted. Generally, the ratio of the mass transfer between a solid and a liquid phase is directly proportional to the surface area of the solid. Hence, it is usually beneficial to use small solid particles of a narrow size distribution. It is worth noticing that fine, well-packed particles generate a significant pressure drop in the reactor system. Thus, too small particles can prove to be impractical. Three general types

of solid-fluid reactors are used, pack-bed, fluidised-bed and mixed-bed. Packed-beds are characterised by the entire column filled with a solid material so that the particle movement is restricted. In a fluidised-bed reactor, the suspended within the channel particles are free-flowing owing to the turbulent flow of the liquid phase. Mixed-beds are a combination of a packed bed and a fluidised bed. The movement of the solid at the bottom of the reactor is restricted, while the top layers are suspended and mixed via the flowing liquid phase. The hydrodynamics of flow through solid-liquid reactors are complex and are outside the literature review. For a detailed description of liquid-solid systems see refs 92 and 93.

### 2.2.2. Residence time distribution

Non-ideal, continuous reactor systems are characterised by unique probability distribution functions describing the time an element of the reaction medium spends in the reactor. Such functions, called residence time distributions, are inherent characteristics of mixing and flow patterns within the reactors. The fact that different elements of the reaction mixture spend different time in the reactor may result in an inconsistent yield between different elements of fluid. Thus, the understanding of the residence time distribution is crucial in reaction engineering.

Two ideal reactor systems are often considered in terms of the residence time distribution, i.e. a continuous-stirred-tank reactor (CSTR) or its cascade and a plug-flow reactor.

An ideal CSTR is assumed to be an ideally mixed reactor vessel with an inlet and an outlet, where reaction media are being constantly passed through the reactor. The residence time of such a model can be expressed as Equation ( 31 ), Figure 2.2-2a.

$$E(t) = \frac{1}{\tau} e^{-\frac{t}{\tau}} \quad (31)$$

where  $\tau$  (s) is the expected residence time of the reactor and  $t$  (s) is the time.

The expected residence time is calculated based on the volume of the reactor,  $V$  ( $\text{m}^3$ ), and the flow rate,  $F$  ( $\text{m}^3 \text{s}^{-1}$ ), Equation ( 32 ).

$$\tau = \frac{V}{F} \quad (32)$$

The residence time distribution of the ideal plug-flow reactor, being a model of the ideal flow through a pipe characterised by ideal radial mixing and non-existent axial mixing, is represented as a Dirac delta function at  $\tau$ , Equation ( 33 ), Figure 2.2-2b.

$$E(t) = \delta(t - \tau) \quad (33)$$

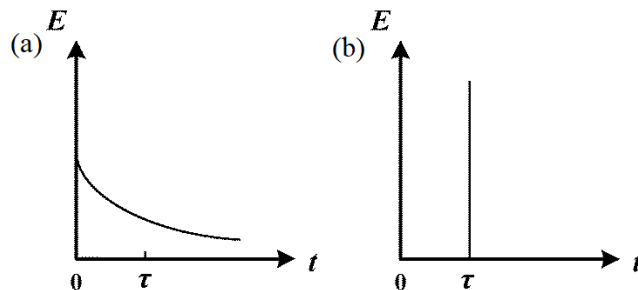


Figure 2.2-2. Residence time distribution of a pulse experiment for the ideal (a) CSTR; (b) plug-flow reactor.

The residence time distributions of non-ideal systems are influenced by deviations from ideal models, i.e. non-ideal mixing and flow patterns, Figure 2.2-3.

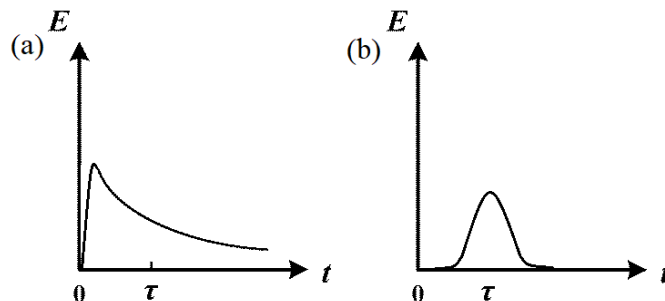


Figure 2.2-3. Residence time distribution of a pulse experiment for non-ideal (a) CSTR; (b) plug-flow reactor.

The residence time distribution of non-ideal CSTRs is often being measured experimentally using either pulse experiments, namely introduction of a small volume of a concentrated tracer at the inlet of the reactor and monitoring the corresponding signal at the outlet. Alternatively, step experiments, where the residence time distribution is investigated by rapidly changing the concentration of the tracer and monitoring the response of the system, can be used.

The mass balance of non-ideal plug-flow reactors can be expressed by Equation ( 34 ):

$$\text{accumulation} = \text{in} - \text{out} \quad ( 34 )$$

alternatively, as Equation ( 35 )

$$\begin{aligned} A_c \partial x \frac{\partial C_i}{\partial t} = & \left( u A_c C_i - A_c D_a \frac{\partial C_i}{\partial x} \right) \\ & - \left[ \left( u A_c C_i - A_c D_a \frac{\partial C_i}{\partial x} \right) + \partial \left( u A_c C_i - A_c D_a \frac{\partial C_i}{\partial x} \right) \right] \end{aligned} \quad ( 35 )$$

where  $A_c$  ( $\text{m}^2$ ) is the cross-sectional diameter of the reactor,  $x$  (m) represents the axial position,  $u$  ( $\text{m s}^{-1}$ ) denotes the linear velocity,  $C_i$  ( $\text{mol dm}^{-3}$ ) is the concentration of the tracer and  $D_a$  ( $\text{m s}^{-1}$ ) corresponds to the axial dispersion coefficient.

Assuming that linear velocity and axial dispersion coefficient are constant, the Equation ( 35 ) takes the form of Equation ( 36 ).

$$\frac{\partial C_i}{\partial t} + u \frac{\partial C_i}{\partial x} = D_a \frac{\partial^2 C_i}{\partial x^2} \quad ( 36 )$$

If  $\theta = \frac{t}{\langle t \rangle} = \frac{tu}{L}$ ;  $X = \frac{x}{L}$  and  $Pe = \frac{Lu}{D_a}$  where  $L$  is the length of the reactor (m) the Equation ( 36 ) can be written as Equation ( 37 ):

$$\frac{\partial C_i}{\partial \theta} + \frac{\partial C_i}{\partial X} = \frac{1}{Pe} \frac{\partial^2 C_i}{\partial Z^2} \quad (37)$$

where  $Pe$  is Peclet number. Peclet number, being a dimensionless number defined as a ratio of the advective mass transport and the diffusive mass transport, is obtained from correlations or measured experimentally.

For a pulsation experiment Equation (37) can be expressed as Equation (38).

$$E(\theta) = \left( \frac{Pe}{4\pi\theta} \right)^{0.5} \exp \left[ \frac{-(1-\theta)^2 Pe}{4\theta} \right] \quad (38)$$

The behaviour of a non-ideal plug-flow reactor can be approximated using the model of the ideal cascade of CSTRs having the same total volume as the investigated non-ideal plug-flow reactor. The residence time distribution of the ideal cascade of CSTRs can be expressed mathematically as Equation (39):

$$E(t) = \frac{1}{\tau} \left( \frac{t}{\tau} \right)^{N-1} \frac{N^N}{(N-1)!} \exp \left[ -\frac{tN}{\tau} \right] \quad (39)$$

where  $N$  is the number of CSTRs. This number must be obtained experimentally. For  $N$  going to infinity, the Equation (39) will represent the residence time distribution of the ideal plug-flow reactor.

### 2.2.3. Heat transfer

The smaller dimensions of flow reactors not only allow the more controlled mass transfer. They also enhance the energy transfer that plays a similarly important role in controlling the selectivity. Furthermore, an ability to efficiently remove heat from the reaction mixture allows expanding the range of conditions that can be used experimentally. Utilizing the flow technology allows running highly exothermic reactions in a much more controlled fashion even at higher temperatures should this benefit the kinetics.

While the heat generation or consumption is an inherent characteristic of the process and can be expressed using adiabatic temperature rise,  $\Delta T_{ad}$  (K), Equation ( 40 ), the delivery or removal of the heat from the reaction system is determined by the reactor and process parameters. The heat transfer from the reaction is governed by thermal conductivity of the reactor walls and their surface area, Equation ( 41 ),

$$\Delta T_{ad} = \frac{\Delta H_{net}}{m_{total} C_{p,r}} \quad (40)$$

where  $\Delta H_{net}$  (J) is net heat evolved in the course of the reaction,  $m_{total}$  (mol) is total content of the reactor,  $C_{p,r}$  (J mol<sup>-1</sup> K<sup>-1</sup>) is cumulative molar heat capacity of the reaction mixture.

$$Q = \frac{kA(T_{hot} - T_{cold})}{d} \quad (41)$$

where  $k$  (W m K<sup>-1</sup>) is thermal conductivity of the barrier, i.e. reactor walls,  $A$  (m<sup>2</sup>) is heat transfer area,  $T_{hot}$  and  $T_{cold}$  (K) are respectively temperatures of the hot and the cold side of the system,  $d$  (m) denotes thickness of the reactor walls.

Finally, the temperature profile inside the reactor is a function of mixing and flow pattern. Thus, to avoid generation of hot-spots inside the reactor, a sufficient mixing must be

provided to allow an adequate conductive or convective heat transfer in the reaction mixture.

The ratio of the heat generated and the heat removed from the reactor can be expressed as  $\beta_{batch}$  for batch systems, Equation ( 42 ), and  $\beta_{flow}$ , Equation ( 43 ), for flow reactors.<sup>63</sup>

$$\beta_{batch} = \frac{\text{heat generated}}{\text{heat removed}} = \frac{\Delta H_{net} d_{reactor}}{6\Delta T_{ad} h} \quad (42)$$

$$\beta_{flow} = \frac{\text{heat generated}}{\text{heat removed}} = \frac{\Delta H_{net} d_{reactor}^2}{4\Delta T_{ad} \kappa} \quad (43)$$

where  $d_{reactor}$  (m) is the diameter of the reaction vessel or reaction tube,  $h$  (W m K<sup>-1</sup>) is the convective mass transfer coefficient, and  $\kappa$  (W m K<sup>-1</sup>) is the thermal conductivity of the reaction mixture. While  $\kappa$  can be conveniently measured,  $h$  is a function of mixing and can be estimated using correlations.<sup>94,95</sup>

For both reactor types, i.e. flow and batch,  $\beta$  should be lower than one to assure efficient heat removal or delivery. Hartman et al. demonstrated the importance of a well-designed reactor system in terms of the energy transfer by providing two examples where  $\beta$  was considerably lower than one for both, the batch and the flow process, and another example where  $\beta_{batch}$  was higher than one and  $\beta_{flow}$  lower than one.<sup>63</sup>

The organocatalytic aldol reaction reported by Odedra and Seeberger<sup>96</sup> characterised by a modest heat of reaction proved to have the  $\beta$  values of approximately  $1 \times 10^{-2}$  for batch and  $4 \times 10^{-4}$  for flow. As verified by Valera et al.,<sup>97</sup> the results from batch and flow are virtually identical, thus a superior heat transfer should not be used as a trigger to conduct this process in flow. On the other hand, for a selective lithiation of 1,2-dibromobenzene with a subsequent electrophilic addition reported by Usutani et al.,<sup>98</sup> operation in a microreactor resulted in the  $\beta$  value of approximately 0.2 and 6.3 for a corresponding batch process. As expected, operation in flow resulted in a much higher yield and selectivity.<sup>63</sup>

### 2.2.4. Photons and electrons

Reduced dimensions of flow reactors do not only enhance mass and energy transfer but also enable chemists to efficiently harvest alternative ways to excite molecules. Photochemical processes require delivery of photons to molecules to form excited states. The excited molecule can either return to the ground state, rearrange and form by-products or react and form a product. Photoredox-catalysis utilises a yet another route, the electron transfer chemistry.<sup>99</sup>

The main obstacle to an intensification of the photoredox-catalysis is the short-lived nature of the excited state. Should the excited state not find an acceptor of the electron, it rapidly fluoresces and returns to the ground state. Owing to the short-life of excited states, it is important to efficiently and uniformly deliver photons of light to the reaction medium. Furthermore, an efficient mixing is required to enable a uniform concentration profile of reactants.<sup>100</sup>

According to the Beer-Lambert Law, the attenuation of light is a linear function of the concentration of the molecule being excited,  $c$  ( $\text{mol m}^{-3}$ ), its attenuation coefficient,  $\varepsilon$  ( $\text{m}^2 \text{mol}^{-1}$ ), and the length of the light path  $l$ , (m), Equation ( 44 ).

$$A = \varepsilon cl \quad (44)$$

Thus the transmittance,  $A$ , is reversely proportional to the length of the light path, Figure 2.2-4.

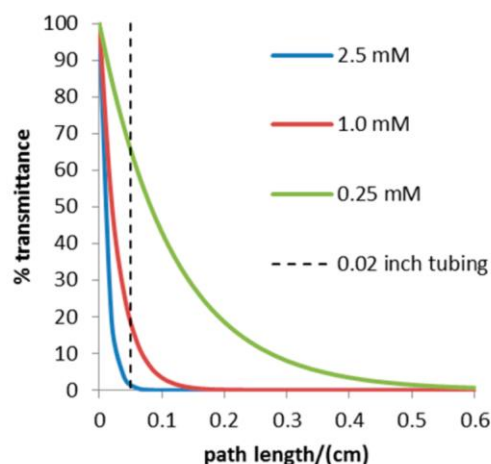


Figure 2.2-4 Transmittance as a function of the path length and concentration of the photoredox catalyst. The dashed vertical dashed line represents the inner diameter of a 0.02" tubing. Reproduced from ref. 71.

Owing to the fact that, for the commonly used catalyst concentrations, less than 40% of light is transmitted past a length of 0.1 cm, typical batch or semi-batch reactors equipped with immersion lamps are severely inefficient. However, when a shorter light path is used as a consequence of employing flow chemistry technology, a much greater efficiency can be achieved, see the dashed line in Figure 2.2-4.

Similarly, the electrochemistry, where the distance between the electrodes is crucial for an efficient transfer of charge, benefits from the technology brought by the flow chemistry.<sup>101</sup> During an electrochemical process, molecules are being reduced at the cathode and oxidised at the anode. To the main challenges of electrochemistry, one can include a nonuniform potential across the working electrode and a high electrical resistance of the reaction media.<sup>102</sup> While the nonuniform potential can be circumvented via a careful placement of electrodes in the reactor system, the issue of the low conductivity of the reaction media cannot be easily solved without using large amounts of electrolytes, changing the solvent or increasing the voltage. However, employing the flow chemistry tools, namely reducing the distance between the electrodes, it is possible to overcome the problem with the low conductivity owing to the directly proportional relationship between the electric resistance of the reactor media and the distance between electrodes. This allows a reduction, or even total removal, of the electrolyte from the reaction media and reduces the Joule heating owing to the much smaller currents used. Furthermore, the electrochemical transformations often involve the evolution of gasses, that can form

bubbles on the surface of the electrodes and reduce their efficiency, in the flow systems, the gas forms slugs resulting in the Taylor flow within the channel, that increases the mass transfer within the system. Thus, it may be beneficial for the reaction.<sup>103</sup>

### **2.2.5. Pressure, temperature and supercritical fluids**

Previous chapters described some of the benefits of smaller dimensions of the flow chemistry tools with a comparison to the classical batch chemistry. However, the flow chemistry offers also an easy access to harsh conditions such as elevated temperatures and pressures. These conditions, inaccessible for a classical round-bottom-flask, allow chemists to accelerate their reactions using high temperatures and, owing to easily generated back pressures, use classical solvents greatly above their boiling points at the atmospheric pressure. This may also allow avoiding the use of solvents at all and operate using neat reactants. Increasing pressures even further allows implementation of new, unconventional solvents such as supercritical fluids; especially supercritical carbon dioxide proved to be successful and found many applications. Easy separation and recyclability of the solvent upon reduction of pressure greatly decrease formation of chemical wastes and accelerates purification.<sup>64,67</sup>

### 2.2.6. Types of reactors

The commonly used laboratory scale flow reactors can be divided into three groups: chips, coils and pack bed reactors, Figure 2.2-5. While the first two, i.e. chip and coil based reactors, are usually implemented for processes exclusively involving fluids and the main difference between them is the scale of operation, packed-bed reactors are the best suited for reactions employing heterogeneous catalysts.

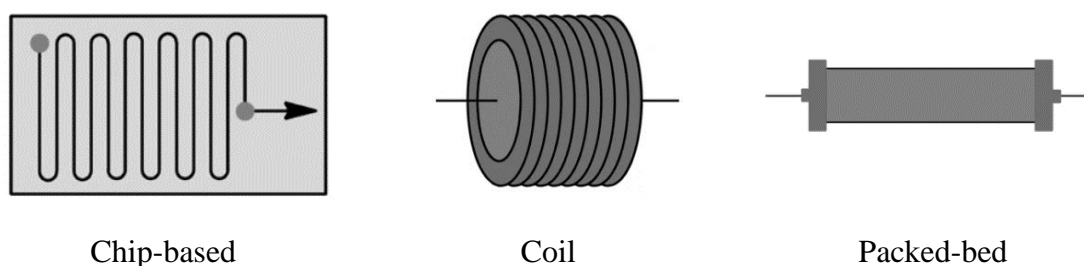


Figure 2.2-5. Commonly used types of flow reactors.

The chip-based units are characterised by the smallest width and depth dimensions in the range of micro or even nanometers. An increased length scale leads to an increased surface-to-volume ratio up to  $10\,000\text{ m}^2\text{m}^{-3}$  or even  $50\,000\text{ m}^2\text{m}^{-3}$ .<sup>70,71</sup> Hence, mass and heat transfer are significantly enhanced. The mass transfer can be further increased by, easy to implement into designs, mixing sections. The chip-based reactors are usually manufactured from polymers, silicon, glass, ceramics or steel.<sup>70,71</sup> Despite their excellent mass and energy transfer, the microreactor based systems are subjects to rapid clogging especially in case of processes involving formation or handling of solids. An another drawback of the chip-based microreactors is their significant cost. The affordable realisations of microreactors made, for example, using the 3D printing technology are generally not chemically resistant. Thus, their use is very limited. Some work has been done on propylene-based 3D printed microreactors.<sup>104</sup> Despite a larger chemical resistance of polypropylene, they still cannot compete with silicon or glass based microreactors. Finally, owing to the width and depth dimensions in the range of micrometres, it may be challenging to scale-up the chip-based reactors. Long microchannels generate significant pressure-drops, thus are impractical. A possible solution is scaling-out. This means operation on a number of identical reactors in

parallel. Nevertheless, the scale-out strategy is challenging in realisation. Namely, it is problematic to provide a uniform distribution of flow rates across a number of reactors.<sup>71</sup>

The coil-based reactors are arguably the most affordable and the simplest. Reactor coils are usually made out of fluoropolymers (PTFE, PFA, FEP) or metals (steel, copper) with internal diameters (IDs) in the range of 1/32" to 1/4". While most of these materials is characterised by a high chemical resistance, their applications are limited by the temperature and pressure rating. The polymer-based coils are suitable for processes with temperatures below 150 °C and, depending on the thickness of the wall and the ID of the tube, pressures in the range of 5-20 bar(g). For more challenging conditions it is common to implement the metal based reactors. Stainless steel reactor coils are particularly popular amongst practitioners. For a long-term exposure to highly corrosive materials, Hastelloy is often used owing to its superior chemical resistance. The copper-based reactors found unique applications owing to their rather high chemical reactivity. They are employed not only as reactors but also as catalysts or heterogeneous precursors of catalysts or other reactants.<sup>105</sup> This aspect of the copper-tube-flow-reactors (CTFR) will be a subject of a separate chapter, Chapter 2.2.7. Similarly to the chip-based reactors, the tubular reactors are prone to clogging. Several techniques have been used to address this issue including treatment with ultrasounds that precludes formation of large agglomerates,<sup>106</sup> however, clogging remains the main disadvantage of the tubular reactors.

Processes involving heterogeneous catalysts or other heterogeneous reactants are usually conducted in the pack-bed reactors. The commercially available pre-packed catalyst columns are commonly applied, for example, to hydrogenation reactions.<sup>65</sup> This type of reactors, prevalent in industrial applications, is the method of choice for heterogeneous catalysis in flow. To the disadvantages of the pack-bed reactors, one can include the chromatographic effect, namely the difference in the residence time of different compounds that results from the bed-compound interactions.<sup>107</sup>

Another frequently used type of flow reactors is a miniature representation of a series of continuously stirred tank reactors (CSTRs). Commercially available systems produced, for example, by AMTech and Cambridge Reactor Design as well as systems reported by Jensen<sup>108</sup> and by Blacker<sup>109</sup> provide researchers with easy to use flow systems. To the main advantages of cascades of CSTRs one can include ability to handle solids as well as access to longer residence times.

### 2.2.7. Copper-tube flow reactors

While the majority of the flow chemistry technologies is characterised by an excellent chemical resistance, one type of reactors benefits from its chemical reactivity. Processes performed in the copper-tube flow reactors (CTFR) became an interesting alternative to the usually heterogeneous copper catalysed batch processes owing to the fact, that the reactor walls can serve as a convenient heterogeneous precursor for the copper-based catalysts. Thus, for such processes, there is no need for additional dosing of solid copper catalysts or using pack-bed reactors. Furthermore, the excellent thermal conductivity of copper allows rapid heating or cooling of the reactor.<sup>110</sup> Hence, CTFRs are suitable for high-temperature applications. A relatively large surface-area-to-volume allows operation at high catalyst concentrations. Thus, when comparing with inert reactors with Cu feeding, faster conversions over a short reactor length can be achieved. Despite the advantages of CTFRs that allow the reduction in the number of phases, CTFRs are criticised owing to the significant copper leaching from the reactors.<sup>105</sup>

CTFRs were successfully implemented to 1,3-dipolar cycloadditions, macrocyclisations, Sonogashira couplings, Ullman-type reactions and decarboxylations.<sup>105</sup> Recently Gemoets et al. implemented a CTFR in their modular flow design for the *meta*-selective C–H arylation of anilines.<sup>111</sup> The last step of the process involved an extraction of the leached copper using an aqueous solution of ammonia. This was necessary owing to a high copper concentration, up to 5000 ppm, in the spent reaction mixture.<sup>111</sup>

Besides classical CTFRs, copper based reactors are also frequently used as extended-channel length microfluidic electrolysis cells.<sup>101,103</sup> In those, metallic copper is used as a material for a cathode or an anode or both.

### 2.2.8. Integrated processes

Syntheses of complex chemical compounds rarely involve only one reaction. Typically, a total synthesis or functionalisation of precursor molecules require a multi-step approach including, besides core processes, for example, an installation and removal of protecting groups, solvent changes and isolations of intermediates. The traditional approach to the multi-step synthesis proceeds through a set of discrete operations done iteratively, Figure 2.2-6a. Such approach promotes the use of auxiliary processes, such as solvent changes or

purifications of intermediates, thus, results in a large number of steps that, ideally, should be removed. Alternatively, multi-step chemical processes can be performed in an integrated fashion, where the number of secondary steps, such as isolations, is reduced to a minimum, Figure 2.2-6b. The integrated approach, inspired by multi-step biosynthetic pathways prevalent in nature,<sup>112</sup> is often being conveniently performed as a continuous flow process merging multiple synthetic steps into a single uninterrupted chain.

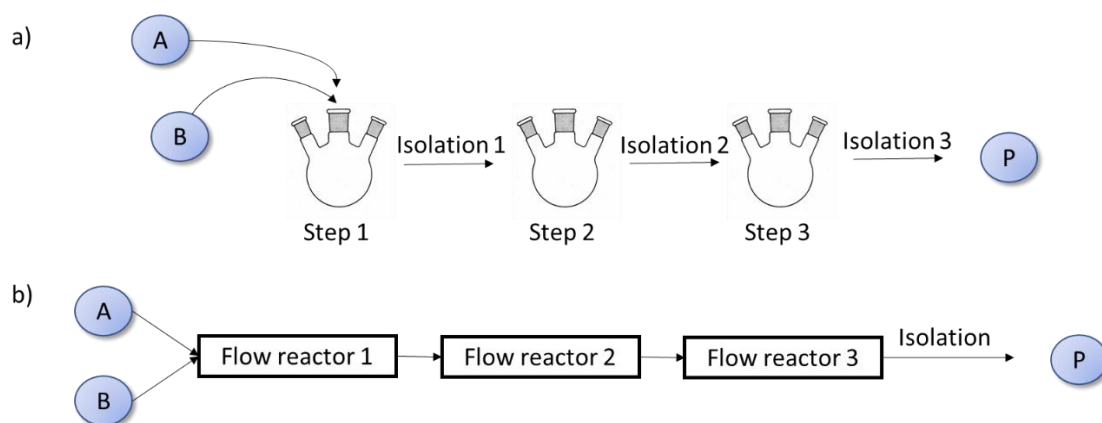


Figure 2.2-6. Multi-step synthesis approaches. Based on ref. 113.

The benefits of telescoped, multi-step syntheses of complex molecules have been demonstrated by, for instance, Tsubogo et al. who developed a multistep continuous-flow synthesis of (R)- and (S)-rolipram.<sup>114</sup> The gram scale-synthesis of the APIs has been performed using exclusively heterogeneous catalysts employing pack-bed reactors. A diligent selection of chemical transformations led to minimisation of solvent changes and reduced formation of by-products. This allowed circumventing the need to isolate intermediates.

Adamo et al. exploited the modularity of flow chemistry to perform an on-demand continuous-flow production of pharmaceuticals in a compact, reconfigurable system.<sup>115</sup> Combining downstream operations, core-processes, as well as upstream steps and enclosing them in a “fridge-size” container, allowed a drastic reduction of the footprint of the setup. The system was tested on several APIs including lidocaine hydrochloride, diazepam and diphenhydramine hydrochloride.

The modularity of flow chemistry can be combined with advantages of batch chemistry and used in a hybrid approach. Implementation of batch and flow technologies in the same process enables engineers to benefit from advantages of these two approaches. Fitzpatrick and Ley demonstrated the utility of this approach in the synthesis of 5-methyl-4-propylthiophene-2-carboxylic acid.<sup>116</sup> Other reports of merging flow and batch processing include formation of aryl fluorides<sup>117</sup>, sequential C–C bond formation<sup>118</sup>, preparation of homoallylic alcohols<sup>119</sup> and cyclopropanation using *in-situ* generated diazo compounds.<sup>120</sup>

Besides the above-mentioned advantages of continuous flow integrated processes, such technology provides researchers with a tool to handle unstable or acutely toxic reagents. For example, the Yoshida group utilised telescoped flow processes to handle organolithium compounds.<sup>69</sup> A similar approach was applied to the *in-situ* generation of other unstable organometallic compounds such as Grignard reagents. Furthermore, *in-situ* generation of, among others, diazomethane, phosgene, azides and cyanides has been reported.<sup>66</sup>

An interesting approach to the multi-step organic synthesis using solid-supported reagents has been developed by the Ley group.<sup>121,122</sup> Various reactants, immobilised on solid supports, can be conveniently used as a molecule assembly technology. If properly designed, such approach should yield a virtually non-existent generation of by-products. Thus purification steps can be omitted.

An integration of discrete steps of synthesis of complex molecules into one continuous process can bring a significant added value in terms of economy, safety and time-scale of the process. Additionally, such technique allows *in-situ* generation of unstable or hazardous reagents. Despite all of this, still much work needs to be done to extend the utility of the integrated flow processes. Efficient techniques of handling solids, continuous purification techniques as well as better control over dispersion need to be developed. Detailed reviews on integrated continuous-flow processes can be found in the literature.<sup>68,70,113,121–124</sup>

### 2.2.9. Scaling of continuous processes

Scaling of chemical batch processes is a nontrivial task that often requires extensive trial-and-error tests. Several commonly used scale-up criteria for the geometrically similar reactors have been developed and used across the industry and academia, Table 2.2-1. These criteria allow maintaining a particular feature of the reaction system constant

however, they are mutually exclusive, Table 2.2-2. Additionally, scaling of a reaction in batch often reveals scale-dependant phenomena that do not play a significant role in the smaller-scale experiments, such as formation of by-products as an effect of differences in mass or energy transfer. Owing to this, scale-up of batch reactors requires significant practical experience as well as thorough knowledge of the process and the influences of the process parameters on the process outcome.

Table 2.2-1. Examples of scale-up criteria for stirred tank reactors. Based on ref. 88.

Criterion name	Example of processes	Physical meaning
Constant energy dissipation rate	Solid distribution;	$\frac{P}{V_L} = \text{const}$
Constant mixing time	Fast reactions	$N = \text{const}$
Constant impeller tip speed	Liquid blending	$U_{\text{imp}} = \text{const}$
Constant Reynolds number	Reactions that require good heat transfer	$Re = \text{const}$
Constant multiphase mass transfer coefficient	Gas-liquid or liquid-liquid reactions	$k_{LA} = \text{const}$

$P$  – power utilised for mixing,  $W$ ;  $V_L$  – volume of the reaction media,  $m^3$ ;  $N$  – frequency of impeller rotation  $s^{-1}$ ;  $U_{\text{imp}}$  – speed of impeller tip,  $ms^{-1}$ ;  $k_{LA}$  – volumetric mass transfer coefficient  $s^{-1}$ .

Since the focus of the thesis is directed onto continuous processes, scaling of batch reactors is outside the scope of the literature review. Detailed literature on scaling-up of batch processes is available.<sup>80,125–128</sup>

Table 2.2-2. Relative changes of reactors parameters in the scale-up procedure. Based on ref. 88.

Parameter change Criterion	$\frac{P_2}{P_1}$	$\frac{\left(\frac{P}{\bar{V}}\right)_2}{\left(\frac{P}{\bar{V}}\right)_1}$	$\frac{N_2}{N_1}$	$\frac{U_{imp2}}{U_{imp1}}$	$\frac{Re_2}{Re_1}$
$\frac{P}{V_L} = \text{const}$	1000	1	0.215	21.5	0.0215
$N = \text{const}$	100000	100	1	10	100
$U_{imp} = \text{const}$	100	0.1	0.1	1	10
$Re = \text{const}$	0.1	0.0001	0.01	0.1	1

Scaling of continuous processes is performed differently. The easiest way to produce larger amounts of a product is longer operational time, owing to the fact that the amount of product is often a linear function of time. Other strategies involve increasing the length or/and the diameter of the flow reactor or scaling-out.

Using longer operational times is the simplest and the safest strategy since parameters of the process remain unchanged. Hence, it is unlikely to observe any, previously unknown, scale-dependant phenomena when applying this approach. Nevertheless, the longer operational times are often impractical and do not allow a significant increase in the scale of the process.

Increasing dimensions of the reactor is arguably the most commonly used strategy. Yet it comes with significant disadvantages. Increasing the length of the flow reactor, whether pack-bed or tubular, while maintaining the diameter unchanged, increases the pressure drop in the system,  $\Delta p$  (Pa), ( 45 ).

$$\Delta p = \lambda \frac{L}{D} \frac{\rho u^2}{2} \quad ( 45 )$$

where  $\lambda$  is the Darcy friction factor,  $L$  (m) is the length of the reactor,  $D$  (m) is the hydraulic diameter of the reactor,  $u$  ( $\text{m s}^{-1}$ ) is the mean velocity of the flow.

Thus, the pressure drop is directly proportional to the reactor length. Large values of the pressure drop require higher pumping costs and result in much higher energy consumption.

On the other hand, increasing the horizontal dimensions of the system, namely the diameter of the reactor, significantly influences mixing and heat transfer performances of the reactor system. The larger diameter results in a longer diffusion time. Thus slower mixing, and larger discrepancies from the ideal plug-flow regime. Hence, at scale, the reaction system may behave significantly differently compared with the small-scale realisation.

Another approach to increasing the scale of the continuous processes is scale-out. This means numbering up of identical reactors. Such strategy allows maintaining dimensions of the individual reactors equal to the small-scale implementations. Thus, no unpredicted scale-dependant phenomena should be discovered. Nevertheless, the scale-out requires a complex flow distribution and elaborate reaction monitoring methods.<sup>72,129</sup> A detailed analysis of flow distribution in different microreactor scale-out geometries can be found in ref. 130.

Generally, design and scaling of chemical processes either in batch or in flow requires extensive knowledge of the reaction. When all physical and chemical phenomena underpinning the behaviour of the reaction system are known, and ideally quantified, the scale-up procedure can be safely performed. However, when the understanding of the process is limited, the scale-up of batch processes requires extensive trial and error procedure. The flow processes, even when the knowledge of the reaction is limited, should be easier to scale owing to the fact that the changes of process parameters, such as, for example, mixing and temperature profile, are significantly lower than in batch. Nevertheless, before a scale-up of a process is performed, one should gain as much information on the process as possible.

Furthermore, flow chemistry is a convenient tool for scaling-down of chemical processes what may be valuable at the stage of reaction discovery thanks to lower consumption of reagents.

### 2.2.10. Summary

The chapter provided an overview of advantages of flow chemistry over classical batch synthesis. The benefits of the increased surface area to volume ratio such as accelerated mixing and superior energy transfer combined with safety aspects, scalability and possibilities of running integrated processes in flow resulted in an increased interest in the flow technology. Furthermore, flow reactors can bring a significant added value to the automation of organic chemistry.

However, despite its advantages, flow chemistry still cannot compete with flexibility and versatility of batch reactors, that can serve as not only reaction vessels, but can also accommodate work-up steps such as, among others, extractions. Furthermore, the same round-bottom flask can be used for isolation of final compounds via crystallisation or even distillation. Flow reactors are commonly designed for only one specific application. Thus, in an academic environment, the CAPEX is usually much higher. Additionally, issues with handling of solids and some aspects of scaling-up, especially for reactions characterised by long residence times, limit the scope of applications of the flow chemistry. Finally, start-up and shut-down procedures for continuous flow processes can be complex, and much attention must be paid to their development.

Keeping in mind advantages and disadvantages of flow chemistry, it is important to realise, that this technology is only one of the tools of reaction engineering. A diligent choice of the appropriate technology, whether continuous or batch, should be made based on the available process knowledge. Tools and strategies for developing of process knowledge are discussed in detail in Chapter 2.1.

Several flow-charts has been developed to aid researchers in the choice of the appropriate technology for the investigated process.<sup>63,71,97</sup> Based on these, and personal experience, an extended decision-tree is suggested in Figure 2.2-7.

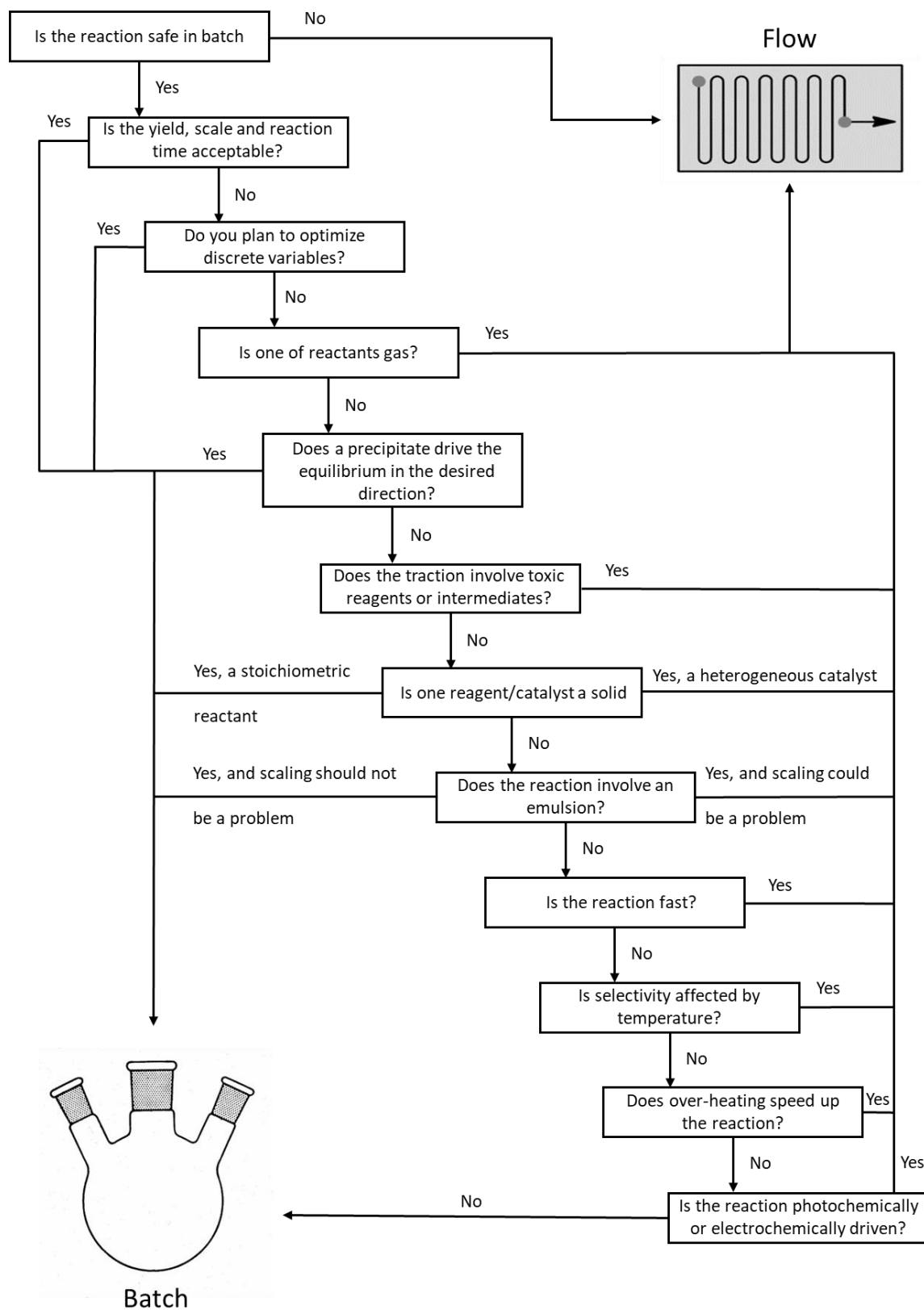


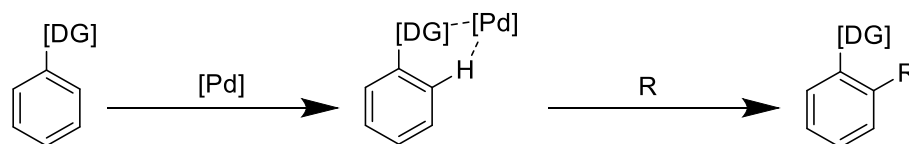
Figure 2.2-7. Decision diagram for continuous processing. Based on ref. 71.

### 2.3. Palladium catalysed C–H activation reactions

Over the last several decades, strategies for the synthesis of organic compounds have undergone a tremendous change. Inefficient and unsustainable non-catalytic transformations found numerous alternatives in environmentally and economically superior catalytic transformations. Owing to the significant advantages of catalytic transformations, they found a plethora of applications in many aspects of organic chemistry in both industry and academia. However, a catalytic functionalisation often requires a pre-functionalisation of the substrate via replacement of unreactive C–H bonds with carbon-halogen bonds or introduction of other suitable leaving groups. This results in significantly longer synthetic routes and an increase in cost. Nevertheless, the functionalisation of molecules via, for example, C–O, C–N or C–C bond formation using catalytic processes based on C–X bond functionalisations, such as Suzuki–Miyaura coupling, Buchwald–Hartwig amination or Sonogoshira coupling, found numerous applications in industrial syntheses of fine chemicals and pharmaceuticals.<sup>131</sup> However, circumventing the problem of the pre-functionalisation of the substrates would yield shorter, greener and more industrially appealing routes. Yet, it cannot be achieved without an efficient strategy for a selective functionalisation of one of the most unreactive bonds, the carbon-hydrogen bond.

First reports of non-catalytic functionalisations of C–H bonds via insertion of transition metals into the C–H bonds resulting in C–[TM] bond being available for further functionalisation were published several decades ago.<sup>132,133</sup> Within the last decade, a significant number of catalytic C–H functionalisations utilizing transition metals such as palladium, platinum, ruthenium, rhodium, copper, nickel or even iron was described in the literature and gained an unprecedented attention within the scientific community.<sup>134–138</sup> Palladium salts, in particular, have enjoyed a great deal of success in effecting C–H activation reactions, especially for reactions under milder conditions.

However, to be able to functionalize the molecules selectively, the strategies for differentiating between numerous C–H bonds are required. The most commonly used and, arguably, the most successful strategy proved to be the functional-group-directed C–H activation, Scheme 2.3-1. Lewis basic heteroatoms within the directing motif, based on their coordinating ability, can attract transition metal catalysts and direct the metal onto the selected C–H bond being adjacent to the heteroatom.



*Scheme 2.3-1. Schematic representation of the directing group effect on a palladium catalysed C–H bond activation.*

Other strategies include, among others, steric modifications of the metal centre of the catalyst allowing it to access only selected C–H bonds.<sup>139</sup> However, this strategy requires a precise design of the catalyst collectively with its ligands.

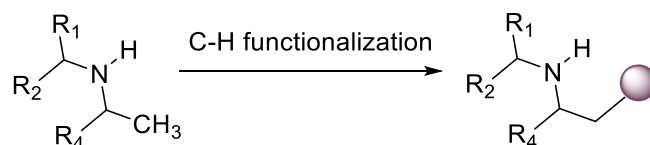
The following chapter focuses on the functional-group-directed C(sp<sup>3</sup>)–H activation of secondary aliphatic amines and C–H carbonylation of the same group of substrates, owing to the fact, that these families of reactions were of the particular interest in the present work.

### 2.3.1. C(sp<sup>3</sup>)–H activation of secondary aliphatic amines

Although many advances have been made in the field of aromatic or aliphatic C(sp<sup>2</sup>)–H bonds activation, functionalisation of the less reactive C(sp<sup>3</sup>)–H bonds in aliphatic molecules still proves to be a great challenge.<sup>140</sup> Due to a lower reactivity of C(sp<sup>3</sup>)–H bonds, their activation is often possible only when a polar functional group, such as a carboxylic acid group,<sup>141,142</sup> a heteroarene<sup>143</sup> or a hydroxyl functionality,<sup>144</sup> is adjacent to the C(sp<sup>3</sup>)–H bond. Despite these advances in C(sp<sup>3</sup>)–H activation, the unprotected aliphatic amine scaffold, being a common functional group prevalent in biologically active molecules and fine chemical products, still proves to be challenging in enabling C–H activation, Scheme 2.3-2. This may be due to several obstacles that can impede the reactivity.

Firstly and most importantly, a high affinity of transition metals such as palladium to the unprotected aliphatic amine scaffold results in formation of stable bis(amine)-Pd complexes. These complexes can be thermodynamically too stable under operating conditions to allow a release of mono(amine)-Pd complexes that could undergo a C–H activation, thus their presence can preclude reactions. Additionally, amine substrates are susceptible to the  $\beta$ -hydride elimination pathway leading towards an oxidative degradation of the substrate and reduction of the catalyst that, upon precipitation and aggregation, forms

“palladium black”, an inactive form of Pd<sup>0</sup> particles. Furthermore, other polar functional groups can compete with the amine motif for coordination of the palladium species. This may lead to a decreased selectivity. To overcome these obstacles, the nucleophilicity of the nitrogen atom must be adjusted using strongly electron withdrawing groups<sup>145</sup> or directing auxiliaries.<sup>146,147</sup> Alternatively, an intensified steric environment can be created in the proximity to the amine scaffold.<sup>148,149</sup>



*Scheme 2.3-2. C(sp<sup>3</sup>)-H functionalisation of a secondary amine.*

Notwithstanding the demonstrated success of synthetic strategies based in adjusting the nucleophilicity of the nitrogen atom, the structural and functional modifications incorporated into amine substrates that are required to enable the C–H activation can, for some cases, reduce the applicability of the amine products. In the present work, the investigated C–H activation processes employ an alternative strategy, namely the steric enabled C(sp<sup>3</sup>)-H bond activation, thus in the present work attention is paid exclusively to this strategy.

The literature on C–H activation of aliphatic amines is very limited. Several reports were made by the Gaunt group where they reported a C–N bond formation leading towards aziridines,<sup>148,150</sup> a C–H arylation of aliphatic amines,<sup>151</sup> a cobalt-catalysed C–H carbonylative cyclisation of aliphatic amines<sup>152</sup> and a ligand-assisted palladium-catalysed C–H alkenylation of aliphatic amines for the synthesis of functionalized pyrrolidines.<sup>153</sup> Owing to not so many scientific reports from this field, there is still very little understanding of the mechanistic and kinetic background of these processes.

### 2.3.2. C–H oxidative carbonylation

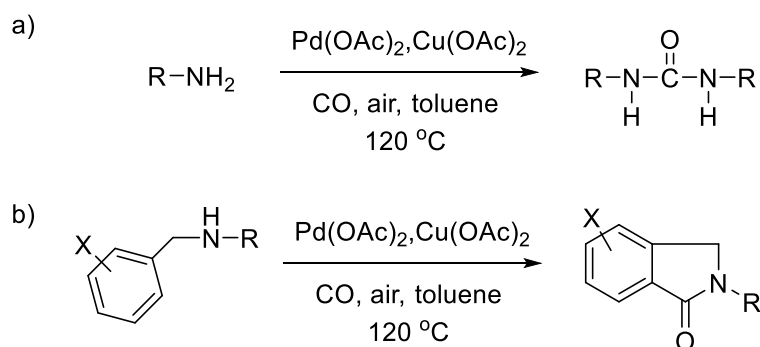
Carbon monoxide can be incorporated into an organic molecule via several strategies: substitutive carbonylation – a process of substitution of a functional group with a CO-Y moiety, Scheme 2.3-3a, additive carbonylation – a process of an addition of a form of CO



However, the classical carbonylation processes often require harsh conditions, and their starting materials, R–X electrophiles, must first be prepared from the corresponding R–H nucleophiles,<sup>157</sup> which severely lowers the step and the atom economy of the whole process. On the other hand, the oxidative carbonylations offer direct functionalisation of R–H bonds, eliminating the need to generate the activated substrate.<sup>162–164</sup> Despite this obvious advantage, citing Ullmann's Encyclopaedia of Industrial Chemistry, “An industrial application of the oxidative carbonylation is not yet in sight”.<sup>165</sup> This is due to a notorious complexity and inefficiency of oxidative carbonylations: the reactions are multiphase, involve dynamic changes of physicochemical properties of the system during the reaction, and generally are poorly mechanistically understood. This makes predicting the conditions for the scale-up highly improbable and the process development requires extensive trial-and-error approach. Similar obstacles preclude discovery of new processes. Nevertheless, due to a great attention paid to development of these reactions, a significant number of oxidative carbonylations of aromatic and unsaturated aliphatic compounds has been reported.<sup>154,162–164</sup> Yet, a direct functionalisation of alkanes through the C–H oxidative carbonylation remains challenging due to the much lower reactivity of aliphatic C–H bonds. Owing to this, very few reports of such processes can be found in the literature. Due to the focus of the present work being the oxidative C–H activation of aliphatic amines the attention will be directed to this specific type of substrates.

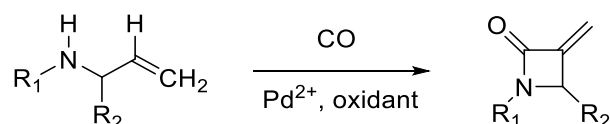
C–H oxidative carbonylation of aliphatic amines is subject to the same limitations as C–H activation processes of aliphatic amines listed in the previous chapter. Furthermore, owing to the heterogeneity of the carbonylation reactions, the physicochemical behaviour of such systems is an additional complication. Moreover, the acute toxicity of CO raises significant safety concerns and requires special safety protocols. Some attention has been paid to *in situ* generation of CO,<sup>166,167</sup> however much work needs to be done to design a robust, cost-efficient, sustainable and scalable procedure that could potentially compete with the classical CO delivery from gas cylinders. Additionally, currently generating elevated pressures of CO using CO precursors is not feasible.

An important report of the oxidative carbonylation of amines is the Orito carbonylation<sup>168</sup> giving access to ureas from primary amines and CO, Scheme 2.3-4a, as well as benzolactams by aromatic carbonylation of secondary amines, Scheme 2.3-4b.



Scheme 2.3-4. Examples of Orito carbonylation.

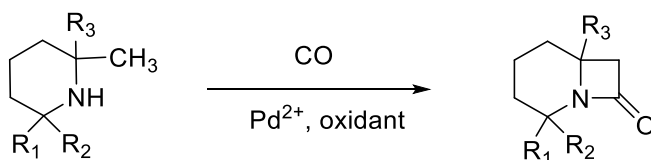
Other significant reports include formation of nitrogen-containing heterocycles such as  $\beta$ - or  $\gamma$ -lactams. For example, Lui et al. reported a palladium-catalysed oxidative carbonylation of *N*-allyl amines for the synthesis of  $\beta$ -lactams, Scheme 2.3-5.<sup>169</sup>



Scheme 2.3-5. Palladium-catalyzed oxidative carbonylation of *N*-allyl amines for the synthesis of  $\beta$ -lactams.

Further reports of nitrogen-containing heterocycles are available in the literature. A comprehensive review on this field was published by Beller.<sup>164</sup>

Moreover, the Gaunt group recently reported a palladium-catalysed C–H carbonylation of sterically hindered aliphatic amines, Scheme 2.3-6.<sup>148</sup>



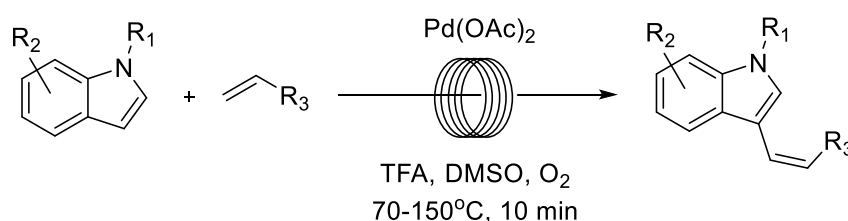
Scheme 2.3-6. Palladium-catalysed C–H carbonylation of sterically hindered aliphatic amines.

### 2.3.3. C–H activation in flow

Due to a relatively small number of reported C–H activation reactions, the development of continuous processes based on this methodology is in its infancy. Hence, only a handful of processes have been published. The currently observed significant interest in the field of continuous C–H activation processes should yield a larger body of literature on this topic in the near future.

Process design based on the available C–H activation reactions is challenging owing to the inherent complexity of the reaction systems. With an often limited mechanistic understanding of new reactions, it is rarely straightforward to determine the best reactor configuration or predict their behaviour at scale, which can make the design of an optimal process difficult, regardless of whether it is a batch, a semi-batch, or a continuous process.

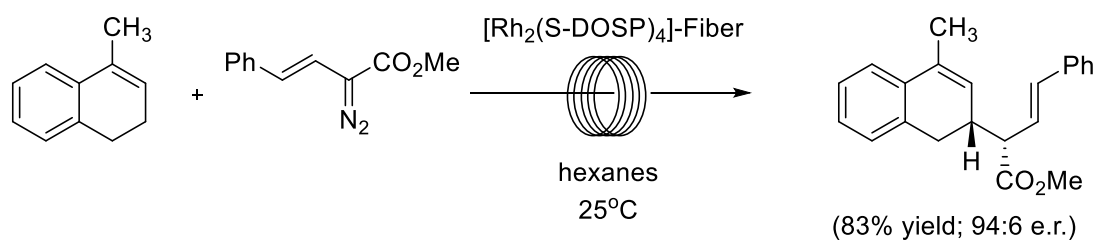
Arguably, the first report of a continuous process for a C–H activation reaction was made by Gemoets et al. for the selective C3-olefination of indoles, Scheme 2.3-7.<sup>170</sup>



*Scheme 2.3-7. C3-olefination of indoles in flow. TFA: trifluoroacetic acid, DMSO: dimethyl sulfoxide.*

Operation in the slug-flow regime enhanced the mass transfer between the gas and the liquid phase. Thus, significantly accelerated the reaction compared with the initial report of the batch process; 4 h in batch vs 10 min in flow. The process was tested on ten olefins, using the same indole scaffold, and five different indoles, using ethyl acrylate as the olefin. All tested examples resulted in relatively high yields between 27 and 92%. For some substrates, a longer residence time, up to 20 min, was required.

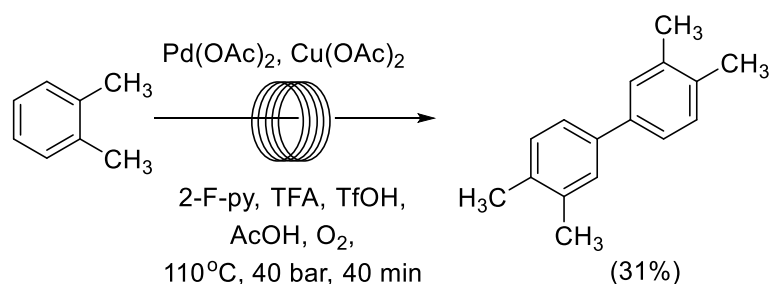
Moschetta et al. performed a sequential combined C–H functionalisation/Cope rearrangement reaction in a developed hollow fiber reactor, Scheme 2.3-8.<sup>171</sup>



*Scheme 2.3-8. C–H functionalisation/Cope rearrangement reaction in a hollow fibre reactor.*

The hollow fibre reactor with an oxide-grafted organometallic rhodium catalyst performed slightly worse compared with the results obtained using a classical batch protocol with a homogeneous catalyst.<sup>171</sup> However, high TONs exceeding 1000 allow minimisation of the amount of the catalyst used, thus less precious metals is used in the synthesis.

Erdmann et al. reported a continuous palladium-catalysed aerobic oxidative coupling of *o*-xylene, Scheme 2.3-9.<sup>172</sup>

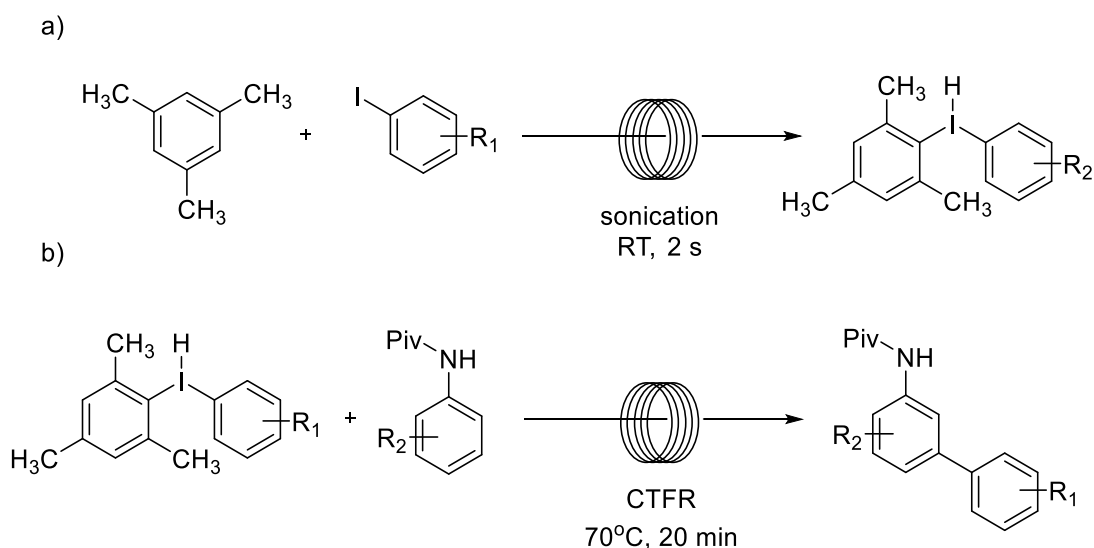


*Scheme 2.3-9. Continuous palladium-catalysed aerobic oxidative coupling of o-xylene. TfOH is trifluoromethyl sulfonic acid, 2-F-py is 2-fluoro-pyridine.*

Operation under elevated temperature and pressure allowed a significant reduction in the reaction time from 17 h down to 40 min. The yield of the flow process was significantly higher than the one of the corresponding batch process, 8% in batch vs 31% in flow. However, these improvements were achieved at the cost of 50 times larger catalyst loading, 5 mol% in flow vs 0.1 mol% in batch. The selectivity was also lower, 60% in flow against 88% in batch.

Recently, Gemoets described a modular continuous-flow synthesis of meta-arylated anilines using diaryliodonium salts.<sup>111</sup> The first step of the process involves synthesis of diaryliodonium salts at remarkably short residence times, Scheme 2.3-10a. Secondly, the

formed diaryliodonium salts are reacted with the corresponding anilines to form meta-arylated anilines, Scheme 2.3-10b. Unlike the batch process developed by Phipps and Gaunt,<sup>173</sup> the developed flow protocol did not require dosing of a copper-based catalyst, but the catalytically active copper species were *in situ* generated from the copper-tube flow reactor (CTFR). Remarkably, the generated products did not require any purification.



Scheme 2.3-10. Meta-selective C-H arylation of anilines. Piv denotes pivalate.

These are, to the author's best knowledge, all reported examples of C-H activation reactions performed in flow. Notably, to-date there are no examples of continuous C(sp<sup>3</sup>)-H activation of aliphatic substrates and only one example of aliphatic C-H activation performed in a continuous setup.<sup>171</sup>

### 2.3.4. Carbonylation in flow

Similarly to C-H activation reactions, carbonylation reactions in flow are at the very early stage of development. Only several reports of the flow processes for classical carbonylations were published and, to the author's best knowledge, no examples of oxidative carbonylations performed in continuous-flow systems exist in the literature. Nevertheless, the potential added value to the process generated by performing such reactions in flow is significant. The benefits of the continuous processes against the batch processing in case of the carbonylation reactions include an easier access to elevated

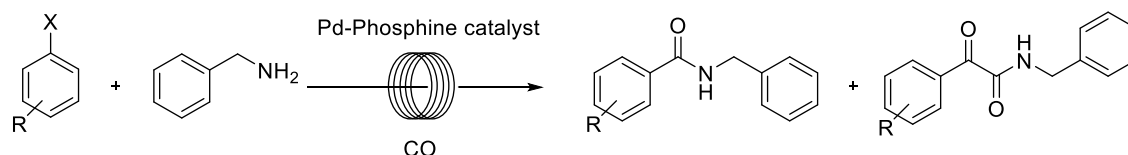
pressures of CO and elevated temperatures that are often required to increase the efficiency of the carbonylation processes. Furthermore, operating in flow minimises the reactor headspace, and hence, lowers the inventory of CO in the reaction system. Additionally, the continuous flow processes are arguably much easier to control and more reproducible.

The lack of examples of oxidative carbonylations performed in continuous flow setups is likely due to the heterogeneity of the reaction mixture, namely the presence of the virtually insoluble copper or silver-based oxidants, as well as CO in the gas phase. Generally, there are very few examples of multiphase catalytic flow processes that include a continuous liquid phase, a dispersed gas phase and a dispersed solid phases, as the majority of studies were performed with a gas-liquid or a liquid-liquid flow through a stationary solid phase.<sup>174</sup> However, some work on a co-flow of dispersed solids in a gas-liquid bi-phasic main flow was reported.<sup>175</sup> Nevertheless, such systems are arguably difficult to control and may result in reproducibility issues. Thus, may be problematic at scale.

A prerequisite to designing of a flow setup for a carbonylation reaction is an ability to introduce gaseous reactants, mostly CO, to the reactor. There are generally two ways to achieve this. The classical operation in a multi-phase flow in either the annular or the slug flow regime proved to be the most versatile for the tubular flow reactors and are the most commonly applied techniques.<sup>65</sup> They provide an excellent mass transfer between the gas and the liquid phase and are easy to implement. The other possibility is a membrane contactor system. At the laboratory scale, Teflon AF2400 is frequently employed in the so-called Tube-in-Tube reactors for organic syntheses.<sup>176</sup> Teflon AF2400 tubing, owing to its excellent gas permeability and chemical resistance, is suitable for corrosive gas-liquid systems. However, the membrane is subject to a rapid clogging, which severely limits the applications of the Tube-in-Tube reactors.<sup>65</sup> Nevertheless, the membrane systems based on Teflon AF2400 have found numerous applications in research laboratories. Ready-to-use, commercial reactor systems are now available, for example, the Gastropod Gas-Reaction Module from Cambridge Reactor Design.

One of the first examples of carbonylation reaction performed in a continuous flow was the synthesis of *N*-benzylamides via a carbonylative cross-coupling reaction.<sup>177</sup> As the by-product of the over-carbonylation,  $\alpha$ -ketoamide was obtained. This was contrary to the corresponding batch processes, where only products of the single carbonylation were observed, Scheme 2.3-11.<sup>177</sup> Moderate yields of the process in the range of 12-58% were

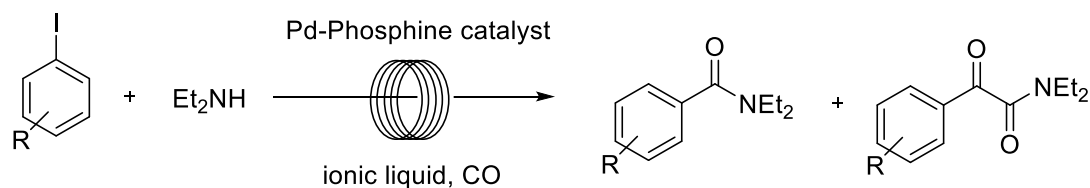
a slight improvement compared with the corresponding batch process (11-25%). Operation in the annular flow regime provided superior, compared with the corresponding batch process, gas-liquid mass transfer.



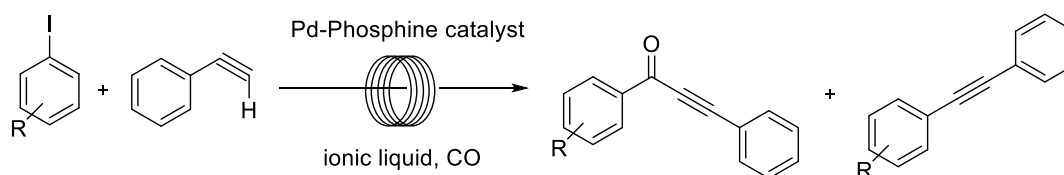
*Scheme 2.3-11. Synthesis of N-benzylamides and  $\alpha$ -ketoamide via carbonylative cross-coupling.*

The same group reported an effective method for a continuous flow carbonylation reaction using  $^{11}\text{C}$  carbon monoxide.<sup>178</sup> Employing the same reaction system, they obtained good yields (23-99%) and radiochemical purities above 70%.

Rahman et al. reported a Pd-catalyzed amidation of aryl iodides with diethylamine and carbonylative Sonogashira cross-coupling, Scheme 2.3-12 and Scheme 2.3-13.<sup>179</sup> Interestingly; the reactions were performed in the ionic liquid ( $[\text{MBlIn}]\text{PF}_6$ ) in the slug flow regime. Again, the results were a slight improvement against the corresponding batch processes.<sup>179</sup> Similarly to the work of Miller et al.,<sup>177</sup> they also observed both the single and the double carbonylation products.

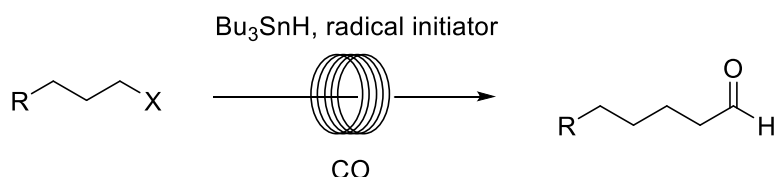


*Scheme 2.3-12. Palladium-catalyzed single/double carbonylation of aryl iodides.*



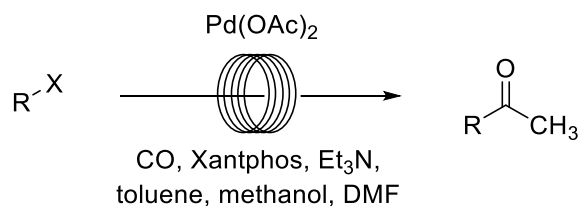
*Scheme 2.3-13. Palladium-catalyzed carbonylative Sonogashira cross-coupling.*

The Ryu group continued their research on the continuous carbonylative reactions and reported a radical carbonylation of aliphatic halides, Scheme 2.3-14.<sup>180</sup> The reaction required high pressures in the range of 20-85 atm; however, was characterised by short residence times, 12 min. The process resulted in moderate to high yields.



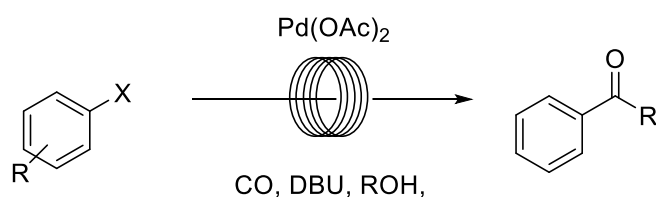
*Scheme 2.3-14. Radical carbonylation of aliphatic halides.*

The work on carbonylation reactions in flow systems using the membrane contactors was pioneered by the Ley group. Koos et al. reported a continuous flow process for the palladium methoxycarbonylation of aryl heteroaromatic and vinyl iodides and an aryl bromide, Scheme 2.3-15.<sup>176</sup> Most of the 15 tested substrates resulted in moderate-to-good yields. Koos et al. employed, the so-called conventional Tube-in-Tube reactor, where the inner tube is filled with the liquid phase, and the gas reactants diffuse from the outer tube to the liquid phase. Such system possesses a significant drawback, the outer tube filled with the gaseous reactant is characterised by a small heat transfer coefficient. Thus, heating of the reaction mixture is highly inefficient. Koos et al., in their work, used the membrane system to pre-saturate the mixture of solvents with CO. Later, the saturated mixture of solvents was mixed with the starting material and the catalyst. Finally, the complete reaction mixture was passed into the heated reaction coils. Such approach, namely pre-saturation of the solvent with the gaseous reactant, results in a larger footprint of the reaction system. Additionally, the amount of dissolved gas may be insufficient to operate at high concentrations of the starting material. Thus, may result in the excessive generation of solvent waste.



*Scheme 2.3-15. Palladium catalysed methoxycarbonylation of aryl, heteroaromatic and vinyl iodides and an aryl bromide.*

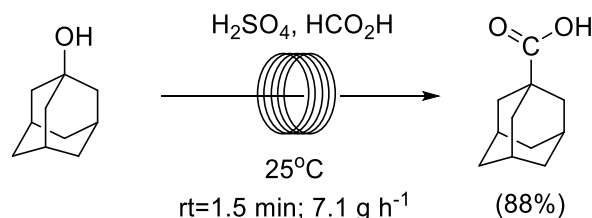
A similar reaction system was reported by Mercadante and Leadbeater.<sup>181</sup> They presented an approach to the continuous-flow alkoxy carbonylation reactions of aryl iodides, Scheme 2.3-16, using the reverse configuration of the membrane system - liquid phase in the outer tubing. All eight reported examples resulted in high-to-excellent yields, 91-99%, measured using <sup>1</sup>H NMR spectroscopy. The reverse configuration of the membrane system allowed simultaneous heating of the liquid phase and continuous delivery of CO. This resulted in a simplification of the reaction system and allowed operation under constant concentration of CO, being equal to the solubility of CO under operational conditions, providing the flux of CO is larger than the rate of the reaction. Interestingly, when the same group compared the results of the same alkoxy carbonylation reactions performed in the membrane system and the slug flow biphasic system they obtained the significantly better results using the Tube-in-Tube reactor.<sup>182</sup>



*Scheme 2.3-16. Palladium-catalysed alkoxy carbonylation of aryl iodides.*

The Ryu group devised an interesting approach to combining advantages of the membrane systems and the *in-situ* generated CO from formic acid and concentrated sulfuric acid. They demonstrated the utility of the developed setup on Heck aminocarbonylation.<sup>167</sup> A similar method was established by Fukuyama et al., however, instead of using the membrane system, they decided to generate CO in the same stream where CO was consumed via Koch-Haaf reaction of adamantanol, Scheme 2.3-17.<sup>183</sup> The designed protocol was

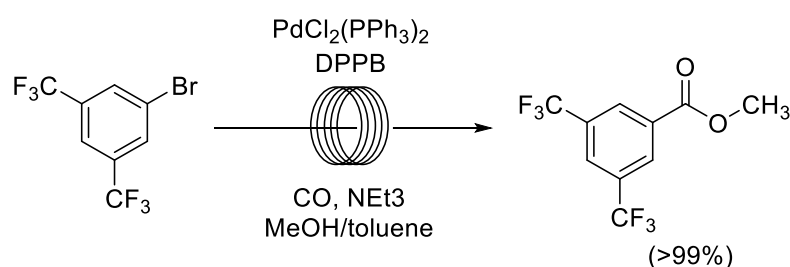
successfully scaled-up resulting in the multigram-scale synthesis of 1-adamantane carboxylic acid, 7.1 g per hour, 88% isolated yield.



*Scheme 2.3-17. Koch–Haaf reaction of adamantanols.*

Recently, the Ley group reported an extension of the utility of the developed membrane system by aminocarbonylation, alkoxy carbonylation, hydroxycarbonylation, formation of lactams and one example of a synthesis of a lactone. Interestingly, in the hydrazine-promoted amino-carbonylation process, the authors employed two membrane systems to introduce two separate gaseous reactants, CO and dimethylamine.<sup>184</sup>

Akinaga et al. reported a kilogram scale Heck carbonylation, Scheme 2.3-18. Using an almost stoichiometric amount of carbon monoxide in the slug flow regime they achieved the nearly quantitative yield, >99%, at the moderate residence time of 55 min. Using a 900 ml stainless-steel tubular reactor with a flow rate of 7.3 ml min<sup>-1</sup> resulted in production of 1.86 kg of the product per 24 hours.<sup>185</sup>



*Scheme 2.3-18. Heck carbonylation of 1-bromo-3,4-bis(trifluoromethyl)benzene.*

A number of other continuous carbonylation processes were reported, and due to a significant interest in the field, new reactions are being regularly published. Comprehensive reviews on continuous carbonylation processes can be found in the literature.<sup>65,71,186</sup>

Notably, to the author's best knowledge, there are no examples of oxidative carbonylations performed in a continuous flow system. All examples presented in this chapter relate to classical, reductive carbonylations.

## 2.4. Life-cycle assessment

Pollution prevention was, and still is, a significant area of interest in the chemical engineering community. The concept of green chemistry, formulated as a set of twelve principles nearly thirty years ago,<sup>187</sup> gained a significant interest from both industry and academia. Applying the twelve principles outlined by Anastas and Warner as design rules for novel processes can help to achieve the intentional goal of sustainability.

Prevention	It is better to prevent waste than to treat or clean up waste after it has been created.
Atom economy	Synthetic methods should be designed to maximise the incorporation of all materials used in the process into the final product.
Less hazardous chemical syntheses	Wherever practicable, synthetic methods should be designed to use and generate substances that possess little or no toxicity to human health and the environment.
Designing safer chemicals	Chemical products should be designed to affect their desired function while minimising their toxicity.
Safer solvents and auxiliaries	The use of auxiliary substances (e.g., solvents, separation agents, etc.) should be made unnecessary wherever possible and innocuous when used.
Design for energy efficiency	Energy requirements of chemical processes should be recognised for their environmental and economic impacts and should be minimised. If possible, synthetic methods should be conducted at ambient temperature and pressure.
Use of renewable feedstocks	A raw material or feedstock should be renewable rather than depleting whenever technically and economically practicable.

Reduce derivatives	Unnecessary derivatisation (use of blocking groups, protection/deprotection, temporary modification of physical/chemical processes) should be minimised or avoided if possible because such steps require additional reagents and can generate waste.
Catalysis	Catalytic reagents (as selective as possible) are superior to stoichiometric reagents.
Design for degradation	Chemical products should be designed so that at the end of their function they break down into innocuous degradation products and do not persist in the environment.
Real-time analysis for pollution prevention	Analytical methodologies need to be further developed to allow for real-time, in-process monitoring and control prior to the formation of hazardous substances.
Inherently safer chemistry for accident prevention	Substances and the form of a substance used in a chemical process should be chosen to minimise the potential for chemical accidents, including releases, explosions, and fires.

Figure 2.4-1. Twelve principles of green chemistry. Based on ref. 188.

Simultaneously to the development of twelve principles of green chemistry, the chemical engineering community driven by the globalisation of the markets, acceleration of partnerships and an unprecedented rate of development of new technologies, developed the idea of green chemical engineering. It was done in an effort to mitigate the environmental burden of chemical processes and develop new, greener alternatives to the currently practised processes. Besides environmental aspects, greener processes can prove to be economically superior owing to fewer wastes being generated or less energy being consumed in the course of the process. The concept of green chemical engineering promotes, among others, process intensification<sup>189</sup> and an integrated, as well as multidisciplinary, approach to process engineering.<sup>190</sup>

General appreciation and acceptance of green chemistry, as well as green chemical engineering principles, resulted in a significant change in the way industrial processes are being performed. Besides replacement of some of the outdated and environmentally poorly performing processes, there are examples of internal practises or regulations aiming towards assurance that newly designed products or processes will meet sustainability and safety criterions.<sup>191</sup>

To ensure that the developed process option is environmentally superior there must be a way to assess the environmental sustainability of the process in the most comprehensive and accurate manner. Even though a number of metrics to assess such impact has been developed and applied in academic as well as industrial environment, scientists lack consensus in which one applies to the most of case-studies and which one provides its users with the most comprehensive answer.

The simplest, nonetheless quite powerful, metric is yield, Equation ( 46 ). Measuring the efficiency of the process by the amount of the substrate that is transformed into product allows a rough comparison between different process options.

$$\text{yield} = \frac{\text{mol product}}{\text{mol substrate}} \quad (46)$$

Owing to its simplicity, yield does not take into account the amount of waste generated by the investigated process. This issue was answered by the development of Sheldon's  $E_{factor}$  which calculates the amount of waste generated to produce 1 kg of the chemical product, Equation ( 47 ).<sup>192</sup>

$$E_{factor} = \frac{\text{kg waste}}{\text{kg of product}} \quad (47)$$

Notably, water as a waste stream is excluded from the  $E_{factor}$  calculation due to unrealistic values of the  $E_{factor}$  that may be difficult to compare and analyse.<sup>192</sup> To tackle this, numerous intensity based metrics were developed including the Mass Intensity, the Solvent Intensity and the Water Intensity and they suppressed the usage of the  $E_{factor}$  greatly.<sup>193</sup>

However, even the most detailed analysis of the process options based on the  $E_{factor}$  or its modifications will not reveal in-depth differences in the environmental impact owing to a very low sensitivity of the  $E_{factor}$  to the operations prior to the process itself, meaning that the  $E_{factor}$  can be meaningfully changed only if one of the process options is significantly different or results in a notably different yield.

Assessment of a process within broader boundaries requires a very different approach. Evaluation of environmental impacts of a technology performed considering the contribution to impacts from the transport and manufacture of all material inputs into the technology starting from raw materials, the so-called cradle-to-gate boundary, or even accounting for the impacts of the use of the products and their post-use fate, the so-called cradle-to-cradle boundary is the domain of the Life Cycle Assessment (LCA) as outlined in ISO 14040/14044. Owing to the boundaries of the assessment, LCA is particularly useful when comparing the process options, which modifications may significantly affect the material or energy fluxes in the upstream stages of the process.<sup>194</sup>

According to ISO 14040/14044, LCA is performed in four discrete phases, i.e. Goal and Scope Definition, Inventory Analysis, Impact Assessment and Interpretation.<sup>194</sup>

Goal and Scope Definition is an explicit statement of the ultimate aim of the study and sets out the context. It describes the system boundaries, the functional unit and the allocation methods used. Furthermore, all assumptions, analysed impact categories and limitations of the study shall be clearly and unbiasedly stated. Inventory Analysis formulates detailed mass and energy balances for all cells of the generated model and calculates burdens generated by each of them. Impact Assessment translates the burdens of all individual objects of the inventory on individual impact categories. Impact Assessment can be performed at a different depth of analysis, Table 2.4-1. A direct estimation of environmental intervention based on materials and energy fluxes can be translated into environmental problems formulating a “midpoint” analysis. Even though non-trivial, a further translation into damage or “endpoint” categories is possible. Interpretation consists of analysis of the obtained data, comparison of the individual process scenarios and presentation of these.<sup>195</sup>

Table 2.4-1. Burdens, mid-point and end-point impact categories.

Environmental intervention (burdens)	Environmental problems (“midpoint” categories)	Damage (“endpoint” categories)
Use of materials	Depletion of abiotic resources	Human-made environment
Use of energy	Depletion of biotic resources	Biotic natural environment
Emissions to water	Impacts of land use	Abiotic natural environment
Emissions to air	Climate change	Biotic natural resources
Solid waste	Stratospheric ozone depletion	Abiotic natural resources
	Acidification	Human health
	Eutrophication	
	Photochemical oxidants	
	Human toxicity	
	Eco-toxicity	

ReCiPe 2008, aiming to harmonise the standards of the LCA analyses, compiled a set of impact categories for the “midpoint” assessment that are generally accepted by the scientific community, Table 2.4-1.<sup>196</sup> ReCiPe 2008 also contains categories for the “endpoint” assessment. However, the majority of reported studies does not assess the “endpoint” impact categories and operate using only the “midpoint” impacts. It may be due to significant uncertainties in translation between the “midpoints” and the “endpoints” owing to a much more complex nature of the latter. For instance, it may prove to be challenging to assess the impact of a certain process on human health quantitatively. Hence, it is arguably accepted to report only the “midpoint” impacts.

LCA is often being criticised for difficult to interpret results, inconsistency in applied boundaries and numerous assumptions made while constructing models.<sup>197,198</sup> The assumptions of, for example, amount of energy consumed, yield of the process, recyclability of some of the materials used, etc., are required when the information on the current best industrial practise is not available. For models based on numerous assumptions, it is necessary to perform a sensitivity analysis to assess their influence on the final result. Regarding the difficulties in the interpretation of results, usually, a reference technology is required to assess the sustainability of the process. Analysis based solely on the values of the “midpoint” or the “endpoint” results may be indeed difficult in interpretation.<sup>195</sup>

Table 2.4-2. Impact categories outlined in ReCiPe 2008 based on ref. 196.

Abbreviation	Impact category	Unit
GWP	Climate change	kg of CO <sub>2</sub> – equivalents (eq.) per functional unit (FU)
FDP	Fossil fuels depletion potential	kg of oil per FU
HTP	Human toxicity potential	kg of 1,4-dichlorobenzene (1,4-DCB) – eq. per FU
MEP	Marine eutrophication potential	kg of nitrogen – eq. per FU
MDP	Metal depletion potential	kg of Fe – eq. per FU
NLTP	Natural land transformation potential	m <sup>2</sup> per FU
ODP	Ozone depletion potential	kg of chlorofluorocarbon-11 per FU
POFP	Photochemical oxidant formation potential	kg of non-methane volatile organic compounds (MNVOC) – eq. per FU
TAP	Terrestrial acidification potential	kg of SO <sub>2</sub> – eq. per FU
TETP	Terrestrial ecotoxicity potential	kg of 1,4-DCB – eq. per FU

One of the common uses of LCA is assessment of the sustainability of several competitive process options. Such analysis, alongside for example cost estimation, is often used in the choice of a process technology in the industry. The most significant advantage of such analysis is ease of interpretation of the results. Having the values of impacts of several process options allows choosing the most sustainable or, taking into account also other criteria, the most appropriate one.<sup>195</sup>

## 2.5. Conclusions

Even though the field of C–H activation received an unprecedented attention from the scientific environment, virtually no examples of industrial applications, or even intensified processes designed in academia, of these seemingly ideal transformations exist. It may be due to, amongst others, lack of sufficient mechanistic and kinetic understanding and usage of large amounts of precious metal catalysts. The present work aims to employ tools and methods of building process knowledge to attain a sufficient kinetic and mechanistic understanding of investigated C–H activation processes and develop intensified, ideally continuous, processes for them. Identified in the course of processes development inherent inefficiencies can hopefully allow to devise generic rules of intensified process design for the investigated family of C–H activation reactions.

The literature review presented some of the available tools and techniques used in building kinetic and mechanistic understanding of the processes that can be employed in design of intensified processes. Nextly, flow chemistry, being a tool of process intensification was described. Finally, an introduction to C–H activation reactions was presented. Even though all of the above mentioned topics are in the forefront of the respective fields, very little collaborative efforts are made to employ all of them in one project. This work aims to fill this gap. An example of using chemical engineering techniques of process development combined with process intensification and usage of novel chemical transformations may prove to be a valuable example of collaborative approach to process development and can potentially bring a significant added value to the fields of organic chemistry, C–H activation, process development and process intensification.

## Chapter 3. Experimental section

### General methods.

Proton nuclear magnetic resonance ( $^1\text{H}$  NMR) spectra were recorded at ambient temperature on a Bruker AM 400 (400 MHz) or an Avance 500 (500 MHz) spectrometer. Chemical shifts ( $\delta$ ) are reported in ppm and quoted to the nearest 0.01 ppm relative to the residual protons in chloroform-*d* (7.26 ppm), benzene-*d*<sub>6</sub> (7.16 ppm), dimethyl sulfoxide *d*<sub>6</sub> (2.05 ppm), methanol-*d*<sub>4</sub> (3.31 ppm) or acetonitrile-*d*<sub>3</sub> (1.94 ppm) and coupling constants (*J*) are quoted in Hertz (Hz). Data are reported as follows: Chemical shift (number of protons, multiplicity, coupling constants). Coupling constants were quoted to the nearest 0.1 Hz and multiplicity reported according to the following convention: s = singlet, d = doublet, t = triplet, q = quartet, qn = quintet, sext = sextet, sp = septet, m = multiplet, br = broad. Where coincident coupling constants have been observed, the apparent (app) multiplicity of the proton resonance has been reported. Carbon nuclear magnetic resonance ( $^{13}\text{C}$  NMR) spectra were recorded at ambient temperature on a Bruker AM 400 (101 MHz) or an Avance 500 (126 MHz) spectrometer. Chemical shift ( $\delta$ ) was measured in ppm and quoted to the nearest 0.1 ppm relative to the residual solvent peaks in chloroform-*d* (77.16 ppm), benzene-*d*<sub>6</sub> (128.06 ppm), dimethylsulfoxide-*d*<sub>6</sub> (39.25 ppm), methanol-*d*<sub>4</sub> (49.00 ppm) or acetonitrile-*d*<sub>3</sub> (1.32 ppm). Infrared (IR) spectra were recorded on a Perkin Elmer FT-IR Spectrometer fitted with an ATR sampling accessory as either solids or neat films, either through direct application or deposited in chloroform, with absorptions reported in wavenumbers ( $\text{cm}^{-1}$ ). Analytical thin layer chromatography (TLC) was performed using pre-coated Merck glass-backed silica gel plates (Silicagel 60 F254). Flash column chromatography was undertaken on Fluka or Material Harvest silica gel (230–400 mesh) under a positive pressure of nitrogen unless otherwise stated. Visualisation was achieved using ultraviolet light (254 nm) and chemical staining with ceric ammonium molybdate or basic potassium permanganate solutions.

The experimental work was performed in the Department of Chemical Engineering and Biotechnology and Department of Chemistry, University of Cambridge.

All reactants were purchased from Sigma-Aldrich, AlfaAesar or Fluorochem at highest available purity and, unless stated otherwise, used without additional purifications.

### **3.1. Continuous-flow synthesis and derivatisation of aziridines through palladium-catalyzed C(sp<sup>3</sup>) C–H activation**

General experimental procedures for Chapter 4.1 are described below. For all experimental procedures toluene, acetic acid and acetic anhydride were distilled and kept under inert atmosphere prior to being used in reactions.

#### Procedure 1

5 ml of a solution containing diacetoxyiodobenzene (PIDA) (1.5 equiv.), palladium (II) acetate (Pd(OAc)<sub>2</sub>) and internal standard in toluene was placed in a dry microwave vial and sealed with a Teflon cap. After preheating in a silicone oil bath, the starting material was added via a microsyringe. Aliquots were taken over the specified time, and the reaction progress was monitored via a gas chromatography analysis using 1,1,2,2-tetrachloroethane as an internal standard.

Unless otherwise stated, agitation was performed using a cylindrical stirrer bar (5 mm diameter); agitation rate: 300 RPM delivered by IKA RCT basic magnetic stirrer. The temperature was controlled using a silicone oil bath heated by a hot-plate (IKA RCT basic) equipped with ETS-D5 PID controller. Oil was preheated prior to the experiments and temperature was kept constant for at least 30 minutes.

#### Procedure 2

5 ml of a solution containing PIDA (1.5 equiv.), Pd(OAc)<sub>2</sub> and internal standard in toluene was placed in a dry microwave vial and sealed with a Teflon cap. The starting material was added via a microsyringe. Feed stream was introduced using a syringe pump. Aliquots were taken over the specified time, and the reaction progress was monitored via GC analysis using 1,1,2,2-tetrachloroethane as an internal standard.

Unless otherwise stated, agitation was performed using a cylindrical stirrer bar (5 mm diameter); agitation rate: 300 RPM delivered by IKA RCT basic magnetic stirrer. The temperature was controlled using a silicone oil bath heated by a hot-plate (IKA RCT basic) equipped with ETS-D5 PID controller. Oil was preheated prior to the experiments and temperature was kept constant for at least 30 minutes.

#### Procedure 3

5 ml of a solution containing PIDA (1.5 equiv.), Pd(OAc)<sub>2</sub> and internal standard in toluene was prepared and placed in a syringe. The starting material was placed in a syringe as a solution in toluene. Solutions were pumped using syringe pumps at specified flow rates and mixed before entering the micro-reactor using a Y-mixer. The reaction was carried out in a custom build 240  $\mu$ l temperature controlled microreactor equipped with a 6 bar(g) back-pressure regulator. Solutions leaving the reactor were cooled down in an ice bath and collected. The reaction progress was monitored via GC analysis using 1,1,2,2-tetrachloroethane as an internal standard.

#### Procedure 4

5 ml of a solution containing PIDA (1.5 equiv.), Pd(OAc)<sub>2</sub> and internal standard in toluene was prepared in a container. The starting material was placed in the second container as a solution in toluene. Solutions were pumped using the Vapourtec R system HPLC pumps at specified flow rates and mixed before entering the micro-reactor using a Y-mixer. The reaction was carried out in a Vapourtec R system 10 ml PFE tubular reactor (1/16" inner diameter) equipped with a 6 bar(g) back-pressure regulator. Solutions leaving the reactor were cooled down in an ice bath and collected. The reaction progress was monitored via GC analysis using 1,1,2,2-tetrachloroethane as an internal standard.

#### 2,2,6-Trimethyl-4-oxa-1-azabicyclo[4.1.0]heptan-5-one

<sup>1</sup>H NMR (400 MHz, CDCl<sub>3</sub>):  $\delta$  3.99 (d, J = 12.1 Hz, 1H, H-1), 3.87 (d, J = 12.1 Hz, 1H, H-1), 2.45 (s, 1H, H-6), 1.90 (s, 1H, H-6), 1.45 (s, 3H, H-7), 1.29 (s, 3H, H-3/4), 1.13 (s, 3H, H-3/4); <sup>13</sup>C NMR (100 MHz, CDCl<sub>3</sub>):  $\delta$  170.8 (C-8), 71.7 (C-1), 50.0 (C-5), 36.0 (C-2), 32.9 (C-6), 25.6 (C-7), 23.7 (C-3/4), 20.9 (C-3/4); IR  $\nu_{\max}/\text{cm}^{-1}$  (film): 2973, 2934, 1721 (C=O), 1498, 1467, 1406, 1378, 1327, 1303, 1283, 1255, 1217, 1198, 1131, 1056, 1041, 981, 956, 905, 848, 768, 745, 700

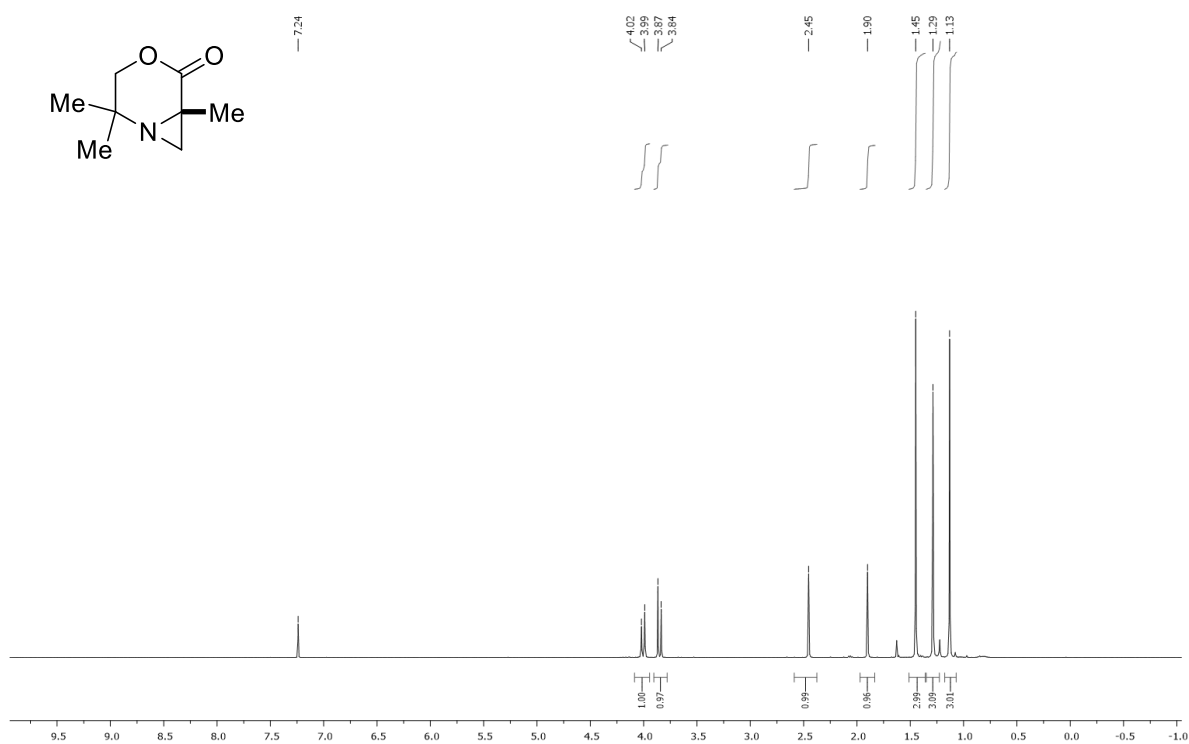


Figure 3.1-1. <sup>1</sup>H NMR (CDCl<sub>3</sub>, 400 MHz) 2,2,6-Trimethyl-4-oxa-1-azabicyclo[4.1.0]heptan-5-one

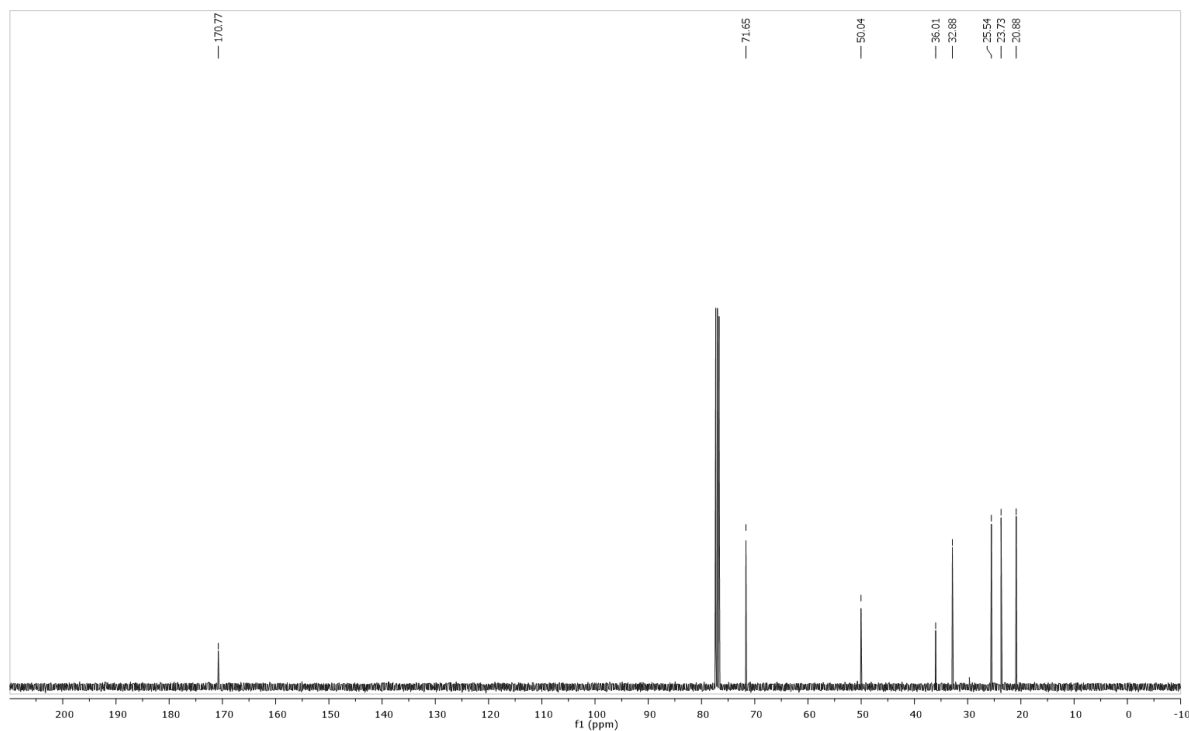


Figure 3.1-2. <sup>13</sup>C NMR (CDCl<sub>3</sub>, 100 MHz) 2,2,6-Trimethyl-4-oxa-1-azabicyclo[4.1.0]heptan-5-one

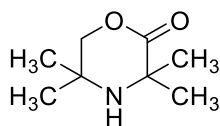


Figure 3.1-3. 3,3,5,5-Tetramethylmorpholin-2-one

2-Amino-2-methyl-1-propanol (10.0 g, 112 mmol, 1.0 equiv), acetone (82 ml, 1.12 mol, 10.0 equiv) and chloroform (13.5 ml, 168 mmol, 1.5 equiv) were added under nitrogen to a 500 ml three-neck flask equipped with a thermometer. The mixture was cooled with an acetone/ice bath and stirred vigorously. Powdered sodium hydroxide (22.4 g, 560 mmol, 5.0 equiv) was then added portion-wise while keeping the internal temperature below 5 °C. After completion of the addition, the thick solution was vigorously stirred for 2 hours, keeping the temperature below 10 °C. The solution was then allowed to warm to room temperature over 16 hours. The white solid was filtered, rinsed with acetone and twice with methanol (2 x 100 ml). The combined filtrates were concentrated under vacuum to afford the crude sodium carboxylate which was then refluxed for 6 hours in concentrated hydrochloric acid (100 ml). After cooling to room temperature, the hydrochloric acid was removed in vacuo. The flask was then placed in an ice bath, and a saturated solution of sodium bicarbonate was carefully added until the mixture became basic. The solution was extracted with ethyl acetate (3 x 50 ml), and the combined organics were washed with brine (50 ml), dried (MgSO<sub>4</sub>) and concentrated in vacuo. The product was purified by Kugelrohr distillation (0.38 mbar, approximately 95 °C) to give a colourless liquid (8.9 g, 56.7 mmol, 50.6%).

<sup>1</sup>H NMR (400 MHz, CDCl<sub>3</sub>): δ 4.10 (s, 2H, H-1), 1.36 (s, 6H, H-6), 1.12 (s, 6H, H-3); <sup>13</sup>C NMR (100 MHz, CDCl<sub>3</sub>): δ 175.2 (C-7), 78.1 (C-1), 54.6 (C-5), 49.1 (C-2), 30.6 (C-6), 26.4 (C-3); IR  $\nu_{\max}$ /cm<sup>-1</sup> (film): 3336 (N-H), 2973, 1726 (C=O), 1473, 1399, 1379, 1286, 1259, 1235, 1196, 1127, 1047, 915, 890, 806, 751

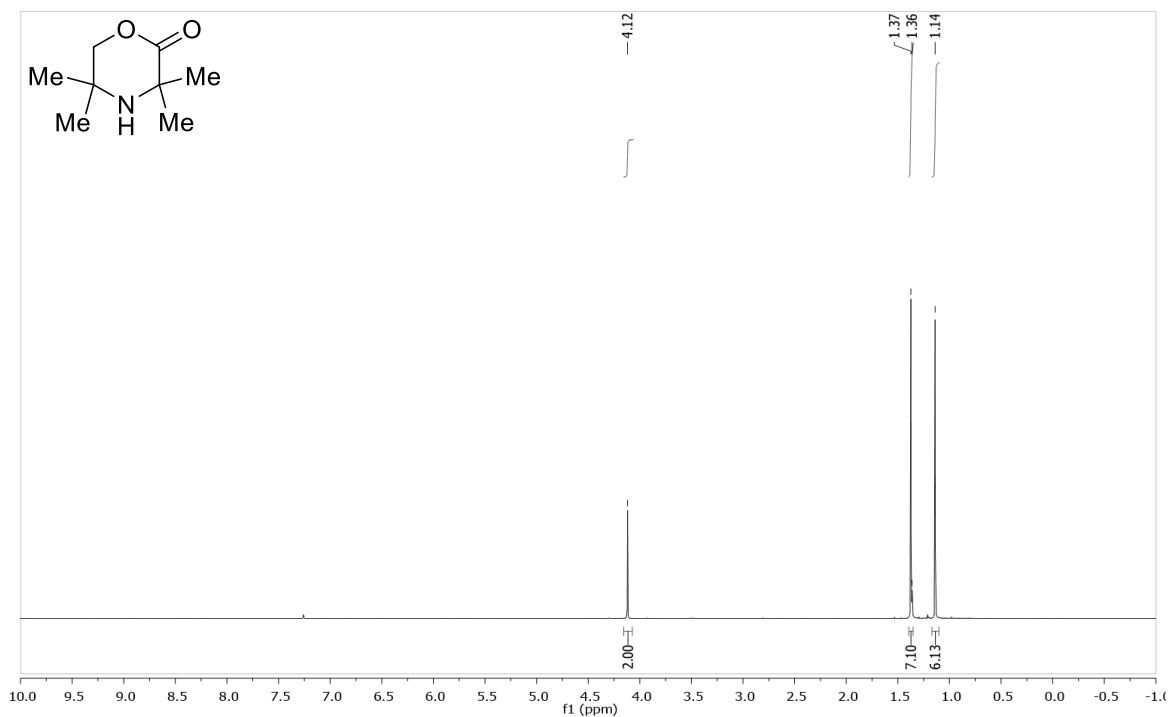


Figure 3.1-4.  $^1\text{H}$  NMR ( $\text{CDCl}_3$ , 400 MHz) 3,3,5,5-Tetramethylmorpholin-2-one

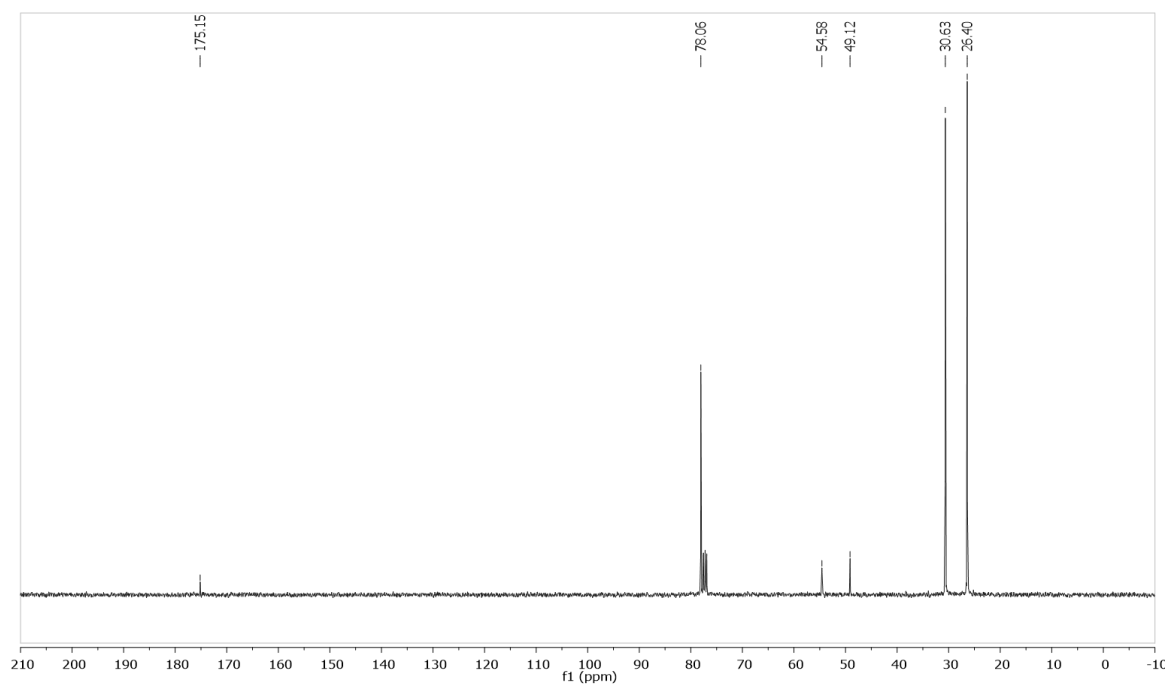


Figure 3.1-5.  $^{13}\text{C}$  NMR ( $\text{CDCl}_3$ , 100 MHz) 3,3,5,5-Tetramethylmorpholin-2-one

For the present work, an Agilent 6850 Network GC, equipped with an automated liquid sampler (ALS) and a HP-1 30 m x 0.32 mm x 0.25  $\mu\text{m}$  column, was employed. Helium was used as carrier (2.271 mL min<sup>-1</sup> and 12.748 psi) and air as make-up gas. The samples were analysed using auto injection with an injection volume of 1  $\mu\text{L}$ , split mode and split ratio of 200:1. The initial temperature of 100 °C was held for 1 minute and then ramped at 30 °C min<sup>-1</sup> to 250 °C with 1 minute hold time, resulting in an overall method time of 7 minutes. This method allowed sufficient separation of peaks corresponding to the product and the substrates, Figure 3.1-6.

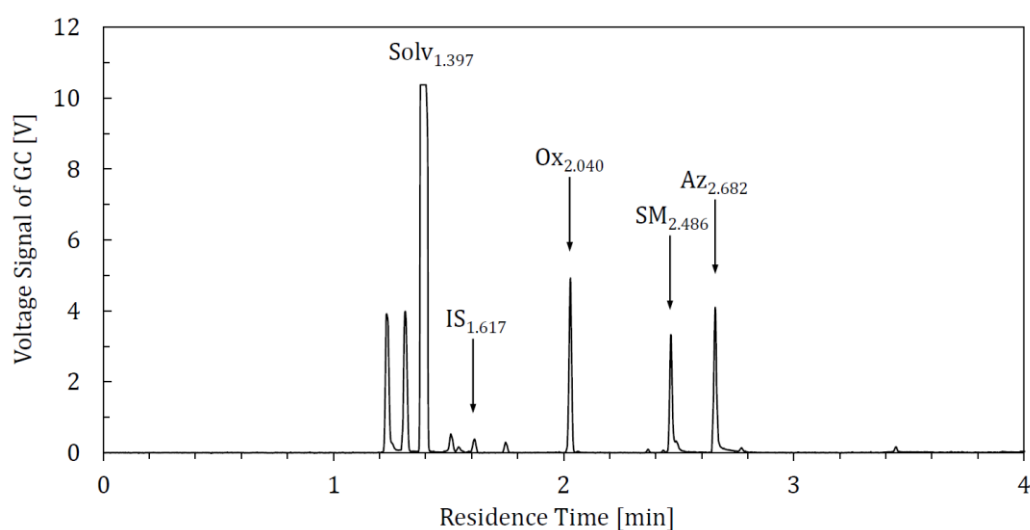


Figure 3.1-6. An example of a GC analysis. Solv: toluene, IS: internal standard, Ox: PIDA, SM: Starting material, AZ: Product.

Due to small changes in the sampling volume of the GC and its internal components, the sample to be measured has to be equipped with a known concentration of internal standard (IS). As possible measurement errors would affect all components in the sample the same way, a comparison between the analyte peak and its concentration with those of the IS would remain constant. Thus, from the known amount of contained IS and the resulting peak area, the amount of analyte could be calculated given the corresponding peak area. 1,1,2,2-Tetrachloroethane was applied as IS in the present work, because it behaved inert, was not used in the investigated chemistry for any other purpose and resulted in an unambiguous peak at the GC detector. For analysing the GC data and integration of the peak areas, the software Agilent 62 7.1 Experimental Set-up Chemstation was employed.

Calibration curves for several known concentrations of starting material SM and product Az were created using a defined amount of 0.0012 mL IS per mL solution, Figure 3.1-7.

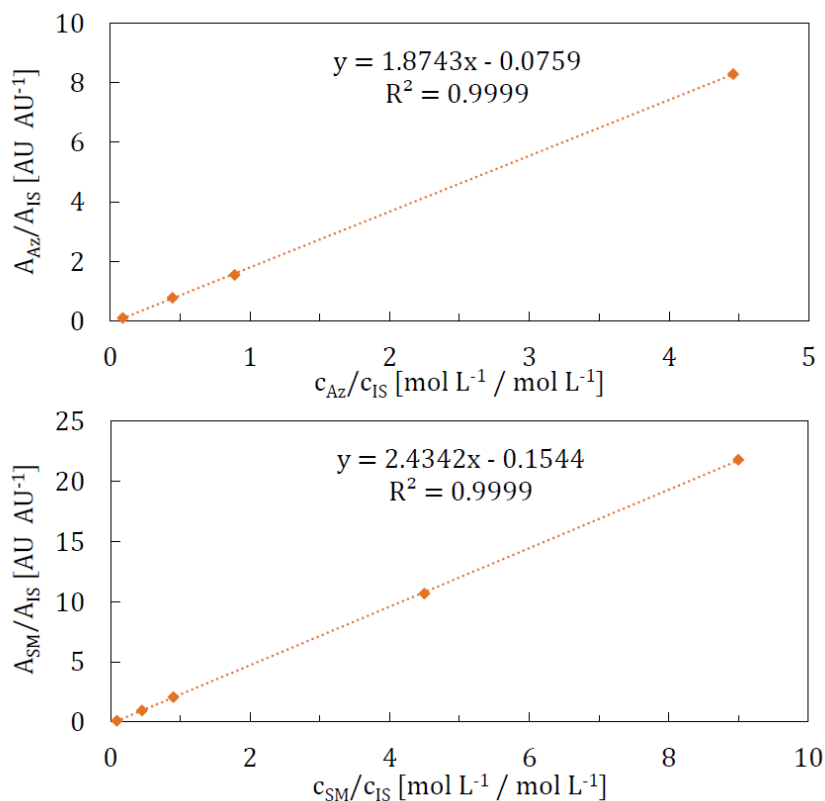


Figure 3.1-7. A calibration curve for the GC analysis, using an internal standard (IS), was established for the product (Az) in the upper and for the starting material (SA) in the lower plot.

Density functional theory (DFT) modelling was performed using Gaussian09; geometries of all structures (minima and saddle points) were optimized at the  $\omega$ B97xd/cc-PVDZ level in implicit solvent (using the SMD solvation model) using the SDD model potential for Pd; subsequent vibrational frequency calculations were performed at the same level for all calculated structures. All transition states thus found possess exactly one negative Hessian eigenvalue, while all other stationary points were confirmed to be genuine minima on the potential energy surface (PES). Intrinsic reaction coordinate (IRC) analysis was performed to unambiguously assign the located transition states for all the potential reaction pathways. Electronic energies were obtained by performing single point calculations at the  $\omega$ B97xd/cc-pVTZ level in an implicit solvent using the SDD model potential for Pd.

Enthalpies are reported as sums of  $\Delta E$ , zero-point vibrational energy (ZPVE) corrections, and thermal corrections at 298 K. Gibbs energies were calculated as  $\Delta G = \Delta H - T\Delta S$  at 298 K where enthalpies and entropies were obtained by using standard statistical mechanical formulae for the ideal gas, rigid rotor, and harmonic oscillator approximations following the normal-mode analysis in vacuum.<sup>199</sup> Coordinates of all modelled intermediates and transition states are given in Appendix 1.

### 3.1.1. Black-box optimisation

Experiments were performed in a semi-automated system consisting of a Vapourtec R2+/R4 system with a standard 10 ml coiled reactor, in-line UV and GC analysis and a computer to process data and operate all instruments.

The Vapourtec R2+/R4 consists of a system of HPLC pumps, pressure sensors and an air cooled/heated tubular reactor equipped with a Pt100 temperature sensor. Sample loops were provided to reduce the amount of the reaction mixture consumed; segments of reactants were introduced from the loops into a continuous flow of a solvent and directed into the reactor. Despite obvious advantages coming from using only a small volume of the reaction mixture, this approach suffers from several drawbacks; slugs of the reaction mixture are affected by dispersion, and additionally, especially for automated systems, accurate systems for detection of slugs are required to be able to sample and analyse them.

Laminar flow through pipes is subject to the dispersive mass transfer which is caused by non-ideal flow patterns, i.e. deviations from the ideal plug-flow regime. Axial mass transfer caused by dispersion results in a non-ideal concentration profile of the reaction segment. To avoid this phenomenon the residence time distribution (RTD) was measured aiming to determine the minimum size of the segment having at least a part of it of the same characteristics as a theoretical ideal plug-flow segment. Experiments were performed by pumping segments of the standard reaction mixture (experiment 1, Table 4.1-1) through the system and recording the intensity of the UV signal at  $362.8 \text{ cm}^{-1}$ , where the reaction mixture had the highest signal intensity, Figure 3.1-8.

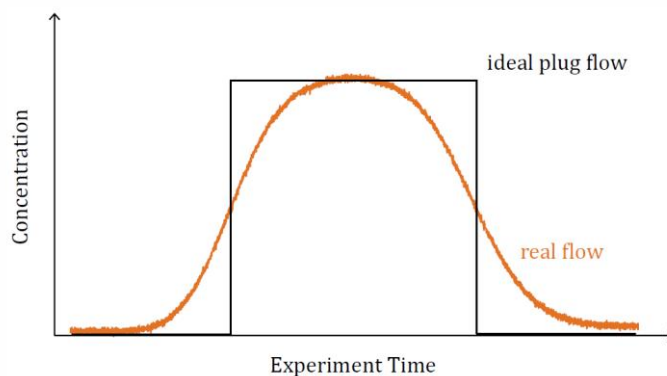


Figure 3.1-8 Example of residence time distribution experiment. Theoretical result for ideal plug-flow is added in the figure. 2 ml reaction mixture segment was used. Concentration is represented by UV signal measured by in-line UV cell.

It was observed that, to avoid dispersion, i.e. the signal for the real flow is equal to a theoretical ideal plug-flow signal for at least one time increment, 2 ml reaction mixture segments are required. Thus, this size of the sample loops was used.

The in-line UV cell used for the RTD measurements was also employed as the detector of the reaction mixture segment during the reaction. Since UV signal can be translated into concentration using the Lambert-Beer law a calibration curve was prepared, where UV signal intensity was expressed as a function of the concentration of palladium (II) acetate, Figure 3.1-9.

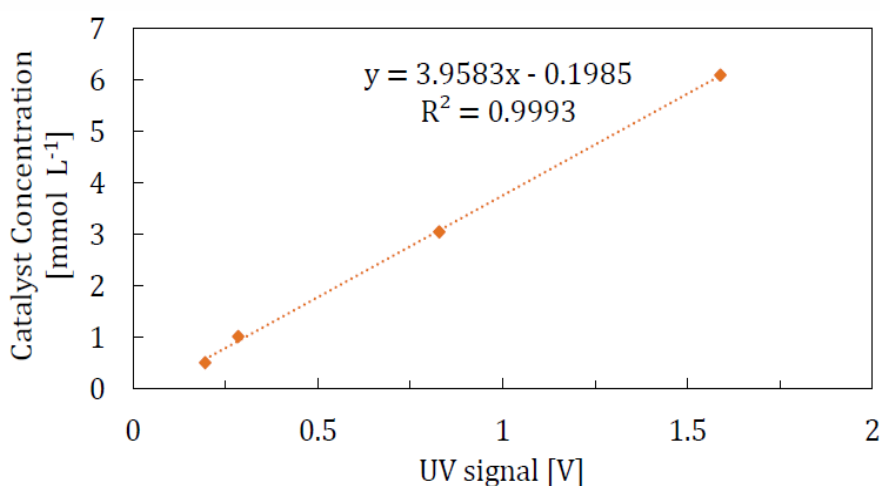


Figure 3.1-9 Calibration curve for the UV cell.

Knowing the initial concentration of the catalyst in the reaction mixture, the expected intensity of the UV signal can be calculated. Thus the system can detect with high precision when the segment of the reaction mixture passed the cell. Based on the volume of tubing between UV cell and GC as well as the flow rate, time, when GC sampling should be triggered, was automatically calculated for every experiment.

The GC analysis was performed using an Agilent 6850 Network GC, equipped with an automated liquid sampler (ALS) and an HP-1 30 m x 0.32 mm x 0.25  $\mu$ l column, was employed. A custom built GC vial was designed by Daniel Geier and Ralf Thelen from the Institut für Technische und Makromolekulare Chemie (ITMC) at RWTH Aachen University and manufactured in-house in Cambridge.<sup>20</sup> The vial consisted of a chamber with a small “fountain” in the middle of it where the solvent or the reaction mixture was continuously overflowing. Sampling was conducted using an automated liquid sampler supplied by Agilent in the middle of the “fountain” through a Teflon septum sealing the whole chamber. Excess of the reaction mixture was directed from the vial to a waste container.

All communication between instruments was custom-coded in LabVIEW and communication with Vapourtec was via its proprietary Excel interface, Figure 3.1-10.

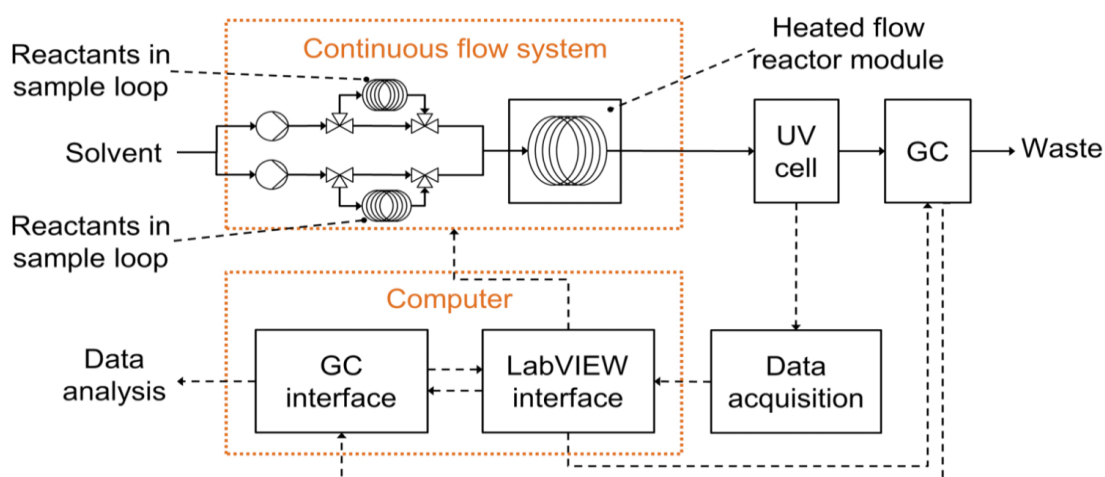


Figure 3.1-10 Schematics of the semi-automated continuous-flow system used for the black box sequential optimisation.

### 3.1.1.1. Data processing

Generated experimental data was processed using the MOAL algorithm (Multi Objective Active Learner)<sup>29</sup> aiming to optimise the conditions against two objectives:

- Yield that should be higher than 99%
- Cost that should be as low as possible

The cost function was defined as Equation ( 48 ):

$$cost = \frac{cost_{el}W_{el} + \sum cost_i m_i}{m_{Product}} \quad (48)$$

where  $cost_{el}$  and  $cost_i$  represent the electricity and material cost, whereas  $W_{el}$  and  $m_i$  denote the consumed electricity and mass of materials, respectively. The product output,  $m_{Product}$ , is defined as Equation ( 49 ):

$$m_{Product} = \frac{m_{Product}}{t_{reaction}} \quad (49)$$

where  $m_{Products}$  is the mass of synthesised product and  $t_{reaction}$  is the time necessary to complete the reaction.

The MOAL algorithm is a tool for the multi-objective target optimisations of reaction conditions. It has been developed by Peremezhney in his PhD thesis<sup>200</sup> and successfully applied for the investigation of emulsion co-polymerisation reactions in the work of Houben.<sup>201</sup> An overview of its structure is given in Figure 3.1-11. To work properly, the algorithm needs fully specified targets  $\mathbf{Y}_{target}$  for the optimisation and defined input variables  $\mathbf{X}$  as the degrees of freedom. The latter has to be bound by its possible values by corresponding constraints. As the algorithm is based on Gaussian process machine learning techniques,<sup>202</sup> an initial training set, consisting of values for the input variables  $\mathbf{X}_{tr}$  and measurements of the associated target variables  $\mathbf{Y}(\mathbf{X}_{tr})$ , has to be assembled. Furthermore, a set of the candidate solutions  $\mathbf{X}_L$  for the optimal results has to be generated by a random selection of points within the constrained input variable space, because the algorithm works with discrete evaluation techniques for the optimisation. After all necessary elements for the algorithm are provided, the initial training set is used to train the MOAL for the first time. The resulting output is a suggestion for an optimal input variable values  $\tilde{\mathbf{X}}_{optimal}$ ,

which are supposed to lead to the desired target. In the next step, an experiment or simulation is conducted, using the results  $\tilde{\mathbf{X}}_{optimal}$  from the MOAL algorithm. With this, the corresponding measurements of the target variable values  $\mathbf{Y}(\tilde{\mathbf{X}}_{optimal})$  are obtained. To check whether the target is reached by application of  $\tilde{\mathbf{X}}_{optimal}$  or not, the experiment or simulation results are assessed against the target values. If the task is fulfilled and reaction conditions are found, which leads to the desired target, then the solution  $\tilde{\mathbf{X}}_{optimal}$ , proposed as optimal, becomes the real optimal solution  $\mathbf{X}_{optimal}$  and the algorithm finishes the optimisation. If this is not the case and the targets are not reached, then the set of  $[\tilde{\mathbf{X}}_{optimal}, \mathbf{Y}(\tilde{\mathbf{X}}_{optimal})]$  is used to extend the initial training set. Thus, one more training point is available in the next iteration. The algorithm is retrained on the new set to improve its prediction and outputs a different proposal for optimal input variable values  $\tilde{\mathbf{X}}_{optimal}$ .

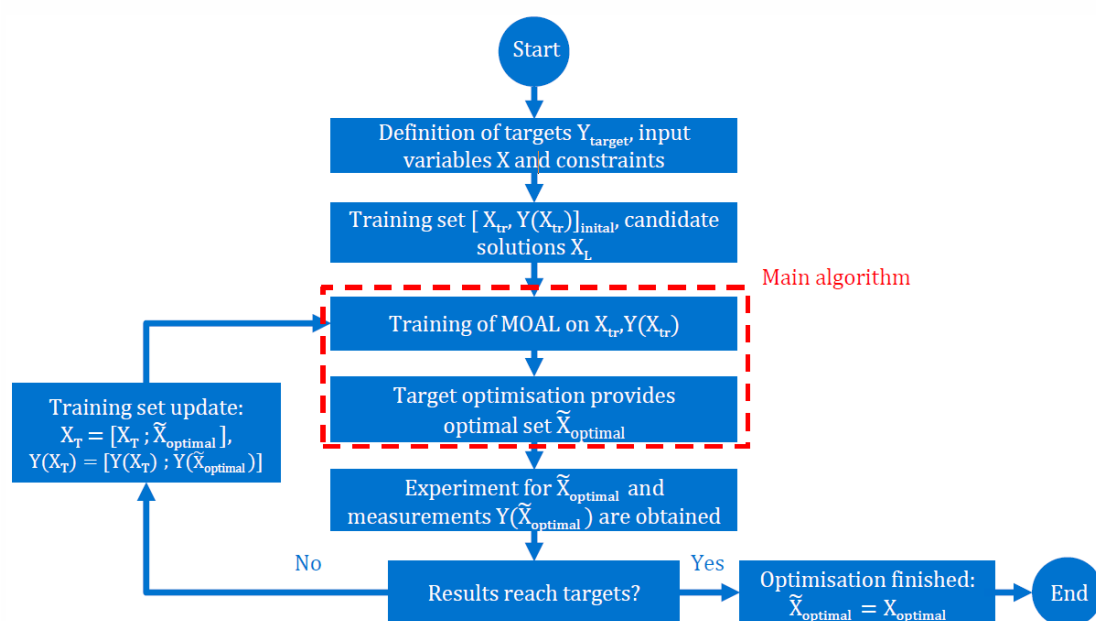


Figure 3.1-11 An overview of the MOAL algorithm including the training feedback loop.

In the present work, a grid of 2000 randomly selected candidate solutions  $\mathbf{X}_L$ , uniformly distributed within the allowed space of values, was employed. Furthermore, the vector of input variables and thus degrees of freedom for the optimisation was  $[T; t_{reac}; c_{SM}; c_{AcOH}; c_{Cat}]$ . The space of possible values was constrained as presented in Table 3.1-1. The restrictions imposed on the algorithm used in setting-up the optimisation were caused by

solubility issues and temperature stability of the reactants. Several additional constraints were designed to reduce the experimental space available to the algorithm.

*Table 3.1-1 Constraints used in the black box optimisation.*

Constrain	Lowest value	Highest value
Temperature [°C]	60	110
Initial concentration of the substrate [mol l <sup>-1</sup> ]	0	0.1
Initial concentration of acetic acid [mol l <sup>-1</sup> ]	0	4
Initial concentration of palladium acetate [mol l <sup>-1</sup> ]	0	0.01
Concentration of PIDA [mol l <sup>-1</sup> ]	1.2 * initial concentration of the substrate	
Concentration of PIDA [mol l <sup>-1</sup> ] <sup>(a)</sup>	0	(concentration of acetic acid +1.2872)/34.441
Concentration of acetic anhydride [mol l <sup>-1</sup> ]	0.2	
Ratio of the substrate and acetic acid concentration [mol l <sup>-1</sup> ]	0	100
Residence time [min]	1	120

<sup>(a)</sup> Limitation imposed by solubility of the PIDA

### 3.2. $\beta$ -C–H carbonylation of aliphatic amines to $\beta$ -lactams

Substrates were synthesised according to the protocols described by Willcox and Chappell et al. and characterisation via  $^1\text{H}$  and  $^{13}\text{C}$  NMR analysis was consistent with previously reported data.<sup>203</sup>

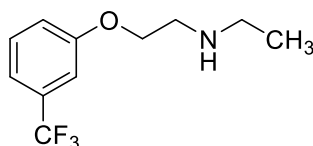


Figure 3.2-1. *N*-Ethyl-2-((6-(trifluoromethyl)pyridin-2-yl)oxy)ethan-amine

Sodium hydride (720 mg, 18.0 mmol, 60% in mineral oil) was added portion-wise to a solution of 2-(ethylamino)ethan-1-ol (1.46 mL, 15.0 mmol) in tetrahydrofuran (15 mL) at 0 °C and stirred for 30 min. To this was added a solution of 2-chloro-6-trifluoromethylpyridine (3.00 g, 16.5 mmol) in tetrahydrofuran (10 mL) drop-wise. The mixture was allowed to warm to ambient temperature then stirred for 16 h. The reaction mixture was quenched with water (20 mL) and extracted with dichloromethane (2 x 20 mL). The combined organic phases were washed with brine (20 mL), dried (magnesium sulfate) and concentrated *in vacuo*. The crude residue was purified by Kugelrohr distillation to afford the product as a colourless liquid (2.10 g, 9.00 mmol, 60%);  $R_f = 0.17$  (dichloromethane/methanol 9:1 (v/v)).

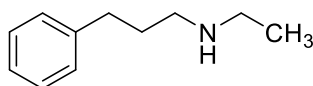


Figure 3.2-2. *N*-Ethyl-3-phenylpropan-1-amine

To a solution of hydrocinnamoyl chloride (3.00 mL, 20.0 mmol) and triethylamine (5.6 mL, 40.1 mmol) in dichloromethane (30 mL) was added ethylamine (2M in tetrahydrofuran, 10.0 mL, 20.0 mmol). The resulting mixture was stirred for 3 h. at ambient temperature then concentrated *in vacuo*. The crude material was used without further purification. The amide was dissolved in tetrahydrofuran and cooled to 0 °C. Lithium

aluminium hydride (2.4 M in tetrahydrofuran, 19 mL, 45.6 mmol) was added dropwise, and upon complete addition, the mixture was warmed to reflux for 3 h. The reaction mixture was quenched with water (2.0 mL), sodium hydroxide (15%, 2.0 mL) and water (6.0 mL) and extracted with dichloromethane (2 x 20 mL). The combined organic phases were washed with brine (20 mL), dried (magnesium sulfate) and concentrated in vacuo. The residue was purified by Kugelrohr distillation to afford the title compound as a colourless liquid (2.06 g, 12.6 mmol, 63%).

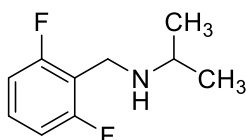


Figure 3.2-3. *N*-(2,6-Difluorobenzyl)propan-2-amine

To a solution of 2,6-difluorobenzylamine (1.00 mL, 8.40 mmol) and acetone (1.2 equiv, 614  $\mu$ L, 8.40 mmol) in dichloromethane (50 mL) was added sodium triacetoxyborohydride (1.5 equiv, 2.67g., 12.5 mmol) and glacial acetic acid (700  $\mu$ L) at 0 °C. The mixture was allowed to warm to ambient temperature then stirred for 16 h. Upon complete consumption of amine (GCMS), the mixture was quenched with saturated sodium bicarbonate (50 mL) and extracted with diethyl ether (50 mL). The organic phase was washed with brine (20 mL), dried (sodium sulfate) and concentrated to give the crude free amine. The crude product was purified by column chromatography followed by Kugelrohr distillation to provide the desired compound as a colourless liquid (1.33 g, 7.20 mmol, 85%).

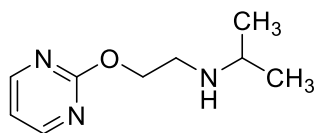


Figure 3.2-4. *N*-(2-(Pyrimidin-2-yloxy)ethyl)propan-2-amine

Sodium hydride (720 mg, 18.0 mmol, 60% in mineral oil) was added portion-wise to a solution of 2-(isopropylamino)ethan-1-ol (1.72 mL, 15.0 mmol) in tetrahydrofuran (15 mL) at 0 °C and stirred for 30 minutes. To this was added a solution of 2-chloropyrimidine (1.90 g, 16.5 mmol) in tetrahydrofuran (10 mL) dropwise. The mixture was allowed to warm to ambient temperature then stirred for 16 h. The reaction mixture was quenched with water (20 mL) and extracted with dichloromethane (2 x 20 mL). The combined organic phases were washed with brine (20 mL), dried (magnesium sulfate) and concentrated in vacuo. The crude residue was purified by Kugelrohr distillation to afford the product as a colourless liquid (1.68 g, 9.27 mmol, 62%).

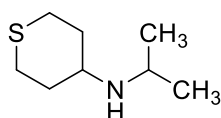


Figure 3.2-5. *N*-isopropyltetrahydro-2H-thiopyran-4-amine

To a solution of tetrahydro-2H-thiopyran-4-one (5.80 g, 50.0 mmol) in isopropylamine (50 mL) was added powdered 4Å molecular sieves (~5.0 g) and stirred at ambient temperature for 16 h. The mixture was filtered and concentrated in vacuo. The crude product was taken up in methanol (50 mL) and cooled to 0 °C. Sodium borohydride (3.76 g, 105 mmol) was added portionwise, and the mixture allowed to warm to ambient temperature and stirred for an additional 1 h. The reaction mixture was quenched with water (20 mL) and extracted with dichloromethane (2 x 20 mL). The combined organic phases were washed with brine (20 mL), dried (magnesium sulfate) and concentrated in vacuo. The crude residue was purified by column chromatography (silica, dichloromethane to 9:1 dichloromethane/methanol) to afford the product as a colourless solid (3.98 g, 25.0 mmol, 50%).

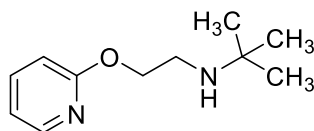


Figure 3.2-6. 2-Methyl-N-(2-(pyridin-2-yloxy)ethyl)propan-2-amine

2-(tert-Butylamino)ethan-1-ol (2.34 g, 20.0 mmol) was dissolved in 1,4-dioxane (30 mL) and NaH (800 mg, 60% dispersion in oil, 20.0 mmol) was added portion-wise. The solution was refluxed for 30 minutes, then allowed to cool to ambient temperature and 2-chloropyridine (1.9 mL, 20.0 mmol) was added. The reaction mixture was refluxed for 18 h, concentrated in vacuo and the residue suspended in water and extracted with dichloromethane (20 mL). The organic phase was dried (magnesium sulfate), concentrated in vacuo and the residue purified by Kugelrohr distillation to afford the title compound as a colourless liquid (2.43 g, 12.5 mmol, 62%).

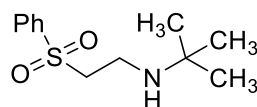


Figure 3.2-7. 2-Methyl-N-(2-(phenylsulfonyl)ethyl)propan-2-amine

To a solution of tert-butyl amine (3.15 mL, 30.0 mmol) in ethanol (13 mL) at 0 °C was added, via addition funnel, a solution of phenyl vinyl sulfone (2.50 mL, 15.0 mmol) in ethanol (7 mL). The reaction mixture was allowed to warm to ambient temperature then stirred at ambient temperature for 24 h, concentrated in vacuo and the residue purified by Kugelrohr distillation to afford the pure compound as a colourless oil (3.62 g, 15.0 mmol, quant.).

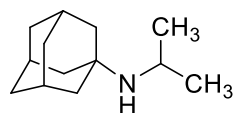


Figure 3.2-8. *N*-Isopropyladamantan-1-amine

The appropriate acetone (1.10 mL, 15.0 mmol) was dissolved in titanium(IV) isopropoxide (5.89 mL, 20.0 mmol) followed by the addition of 1-adamantylamine (2.27 g, 15.0 mmol) and stirred at ambient temperature overnight before cooling to 0 °C and adding methanol to the reaction mixture. Sodium borohydride (946 mg, 25.0 mmol) was added portion wise, and the reaction mixture stirred at 0 °C for 20 minutes then ambient temperature for the specified time. The reaction was quenched by the addition of an aqueous sodium hydroxide (1 M, 50 mL) and then diluted with dichloromethane (50 mL). The mixture was filtered through Celite, eluting with dichloromethane. The organic phase was separated, dried (magnesium sulfate) and concentrated in vacuo. The crude product was purified by Kugelrohr distillation to afford the title compound as a colourless oil (1.31 g, 6.8 mmol, 45%).

General procedures for  $\beta$ -C–H carbonylation of aliphatic amines to  $\beta$ -lactams.

#### General procedure A

A 1/8" outer diameter copper pipe reactor (V=10 ml) was connected to Isco 100D syringe pump, and Bronkhorst EL-FLOW Select MFC calibrated for multiple gasses. The reactor was placed in a silicone oil bath and pre-heated. A back pressure regulator (BPR-10 from Zaiput Flow Technologies) was fitted, and the pressure was set to the desired value. To condition the reactor, toluene and 6.25% CO balanced using synthetic air (1/1; v/v) was passed through the reactor for 30 min at 0.1 ml min<sup>-1</sup> flowrate for both gas and liquid phase at 150 °C. At the outlet of the reactor (after the BPR) an additional stream of compressed air was delivered to dilute remaining CO.

Reaction mixture preparation; 1,4-benzoquinone (1.5 equiv.) was added to toluene and stirred for 10 minutes. After stirring the mixture was filtered through a 20 $\mu$ m nylon filter (to remove insoluble impurities). Palladium acetate (5 mol%), adamantane-carboxylic acid

(12 mol%), pyridine (20 mol%) and an amine were added, and the mixture was stirred until a homogeneous solution was obtained.

The reaction was started by filling the reactor with toluene. The mass flow rate of 6.25% CO balanced using synthetic air was set to a corresponding value and allowed to stabilise for 5 min. Upon a stable gas flowrate, the reaction mixture was pumped into the reactor. The volume of gas slugs was at least equal to the volume of liquid slugs. Steady state was assumed after two residence times.

The temperature was controlled using a silicone oil bath heated by a hot-plate (IKA RCT basic) equipped with an ETS-D5 PID controller. Silicone oil was preheated prior to the experiments and temperature was kept constant for at least 30 minutes.

The reaction mixture was filtered through Celite, eluting with ethyl acetate and the filtrate was concentrated in vacuo. The residue was purified by flash column chromatography.

#### General procedure B

A 1/8" outer diameter copper pipe reactor ( $V=10$  ml) was connected to Isco 100D syringe pump, and Bronkhorst EL-FLOW Select MFC calibrated for multiple gasses. The reactor was placed in an oil bath and pre-heated. A back pressure regulator (BPR-10 from Zaiput Flow Technologies) was fitted, and the pressure was set to the desired value. To condition the reactor, toluene and 6.25% CO balanced using synthetic air (1/1; v/v) was passed through the reactor for 30 min at  $0.1 \text{ ml min}^{-1}$  flowrate for both gas and liquid phase at  $150^\circ\text{C}$ . At the outlet of the reactor (after the BPR) an additional stream of compressed air was delivered to dilute remaining CO.

Reaction mixture preparation; 1,4-benzoquinone (1.5 equiv.) was added to toluene and stirred for 10 minutes. After stirring the mixture was filtered through  $20 \mu\text{m}$  nylon filter (to remove insoluble impurities). Palladium acetate (5 mol%), adamantane-carboxylic acid (12 mol%), Li-quinoline (10 mol%) and an amine were added, and the mixture was stirred until a homogeneous solution was obtained.

The reaction was started by filling the reactor with toluene. The mass flow rate of 6.25% CO balanced using synthetic air was set to a corresponding value and allowed to stabilise for 5 min. Upon a stable gas flowrate, the reaction mixture was pumped into the reactor.

The volume of gas slugs was at least equal to the volume of liquid slugs. Steady state was assumed after two residence times.

The temperature was controlled using a silicone oil bath heated by a hot-plate (IKA RCT basic) equipped with an ETS-D5 PID controller. Oil was preheated prior to the experiments and temperature was kept constant for at least 30 minutes.

The reaction mixture was filtered through Celite, eluting with ethyl acetate and the filtrate was concentrated in vacuo. The residue was purified by flash column chromatography.

### General procedure C

A 1/8" outer diameter copper pipe reactor ( $V=10$  ml) was connected to Isco 100D syringe pump, and Bronkhorst EL-FLOW Select MFC calibrated for multiple gasses. The reactor was placed in an oil bath and pre-heated. A back pressure regulator (BPR-10 from Zaiput Flow Technologies) was fitted, and the pressure was set to the desired value. To condition the reactor, toluene and 6.25% CO balanced using synthetic air (1/1; v/v) was passed through the reactor for 30 min at  $0.1 \text{ ml min}^{-1}$  flowrate for both gas and liquid phase at  $150$  °C. At the outlet of the reactor (after the BPR) an additional stream of compressed air was delivered to dilute remaining CO.

Reaction mixture preparation; 4-phenyl-benzoquinone (1.5 equiv.) was added to toluene and stirred for 10 minutes. After stirring the mixture was filtered through  $20 \mu\text{m}$  nylon filter (to remove insoluble impurities). Palladium(II) 2,4,6-trimethylbenzoate (10 mol%), 2,4,6-trimethylbenzoic acid (10 mol%), quinuclidine (10 mol%) and an amine were added, and the mixture was stirred until a homogeneous solution was obtained.

The reaction was started by filling the reactor with toluene. The mass flow rate of 6.25% CO balanced using synthetic air was set to a corresponding value and allowed to stabilise for 5 min. Upon a stable gas flowrate, the reaction mixture was pumped into the reactor. The volume of gas slugs was at least equal to the volume of liquid slugs. Steady state was assumed after two residence times.

The temperature was controlled using a silicone oil bath heated by a hot-plate (IKA RCT basic) equipped with an ETS-D5 PID controller. Oil was preheated prior to the experiments and temperature was kept constant for at least 30 minutes.

The reaction mixture was filtered through Celite, eluting with ethyl acetate and the filtrate was concentrated in vacuo. The residue was purified by flash column chromatography.

#### General procedure D

A stainless-steel autoclave, equipped with a pressure gauge, a liquid phase sampling port, an additional inlet for gas phase (located at the bottom of the autoclave) and a thermocouple was loaded with a mixture of reactants. The reactor was preheated to the temperature close to a boiling point of the solvent using an oil bath. The autoclave was pressurised and stirred vigorously. The temperature of the oil bath was set to an appropriate value, and aliquots of the liquid phase were taken over the specified time. The reaction progress was monitored via gas chromatography (GC) using dodecane as an internal standard or via high-performance liquid chromatography (HPLC) analysis.

Unless otherwise stated, agitation was performed using a cross-shaped stirrer bar (20 mm diameter); agitation rate: 300 RPM delivered by IKA RCT basic magnetic stirrer.

The temperature was controlled using a silicone oil bath heated by a hot-plate (IKA RCT basic) equipped with an ETS-D5 PID controller.

After the specified time the autoclave was cooled down to room temperature, depressurised and unloaded. The reaction mixture was filtered through Celite, eluting with ethyl acetate. The filtrate was concentrated in vacuo. The residue was purified by flash column chromatography.

#### **1-Cyclohexyl-4-methylazetidin-2-one**

$^1\text{H}$  NMR (400 MHz,  $\text{CDCl}_3$ )  $\delta$ : 3.71 (1H, qnd,  $J = 6.0, 2.0$  Hz), 3.42 (1H, tt,  $J = 11.7, 3.9$  Hz), 2.97 (1H, dd,  $J = 14.3, 5.0$  Hz), 2.41 (1H, dd,  $J = 14.4, 2.2$  Hz), 1.88 (2H, br t,  $J = 13.2$  Hz), 1.77 (2H, br t,  $J = 14.6$  Hz), 1.65– 1.61 (1H, m), 1.51 (1H, qd,  $J = 12.3, 3.4$  Hz), 1.39 (1H, qd,  $J = 12.2, 3.4$  Hz), 1.34 (3H, d,  $J = 6.0$  Hz), 1.26 (2H, tt,  $J = 12.2, 3.1$  Hz), 1.14 (1H, qn,  $J = 12.5, 3.3$  Hz);

$^{13}\text{C}$  NMR (100 MHz,  $\text{CDCl}_3$ )  $\delta$ : 166.3, 51.8, 46.3, 43.3, 32.1, 30.7, 25.4, 25.3, 20.7;

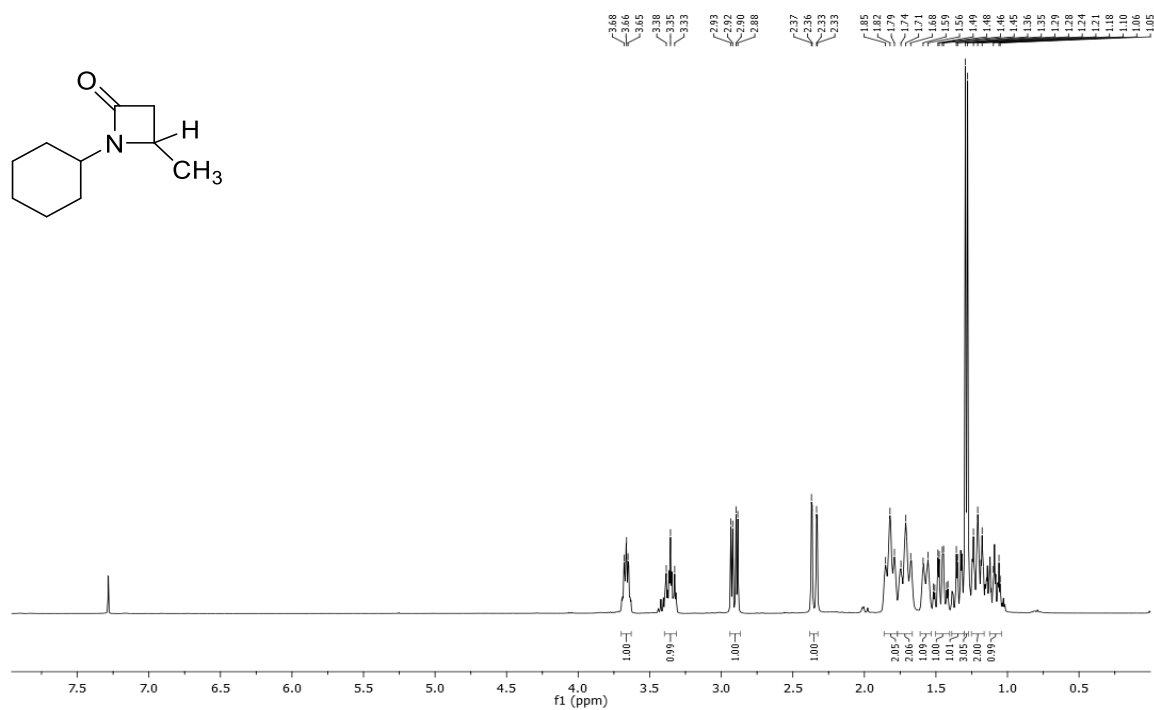


Figure 3.2-9. <sup>1</sup>H NMR (CDCl<sub>3</sub>, 400 MHz) 1-Cyclohexyl-4-methylazetidin-2-one

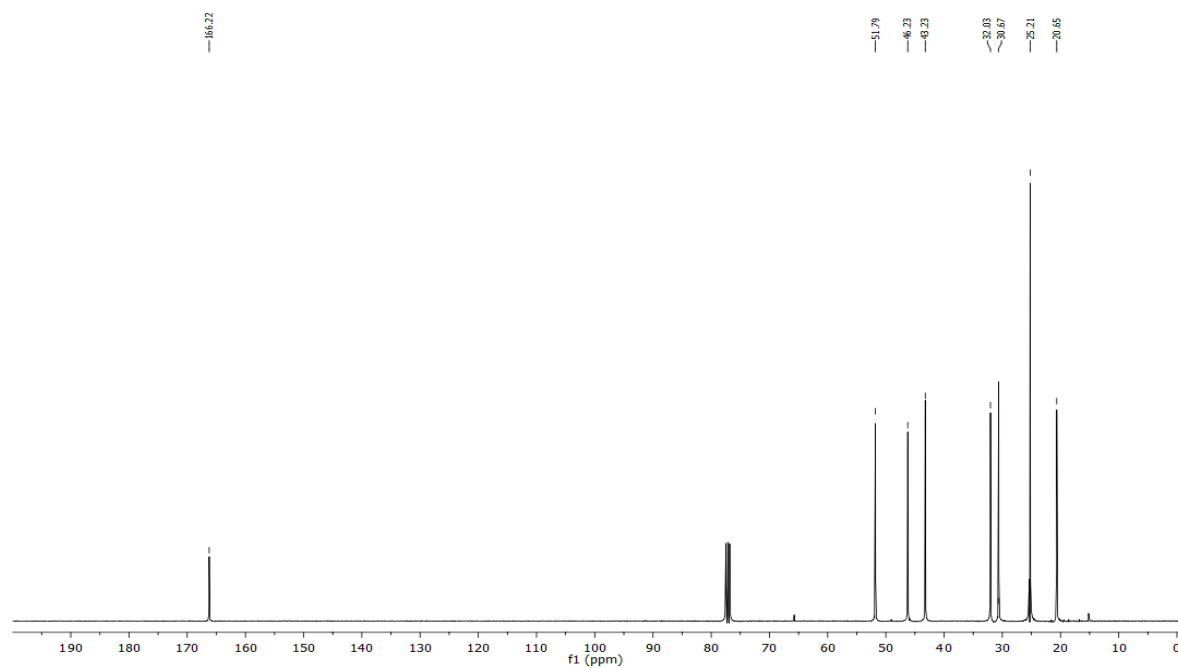
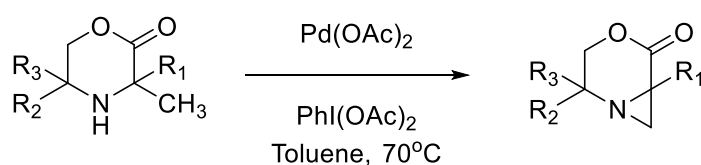


Figure 3.2-10. <sup>13</sup>C NMR (CDCl<sub>3</sub>, 100 MHz) 1-Cyclohexyl-4-methylazetidin-2-one

## Chapter 4. Results and data analysis

### 4.1. Continuous-flow synthesis and derivatisation of aziridines through palladium-catalyzed C(sp<sup>3</sup>) C–H activation

The reaction discovered by McNally<sup>148</sup> is an important advancement in the field of functional group directed C–H activation of secondary amines, Scheme 4.1-1. Giving easy access to the versatile strained nitrogen heterocycles, it opens possibilities for late-stage functionalisations of secondary amines that are a backbone of many important pharmaceuticals, chemical reagents and polymeric materials. A fully substituted, unsymmetrical secondary amine, morpholinone, undergoes a selective C–H activation on a methyl group adjacent to the carbonyl group forming aziridines. Owing to its low efficiency and lack of scalability, the reaction could potentially benefit from a hierarchical process design. The project set out to develop sufficient mechanistic and kinetic understanding of the investigated reaction, and design an intensified scalable process for it.



*Scheme 4.1-1 C–H activation reaction leading towards the synthesis of aziridines. Adapted from ref. 148; PhI(OAc)<sub>2</sub> - (Diacetoxyiodo)benzene; Pd(OAc)<sub>2</sub> – palladium (II) acetate; R – functional groups.*

### 4.1.1. Scope of the reaction

The reaction tolerates a wide range of functional groups, Figure 4.1-1, and opens possibilities for further functionalisation of the aziridine ring via a nucleophilic ring opening.

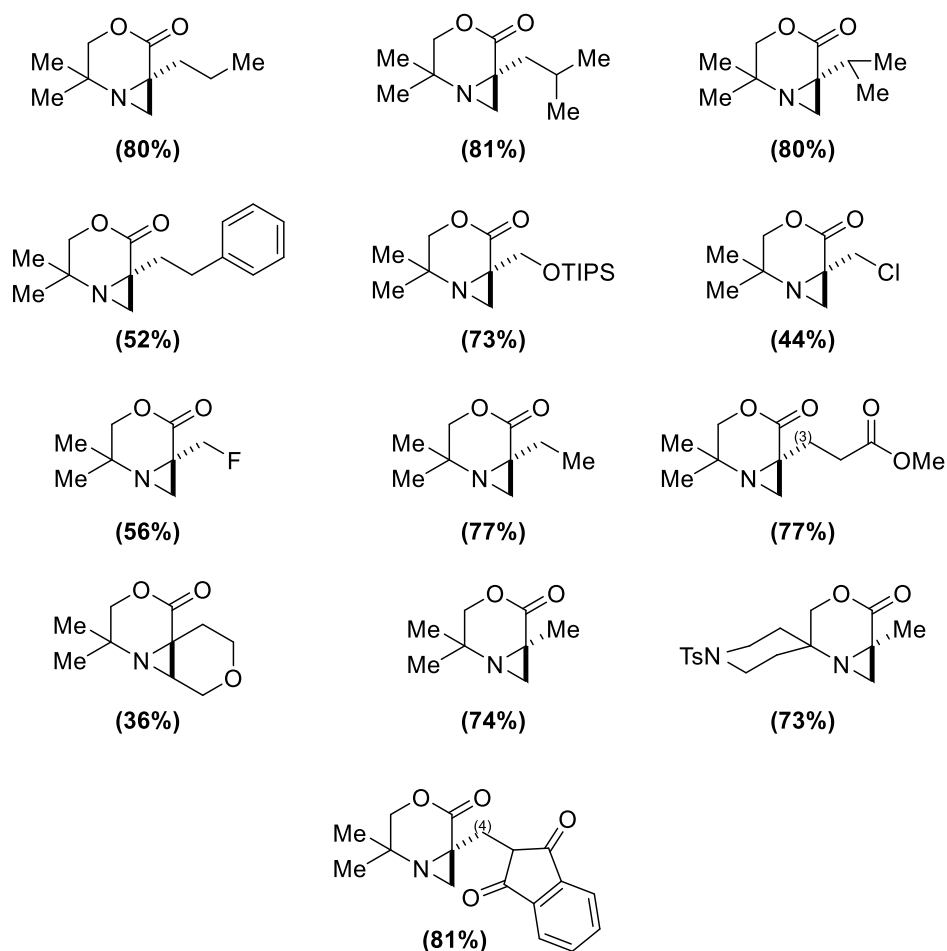


Figure 4.1-1 C-H activation reaction leading towards the synthesis of aziridines substrate scope. Yields are given for the isolated compounds. Adapted from ref. 148.

### 4.1.2. Mechanistic understanding

Because of the unusual chemoselectivity and extremely high regioselectivity of the reaction, the Gaunt group began extensive studies aiming to explain the mechanistic differences between the classical 5-membered ring cyclopalladations<sup>204</sup> and the discovered reaction.

McNally in his work observed that mixing two equivalents of **A** with palladium acetate resulted in a *bis*-amine palladium (II) intermediate **B**, Figure 4.1-2. Upon heating and treatment with a phosphine, a derivative of **D**, a putative C–H activation complex, was obtained and crystallised. As a result of further oxidation by a hypervalent iodine and a C–N reductive elimination, the product, aziridine, was obtained.<sup>148</sup>

Following that, Smalley performed a series of DFT calculations, aiming to explain the regioselectivity of the C–H activation and the chemoselectivity of the C–N reductive elimination.<sup>150</sup> In his work, he discovered the difference in the energy for the concerted metallation-deprotonation pathway of the C–H activation step between the methyl groups adjacent to the carbonyl group and the ones on the other side of the molecule to be equal to 4.89 kcal mol<sup>-1</sup> and explained this by electronic effects of the carbonyl group, increasing acidity of the C–H bonds located closer to the carbonyl.<sup>150</sup> Furthermore, he discovered that the reductive elimination is preceded by acetic acid dissociation, which lowers the energy significantly and provides the aziridine product. Additionally, the last step yields the reformed catalyst that can re-enter the catalytic cycle. McNally and Smalley in their works qualitatively described all species completing the catalytic cycle. The present studies began by probing all available on-line and off-line analytic techniques to measure concentrations of the catalytic species. Unfortunately, only the starting material and the product could be detected quantitatively, probably due to the short-lived nature of the rest of the species and, presumably, their low concentrations.

To support the proposed mechanism and identify the turn-over limiting step, kinetic isotope effect (KIE) was investigated. This powerful technique is commonly used in the field of mechanistic studies. When conducted appropriately it can provide information about which bonds are broken or formed at different stages of the reaction, and, in some cases, about the properties of the transition state through which these bonds are cleaved. This technique is of great importance for C–H activation type processes, where based on KIE

measurements one can conclude whether C–H bond cleavage occurs during the “rate-determining step”.<sup>205</sup>

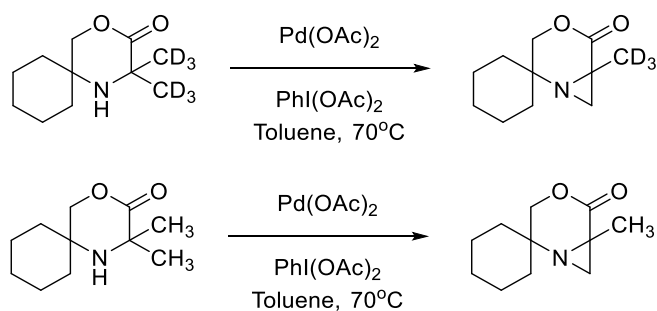
Generally, KIE experiments are conducted by accurate measurement of differences in the observed reaction rate for reaction at the C–H bond versus the analogous C–D bond. Three types of KIE experiments can be identified. The first type relies on measurements of two parallel reactions (i.e. conducted in two separate vessels). The second one involves a reaction where two substrates, C–H and C–D, compete with each other in the same flask. The third one is based on an intramolecular competition between C–H and C–D, thus the substrate must have two positions where C–H activation is possible.<sup>205</sup>

KIE is calculated based on Equation ( 50 )

$$KIE = \frac{k_H}{k_D} \quad (50)$$

where  $k_H$  ( $\text{mol min}^{-1}$ ) is the observed reaction rate for the non-deuterated starting material, and  $k_D$  ( $\text{mol min}^{-1}$ ) is the observed reaction rate for the deuterated starting material.

Aiming to avoid any competition between the two sets of methyl groups, the decision was taken to test the cyclohexane derived morpholinone (Scheme 4.1-2)



*Scheme 4.1-2. KIE experiment.*

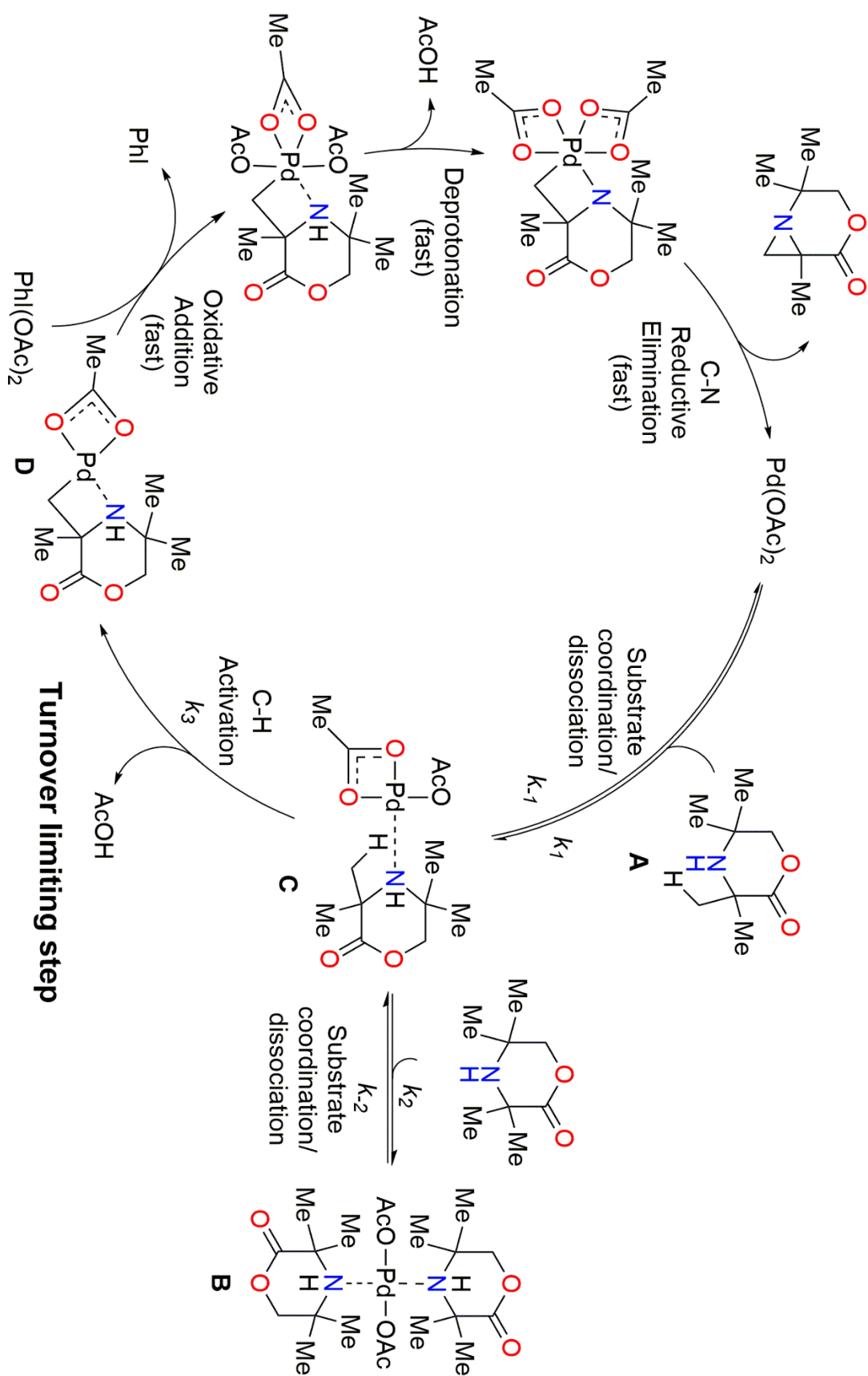


Figure 4.1-2. Proposed mechanistic cycle.

The experiment was performed according to Procedure 1, Chapter 3.1, and based on the first type of the KIE experiments. The calculated KIE value was equal to 3.8, which indicates a primary isotope effect. Hence, it was concluded that the C–H bond cleavage occurs as a part of the turn-over limiting step (TOLS).<sup>205</sup> This observation limits the number of the kinetically relevant species to the ones preceding the TOLS.

Finally, the work aimed to explain the effect of acetic acid on the observed reaction rate. McNally in his work noticed that addition of acetic anhydride allows lowering the catalyst loading from 10 mol% to 5 mol%. Thus, the turnover number (TON) of the catalyst increased significantly.<sup>148</sup> He explained it by removal of the residual water from the system and stabilisation of active palladium species. Furthermore, it was noticed that addition of acetic acid to the reaction mixture greatly increases the observed reaction rate. Being surprised by this fact, and attempting to explain this phenomenon, the author began investigations utilising the quantum-mechanical approach.

Several possibilities of how acetic acid can influence the mechanistic cycle, including a C–H cleavage involving an external acetate ligand, were considered. The calculated Gibbs activation energy for this pathway was equal to 38.0 kcal mol<sup>-1</sup> (**TS-E**). Alternatively, cyclopalladation from the (mono)amine–Pd complex (**A**) to form intermediate (**D**), Figure 4.1-2, was characterised as a single elementary step (through concerted metalation–deprotonation, CMD) with a barrier of 22.9 kcal mol<sup>-1</sup>, Figure 4.1-3, **TS-C**. This pathway was also suggested in a number of similar cases.<sup>206–211</sup> Additionally, it was found that protonation of the amine with acetic acid to give **SM·HOAc** was energetically beneficial by 0.8 kcal mol<sup>-1</sup>. Therefore, it is believed that acetic acid protonates the free amine (**SM**) to give **SM·HOAc**, thereby reducing the free-amine concentration, which in turn reduces the concentration of the off-cycle bis(amine)–Pd complex (**B**). Thus, palladium is maintained in the catalytic cycle instead of being held in the off-cycle complex **B**, Figure 4.1-4.

Thereby, it is believed that the reaction proceeds as demonstrated in Figure 4.1-3, i.e. starting material, **SM**, is being released from its salt, **SM·HOAc**, and coordinates to a molecule of palladium acetate forming the (mono)amine complex, **A**. **A** undergoes a C–H activation through the transition state **TS-C** forming the intermediate **D**. Finally, upon oxidation, deprotonation and reductive elimination, a molecule of the product is formed

(Figure 4.1-4). Despite being thermodynamically the most stable, the formation of bis(amine)-Pd intermediate, **B**, is prohibited kinetically using an excess of acetic acid.

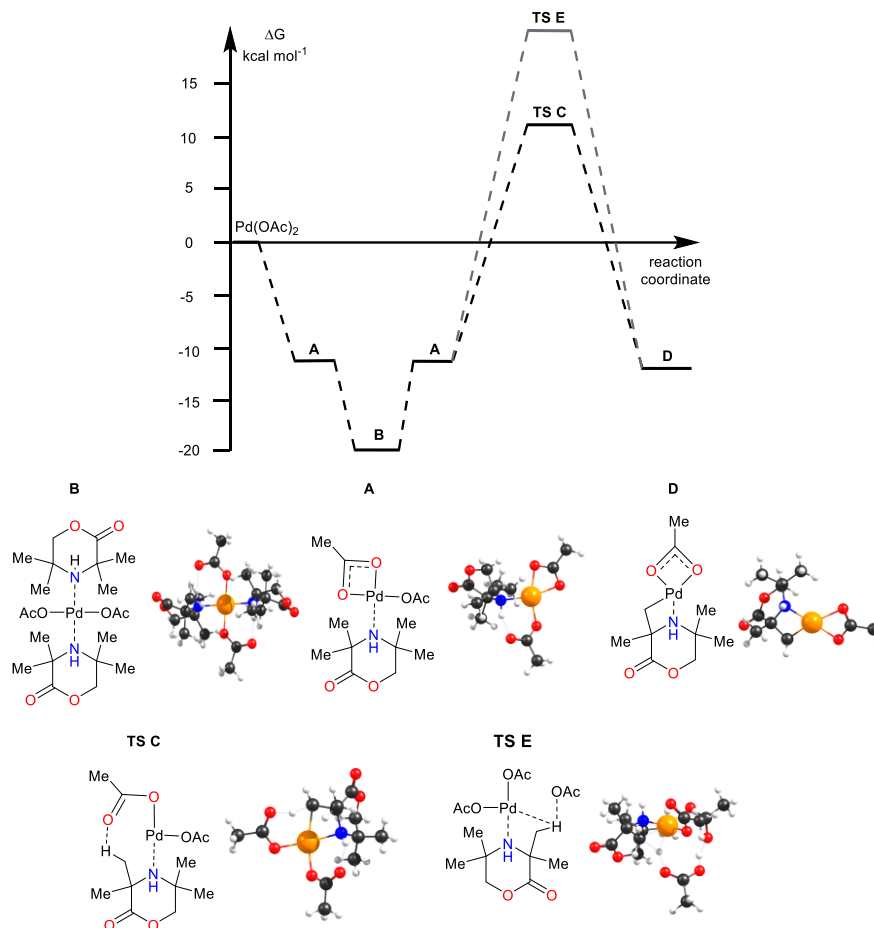


Figure 4.1-3 Energy profile of cyclopalladation proceeding through a CMD mechanism.

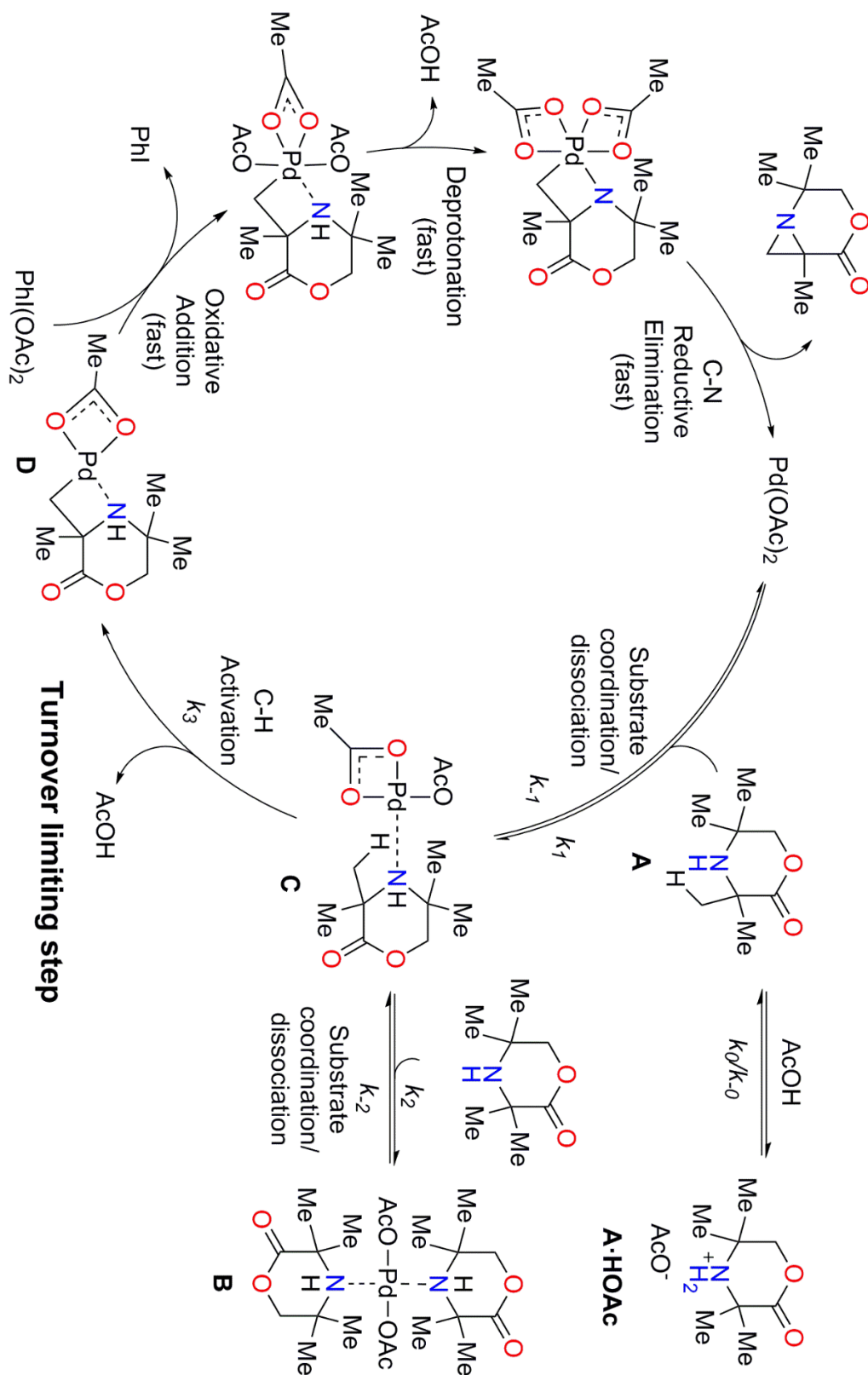


Figure 4.1-4 Proposed mechanistic cycle including the influence of the acetic acid on the mechanistic cycle.

### 4.1.3. Detailed kinetic investigation

The mechanism of the acid-accelerated C–H activation reaction was reduced to the kinetic model incorporating three equilibria ( $K_0$ ,  $K_1$  and  $K_2$ ) and one irreversible reaction ( $k_3$ ) (Figure 4.1-4). The elementary steps following the turnover-limiting step were ignored in setting up the model. This resulted in the set of seven ordinary differential equations and three algebraic equations.

$$\frac{dC_{Pd(OAc)_2}}{dt} = k_3 C_I - k_1 C_{Pd(OAc)_2} C_{SM} + k_{-1} C_{Sam}$$

$$\frac{dC_{SM}}{dt} = -k_0 C_{SM} C_{AcOH} + k_{-0} C_{SMH} - k_1 C_{Pd(OAc)_2} C_{SM} + k_{-1} C_{Sam}$$

$$-k_2 C_{Sam} C_{SM} + k_{-2} C_{Bam}$$

$$\frac{dC_{SMH}}{dt} = k_0 C_{SM} C_{AcOH} - k_{-0} C_{SMH}$$

$$\frac{dC_{Sam}}{dt} = k_1 C_{Pd(OAc)_2} C_{SM} - k_{-1} C_{Sam} - k_2 C_{Sam} C_{SM} + k_{-2} C_{Bam} - k_3 C_{Sam}$$

$$\frac{dC_{Bam}}{dt} = k_2 C_{Sam} C_{SM} - k_{-2} C_{Bam}$$

$$\frac{dC_{I1}}{dt} = k_3 C_{Sam} - k_4 C_{I1}$$

$$\frac{dC_P}{dt} = \frac{dC_{I1}}{dt}$$

$$\frac{dC_{AcOH}}{dt} = -k_0 C_{SM} C_{AcOH} + k_{-0} C_{SMH} + 2k_3 C_{Sam}$$

$$K_0 = \frac{k_0}{k_{-0}}; K_1 = \frac{k_1}{k_{-1}}; K_2 = \frac{k_2}{k_{-2}}$$

where:

$C_{Pd(OAc)_2}$  is the concentration of free palladium acetate

$C_{SM}$  is the concentration of the starting material, (**A**)

$C_{SMH}$  is the concentration of the salt of starting material and acetic acid, (**A**·**HOAc**)

$C_{Sam}$  is the concentration of the *single*-amine intermediate, (**B**)

$C_{Bam}$  is the concentration of the *bis*-amine intermediate, (**C**)

$C_{I1}$  is the concentration of the intermediate 1 (after reaction  $k_3$ ), (**D**)

$C_P$  is the concentration of the product

$C_{AcOH}$  is the concentration of acetic acid.

Firstly, to ensure that the experiments were performed in a strictly kinetically controlled regime, three experiments with agitation rate as the variable, were performed. The following conditions were used:  $C_{SM0}=0.05 \text{ mol l}^{-1}$ ;  $C_{Cat0}=0.005 \text{ mol l}^{-1}$ ;  $C_{AcOH}=0.7 \text{ mol l}^{-1}$ . Mixtures were prepared using the same stock solution, and three different agitation rates were used: 300 RPM, 600 RPM and 900 RPM. Experiments were conducted according to Procedure 1, Chapter 3.1.

Small variations between experiments and homogeneity of the reaction mixture allowed assuming no influence of mass transfer on the observed reaction rate. Providing that temperature of the reactor is kept constant by the appropriate preheating procedure, one can assume that the reaction is in the strictly kinetically controlled regime, Figure 4.1-5.

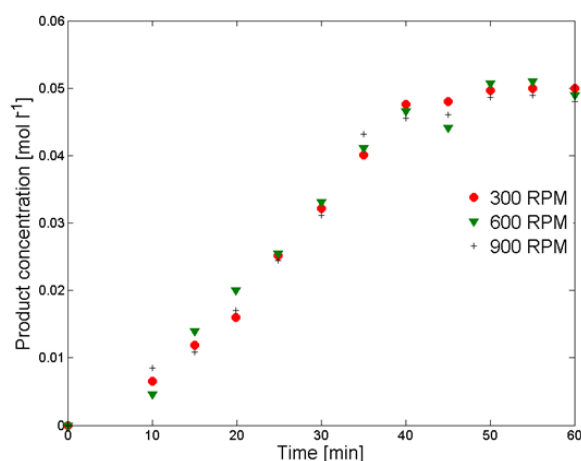


Figure 4.1-5 The influence of agitation on the product concentration as a function of time.

To estimate values of the parameters, a set of 38 experiments was designed. Initially parameters were estimated for a single temperature, 70 °C, and finally, additional experiments, where the temperature was varied, were used to estimate activation energies, Table 4.1-1. To reduce the cost, the experiments were performed only once, and the uncertainty of measurements was calculated based on the standard deviation of experiments performed to prove that the reaction was in the strictly kinetically controlled regime, Figure 4.1-5. Experiments were performed according to Procedure 1, Chapter 3.1.

*Table 4.1-1 Set of experiments used to estimate the kinetic parameters.*

No.	Palladium acetate [mol l <sup>-1</sup> ]	Substrate [mol l <sup>-1</sup> ]	Acetic acid [mol l <sup>-1</sup> ]	Temperature [°C]
0	0.010	0.1	0	70
1	0.0025	0.05	0.7	70
2	0.0025	0.05	1.4	70
3	0.0025	0.05	2.1	70
4	0.0025	0.05	2.8	70
5	0.0025	0.05	3.5	70
6	0.005	0.05	0.7	70
7	0.005	0.05	1.4	70
8	0.005	0.05	2.1	70
9	0.005	0.05	2.8	70
10	0.005	0.05	3.5	70
11	0.00125	0.05	0.7	70
12	0.00125	0.05	1.4	70
13	0.00125	0.05	2.1	70
14	0.00125	0.05	2.8	70
15	0.00125	0.05	3.5	70
16	0.005	0.1	0.7	70
17	0.005	0.1	1.4	70
18	0.005	0.1	2.1	70
19	0.005	0.1	2.8	70

No.	Palladium acetate [mol l <sup>-1</sup> ]	Substrate [mol l <sup>-1</sup> ]	Acetic acid [mol l <sup>-1</sup> ]	Temperature [°C]
20	0.005	0.1	3.5	70
21	0.0025	0.1	0.7	70
22	0.0025	0.1	1.4	70
23	0.0025	0.1	2.1	70
24	0.0025	0.1	2.8	70
25	0.0025	0.1	3.5	70
26	0.00125	0.1	0.7	70
27	0.00125	0.1	1.4	70
28	0.00125	0.1	2.1	70
29	0.00125	0.1	2.8	70
30	0.00125	0.1	3.5	70
31	0.005	0.2	0.7	70
32	0.005	0.2	1.4	70
33	0.005	0.2	2.1	70
34	0.005	0.2	2.8	70
35	0.005	0.2	3.5	70
36	0.005	0.05	0.7	80
37	0.005	0.05	0.7	90
38	0.005	0.05	0.7	100

The kinetic parameters were fitted to the experimental data using gPROMS ModelBuilder 4.0.0.<sup>212</sup> The assumption was made that the kinetic constants following the turn-over limiting step are greater than the value of the  $k_3$ . Thus there is no need to estimate them. Additionally, the Gibbs energies of activation were calculated based on Eyring equation,<sup>213</sup> where the initial guesses of the parameter estimation were calculated from the Gibbs energies obtained from the DFT studies. The full set of experimental results and the fit between the model and the experimental results are shown in Appendix 2.

The values of the parameters obtained during the parameter estimation are in a rather good agreement with the energies predicted via the DFT studies (Table 4.1-2). This supports the performed mechanistic studies and can suggest that the developed mechanism is an accurate representation of the reaction. Small correlations between most of the kinetic

parameters (Table 4.1-3) proved their independence. The larger correlation between  $K_0$  and  $K_2$  can be explained by their competitive nature with respect to the starting material (Figure 4.1-4). Furthermore, small confidence intervals and t-values greater than the reference t-value for all the estimated parameters evidence the statistical significance and precision of the parameter estimation, .

*Table 4.1-2 Fit between energies obtained during the parameter estimation and DFT modelling.*

Kinetic parameter	Energy theoretical [kcal mol <sup>-1</sup> ]	Energy experimental [kcal mol <sup>-1</sup> ]
$K_0$	-0.75	-0.78
$K_1$	-10.053	-8.78
$K_2$	6.17	5.25
$k_3$	22.92	20.55

*Table 4.1-3 Correlation matrix*

Parameter	$K_0$	$K_1$	$K_2$	$k_3$
$K_0$	1			
$K_1$	0.241	1		
$K_2$	0.859	0.149	1	
$k_3$	-0.375	0.312	0.134	1

Table 4.1-4 Results of parameter estimation for 70 °C.

Model parameter	Final value	Initial guess	Confidence interval			95% t-value	Standard deviation
			90%	95%	99%		
K <sub>0</sub>	16.069	3.3	0.34	0.41	0.54	3.92	0.21
K <sub>1</sub>	1.47x10 <sup>6</sup>	2.52x10 <sup>6</sup>	2708	3227	4248	4.55	1643
K <sub>2</sub>	657.24	8547.15	0.12	0.15	0.19	4.53	0.74
K <sub>3</sub>	0.36	1.30	2.38x10 <sup>-3</sup>	2.83x10 <sup>-3</sup>	3.73x10 <sup>-3</sup>	2.26	1.44x10 <sup>-3</sup>

Reference t-value = 1.94

Furthermore, two semi-batch experiments were performed to test the accuracy of the developed model, Table 4.1-5. Experiments were performed according to Procedure 2, Chapter 3.1.

Table 4.1-5 Design of the semi-batch experiments.

	Palladium acetate [mol l <sup>-1</sup> ]	Substrate [mol l <sup>-1</sup> ]	Acetic acid [mol l <sup>-1</sup> ]	Temperature [°C]	Flow rate [ml min <sup>-1</sup> ]
Initial concentration experiment A	0.005	0	0.5	70	-
Feed concentration experiment A	0	0.025	0	Room temperature	0.02
Initial concentration experiment B	0.005	0.050	2.0	70	-
Feed concentration experiment B	0	0.10	0	Room temperature	0.02

A good agreement between the experimental data and the predicted kinetics for both experimental conditions, Figure 4.1-6, provided further support for the model as a good representation of the molecular processes.

Having evaluated the accuracy and predictive capability of the model, an *in silico* screening for the optimal conditions for running the process was performed. The design of the continuous process model was carried on the assumption of ideal plug-flow reactor. Two restrictive parameters were defined:

1. The reaction temperature could not be higher than 120 °C owing to the thermal instability of palladium acetate.<sup>214</sup>
2. Full conversion must be reached within 10 min for a large space-time yield (STY) to be attained.

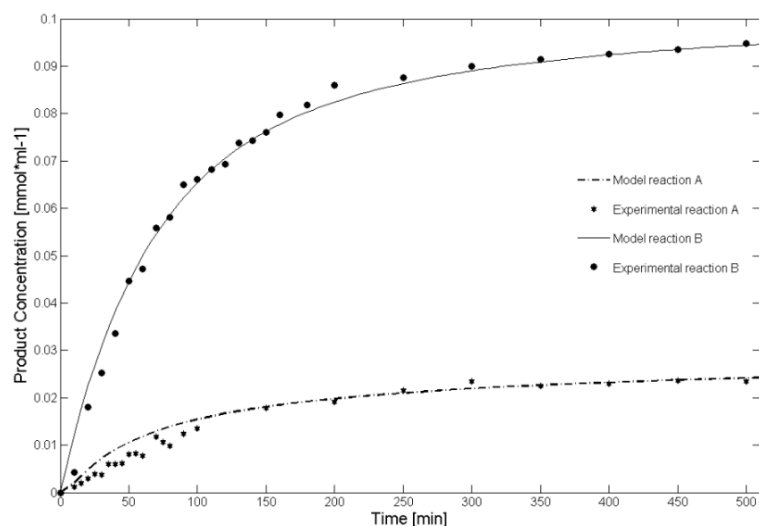


Figure 4.1-6 Comparison of the kinetic model with experimental results for semi-batch experiments.

The model was used to select the operating conditions that fulfilled both requirements, while also considering that high acid concentrations may lead to a degradation of the aziridine product.<sup>150</sup> Optimisation *in silico* using the developed process model was performed with respect to the concentrations of the starting material (**A**), Pd(OAc)<sub>2</sub>, AcOH and with respect to the temperature. The results led to several possible sets of conditions. However, priority was given to the ones characterised by the smallest catalyst loading. Selected optimal conditions were tested experimentally, Figure 4.1-7.

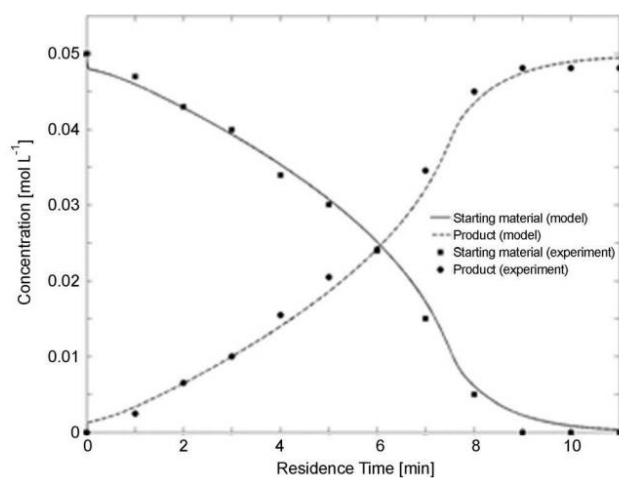


Figure 4.1-7 Results of continuous-flow experiments under optimal conditions.

The final conditions were obtained as follows: 0.1 mol l<sup>-1</sup> SM, 0.5 mol% Pd(OAc)<sub>2</sub>, 10 eq. AcOH, 2 eq Ac<sub>2</sub>O, toluene, 120 °C, 10 min. The continuous flow experiments were performed according to Procedure 3, Chapter 3.1.

#### 4.1.4. Black box optimisation

Following the full deconvolution of the mechanism of the investigated transformation, the sequential black-box optimisation was conducted to compare the experimental cost of the two competing approaches.

The MOAL algorithm was fed with a set of five experiments designed based on the Latin Hypercube sampling (LHS) approach, where a uniform cumulative distribution function (CDF) is taken for each variable, and the variable range is partitioned into five sections (corresponding to five experiments). One random variable value is then taken within each defined range.

Table 4.1-6 Recipes for experiments in the initial training of the black box optimisation.

Experiment number	Residence time [min]	Concentration of the substrate [mol l <sup>-1</sup> ]	Concentration of the catalyst [mol l <sup>-1</sup> ]	Concentration of acetic acid [mol l <sup>-1</sup> ]	Temperature [°C]
1	58.8	0.0322	0.0028	1.5435	60
2	17.0	0.0524	0.0051	2.7894	72
3	41.9	0.0772	0.0071	2.2206	86
4	91.6	0.0181	0.0011	0.0649	97
5	58.8	0.0930	0.0089	3.5487	106

Following the initial set of experiments, the algorithm was iteratively suggesting new sets of conditions, Table 4.1-7. The procedure was repeated until both criteria were satisfied, i.e. the yield was higher than 99%, and the cost function was at least as low as the cost calculated based on the experimental conditions obtained in the course of the *in silico* optimisation described in the previous chapter, Figure 4.1-8 and Figure 4.1-9.

After a single iteration, the results suggested a set of conditions already being more promising than any of the training points. The target for yield was met, as perhaps expected as it was met for two of the training experiments as well, and the value for the cost function was significantly reduced, getting closer to the pre-defined target. While it was observed that experiments 7 and 9 had a large margin of error with regards to the targets, this is due to the exploratory function of the algorithm, Figure 4.1-8.

Using the black box optimisation, the set of suitable conditions was found performing a rather small amount of experimental work. The conditions comparable to the ones obtained in the previous chapter were found after generating only 11 data points, where, in the classical approach, around 400 experimental points were generated. The rapid search for conditions using the semi-automated system, allowed shortening the time necessary to find the suitable conditions, although it did not provide any process knowledge. Without the prior knowledge of the influence of acetic acid on the observed reaction rate, the black box optimisation would not yield such a good result.

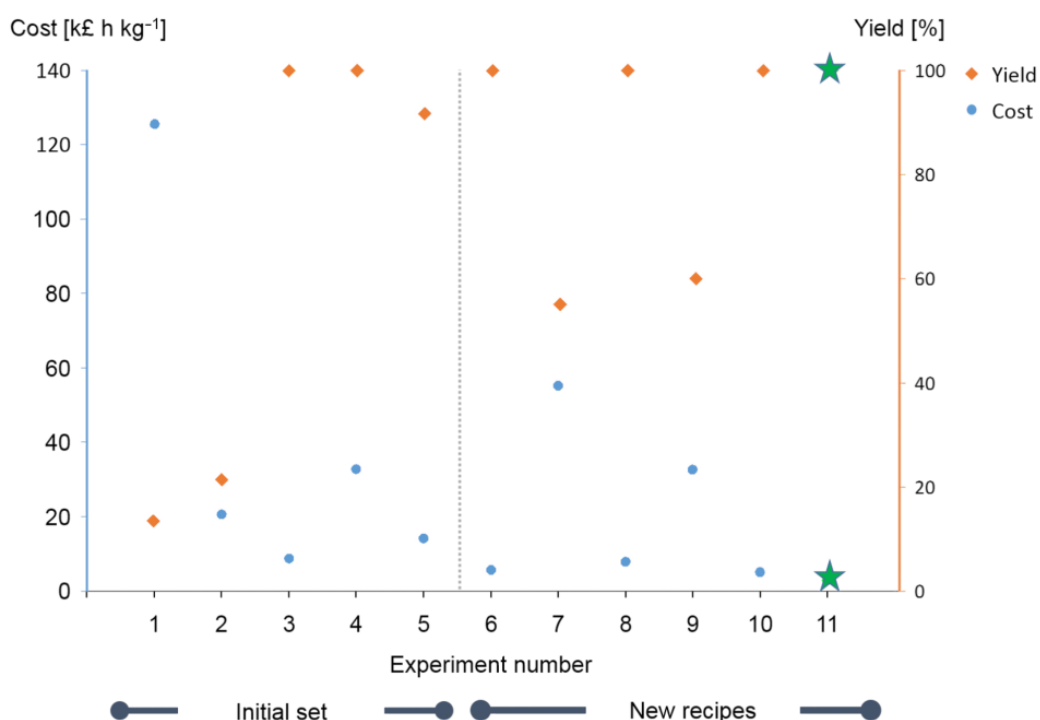


Figure 4.1-8 Results of the black box optimisation. Blue “dots” correspond to the cost function – left vertical axis; Orange “diamonds” correspond to the yield – right vertical axis.

Table 4.1-7 Recipes for experiments suggested by the algorithm.

Experiment number	Residence time [min]	Concentration of 1 (the substrate) [mol l <sup>-1</sup> ]	Concentration of the catalyst [mol l <sup>-1</sup> ]	Concentration of acetic acid [mol l <sup>-1</sup> ]	Temperature [°C]
6	30.8	0.0756	0.0055	2.3368	109
7	35.9	0.0057	0.0004	0.0717	109
8	51.1	0.0993	0.0047	3.1000	96
9	115.7	0.0887	0.0043	3.5923	105
10	25.6	0.0998	0.0084	3.0330	86
11	15.3	0.0859	0.0072	2.3927	102

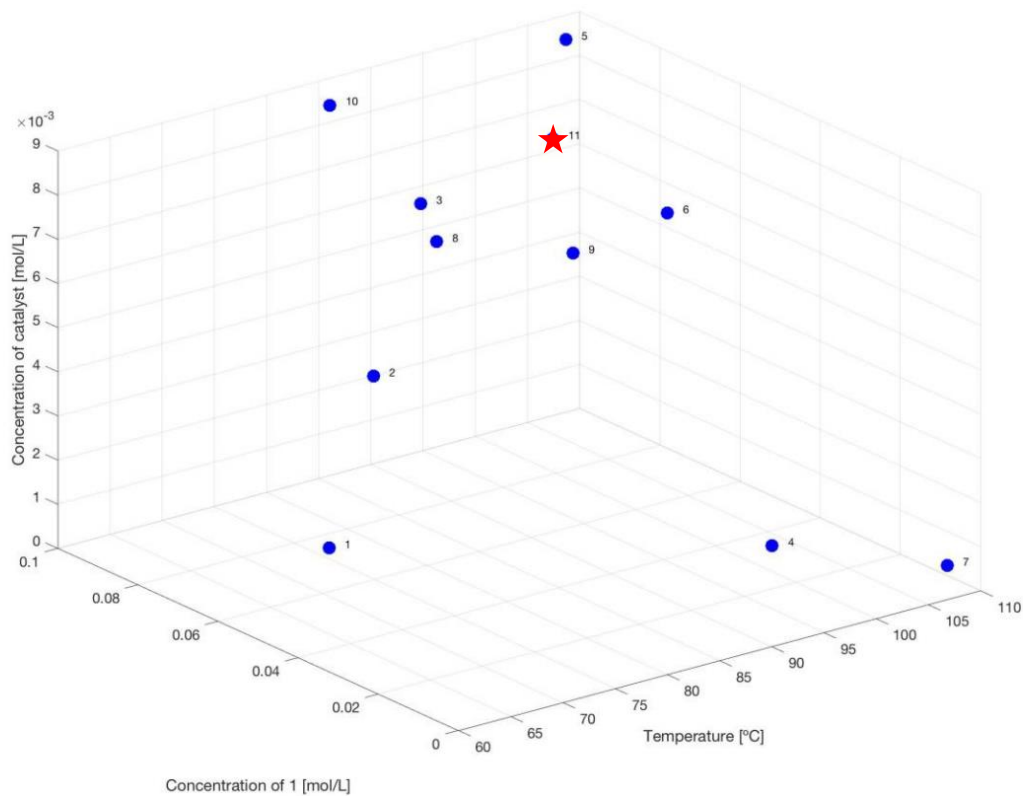


Figure 4.1-9 Trajectory of the black box optimisation. The red star represents the final set of conditions.

### 4.1.5. Design of the reactor and separation system for the aziridination reaction

Having obtained the set of suitable conditions for a continuous flow process, the design of a suitable reactor system was performed. The following aspects were investigated:

- Flow reactor
- Purification technique

Owing to the homogeneous nature of the reaction mixture, the design of the flow reactor was greatly simplified. The decision was made to use:

- On the micro-scale, a custom built 240  $\mu$ l silicon-glass microreactor equipped with a heat exchanger.
- On the meso-scale, a commercially available 10 ml tubular PFE reactor supplied by Vapourtec. The diameter of the PFE tube equal to 1/16".

On the micro-scale, the temperature was controlled via a temperature controlled circulator using ethylene glycol as a heating/cooling medium. On the meso-scale, Vapourtec R2+/R4 was used.

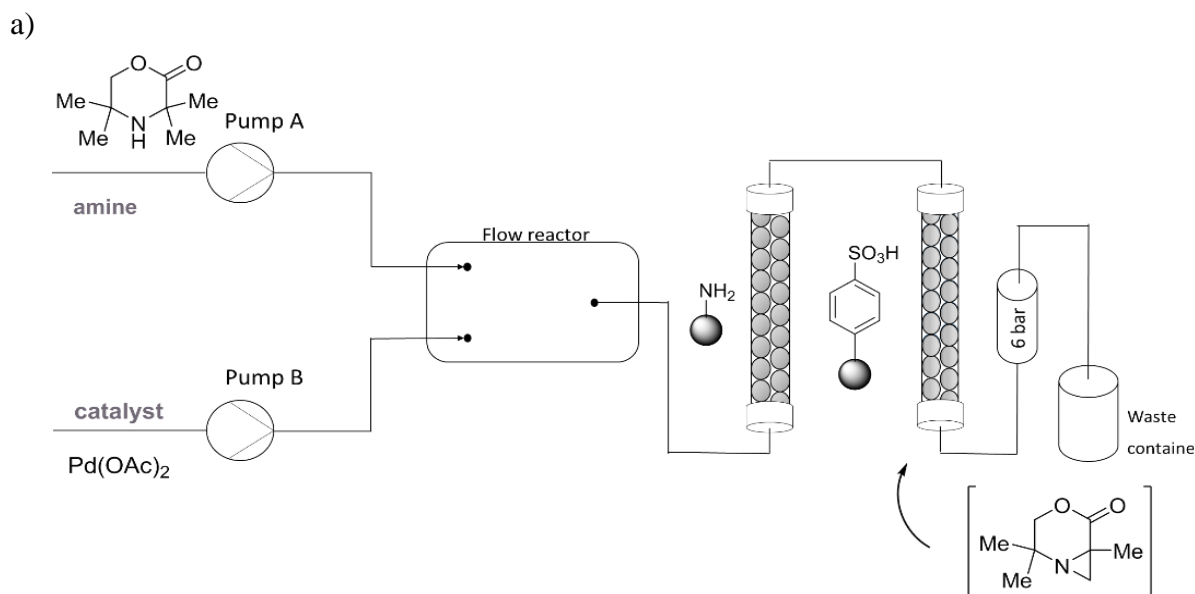
The decision was taken to design a suitable purification system allowing separation of the product and the catalyst of the investigated reaction. Following unsuccessful trials involving bi-phasic extraction using a range of available solvents and crystallisation, where palladium particles "coated" crystals of the product generated upon addition of a solution of hydrochloric acid in dioxane, the decision was taken to use a system of scavenging columns.

The first column, designed to catch the palladium catalyst, could not be filled with the most powerful, acid-based, metal scavengers because they would scavenge both the catalyst and the aziridine product. Nevertheless, it was found that the commercially available QuadraSil AP (with a pendant primary amine) supplied by Johnson Matthey successfully coordinated only to palladium species, thus enabled removal of the catalyst from the spent reaction mixture.

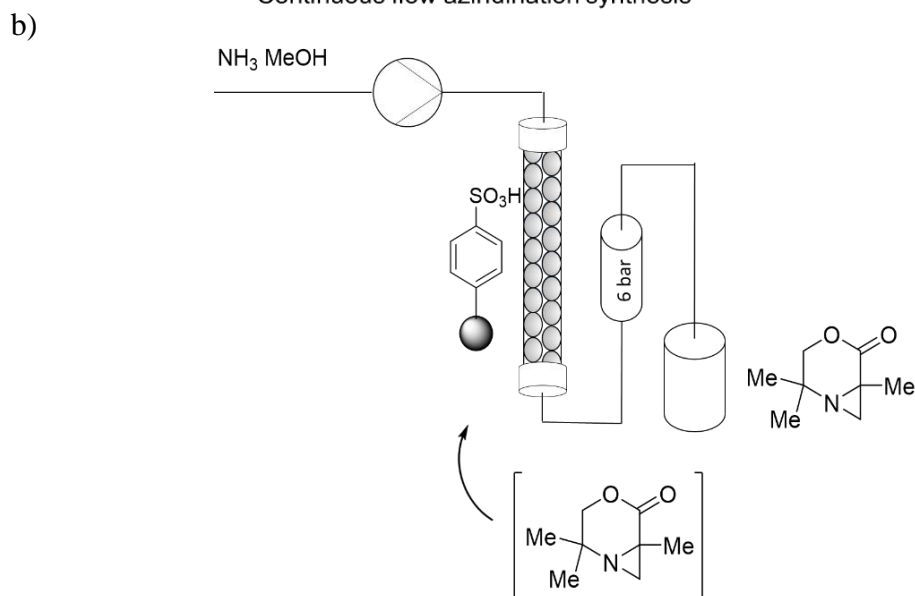
In the second separation step, the amine product could be separated from the reaction mixture using a silica gel functionalized with strongly acidic groups. In this study, the Isolute SCX-3 gel (with pendant sulfonic acid groups) was used as the amine scavenger.

The product can be washed on the gel and subsequently removed by a high pH eluent. Due to experimental practicality, a 4N solution of ammonia in methanol was used. Finally, after evaporation of the solvent, the aziridine product of high purity was collected.

The synthesis was run according to Procedure 4, Chapter 3.1. After exiting the temperature controlled flow reactor, the reaction mixture was passed over the first scavenging column. The reaction mixture leaving the first scavenging column was passed over the second scavenging column, and finally, the spent reaction mixture was passed via a back pressure regulator, setting the system pressure to 6 bar(g), and directed to a waste container, Figure 4.1-10a. To elute the product from the second column, firstly a fresh solvent was passed through the column to elute any residual waste (5 column volumes), and finally, a solution of ammonia in methanol (4N) was passed through the column to neutralise the charge on the gel. A solution of the aziridine product was collected, and upon solvent evaporation, the product of high purity was obtained in 90% yield, Figure 4.1-10b.



## Continuous flow aziridination synthesis



## Releasing of the product from the 'catch' column

Figure 4.1-10 Flow process for the aziridination C–H activation reaction. a) Flow reactor: silicon/glass microfluidic reactor or PFE tubular reactor. The first column separates the catalyst from the spent mixture; the second column separates the product. Reactants were delivered via: pump A (starting material, oxidant, acetic acid), pump B (catalyst, acetic acid, acetic anhydride). A 6 bar pressure regulator was fitted; b) Elution of the product from the “catch” column.

Under the selected set of conditions, a space-time yield of  $0.463 \text{ kg l(reactor)}^{-1} \text{ h}^{-1}$  was achieved. Using the Vapourtec system, allowed synthesis of 4.68 mmol (0.78 g) per hour of the product. The Vapourtec R-Series is designed to operate autonomously and the operational time is only limited by the capacity of the scavenger columns. This limitation can easily be overcome with a setup including two sets of columns: one operational and one in a standby mode. Additionally, thanks to the homogeneity of the mixture and low dependence on mass transfer, the reactor system should prove to be easily scalable giving access to even larger amounts of aziridine products.

#### 4.1.6. Nucleophilic ring opening reaction

To extend the synthetic utility of the continuous-flow C–H activation procedure, the possibility of coupling of the C–H activation step to a subsequent reaction in a single flow process was investigated. It had been previously shown that the aziridine products could be functionalized through ring-opening reactions with various nucleophiles, such as carboxylic acids, azides, thiols, and halogens.<sup>148,215</sup> To further highlight the benefits of translating this batch process into flow, it was aimed to develop a robust procedure suitable for opening aziridines with weak nucleophiles and reagents that could be potentially hazardous when used in batch.

McNally suggested that the ring-opening reaction requires presence of either a strong Brønsted or Lewis acid to activate the aziridine.<sup>148</sup> In the current system, it was questioned whether a strongly acidic scavenging resin might also function as the catalyst for the aziridine ring opening, thereby reducing the number of chemical operations and streamlining the overall transformation.

The final choice of the second column scavenger was preceded by a screening of possible acidic scavengers for activity in the nucleophilic ring opening reaction. The following silica-based gels were tested: QuadraSil<sup>®</sup> MP (3-mercaptopropyl-functionalized silica gel), QuadraSil<sup>®</sup> SA (propyl sulfonic acid functionalized silica), ISOLUTE<sup>®</sup> SCX-3 (ethylbenzene sulfonic acid functionalized silica gel).

From the tested silica gels, QuadraSil<sup>®</sup> SA and ISOLUTE<sup>®</sup> SCX-3 successfully catalysed the nucleophilic ring opening. Gels were tested using 2,2,6-trimethyl-4-oxa-1-azabicyclo[4.1.0]heptan-5-one as the substrate and methanol as the nucleophile. The

scavenger column loaded with the aziridine was heated to 60 °C, and the stream of the nucleophile was pumped for 30 minutes at 0.1 ml min<sup>-1</sup> flowrate. The methodology was tested using three selected weak nucleophiles: water, methanol and *in situ* generated hydrazoic acid. All tested nucleophiles gave high isolated yields ranging from 92% to 72%, Figure 4.1-11. The use of a solid-state support significantly simplified the reaction procedure, minimised the number of purification steps, and shortened the reaction time considerably.

Although several reactions were previously described for the aziridine ring opening in a continuous flow,<sup>216</sup> none have been performed using an immobilisation–activation strategy. High purity of the crude mixture (>95%, <sup>1</sup>H NMR) allows direct transformations of the synthesised amines without any additional treatment. This protocol could be used more generally for the opening of various aziridines through the effective “catch–release” flow process. Furthermore, the otherwise time-consuming and hazardous reactions with hydrazoic acid precursors can be conducted much more safely.

Results of the NMR analysis of all purified molecules can be found in Appendix 3.

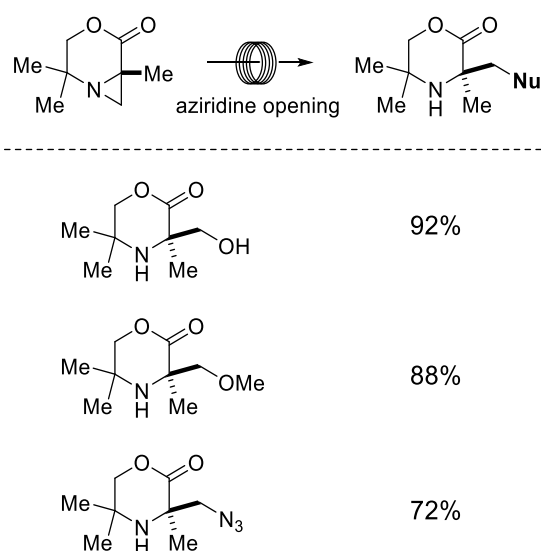
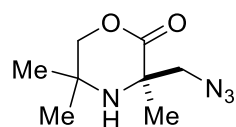


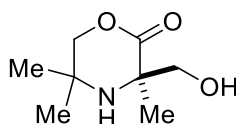
Figure 4.1-11 Tested scope of the nucleophilic ring opening of aziridine product. Yields are given for the isolated compounds.

3-(Azidomethyl)-3,5,5-trimethylmorpholin-2-one; CDCl<sub>3</sub>, 400MHz (<sup>1</sup>H) 100MHz (<sup>13</sup>C)



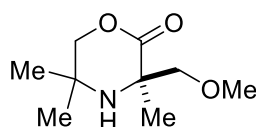
<sup>1</sup>H NMR (400 MHz, CDCl<sub>3</sub>) δ: 4.20 (d, J = 2.0 Hz, 1H, H-1), 4.13 (d, J = 2.0 Hz, 1H, H-1), 3.57 (d, J = 3.0 Hz, 1H, H-6), 3.20 (d, J = 3.0 Hz, 1H, H-6), 1.41 (s, 3H, H-7), 1.23 (s, 3H, H-3/4), 1.19 (s, 3H, H-3/4); <sup>13</sup>C NMR (100 MHz, CDCl<sub>3</sub>) δ: 172.4, 78.0, 60.6, 58.8, 48.9, 27.2, 26.2, 26.0; IR ν<sub>max</sub>/cm<sup>-1</sup>(film): 3332, 2973, 2097, 1728, 1286, 1045; m/z HRMS: (ESI) found [M+H]<sup>+</sup> 199.1186, C<sub>8</sub>H<sub>15</sub>N<sub>4</sub>O requires 199.1190

3-(Hydroxymethyl)-3,5,5-trimethylmorpholin-2-one; CDCl<sub>3</sub>, 400MHz (<sup>1</sup>H) 100MHz (<sup>13</sup>C)



<sup>1</sup>H NMR (400 MHz, CDCl<sub>3</sub>) δ: 4.14 (d, J = 3.0 Hz, 1H, H-1), 4.13 (d, J = 3.0 Hz, 1H, H-1), 3.70 (d, J = 3.0 Hz, 1H, H-6), 3.35 (d, J = 3.0 Hz, 1H, H-6), 1.38 (s, 3H, H-7), 1.24 (s, 3H, H-3/4), 1.17 (s, 3H, H-3/4); <sup>13</sup>C NMR (100 MHz, CDCl<sub>3</sub>) δ: 173.9, 77.6, 69.2, 58.9, 48.9, 26.2, 26.1, 25.6; IR ν<sub>max</sub>/cm<sup>-1</sup>(film): 3313 (br, O-H), 2974, 1721 (C=O), 1284, 1047; m/z HRMS (ESI) found [M+H]<sup>+</sup> 174.1121, C<sub>8</sub>H<sub>16</sub>NO<sub>3</sub> requires 174.1125

3-(Methoxymethyl)-3,5,5-trimethylmorpholin-2-one; CDCl<sub>3</sub>, 400MHz (<sup>1</sup>H) 100MHz (<sup>13</sup>C)



<sup>1</sup>H NMR (400 MHz, CDCl<sub>3</sub>) δ: 4.14 (d, J = 2.0 Hz, 1H, H-1), 4.12 (d, J = 2.0 Hz, 1H, H-1), 3.62 (d, J = 3.0 Hz, 1H, H-6), 3.33 (s, 3H, H-7), 3.21 (d, J = 3.0 Hz, 1H, H-6), 1.33 (s, 3H, H-8), 1.23 (s, 3H, H-3/4), 1.13 (s, 3H, H-3/4); <sup>13</sup>C NMR (100 MHz, CDCl<sub>3</sub>) δ: 173.3, 79.6, 78.5, 59.2, 58.7, 48.5, 26.6, 26.1, 25.1; IR ν<sub>max</sub>/cm<sup>-1</sup>(film): 2970, 1733 (C=O), 1284, 1104, 1049; m/z HRMS (ESI) found [M+H]<sup>+</sup> 188.1279, C<sub>8</sub>H<sub>16</sub>NO<sub>3</sub> requires 188.1281

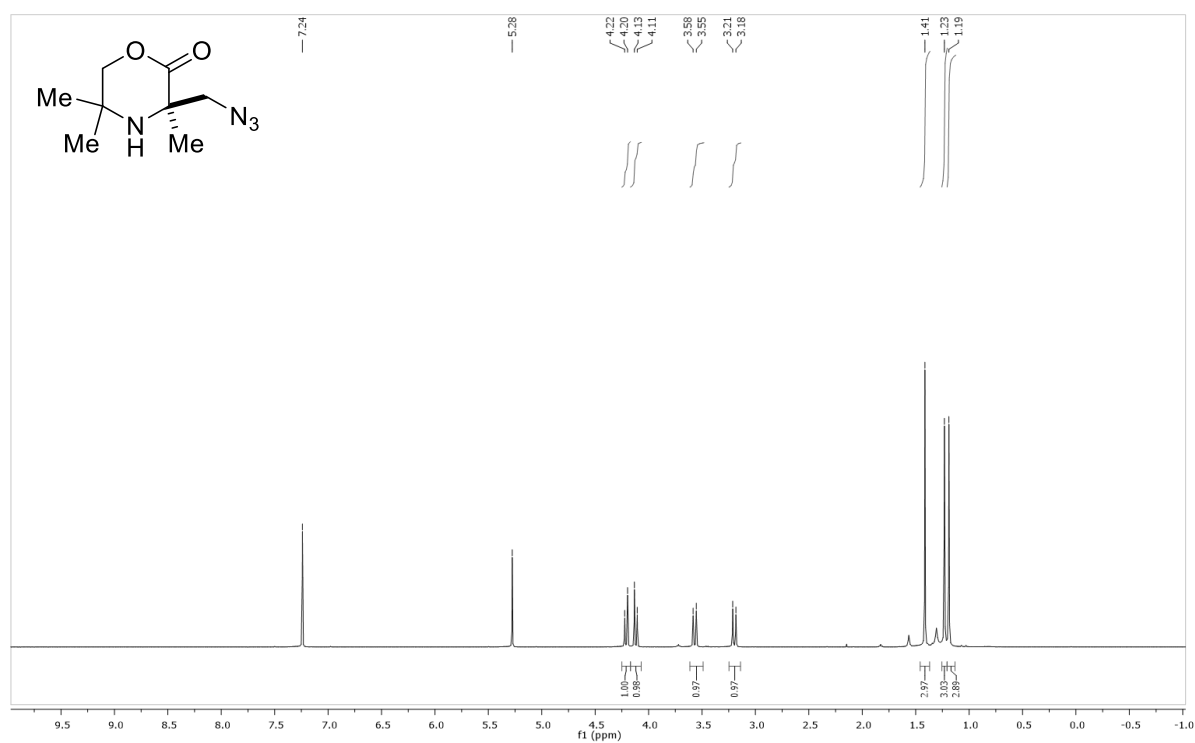


Figure 4.1-12.  $^1\text{H}$  NMR ( $\text{CDCl}_3$ , 400 MHz) 3-(Azidomethyl)-3,5,5-trimethylmorpholin-2-one

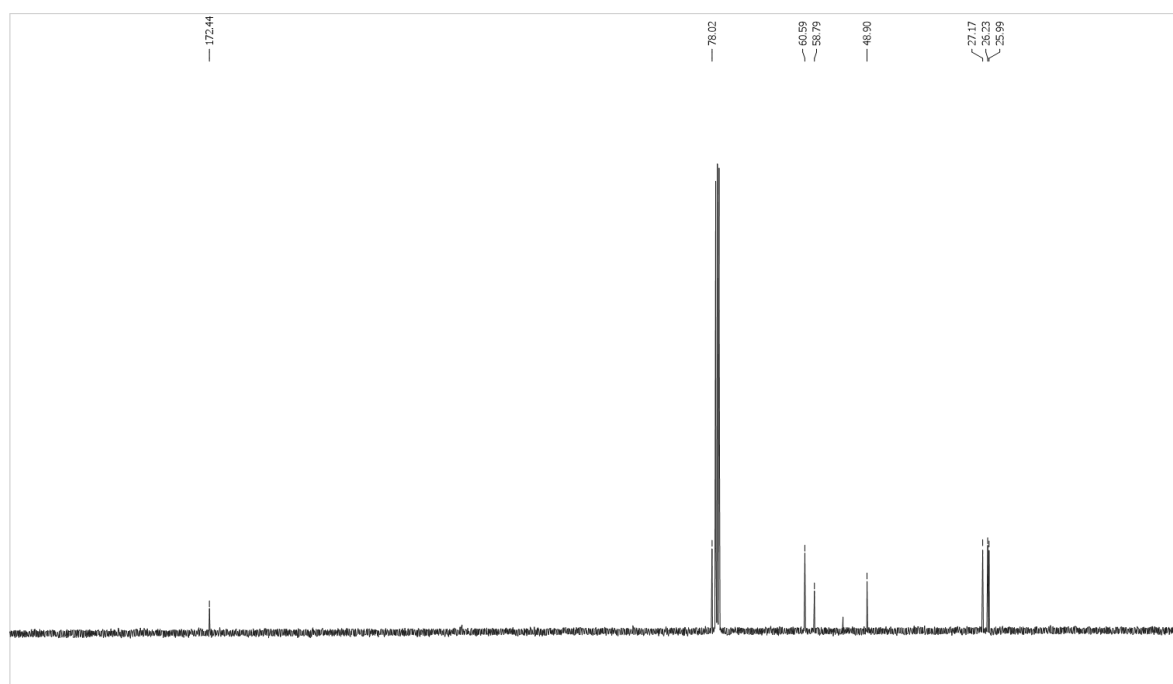


Figure 4.1-13.  $^{13}\text{C}$  NMR ( $\text{CDCl}_3$ , 100 MHz) 3-(Azidomethyl)-3,5,5-trimethylmorpholin-2-one

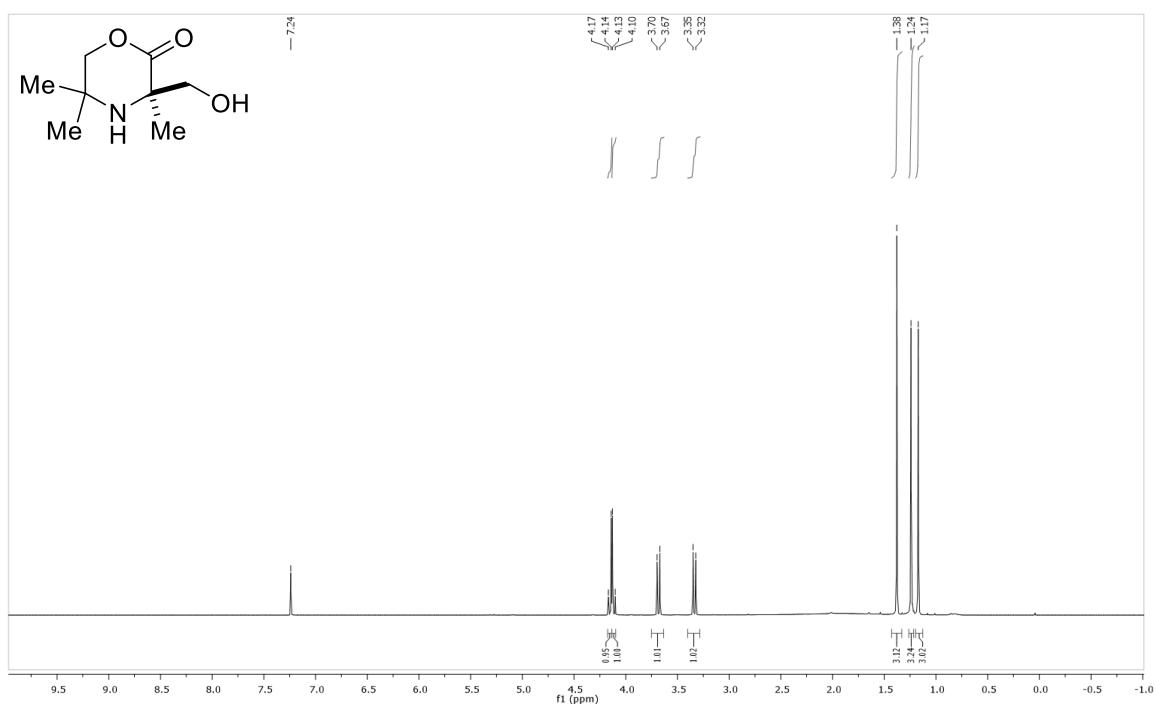


Figure 4.1-14. <sup>1</sup>H NMR (CDCl<sub>3</sub>, 400 MHz) 3-(Hydroxymethyl)-3,5,5-trimethylmorpholin-2-one

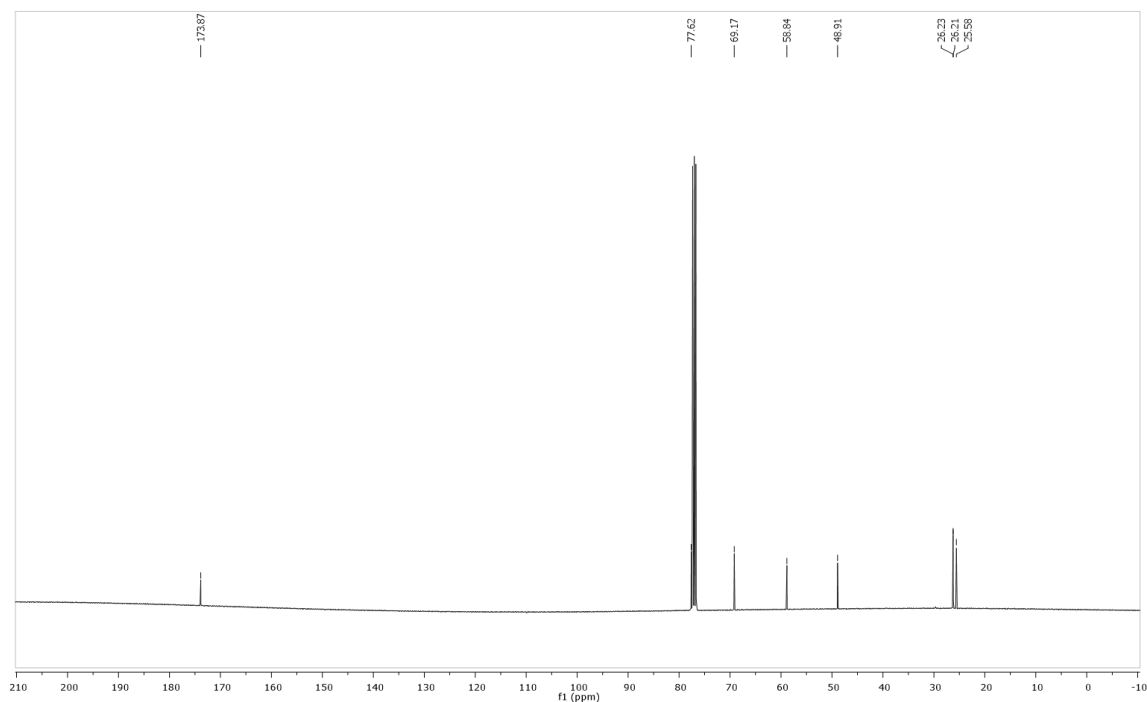


Figure 4.1-15. <sup>13</sup>C NMR (CDCl<sub>3</sub>, 100 MHz) 3-(Hydroxymethyl)-3,5,5-trimethylmorpholin-2-one

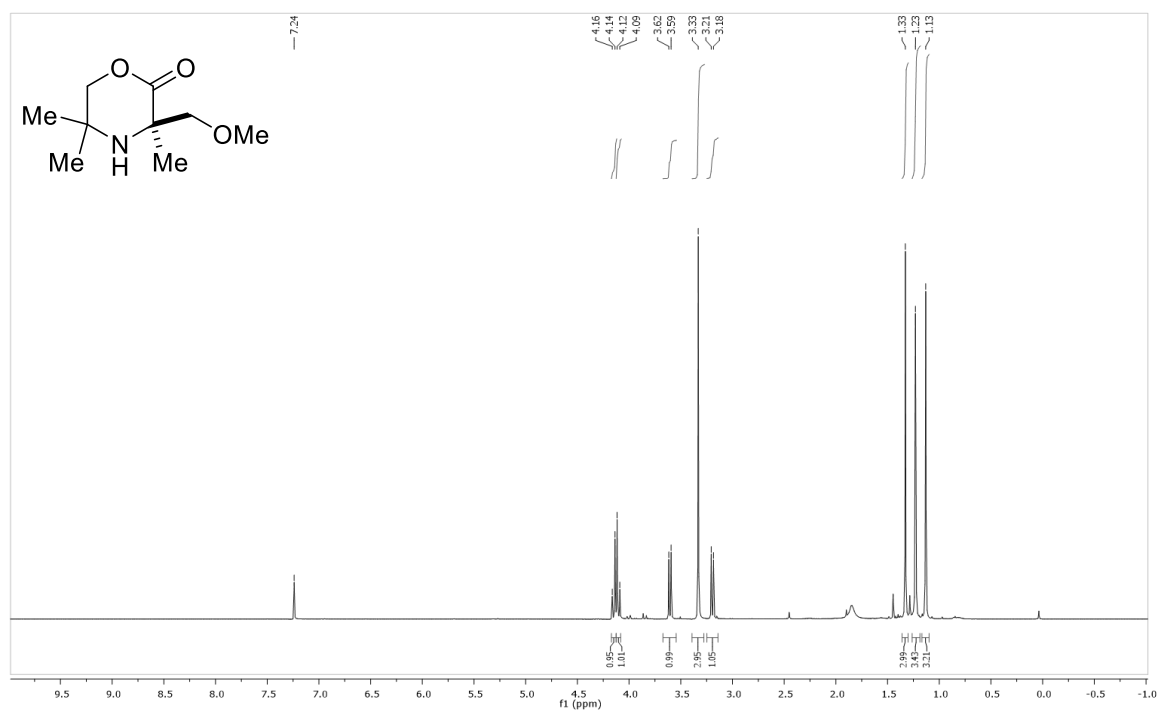


Figure 4.1-16.  $^1\text{H NMR}$  (CDCl<sub>3</sub>, 400 MHz) 3-(Methoxymethyl)-3,5,5-trimethylmorpholin-2-one

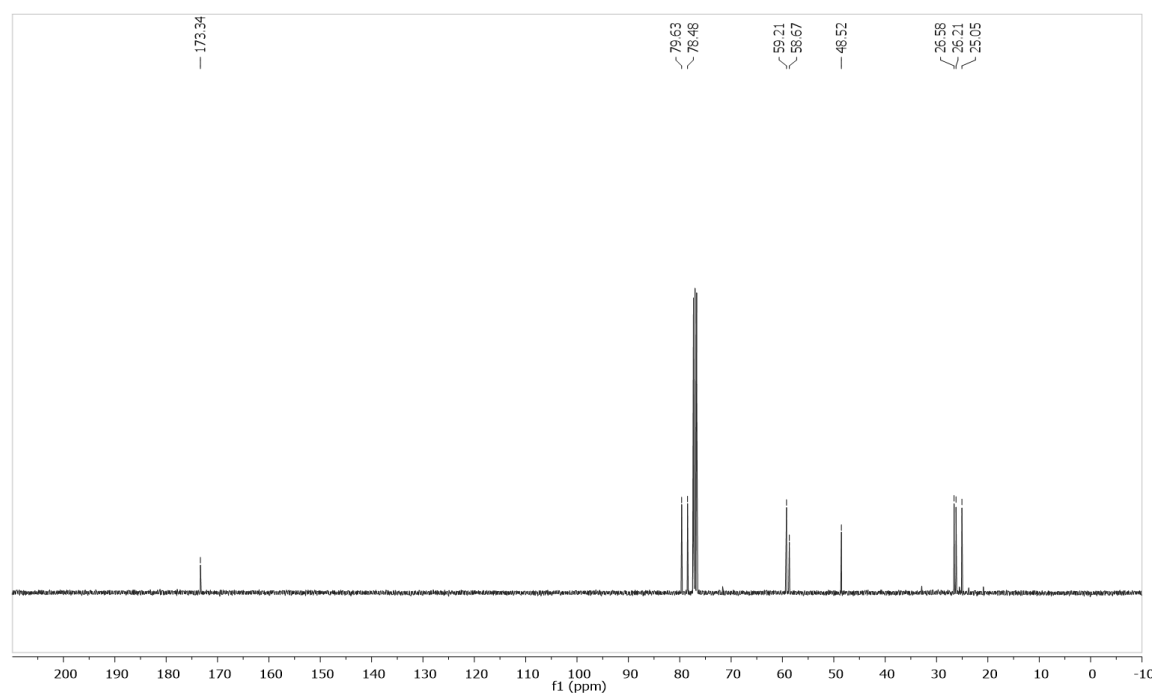


Figure 4.1-17.  $^{13}\text{C NMR}$  (CDCl<sub>3</sub>, 100 MHz) 3-(Methoxymethyl)-3,5,5-trimethylmorpholin-2-one

### 4.1.7. Discussion

The developed thorough mechanistic and kinetic understanding was used to design a continuous flow process for the investigated reaction. Thanks to the explanation of the role of acetic acid, not only a complete understanding of the mechanism was built, but also a convenient way of process intensification, through the introduction of a second off-cycle intermediate, was discovered.

The mechanistic and kinetic studies revealed an obstacle inherent to palladium catalysed C–H activation of amines. The presence of a stable *bis*-amine intermediate results in low observed reaction rates and, in certain cases, can preclude the reactivity. The search for ways to destabilise this complex revealed that one could generate a second off-cycle intermediate in order to inhibit formation of the *bis*-amine complex kinetically. Even though this solution may not be versatile, especially for reactions incompatible with an acidic environment, it may prove to be useful for a cost-effective process intensification of this family of reactions. The choice of acid may play a crucial role here. In the presented case, acetic acid was strong enough to generate a stable salt of the morpholinone; other substrates may require acids of a different pKa.

Additionally, a slightly acidic environment allowed increasing the maximum turnover number (TON) from initial 20 to nearly 200. This increase, achieved without using expensive ligands, can also be applicable to a range of similar processes and can help in further reduction of the environmental impact of palladium-catalysed processes.

Despite being experimentally expensive, building a full mechanistic model provides the most process knowledge. Thus, it lowers the uncertainty of designed processes. After assuring that the reaction is performed in a strictly kinetically controlled regime, a set of experiments was used to estimate model parameters. Analysis of the estimation revealed that the obtained parameters are statistically significant and, additionally, the values of activation energies are in a rather good agreement with the energies obtained during DFT modelling.

The predictive model should be applicable also to conditions where the model has not been previously tested. This was demonstrated via the semi-batch experiments. Finally, being in possession of the detailed understanding of the mechanism and the kinetics of the reaction allowed a rapid *in silico* search for optimal process conditions, Figure 4.1-18.

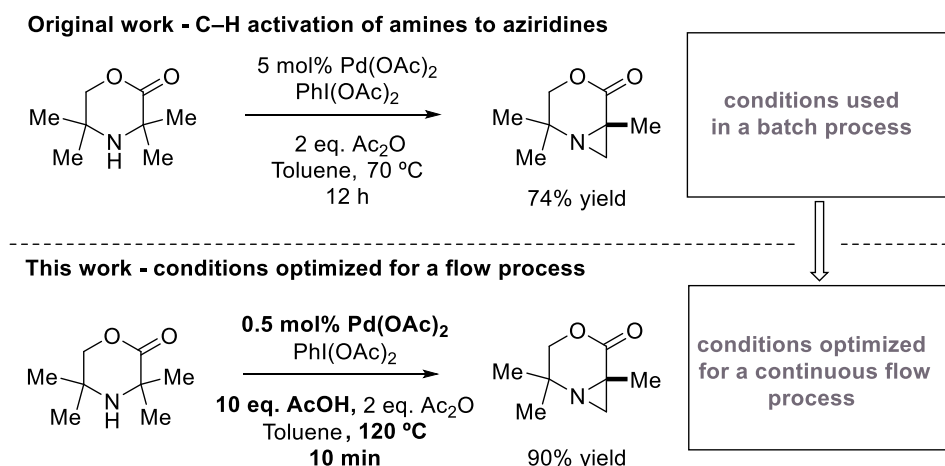


Figure 4.1-18 Development of the continuous process for the aziridination reaction.

The conditions optimised for a continuous process allowed not only reduction of the catalyst loading by a factor of 10, but also, shortened the time necessary to achieve full conversion from initial 12 h to 10 min. Furthermore, the yield of the reaction increased to a level close to the stoichiometric conversion. The applied conditions resulted in full consumption of the starting material. The inevitable ullage of the material is presumably due to thermal decomposition of the starting material and losses during purification.

The comparison of the experimental cost of the full deconvolution of the process complexity and the black box approach demonstrated the utility of statistical tools in the search for suitable conditions to run the process. Without building any process knowledge, it was shown that one could reduce the experimental cost drastically. In the presented case, 11 points have been used in contrast to approximately 400 measurements for the detailed mechanistic studies what gives almost 37 times faster optimisation. However, it would not be possible without possessing a thorough understanding of the process. Purely statistical tools would not discover that addition of acetic acid can accelerate the reaction. Thus, the optimisation would be limited to the space of possible conditions similar to the ones described by McNally.<sup>148</sup> Nevertheless, this methodology demonstrated its utility as an inexpensive and rapid tool for search of suitable conditions to run the process.

The design of the reactor system by a choice of an appropriate reactor and coupling it with a purification method was practised. Due to the homogeneous nature of the reaction, the selection of the reactor was greatly simplified and mostly concerned the scale of the process by choice of a suitable volume. On the micro-scale, a 240  $\mu$ l silicon/glass microreactor was

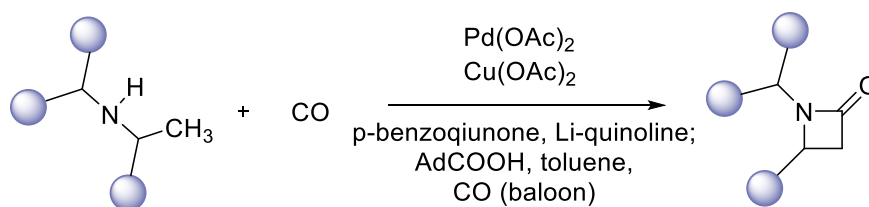
used. A realisation of the meso-scale was achieved in a commercially available 10 ml tubular PFE reactor supplied by Vapourtec. If required, a further scale-up or scale-down should be easily achieved by changing the reactor volume.

Since the process uses an expensive palladium catalyst, the decision was taken to separate, and if possible also recycle it. The efficient separation of the catalyst and the product of the reaction was achieved by employing a set of scavenging columns, from which the first one separated the palladium species from the reaction mixture, and the second one, under operational conditions, caught only the product. A convenient elution protocol allows a rapid and efficient collection of a high purity product and the spent catalyst.

It was also questioned whether a strongly acidic silica gel could act as an efficient catalyst for a nucleophilic ring opening reaction. It was demonstrated that it could be easily achieved using sulfonic acids and the utility of this protocol was tested using weak nucleophiles. Up to the author's best knowledge, this is the first continuous process for the aziridine ring opening reaction using a solid supported substrate and one of the first C–H activation processes in flow. The designed process should be applicable to a wide range of processes characterised by similar conditions and can aid in more efficient and faster process design for C–H activation reactions. Additionally, telescoping of consecutive reactions allows reduction in the number of purification steps. This can not only minimise the environmental impact and the cost of the whole process but also allow decreasing the footprint of the setup.

## 4.2. $\beta$ -C–H carbonylation of aliphatic amines to $\beta$ -lactams

The recently published by Willcox and Chappell et al.<sup>203</sup> process gives an easy access to the  $\beta$ -lactam feature via a C(sp<sup>3</sup>)–H oxidative carbonylation of secondary amines (Scheme 4.2-1). The use of readily available, unprotected amines combined with a wide range of tolerated functional groups can find broad applications in organic synthesis. The utility of this reaction in the late-stage functionalisation of complex molecules has been demonstrated in the original study; a selection of pharmaceutical derivatives and biologically active molecules was successfully carbonylated using the described protocol, giving high yields and selectivity towards  $\beta$ -lactams.<sup>203</sup>



*Scheme 4.2-1  $\beta$ -C–H carbonylation of aliphatic amines to  $\beta$ -lactams. AdCOOH = 1-adamantanecarboxylic acid. Conditions: 10 mol% Pd(OAc)<sub>2</sub>, 10 mol% Cu(OAc)<sub>2</sub>, 1 eq p-benzoquinone, 30 mol% AdCOOH, 10 mol% Li-quinoline, PhMe, 120 °C, 12 h.*

Notwithstanding its broad scope and wide applicability, the process suffers from the inefficiencies typical to oxidative carbonylations, see Chapter 2.3.2.

To extend the utility of the discovered reaction, further studies of the kinetics and the mechanism of the process were required. Based on a deeper mechanistic understanding and process intensification, a scalable process could be designed.

### 4.2.1. Kinetic investigation

Despite extensive DFT studies performed by Willcox and Chappell et al.,<sup>203</sup> it was not possible to use them to build a detailed kinetic model due to inability to measure concentrations of intermediates.

The reaction involves three phases. Hence, the intrinsic chemical kinetics may be affected by a number of possible physical processes, such as interphase mass transport, solubility, mixing and so on, which would affect the observed activation energy. Therefore, a model that describes the combination of the chemical and physical processes is required to describe this reaction correctly.

Table 4.2-1 Standard conditions used for carbonylation experiments.

Substrate ( <i>N</i> -Cyclohexylisopropylamine)	0.05 mol dm <sup>-3</sup>
Pd(OAc) <sub>2</sub>	0.005 mol dm <sup>-3</sup> (10 mol%)
Cu(OAc) <sub>2</sub>	0.005 mol dm <sup>-3</sup> (10 mol%)
p-benzoquinone	0.075 mol dm <sup>-3</sup> (150 mol%)
AdCOOH	0.015 mol dm <sup>-3</sup> (30 mol%)
Li-quinoline	0.004 mol dm <sup>-3</sup> (10 mol%)
Toluene	10 ml
CO / Air 6.25% v/v	10 bar(g)
Temperature	120 °C
Agitation rate	300 RPM (2 cm cross-shaped magnetic bar)

The investigations began by an attempt of estimation of mass transfer between the gas and the liquid phase by *in situ* measurement of the dissolved CO using ATR mid-FTIR spectroscopy. This analytical technique proved to be successful in the previous studies.<sup>176</sup> However, due to the elevated temperature, the IR signal was too weak for the quantitative analysis even at elevated pressures of up to 20 bar(g). If the liquid phase CO concentration is unknown, it is more challenging to ensure that the reaction is performed strictly under the kinetic control regime. Thus, only an apparent rate of the reaction, being a cumulative function of both, the chemical and the physical processes taking place in the system, can

be estimated. Such understanding does not allow an *in silico* search for optimal conditions, because the observed behaviour may be valid only within the tested range of conditions.

Owing to an inability to measure gas-liquid mass transfer, it was necessary to reduce the complexity of the kinetic model. Studies were performed using the Reaction Progress Kinetic Analysis<sup>40</sup> that allowed investigation of the apparent orders of the influence of separate reaction species. Notably, due to an inability to ensure that the experiments were performed under strict kinetic control, the obtained orders may not represent the true mechanism. The observed behaviour may be a result of a mass transfer limitation, a starvation of the process of one of the reactants or an interplay of both. Thus, no conclusions may be drawn from the kinetic studies until the activation energies are estimated. Small values of the activation energies may suggest that the observed behaviour is due to the physical limitations of the system.

In previous studies of a similar system, formation of a catalytically inactive bis-amine-palladium complex, being a product of coordination of two molecules of the starting material to the palladium catalyst, was observed.<sup>150,217</sup> Formation of this off-cycle intermediate results in a negative order influence of the concentration of the starting material on the apparent reaction rate. Since in the currently investigated process, formation of the bis-amine-palladium complex is also possible, a similar behaviour was anticipated. As expected, the concentration of the starting material proved to have an apparent negative order, Figure 4.2-1.

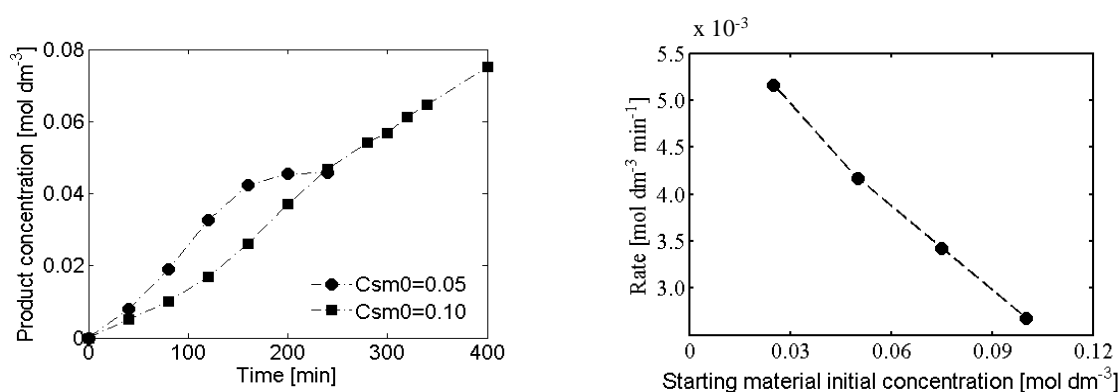


Figure 4.2-1. Influence of the concentration of the starting material on the observed reaction rate for standard conditions. Trend lines added for the convenience of the eye.  $C_{sm0}$ : initial concentration of starting material.  $p=7$  bar(g).

The influence of the concentration of the palladium catalyst on the reaction rate shows a complex behaviour. The increase from 5 to 10 mol% caused acceleration of the reaction. However, the acceleration was significantly smaller than expected, Figure 4.2-2. A further increase in the catalyst concentration did not bring any substantial change in the reaction rate. This behaviour could be explained by a mass transfer related limitation, most likely due to either the low solubility or insufficient flux of carbon monoxide to the liquid phase. Should this hypothesis be true, an increase in CO partial pressure should result in an increase in the observed reaction rate.

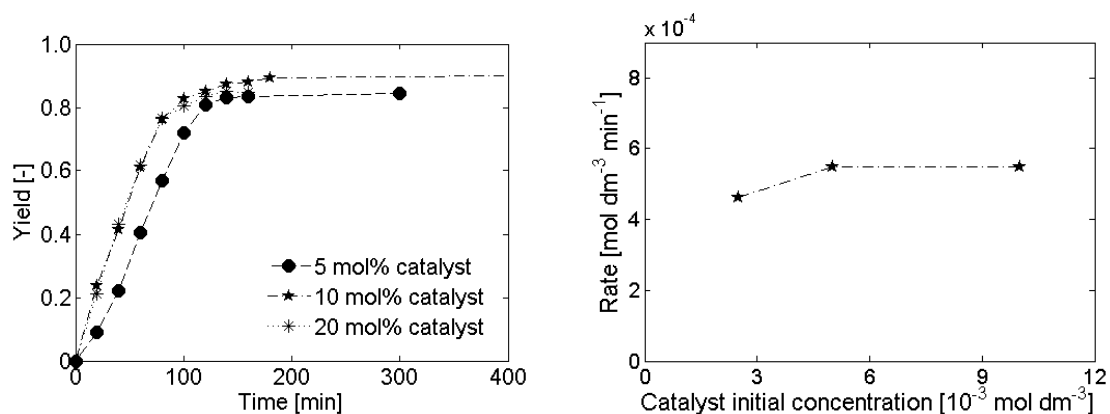


Figure 4.2-2. Influence of the catalyst loading on the observed reaction rate for standard conditions. Trend lines added for the convenience of the eye.

Investigating the influence of pressure, it was observed that an increase in pressure not only increased the reaction rate, but also resulted in higher yields, Figure 4.2-3. The positive trend reversed at around 12 bar(g), where a significant decrease of the yield was noticed, presumably owing to the strongly reductive nature of carbon monoxide that potentially can reduce  $\text{Pd}^{\text{II}}$  to  $\text{Pd}^0$ .  $\text{Pd}^0$  upon precipitation and aggregation forms so-called palladium black.

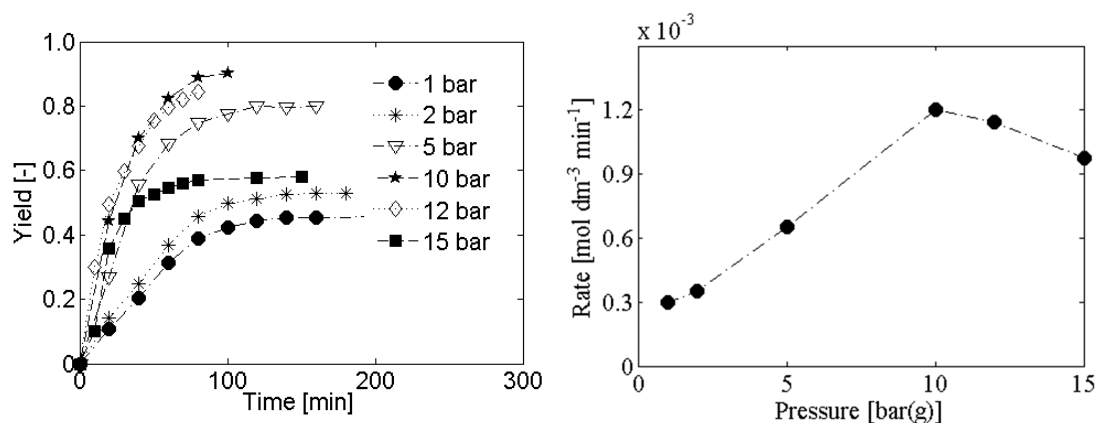


Figure 4.2-3. Influence of the gauge pressure of 6.25% CO balanced by air v/v on the observed reaction rate for standard conditions. Trend lines added for the convenience of the eye.

Increasing the total pressure simultaneously increases the oxygen partial pressure and, hence, the concentration of the dissolved oxygen. This could, potentially, accelerate the oxygen-copper-palladium redox cycle and thus, increase the apparent reaction rate. To exclude this possibility, several experiments varying the concentration of copper (II) acetate using the same partial pressure of oxygen were conducted. There was no increase in the observed reaction rate, Figure 4.2-4. Hence, it was concluded that the re-oxidation of palladium is not a turnover-limiting step.

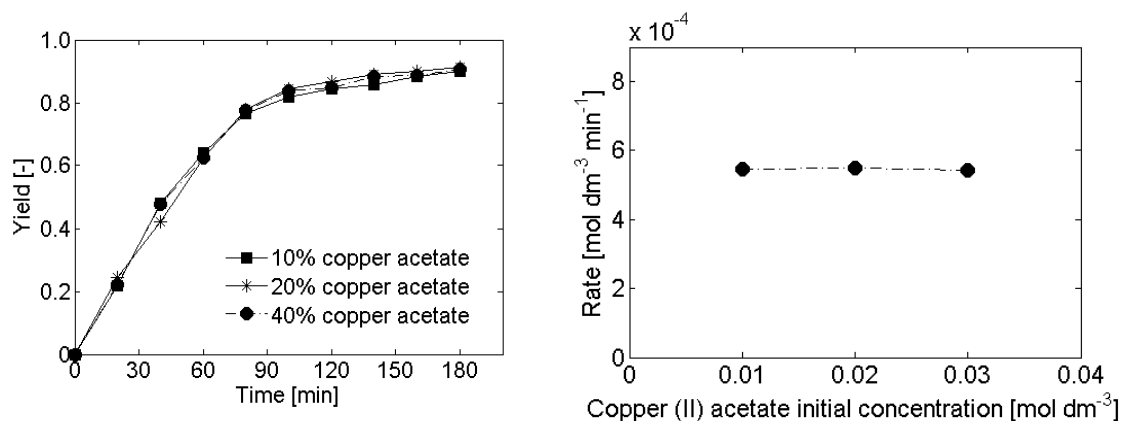


Figure 4.2-4. Influence of the concentration of copper acetate on the observed reaction rate for standard conditions. Trend lines added for the convenience of the eye.

The presence of 5 mol% of the ligand, Li-quinoline, elevated the yield of the reaction by more than 20%. The further increase in Li-quinoline concentration did not supplementary improve the yield, Figure 4.2-5. The rate is zero-order with respect to the ligand. Similarly, 1,4-benzoquinone, that was required in the concentration slightly higher than the stoichiometric amount to achieve the highest yields, proved to have no influence on the rate of the reaction, Figure 4.2-6. This suggests that both, Li-quinoline and p-benzoquinone, enter the catalytic cycle after the turnover-limiting step. Thus, can be omitted in setting up the kinetic model. When testing the effects of 1-adamantane carboxylic acid, it was observed that it had an initially positive influence on both the yield and the reaction rate. At the concentration higher than double of the concentration of the catalyst, the trend has reversed and the yield as well as the rate decreased, Figure 4.2-7.

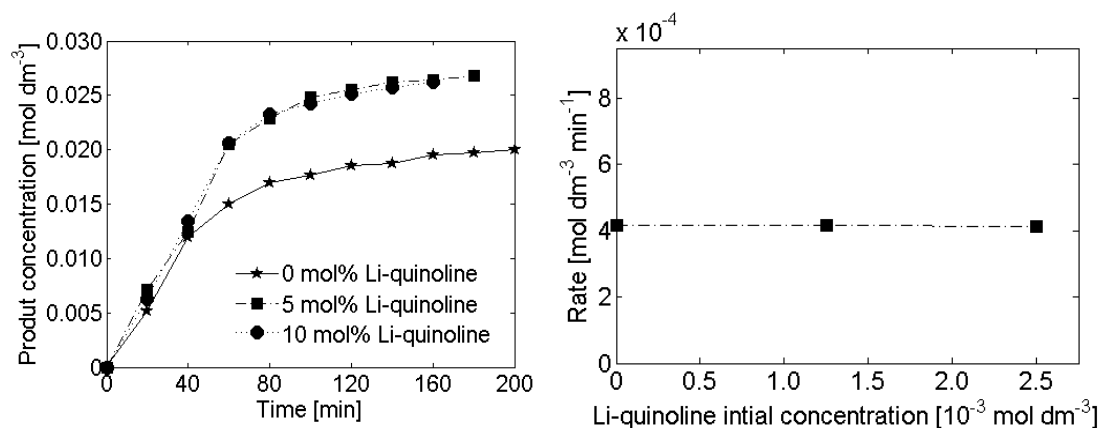


Figure 4.2-5. Influence of the concentration of Li-quinoline on the observed reaction rate for standard conditions. Trend lines added for the convenience of the eye.  $p=7$  bar(g).

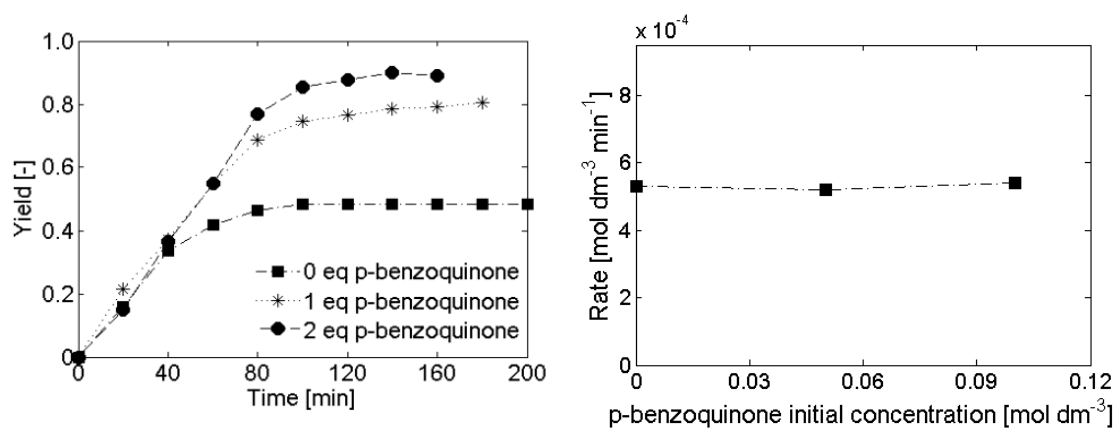


Figure 4.2-6. Influence of the concentration of *p*-benzoquinone on the observed reaction rate for standard conditions. Trend lines added for the convenience of the eye.

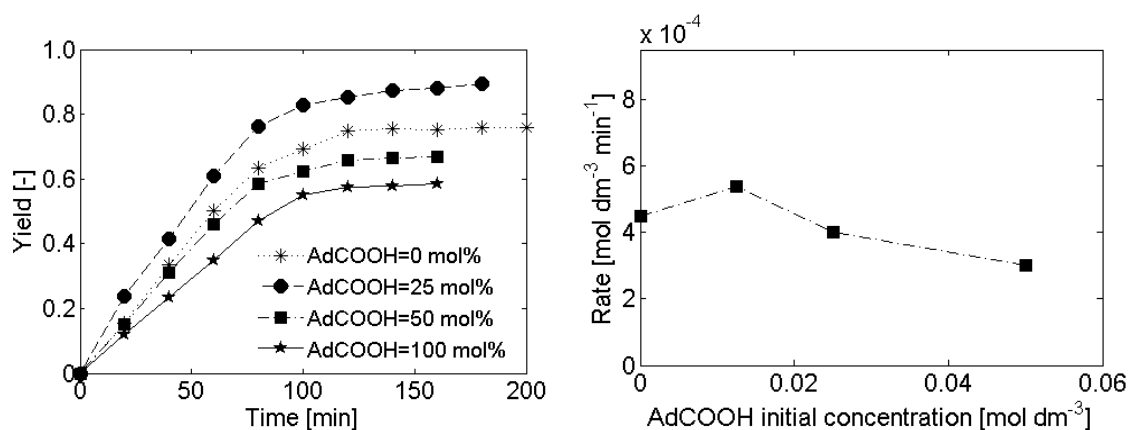


Figure 4.2-7. Influence of the concentration of 1-adamantanecarboxylic acid on the observed reaction rate for standard conditions. Trend lines added for the convenience of the eye.

Based on the deconvolution of the orders of the influence of the species used in the reaction on the observed reaction rate, Table 4.2-2, the simplified catalytic cycle was proposed, see Figure 4.2-8.

Table 4.2-2 A summary of the influence of the substrates on the observed reaction rate and their use in setting up a kinetic model.

Compound	Order of the influence	Used in the model as
Substrate	Negative	Variable
Pd(OAc) <sub>2</sub>	Positive	Variable
Cu(OAc) <sub>2</sub>	Zero	Constant
AdCOOH	Negative	Constant
Li-quinoline	Zero	Constant
Pressure	Positive	Variable

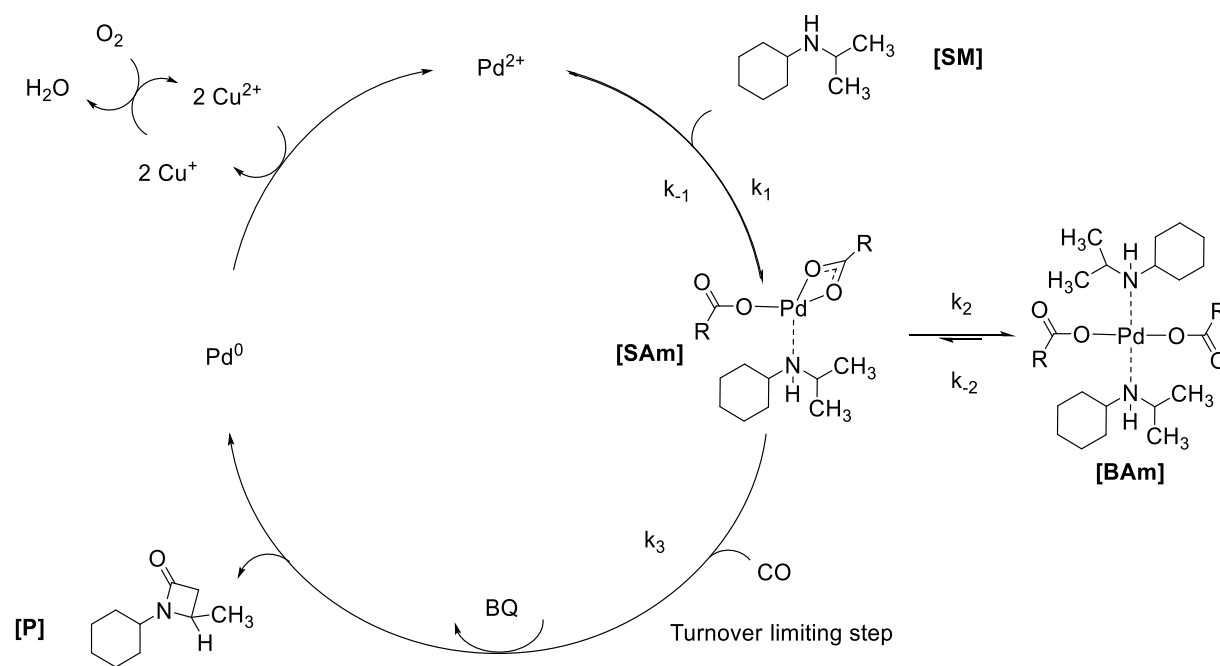


Figure 4.2-8 Proposed, simplified catalytic cycle. Ad- denotes adamantane.

The mass balance of palladium species can be written in the form of Equation ( 51 ).

$$[Pd]_{total} = [Pd^{2+}] + [SAm] + [BAm] \quad (51)$$

Assuming a quasi-steady state, the off- and on-cycle equilibria can be expressed as Equations ( 52 ) and ( 53 ).

$$k_{-1} [SAm] = k_1 [Pd^{2+}] [SM] \quad (52)$$

$$k_2 [SAm] [SM] = k_{-2} [BAm] \quad (53)$$

Thus:

$$[Pd]_{total} = [SAm] \left[ \frac{k_{-1}}{k_1 [SM]} + 1 + \frac{k_2 [SM]}{k_{-2}} \right] \quad (54)$$

Then, the reaction rate can be written in the form of Equation ( 55 )

$$rate = \frac{d[P]}{dt} = k_3 [SAm] [CO] = \frac{k_3 [CO] [Pd]_{total}}{1 + \frac{k_{-1}}{k_1 [SM]} + \frac{k_2}{k_{-2}} [SM]} \quad (55)$$

alternatively, Equation ( 56 ).

$$rate = \frac{k_3 [CO] [Pd]_{total}}{1 + \frac{a}{[SM]} + b [SM]} \quad (56)$$

where:

$$a = \frac{k_{-1}}{k_1} \quad (57)$$

$$b = \frac{k_2}{k_{-2}} \quad (58)$$

Additionally, using GC/MS analysis, a by-product of the reaction was identified. Analysis of the fragmentation pattern suggested the formation of an acetylated *N*-cyclohexylisopropylamine, Figure 4.2-9. Comparison of the signal from the reaction mixture with a sample of pure *N*-cyclohexyl-*N*-isopropylacetamide confirmed this hypothesis.

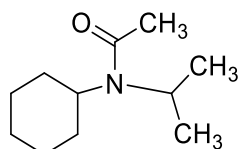


Figure 4.2-9 By-product of the  $\beta$ -C–H carbonylation reaction: *N*-cyclohexyl-*N*-isopropylacetamide.

The experiments performed to investigate the orders of the influence of species taking part in the reaction on the observed reaction rate were used in the parameter estimation using gPROMS<sup>®</sup> Model Builder 4.0.0.<sup>212</sup> The parameters were estimated using the simplified model, Figure 4.2-8 and Equation ( 56 ), for both the product and the by-product of the reaction. Due to lack of reliable data for Henry's law coefficient for carbon monoxide in toluene, the concentration of CO was replaced by pressure in setting up the model. Initially the parameters were estimated for a single temperature (120 °C), and finally, additional experiments, where the temperature was varied, were used to estimate the activation energies. To minimise the number of parameters to estimate, a re-parametrised version of the Arrhenius equation was used, Equation ( 59 ).

$$k = k_{ref} \exp \left[ \frac{Ea}{R} \left( \frac{1}{T} - \frac{1}{T_{ref}} \right) \right] \quad (59)$$

where  $k_{ref}$  is the value of the parameter estimated for the reference temperature ( $T_{ref}$ ); in this specific case 120 °C.

Table 4.2-3 Results of parameter estimation for 120 °C for the simplified mechanism of the carbonylation reaction.

Model parameter	Final value	Initial guess	Confidence interval			95% t-value	Standard deviation
			90%	95%	99%		
k <sub>3P</sub>	894.70	500	27.42	32.71	43.16	2.59	16.58
a <sub>P</sub>	0.072	10	0.033	0.039	0.052	1.607	0.0201
b <sub>P</sub>	0.0011	10	3.34×10 <sup>-5</sup>	3.99×10 <sup>-5</sup>	5.26×10 <sup>-5</sup>	10.079	2.021×10 <sup>-5</sup>
k <sub>3BP</sub>	0.057	1	0.025	0.34	0.044	1.26	0.17
a <sub>BP</sub>	0	1	-	-	-	-	-
a <sub>BP</sub>	0	1	-	-	-	-	-

Reference t-value (95%): 1.65

Table 4.2-4 Correlation matrix for experiments at 120 °C for the carbonylation reaction.

Parameter	$k_{3p}$	$a_p$	$b_p$	$k_{3BP}$
$k_{3p}$	1			
$a_p$	0.996	1		
$b_p$	0.985	0.954	1	
$k_{3BP}$	0.163	0.131	0.201	1

Due to large correlations, Table 4.2-4, it was impossible to estimate the values of the parameters independently. Additionally, for parameters  $a_p$  and  $k_{3BP}$  the t-value was lower than the reference t-value, meaning that the parameter estimation in these cases was not statistically significant, Table 4.2-3.

Because of the large correlations, the number of parameters was reduced, and the rate equation was brought to the form of Equation ( 60 ). Following that, the estimation was repeated.

$$rate = k_3[CO][Pd]_{total} \quad ( 60 )$$

The new model proved to be statistically significant, Table 2.1-1 and Table 4.2-7. Despite its simplicity, the model fitted the reaction rather well (the weighted residual was smaller than  $\chi^2$  value for 95% confidence). Following the estimation of parameters for 120 °C, further experiments were designed to estimate the activation energies. The following temperatures were used: 100 °C, 130 °C, 140 °C and 150 °C.

Table 4.2-5 Results of parameter estimation for 120 °C for the reduced model for simplified mechanism of the carbonylation reaction.

Model parameter	Final value	Initial guess	Confidence interval			Standard deviation
			90%	95%	99%	
k <sub>3p</sub>	792.021	0	27.43	35.31	47.68	17.23
k <sub>3bp</sub>	0.057	0	0.0045	0.0053	0.0071	0.0027

Reference t-value (95%): 1.65

Table 4.2-6 Results of parameter estimation for the reduced model for simplified mechanism of the carbonylation reaction

Model parameter	Final value	Initial guess	Confidence interval			Standard deviation
			90%	95%	99%	
E <sub>ap</sub>	5.011	0	1.11	1.32	1.74	0.67
E <sub>abp</sub>	3.048	0	6.67	7.96	10.50	4.042

Reference t-value (95%): 1.65

Table 4.2-7 Correlation matrix for the simplified mechanism for the carbonylation reaction for 120 °C.

Parameter	$a_p$	$a_{BP}$
$a_p$	1	
$a_{BP}$	0.173	1

Table 4.2-8 Correlation matrix for the simplified mechanism for the carbonylation reaction.

Parameter	$E_{a_p}$	$E_{a_{BP}}$
$E_{a_p}$	1	
$E_{a_{BP}}$	0.0928	1

The estimation of the activation energies yielded a set of parameters that described the system rather well (the weighted residual was smaller than  $\chi^2$  value for 95% confidence), Table 4.2-6 and Table 4.2-8. The reference t-value for the activation energy of the by-product formation was significantly larger than the t-value of the estimation suggesting that the number of experiments used for the parameter estimation was too small to estimate this parameter precisely. This may be caused by the rather small concentration of the by-product formed under operating conditions, being usually in the range of  $10^{-4}$  mol dm<sup>-3</sup>.

The estimation of the activation energy gave a very low value, Table 4.2-6, which, combined with the apparent zero orders of the influence of several reaction species on the reaction rate, suggests that the reaction is starved of one of the reactants. The positive order influence of the partial pressure of CO on the apparent reaction rate means that the limiting factor is the delivery and the equilibrium concentration of CO in the liquid phase. Thus, it was not possible to use the developed kinetic expression to build a predictive model. Hence, it was impossible to perform an *in silico* process design.

To further test the hypothesis of CO starvation, several solvents were selected for a closer investigation. Should the hypothesis of CO starvation be true, in the absence of other possible influences of a solvent change on the catalytic reaction, the solvents characterised by a lower solubility of CO would result in a slower reaction. Due to lack of reliable literature data on Henry's law coefficients for CO in standard organic solvents, an *a priori* thermodynamic method implemented in COSMOtherm was used to predict them.<sup>218</sup>

Furthermore, the decision was taken to test solvents for which a good performance in other carbonylation processes was reported in the literature and to avoid environmentally poor ones. From the selected solvents, only toluene, xylene and esters gave measurable reactivity, Table 4.2-9. DMF, DMSO and MeCN presumably coordinated to Pd<sup>II</sup> species forming kinetically stable complexes. Thus, prohibited the reaction. The reaction in ethyl acetate was slower than the reaction in toluene, which is consistent with the predicted CO solubility in EtOAc being significantly lower than the one in toluene. The greater apparent reaction rate in toluene further supports the hypothesis that the reaction was starved of CO.

*Table 4.2-9 Henry's law coefficients predicted by COSMOtherm at 150 °C.*

Solvent	Henry's law coefficient [bar]	Observed reactivity
Toluene	<b>891.98</b>	<b>yes</b>
p-Xylene	858.35	<b>yes</b>
Acetonitrile	1874.21	no
Ethyl acetate	<b>1255.90</b>	<b>yes</b>
Isopropyl acetate	1135.65	<b>yes</b>
THF	1193.10	no
DMF	1391.02	no
DMSO	1776.34	no

Starvation of the reaction of CO may be the reason of severe inefficiencies of oxidative carbonylation processes performed at ambient pressure since even at the elevated pressure the reaction is CO-limited. The apparent reaction rate of the investigated carbonylation reaction reached a maximum at approximately 10 bar total pressure, and a further increase of pressure resulted in the decrease of the yield. This observation allowed to establish the optimal pressure/concentration of CO to run the process. Based on the available heuristics a set of optimal conditions was identified, Table 4.2-10.

Table 4.2-10. Standard conditions used in process optimisation of the oxidative carbonylation reaction.

<i>N</i> -Cyclohexyl-isopropylamine	0.05 mol dm <sup>-3</sup>
Pd(OAc) <sub>2</sub>	0.005 mol dm <sup>-3</sup> (10 mol%)
Cu(OAc) <sub>2</sub>	0.0025 mol dm <sup>-3</sup> (5 mol%)
<i>p</i> -benzoquinone	0.075 mol dm <sup>-3</sup> (150 mol%)
AdCOOH	0.013 mol dm <sup>-3</sup> (25 mol%)
Li-quinoline	0.0025 mol dm <sup>-3</sup> (5 mol%)
CO / Air 6.25% v/v	10 bar
temperature	120 °C

Reactions were conducted at a 20 mL scale using a 2 cm cross-shaped magnetic bar at an agitation rate 300 rpm.

All experiments in this section were conducted according to Procedure D, Chapter 3.

#### 4.2.2. Process optimisation

Despite using a relatively inexpensive pre-catalyst, namely palladium (II) acetate, 5-10 mol% is still a significant amount of rare metal and raises issues of sustainability (resource use) and safety (Pd toxicity) for potential industrial applications. Therefore, it was highly desirable to increase the turnover number (TON) of the investigated process thus, lower the amount of palladium used in the reaction. The conditions given in Table 4.2-10 were used as a reference point.

Willcox and Chappell et al. discovered that the yield of this reaction could be increased using nitrogen-ligands, namely Li-quinoline or quinuclidine.<sup>203</sup> However, the mechanism of this influence remains unknown. It was questioned whether the ligand plays a direct role in the formation of the product or, rather, coordinates to the palladium species after the product formation, preventing the creation of insoluble species prior to oxidation back to the active catalyst; zero order influence of the Li-quinoline on the apparent reaction rate may suggest the latter. To test this hypothesis, the expensive Li-quinoline was replaced with, arguably, the cheapest and the most environmentally friendly amine-derived ligand, pyridine. Surprisingly, even better results in comparison to the standard conditions were achieved. An increase in TON from the initial 7 to 17 was attained, Table 4.2-11 entry 2.

The fact that pyridine can be used as a ligand supports the hypothesis that the role of the ligand is not directly connected to the formation of the product, but nitrogen-ligands help to solubilise the Pd<sup>0</sup> species and prevent the formation of palladium black. In the course of the further tests, it was discovered that pyridine is a ligand suitable only for some selected substrates. Presumably, this is caused by the formation of palladium-pyridine complexes, which in some cases are thermodynamically more stable than the palladium-substrate complexes. Thus, their presence precludes coordination of the substrate to the palladium catalyst.

Being aware of the solubility issues of Pd<sup>0</sup> complexes and questioning whether all catalytically active species are indeed soluble in toluene, the decision was taken to test other solvents that may be suitable for this reaction. It was discovered that by replacing toluene with ethyl acetate one could achieve an increase in TON and lower the catalyst loading to 1 mol% without a significant decrease in the yield, Table 4.2-11 entry 6. Reactions in ethyl acetate required longer times to completion than the reactions under the same conditions in toluene (for the same conditions 200 min in EtOAc vs 120 min in toluene).

Finally, the investigation of the effect of the gas phase composition on the TON was performed. It was questioned whether removal of oxygen from the system could potentially increase the catalyst stability. Removal of the gas phase oxidant would require an increase in the concentration of the copper oxidant to the stoichiometric amount, but, at the same time, would prohibit formation of water, being the by-product of the re-oxidation of copper. Indeed, TON was significantly higher in this case, and for the optimal set of conditions the catalyst loading was as low as 0.2 mol%, Table 4.2-11 entry 7.

Table 4.2-11. Selected results from the process optimisation.

Entry	Process variant	Catalyst loading (Pd /Cu) [mol%]	Additives [mol%]	Time [min]	Yield of product
1	Initial conditions	10 / 10	10 Li-quinoline	360	68%
2	10 bar CO/Air	5 / 5	5 Li-quinoline	75	84%
3	10 bar CO/N <sub>2</sub>	5 / 200	5 Li-quinoline	85	86%
4	1-10 bar CO	10 / 200	10 Li-quinoline	-	Trace
5	(2) + pyridine	3 / 5	10 pyridine	150	85%
6	(3) + pyridine	1 / 200	10 pyridine	200	78%
7	<b>(5)+ EtOAc</b>	<b>0.2 / 200</b>	<b>10 pyridine</b>	<b>300</b>	<b>84%*</b>

Reactions were performed using 1.5 equiv. *p*-BQ and 25 mol% AdCOOH, *T*=120 °C. Yield marked with an asterisk is given for the isolated compound.

### 4.2.3. Process design

Understanding that the limiting factor precluding intensification of the reaction is the gas-liquid mass transfer, the possibility of translating the process into continuous-flow was studied. Such transition would allow enhancing the mass transfer using, for example, the gas-liquid slug-flow regime in a capillary flow reactor. This type of flow is easy to implement as well as scalable by numbering up, and simultaneously, addresses safety aspects of using high pressures of CO in stirred tank reactors. Operation in flow allows minimisation of a head-space, and hence lowering the amount of CO present in the reactor. Continuous flow processes are also, generally, easier to control and more reproducible.<sup>71</sup> A significant attention has been paid to development of flow chemistry methods for challenging chemical transformations and extensive literature reports from this filed are available.<sup>65,67,70,71,219–222</sup>

Even though classical carbonylation reactions were previously successfully conducted in flow, demonstrating a significant added value in terms of safety and efficiency,<sup>65,184</sup> to the best of author's knowledge, no examples of continuous oxidative carbonylations employing copper oxidants exist in the literature. This is likely due to the heterogeneity of the reaction mixture, namely the presence of copper or silver-based oxidants, that are not soluble in the reaction media, as well as CO in the gas phase. Generally, there are very few examples of multiphase catalytic flow processes that include co-flow of dispersed solids in

the gas-liquid bi-phasic main flow.<sup>175</sup> The majority of studies were performed with gas-liquid or liquid-liquid flows through a stationary solid phase.<sup>174</sup> In the present work, the decision was taken to reduce the number of phases, which would lower the overall complexity of the scale up of the process.

Reduction in the number of phases could not be achieved by increasing pressure to the point of full dissolution of the gas phase, due to the narrow range of the tolerated CO concentrations, nor by implementing membrane systems to continuously deliver gaseous reactants to the liquid phase, due to the inevitable membrane clogging. Thus, there was no possibility of removing the gas phase from the reaction. The reduction in the number of phases must have been done by removing the solid phase, consisting of a significant amount of Cu<sup>II</sup> salt being virtually insoluble in the suitable for the reaction solvents. Inspired by Ceylan,<sup>223</sup> it was questioned whether it is possible to use heterogeneous precursors of Cu<sup>II</sup> salts instead of the continuous delivery of solids. Such possibility was firstly probed by introducing a copper wire into a tubular reactor operating in the gas-liquid slug flow.

The *in situ* oxidised metallic copper was able to re-oxidise the palladium catalyst, Table 4.2-12 entry 1. However, the system proved to be stable only for short periods of time. Encouraged by the positive initial results the decision was taken to expand the contact area between the gas-liquid main stream and the heterogeneous precursor of the copper oxidant. Using a copper-tube-flow reactor (CTFR) resulted in a significant improvement of the stability of the system and the increase in the observed reaction rate, Table 4.2-12 entry 2. To the best of author's knowledge, this was the first example of using a CTFR as an "oxidant". The layer of oxidised Cu was regenerated *in situ* by oxygen present in the gas phase and proved to be stable for at least 8 hours on stream. Using the ICP OES analysis, the amount of copper leaching from the reactor was determined to be in the range of 1200 – 1500 ppm. This amount of copper can be conveniently removed from the reaction mixture using the protocol developed by Gemoets et al.<sup>111</sup> The flow process described in the present work provides easy access to the *in situ* generated Cu<sup>II</sup> species widely used as oxidants and may be significant for the development of other continuous flow oxidative chemical systems. The removal of the 3<sup>rd</sup> phase and operation in the so-called "slug flow" regime increased the mass transfer between the gas and the liquid phases significantly, resulting in a superior space-time-yield.<sup>224</sup>

In the continuous flow setup, toluene was used instead of EtOAc to allow operation at short residence times. Additionally, leaching of Cu was significantly higher when EtOAc was used.

Table 4.2-12. Development of the flow process for the oxidative carbonylation reaction.

Entry	Process variant	Catalyst loading (Pd / Cu) [mol%]	Time [min]	Yield of product [-]
1	Flow (using copper wire)	10 / -	20	80%
2	Flow (using CTFR)	5 / -	5	86%*

Reactions were performed using 1.5 equiv. *p*-BQ and 25 mol% AdCOOH. *T*=150 °C. Reactions were performed in toluene using 6.25 % v/v CO/air mixture. Yield marked with an asterisk is given for the isolated compound.

Having designed the flow processes, the decision was taken to test the selected substrate scope, Figure 4.2-10. The full substrate scope has been described by Willcox and Chappell et al.<sup>203</sup> In the continuous flow setup all substrates worked equally well or better than in the original report.

The utility of the developed process was further investigated on three reactions mechanistically different from the initially tested process, Figure 4.2-11. For all tested cases the process worked very well, despite virtually no optimisation performed. Firstly, the Orito carbonylation of secondary amines to ureas<sup>168</sup> was tested achieving full conversion and almost quantitative yields within 5 minutes. Furthermore, the oxidative carbonylation of *N*-allylamines for the synthesis of  $\beta$ -lactams was performed where, after adjusting the procedure, comparable to previously reported yields were achieved.<sup>169</sup> Used in the original procedure palladium (II) chloride was replaced with palladium (II) acetate due to solubility issues. Additionally, DMF was replaced with toluene to reduce leaching of copper salts from the CTFR.

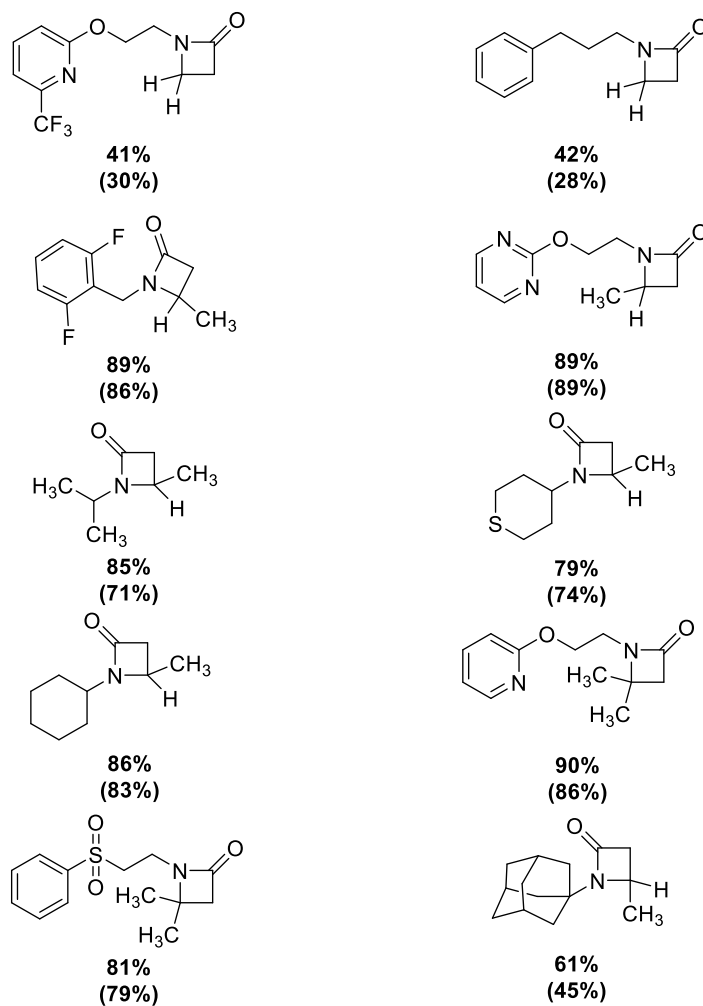


Figure 4.2-10. Selected substrate scope. Yields are given for the isolated compounds. Yields in brackets are from the initial report of Gaunt and co-workers ref. 203.

Finally, the possibility of running the carbonylation of benzoic acids to give dicarboxylic acids was probed.<sup>225</sup> Even though the conditions were significantly different from those published in the original work, the reaction still performed rather well in the developed setup.

NMR characterisation of all isolated compounds can be found in Appendix 4.

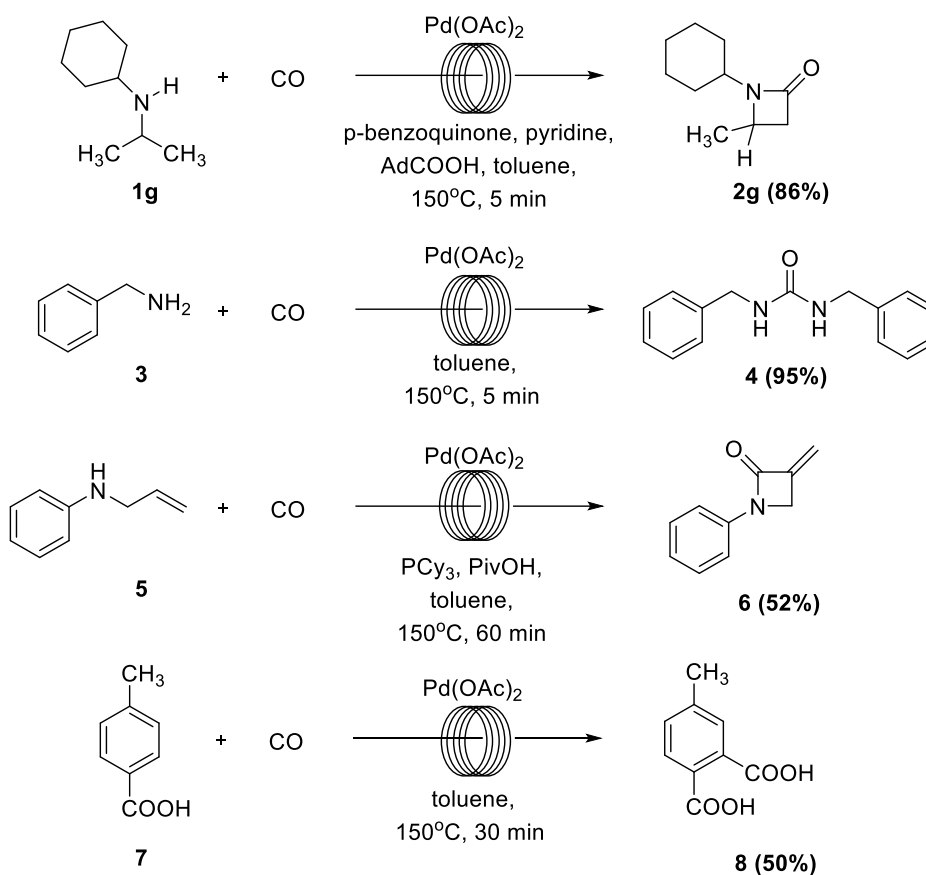


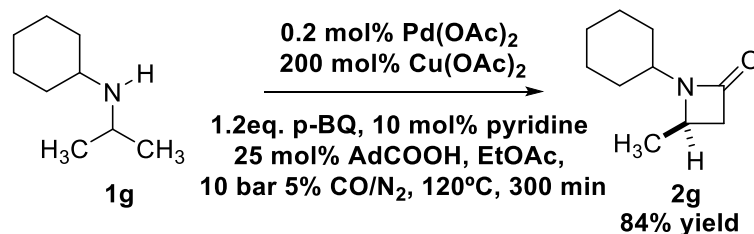
Figure 4.2-11 Selected scope of the process. Yields are given for the isolated compounds. Tests performed under 10 barg of 6.25 % v/v CO balanced by synthetic air.

NMR characterisation of all isolated compounds can be found in Appendix 4.

Furthermore, the decision was taken to design an intensified batch process for this reaction and later compare it with the already developed flow process.

Based on the available heuristics, the most suitable conditions to run the process in batch were selected, Scheme 4.2-2. These conditions were characterised by a very low  $\text{Pd}^{\text{II}}$  catalyst loading, a high yield and a reasonable time to completion. It was questioned whether this process could be scaled-up without significant modifications of the protocol, namely without keeping process parameters describing the mass and energy transfer constant. As expected, doubling the mass of the starting material to approximately 0.5 g, with the corresponding increase in the solvent volume, resulted in notable changes in the behaviour of the process. The larger scale reaction resulted in a reduced rate and a lower yield, Figure 4.2-12. It was hypothesised that the lower reaction rate was due to an insufficient flux of carbon monoxide to the liquid phase, as the gas-liquid interfacial area

remained the same, while the reaction volume has doubled, i.e. the rate of mass transfer per unit of volume of the liquid phase was twice smaller.



*Scheme 4.2-2. Reaction conditions for a batch process for carbonylation reaction. Yield is given for the isolated compound.*

Obtaining an estimate of the  $k_{LA}$  for the reference conditions, one can use it as a scale-up criterion due to the fact that preserving the  $k_{LA}$  value equal or greater than the reference  $k_{LA}$  should result in providing a sufficient flux of the CO to the system. The  $k_{LA}$  value may be maintained by using similar geometries of the reactors, i.e. constant surface-to-volume-ratio, or by providing an additional stream of CO via an injector located at the bottom of the autoclave. The latter was implemented in the present work.

Being unable to measure the concentration of CO in the liquid phase *in situ*, it was only possible to estimate the value of the mass transfer coefficient ( $k_{LA}$ ) for the investigated system. Since the stoichiometry of the reaction requires that the consumption of CO is equal to the rate of the reaction, the rate of the reaction was used to determine the mass transfer coefficient at different scales. Based on Equation ( 61 ) the values of  $k_{LA}$  for experiments at different scales were calculated.

$$rate = \frac{dC_P}{dt} = k_L a (c_g - c_l) dt \quad ( 61 )$$

where  $c_g$  is the concentration of CO in the gas phase and  $c_l$  is the concentration of the CO in the liquid phase.

Table 4.2-13. Estimation of the mass transfer coefficient.

Scale [ml]	$k_{LA}$ [ $\text{min}^{-1}$ ]
20	0.085
30	0.074
40	0.061

In order to scale the reaction maintaining the flux of the CO to the liquid phase, the  $k_{LA}$  value should be kept equal or greater than 0.085 since the small scale (20 ml) process operated at the concentration of CO in liquid phase equal or close to saturation, Figure 4.2-12.

For the system with a constant delivery of CO via an injector the mass transfer coefficient can be expressed in the form of Equation ( 62 ):

$$\text{rate} = \frac{dC_p}{dt} = (k_L a + k_{LA} a_{injector})(c_g - c_l) dt \quad (62)$$

where  $k_{LA} a_{injector}$  is the mass transfer coefficient for the gas delivered through the injector.  $k_{LA} a_{injector}$  can be estimated using Equation ( 63 ):<sup>88</sup>

$$k_{LA} a_{injector} = 0.32 (\vartheta_{gas}^c)^{0.7} \left( \frac{\mu_{H_2O}}{\mu_{solvent}} \right)^{0.84} \quad (63)$$

where  $\vartheta_{gas}^c$ ,  $\text{m s}^{-1}$ , is the velocity of the gas phase per surface area of the reactor,  $\mu_{H_2O}$  and  $\mu_{solvent}$  are respectively the dynamic viscosity of the water and the solvent,  $\text{kg m}^{-1} \text{s}^{-1}$ .

For the investigated process, the flowrate of 7 sccm was sufficient to achieve the reaction rate comparable with the experiments at the small scale, Figure 4.2-12. However, the yield was still significantly lower.

While conducting experiments at the larger scale, the formation of a dense polymer-like by-product was observed. A visual analysis revealed that the by-product entrapped a

significant amount of copper (II) acetate crystals, and presumably also palladium species. NMR analysis exposed that it also contained some starting material as well as product. Aiming to minimise the formation of the polymer-like by-product the decision was taken to enhance mixing, thus prevent settling of the polymer during the reaction. To ensure that a sufficient amount of power required for mixing is delivered to the system, maintaining a constant, or using a greater, energy dissipation rate per volume unit of the liquid phase was suggested, Equation ( 64 )<sup>88</sup>

$$\frac{P}{V_l} = const \quad ( 64 )$$

where  $P$  is the power utilised for mixing, and  $V_l$  is the volume of the liquid phase.

Power required for mixing is proportional to the agitation rate,  $N$ , the diameter of the stirrer,  $d$ , and density of the liquid phase,  $\rho_l$ , Equation ( 65 ).

$$P \sim N^3 d^5 \rho_l \quad ( 65 )$$

The scale-up criterion takes the form of Equation ( 66 ).

$$\frac{N_1^3 d_1^5}{V_1} \leq \frac{N_2^3 d_2^5}{V_2} \quad ( 66 )$$

where 1 corresponds to the small-scale experiments and 2 to the larger scale one.

On the larger scale, a bigger stirrer bar was used (4 cm diameter) and, based on Equation ( 66 ) the minimum agitation rate to ensure efficient mixing should be equal to 113 rpm. In the present study the agitation rate of 300 rpm was retained. This resulted in the yield and the reaction rate comparable to the small-scale experiments, Figure 4.2-12. Notably, the delivery of CO through the injector also contributes to the increase in the energy dissipation

rate of the system. Thus the mixing performance should be even better. Additionally, a possibility of minimising the formation of the polymeric by-product by purification of p-benzoquinone used for the reaction was investigated. Re-crystallisation of the crude p-benzoquinone resulted in a decrease in the formation of the black polymer. However, without efficient mixing, still a significant amount of the polymer-like by-product at the bottom of the autoclave was observed.

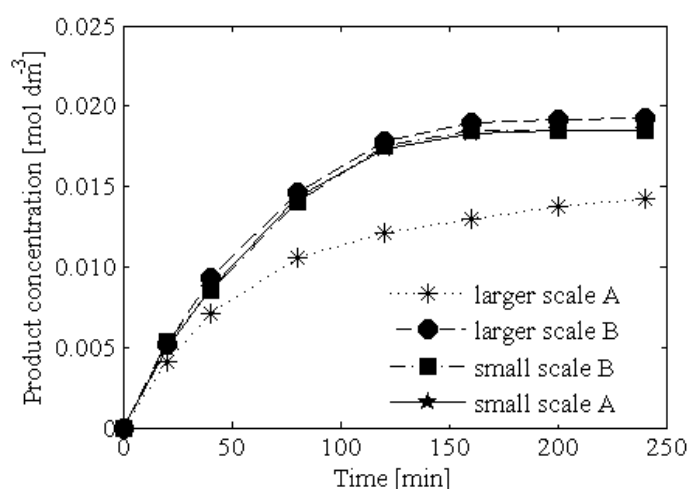


Figure 4.2-12. Scale-up of the batch process. A represents reactions without an additional delivery of CO at the bottom of the reactor and using the small stirrer bar, B reactions with a constant CO delivery and for larger scale also enhanced mixing.

Further increase of the scale was impossible due to limitations of the experimental setup, as well as safety concerns associated with using significant amounts of CO and working with larger amounts of solvents at the temperature above their boiling points at atmospheric pressure. In case of a sudden, unexpected depressurisation of the reactor, a significant amount of a toxic and flammable mixture of solvent vapours and CO would be released. Regardless, the designed protocol should be further scalable by maintaining the surface-to-volume ratio equal to or greater than  $1.14 \text{ cm}^{-1}$ , or the  $k_{\text{LA}}$  value equal to or greater than  $0.085 \text{ min}^{-1}$ . Furthermore, it is suggested to keep the energy dissipation rate constant to ensure efficient mixing.

#### 4.2.4. Environmental sustainability analysis of the developed processes

An analysis of environmental impacts of the developed process options was performed using both simplified metrics and a cradle-to-gate LCA analysis.

##### 4.2.4.1. Simplified metrics

Two simplified metrics were selected to compare the available process options: E-factor and Process Mass Intensity (PMI). Notably, these environmental criteria do not assess the variations in the up-stream operations but compare only the process itself. For all calculations, it was assumed that purification via a flash column chromatography requires 10 kg of solvent per 1 kg of product.

E-factor was defined in Chapter 2.4, Equation ( 47 ). PMI ( $\text{kg kg}^{-1}$ ) is defined as the cumulative mass of raw materials required to produce 1 kg of product, Equation ( 67 ).

$$PMI = \frac{\text{mass of raw materials}}{\text{mass of product}} \quad ( 67 )$$

*Table 4.2-14. Comparable sustainability analysis of the available process options using simplified metrics.*

	E-factor [ $\text{kg kg}^{-1}$ ]	Process Mass Intensity [ $\text{kg kg}^{-1}$ ]
Original work	13.075	13.92
Flow	12.91	13.89
Batch	18.15	18.46

The analysis via the simplified metrics revealed that the flow process is consistently environmentally superior. When considering E-factor and PMI, the batch process proved to generate the most of environmental burden.

The larger value of E-factor for the batch process is caused by the use of a large amount of copper (II) acetate (this process option required the stoichiometric use of a copper salt).

The difference between the flow process and the process published by Willcox and Chappell is the consequence of the lower catalyst loading and the slightly greater yield. The same reasoning applies to the PMI analysis.

While simplified metrics are commonly used to compare process options in both industry and academia, they do not account for any up-stream operations nor reveal which part of the process generates the most of environmental burden. Such understanding requires a broader system approach that can be developed via, for example, LCA studies.

#### 4.2.4.2. LCI assessment

**Functional unit.** The functional unit to which the Life Cycle Impact (LCI) analyses were referred to was 1 kg of product, namely 1 kg of 1-cyclohexyl-4-methylazetidin-2-one.

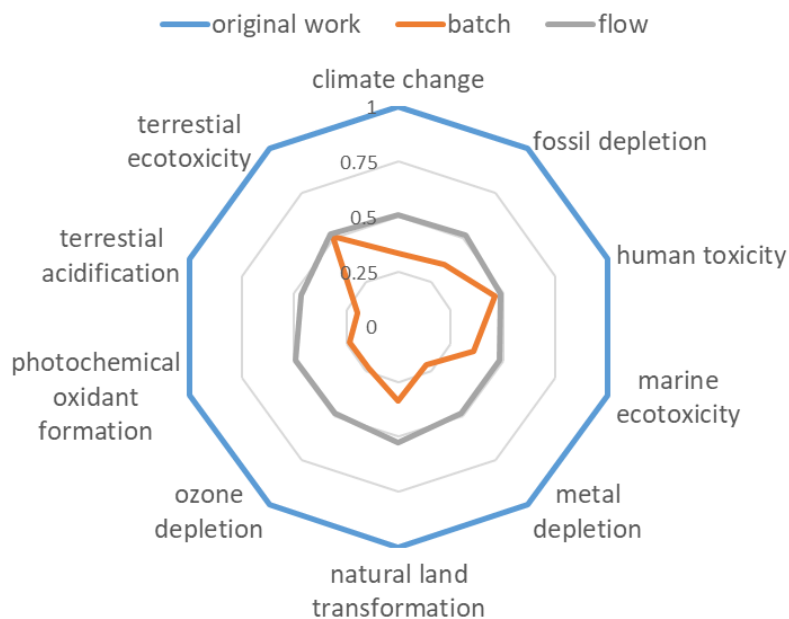
**Data sources.** As a primary source of data used for the impact assessment, the LCI database Ecoinvent v3.2. was used.<sup>226</sup> For molecules not present in the database, the suitable models were built. The synthesis routes were chosen based on data available from manufacturers, encyclopaedias<sup>227,228</sup> or web-based syntheses planners. Description of all developed models can be found in Appendix 5. The LCI analysis and the impact assessment were conducted using Umberto<sup>®</sup> 5.6.<sup>229</sup> The examination was performed using the cradle-to-gate boundary. The LCI assessment was performed following the LCA methodology ReCiPe 2008.<sup>196</sup> The impact potentials included in the ReCiPe 2008, Table 4.2-15, were addressed at the midpoint level.

Table 4.2-15. Impact potentials used in the LCI assessment.

Abbreviation	Impact category	Unit
GWP	Climate change	kg of CO <sub>2</sub> – equivalents (eq.) per functional unit (FU)
FDP	Fossil fuels depletion potential	kg of oil per FU
HTP	Human toxicity potential	kg of 1,4-dichlorobenzene (1,4-DCB) – eq. per FU
MEP	Marine eutrophication potential	kg of nitrogen – eq. per FU
MDP	Metal depletion potential	kg of Fe – eq. per FU
NLTP	Natural land transformation potential	m <sup>2</sup> per FU
ODP	Ozone depletion potential	kg of chlorofluorocarbon-11 per FU
POFP	Photochemical oxidant formation potential	kg of non-methane volatile organic compounds (MNVOC) – eq. per FU
TAP	Terrestrial acidification potential	kg of SO <sub>2</sub> – eq. per FU
TETP	Terrestrial ecotoxicity potential	kg of 1,4-DCB – eq. per FU

**System boundary overview.** The cradle-to-gate system boundaries were applied. Thus, the analysis ended with the purification step of the carbonylation process. For the molecules not present in the Ecoinvent database the analysis was expanded by the suitable syntheses that could be described using molecules that are present in the above-mentioned database. Recycling of all solvents via distillation was included.

**Impact assessment.** The process variant generating the most burden to the environment was, according to the performed LCI assessment, the originally reported technology. This is contrary to the assessment using the simplified metrics. While comparing the batch and the flow processes, for the impact categories besides terrestrial ecotoxicity potential and human toxicity potential, the batch process proved to be environmentally superior. For the last two categories, the impacts were comparable, Figure 4.2-13. Generally, the flow process was characterised by twice smaller impacts than the original process for all indicated in the ReCiPe 2008 midpoint categories. The impacts of the batch process varied between 20% and 50% of the impacts of the reference technology, Figure 4.2-13.



*Figure 4.2-13. Comparison of impacts for the developed process options. Results were normalised against the original work.*

Plotting contributions of all reactants to different impacts as well as of the process itself, as gate-to-gate inventory, allowed to observe that, for most of the impact categories, palladium acetate contributed by far the largest impact, typically in the range of 70-95% of the cumulative impact, Table 4.2-16 and Figure 4.2-14. Only when the batch technology was investigated, owing to the very low palladium use, the situation differed, Table 4.2-16 and Figure 4.2-14. For some of the impact categories of the batch technology, palladium acetate accounted for approximately 50% of the cumulative impact; however, for the impacts of metal depletion potential, ozone depletion potential, photochemical oxidant formation potential and terrestrial acidification potential, palladium acetate still generated more than 90% of the cumulative impact. In the batch technology, the other significant sources of the environmental burden were copper acetate, AdCOOH and the process itself due to operation at high temperature and pressure as well as long time to achieve high conversion.

When analysing the impacts of the production of palladium acetate, it was observed that all of the impact categories were dominated by production of palladium; more than 95% of the accumulated impact for all the investigated categories.

Table 4.2-16. Distribution of impacts between reactants.

	GWP	FDP	HTP	MEP	MDP	NLTP	ODP	POFP	TAP	TETP
Original work										
Pd(OAc) <sub>2</sub>	<b>0.69</b>	<b>0.68</b>	<b>0.94</b>	<b>0.97</b>	<b>1.00</b>	<b>0.86</b>	<b>0.97</b>	<b>0.94</b>	<b>0.95</b>	<b>0.70</b>
SM	0.01	0.01	0.01	0.00	0.00	0.01	0.00	0.01	0.00	0.04
CO	0.00	0.01	0.00	0.00	0.00	0.00	0.00	0.00	0.00	0.00
AdCOOH	0.04	0.05	0.01	0.01	0.00	0.08	0.01	0.01	0.00	0.03
Cu(OAc) <sub>2</sub>	0.00	0.00	0.01	0.01	0.00	0.00	0.00	0.00	0.00	0.01
BQ	0.01	0.01	0.00	0.00	0.00	0.01	0.00	0.00	0.00	0.03
Li*	<b>0.09</b>	<b>0.09</b>	0.01	0.00	0.00	0.02	0.01	0.01	0.04	<b>0.08</b>
Process**	<b>0.16</b>	<b>0.15</b>	0.01	0.00	0.00	0.02	0.01	0.02	0.00	<b>0.11</b>
Flow										
Pd(OAc) <sub>2</sub>	<b>0.66</b>	<b>0.63</b>	<b>0.94</b>	<b>0.97</b>	<b>1.00</b>	<b>0.79</b>	<b>0.96</b>	<b>0.92</b>	<b>0.99</b>	<b>0.65</b>
SM	0.02	0.02	0.01	0.00	0.00	0.02	0.00	0.01	0.00	<b>0.08</b>
CO	0.01	0.02	0.00	0.00	0.00	0.00	0.00	0.00	0.00	0.00
AdCOOH	<b>0.08</b>	<b>0.09</b>	0.03	0.01	0.00	<b>0.15</b>	0.02	0.03	0.00	0.06
BQ	0.01	0.02	0.00	0.01	0.00	0.01	0.00	0.00	0.00	0.06
Pyridine	0.00	0.00	0.00	0.00	0.00	0.00	0.00	0.00	0.00	0.00
Process**	<b>0.22</b>	<b>0.22</b>	0.02	0.01	0.00	0.03	0.01	0.03	0.01	<b>0.15</b>
Batch										
Pd(OAc) <sub>2</sub>	<b>0.41</b>	<b>0.38</b>	<b>0.41</b>	<b>0.53</b>	<b>0.92</b>	<b>0.50</b>	<b>0.82</b>	<b>0.80</b>	<b>0.96</b>	<b>0.27</b>
SM	0.03	0.03	0.02	0.00	0.00	0.03	0.01	0.03	0.01	<b>0.08</b>
CO	0.01	0.02	0.00	0.00	0.00	0.00	0.01	0.00	0.00	0.00
AdCOOH	<b>0.12</b>	<b>0.14</b>	0.03	0.02	0.00	<b>0.24</b>	0.04	0.06	0.01	0.06
Cu(OAc) <sub>2</sub>	0.04	0.05	<b>0.52</b>	<b>0.43</b>	<b>0.08</b>	<b>0.15</b>	0.09	0.04	0.02	<b>0.34</b>
BQ	0.02	0.03	0.00	0.01	0.00	0.02	0.00	0.01	0.00	0.06
Pyridine	0.00	0.00	0.00	0.00	0.00	0.00	0.00	0.00	0.00	0.00
Process**	<b>0.37</b>	<b>0.34</b>	0.02	0.01	0.00	0.05	0.03	0.07	0.01	<b>0.17</b>

\*Li denotes Li-quinoline. \*\*Process denotes the impact from the gate-to-gate inventory.

The overwhelming effect of palladium acetate on all of the investigated impact categories illustrates why industry tends to “loan” precious metals from catalyst producers. Namely, the spent catalyst is collected and sent back to the manufacturer to have it recycled and is being purchased again at a lower cost. Operation in this manner is presumably not only environmentally superior, but also the economy of “loaning” of precious metals should be favourable.

The decision was taken to extend the LCI assessments by adding a metal recovery process to more accurately illustrate the possible environmental impact of the investigated process options.

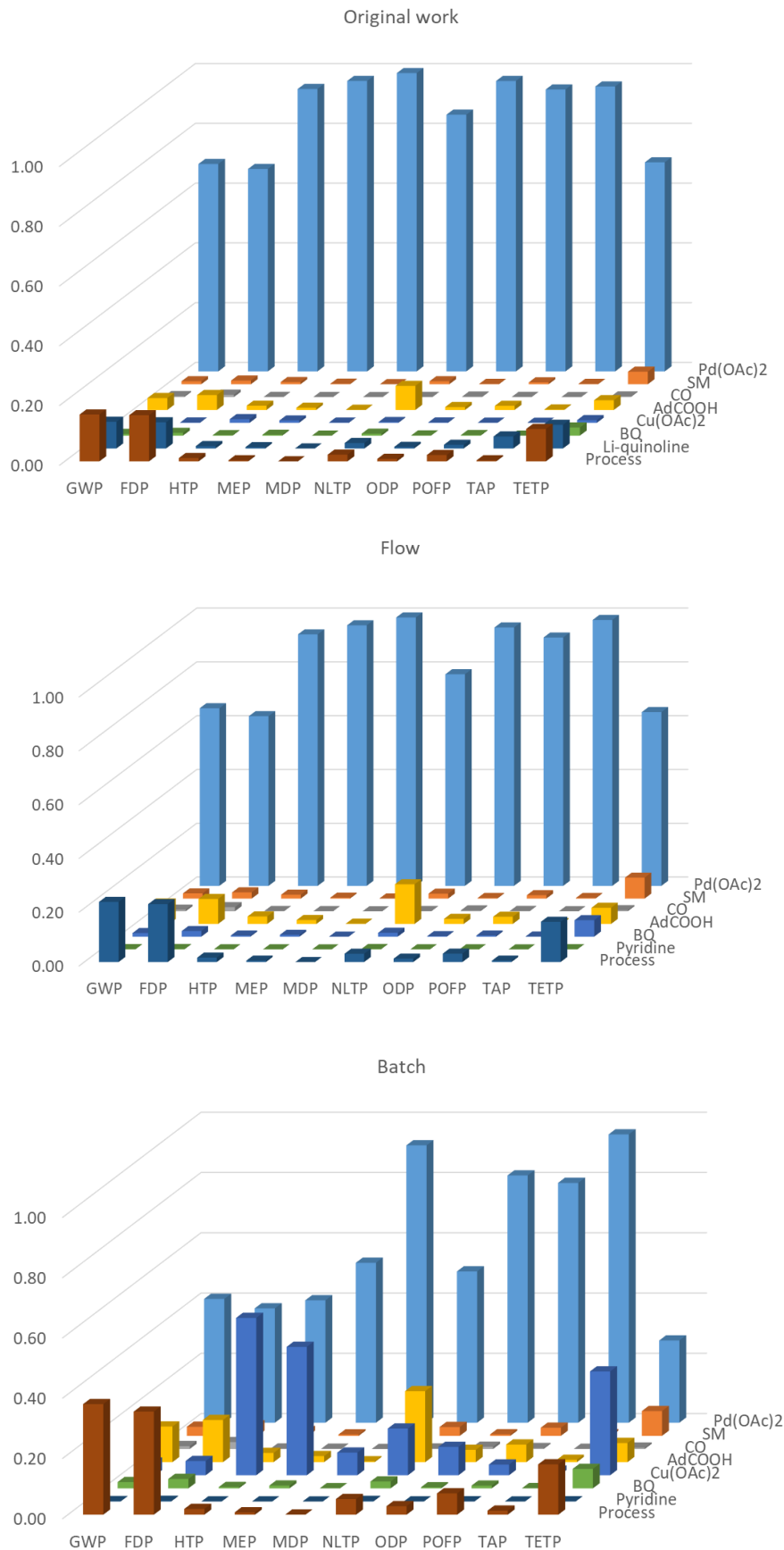
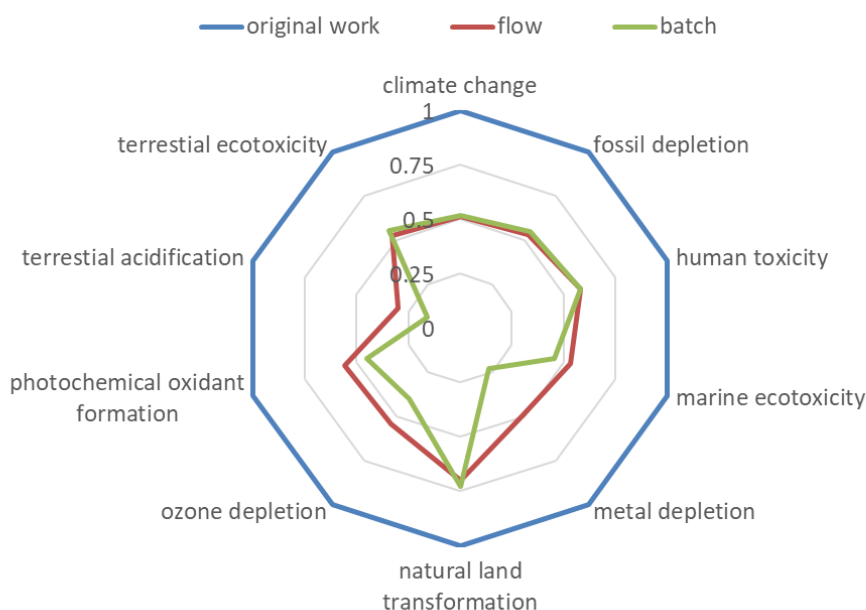


Figure 4.2-14. Distribution of impacts between reactants.

The literature search for a suitable process for recycling of heavy metals revealed that the most commonly used method is electrolysis. Such approach allows, in this specific case, to recover not only palladium species, but also copper.<sup>230</sup> Recycling of metals was included in the process models, and the LCI analysis was repeated. Notably, the yield of the metal recovery was lower than 100%. Thus, both palladium (II) acetate and copper (II) acetate from the primary raw materials were still present in the analysis, albeit in smaller quantities.

When the metal recovery was included in the LCI assessment, the overall result did not change significantly. The batch technology still proved to be environmentally superior in most of the impact categories; only in the cases of natural land transformation potential and terrestrial ecotoxicity potential, the flow process scored lower. However, when accounting for the metal recovery, the results for a significant number of impact categories for the batch and the flow process were virtually identical (terrestrial ecotoxicity potential, climate change potential, fossil depletion potential, human toxicity potential, marine toxicity potential and natural land transformation potential), Figure 4.2-15. When metal depletion potential was considered, the batch process was still by far the most environmentally superior; this was caused by losses during the metal recovery process, Figure 4.2-15.

The originally reported process proved to generate the most of environmental burden. It was characterised by twice larger scores for most of the impact categories (terrestrial ecotoxicity potential, climate change potential, fossil depletion potential, human toxicity potential, marine ecotoxicity potential and photochemical oxidant formation potential). The score for the rest of categories was also significantly larger (between 25% and 90% depending on the reference technology), Figure 4.2-15.



*Figure 4.2-15. Comparison of impacts for the developed process options, accounting for metal recovery. Results were normalised against the original work.*

When individual contributions were investigated, it was observed, that palladium acetate was still responsible for a significant percentage of the cumulative result, especially for the metal depletion potential impact category. Furthermore, for all process options, production of 1-adamantane carboxylic acid, as well as the process itself, contributed significantly to the aggregated impact. The contribution of the process was especially significant for the global warming potential, fossil resources depletion potential and terrestrial ecotoxicity potential, Table 4.2-17 and Figure 4.2-16. This was due to a large amount of energy required for the production of solvents used for purification and the reaction itself.

The aggregated impacts of the batch technology were also largely influenced by production of copper acetate, especially human toxicity potential, marine ecotoxicity potential and natural land transformation potential. Surprisingly, production of copper acetate did not affect the impact category ‘metal depletion potential’ significantly. It can be justified by the efficient recovery of copper as well as its relative abundance, Table 4.2-17 and Figure 4.2-16.

Additionally, in case of the originally reported technology, the ligand, Li-quinoline, was responsible for a significant contribution to the aggregated impacts in most of the categories; for some of them, Li-quinoline was the largest contributor, namely for

photochemical oxidant formation potential, terrestrial acidification potential and terrestrial ecotoxicity potential. The change of the ligand to pyridine in the batch and the flow processes drastically reduced the environmental burden, Table 4.2-17 and Figure 4.2-16.

Table 4.2-17. Distribution of impacts between reactants including metal recovery.

	GWP	FDP	HTP	MEP	MDP	NLTP	ODP	POFP	TAP	TETP
Original work										
Pd(OAc) <sub>2</sub>	<b>0.10</b>	<b>0.10</b>	<b>0.50</b>	<b>0.69</b>	<b>0.98</b>	<b>0.28</b>	<b>0.62</b>	<b>0.47</b>	<b>0.50</b>	<b>0.13</b>
SM	0.03	0.03	0.07	0.02	0.00	0.05	0.01	0.06	0.01	<b>0.12</b>
CO	0.01	0.02	0.01	0.00	0.00	0.00	0.02	0.01	0.00	0.01
AdCOOH	<b>0.11</b>	<b>0.13</b>	<b>0.15</b>	<b>0.10</b>	0.01	<b>0.39</b>	<b>0.12</b>	<b>0.12</b>	0.02	<b>0.10</b>
Cu(OAc) <sub>2</sub>	0.00	0.00	0.01	0.01	0.00	0.00	0.00	0.00	0.00	0.00
BQ	0.02	0.02	0.02	0.01	0.00	0.03	0.01	0.02	0.00	0.01
Li*	<b>0.32</b>	<b>0.30</b>	<b>0.12</b>	<b>0.09</b>	0.00	<b>0.10</b>	<b>0.10</b>	<b>0.50</b>	<b>0.69</b>	<b>0.98</b>
Process**	<b>0.42</b>	<b>0.39</b>	<b>0.13</b>	0.07	0.00	<b>0.12</b>	<b>0.11</b>	<b>0.19</b>	0.04	<b>0.32</b>
Flow										
Pd(OAc) <sub>2</sub>	<b>0.10</b>	<b>0.09</b>	<b>0.42</b>	<b>0.63</b>	<b>0.96</b>	<b>0.20</b>	<b>0.55</b>	<b>0.41</b>	<b>0.81</b>	<b>0.11</b>
SM	0.05	0.06	<b>0.12</b>	0.04	0.01	<b>0.07</b>	0.03	<b>0.10</b>	0.04	<b>0.23</b>
CO	0.02	0.04	0.01	0.01	0.00	0.00	0.04	0.01	0.00	0.01
AdCOOH	0.20	<b>0.23</b>	<b>0.24</b>	<b>0.19</b>	0.02	<b>0.55</b>	<b>0.21</b>	<b>0.21</b>	0.05	<b>0.18</b>
BQ	0.04	0.05	0.04	0.02	0.00	0.05	0.02	0.03	0.01	0.02
Pyridine	0.00	0.00	0.00	0.00	0.00	0.00	0.00	0.00	0.00	0.00
Process**	0.60	<b>0.53</b>	<b>0.17</b>	<b>0.11</b>	0.00	<b>0.13</b>	<b>0.15</b>	<b>0.25</b>	<b>0.09</b>	<b>0.45</b>
Batch										
Pd(OAc) <sub>2</sub>	0.04	0.04	<b>0.17</b>	<b>0.30</b>	<b>0.85</b>	<b>0.08</b>	<b>0.30</b>	<b>0.21</b>	<b>0.62</b>	0.04
SM	0.05	0.06	<b>0.13</b>	0.05	0.01	0.07	0.04	<b>0.12</b>	0.07	<b>0.22</b>
CO	0.02	0.04	0.01	0.01	0.00	0.00	0.05	0.01	0.01	0.01
AdCOOH	0.20	<b>0.22</b>	<b>0.23</b>	<b>0.22</b>	0.05	<b>0.53</b>	<b>0.28</b>	<b>0.26</b>	<b>0.10</b>	<b>0.15</b>
Cu(OAc) <sub>2</sub>	0.02	0.03	<b>0.24</b>	<b>0.26</b>	<b>0.08</b>	<b>0.13</b>	<b>0.08</b>	0.03	0.02	<b>0.09</b>
BQ	0.04	0.05	0.04	0.02	0.01	0.05	0.03	0.04	0.01	0.02
Pyridine	0.00	0.00	0.00	0.00	0.00	0.00	0.00	0.00	0.00	0.00
Process**	<b>0.64</b>	<b>0.56</b>	<b>0.18</b>	<b>0.13</b>	0.01	<b>0.13</b>	<b>0.22</b>	<b>0.33</b>	<b>0.18</b>	<b>0.46</b>

\*Li denotes Li-quinoline. \*\*Process denotes the impact from the gate-to-gate inventory.

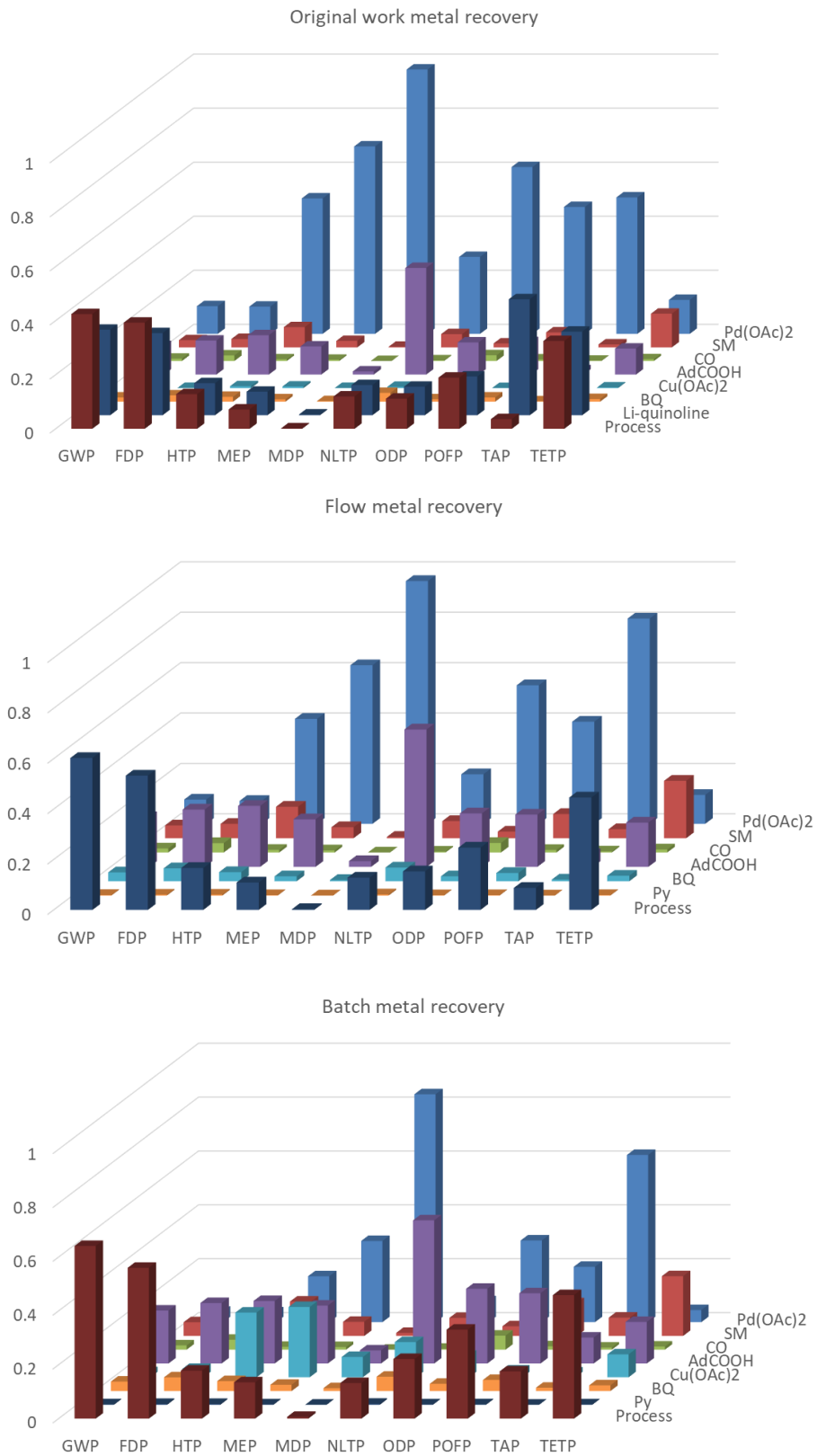


Figure 4.2-16. Distribution of impacts between reactants including metal recovery.

Owing to the fact that the developed the LCI models were based on several assumptions, the decision was taken to perform a sensitivity analysis to evaluate the impact of the assumptions on the final result. All assumptions are described in Appendix 5.

Since it is uncommon to report energy requirements of either patented or published procedures, the vast majority of assumptions concerned the energy consumption. The mass balances were described reasonably well in the chosen procedures. Having this in mind, it was decided to investigate the influence of the variations in the energy consumption of significant contributors to the aggregated impacts (values in bold in Table 4.2-17). Discrepancies of up to 25% of the final value were computed, Figure 4.2-17.

It is clear that varying the energy consumption by up to 25% does not change the final result significantly. The batch process still proved to be slightly more environmentally benign than the flow process. The originally reported technology, according to the performed LCI analysis, scored the worst.

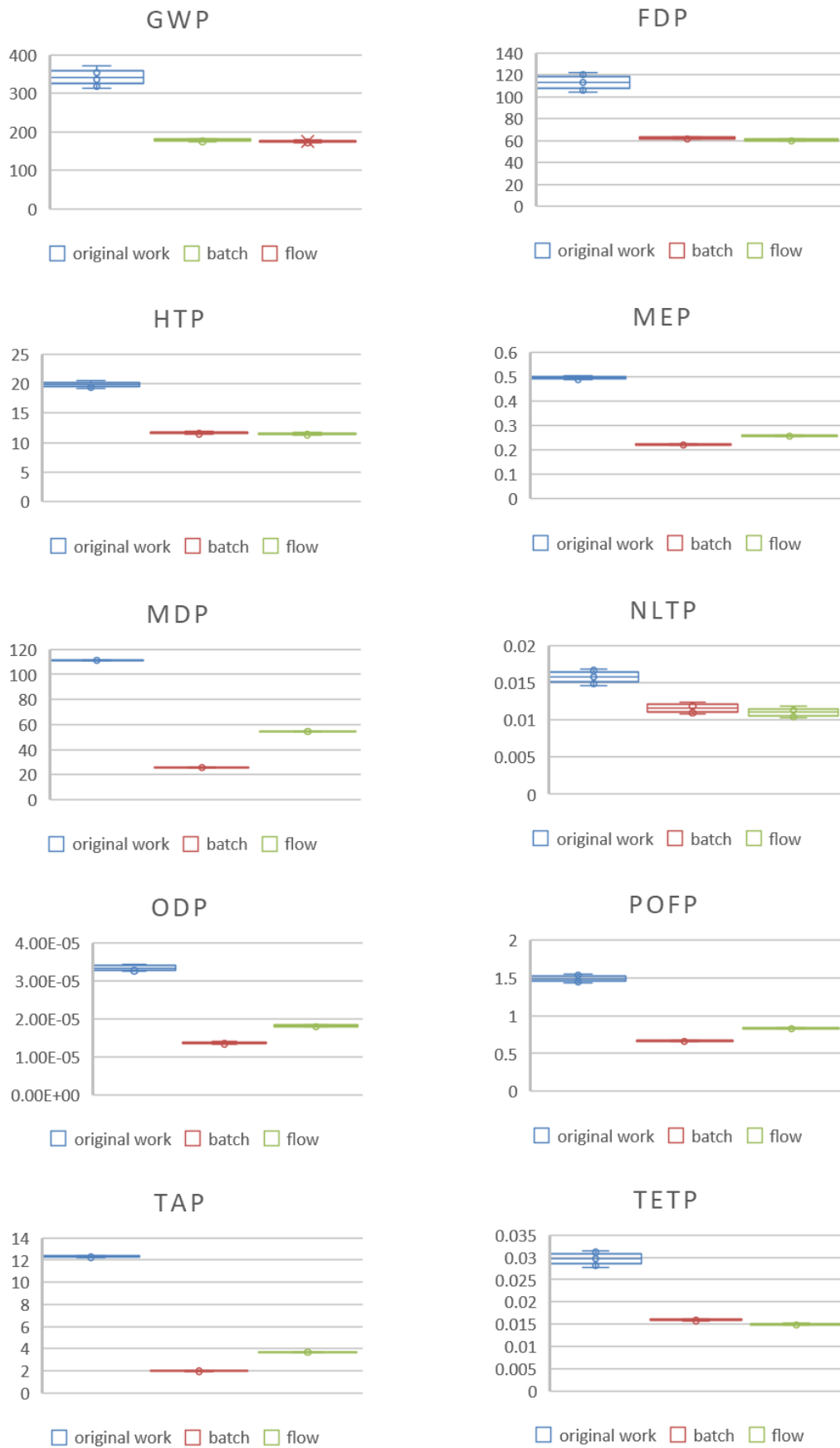


Figure 4.2-17. Sensitivity analysis of the developed LCI assessment.

### 4.2.5. Discussion

In the course of the project a partial deconvolution of the observed behaviour of the oxidative carbonylation of secondary amines to give  $\beta$ -lactams was performed. The identified trends, limitations as well as orders of influence on the observed reaction rate were used in setting up a simplified model that represented the behaviour of the process within the tested range of conditions with a rather high accuracy.

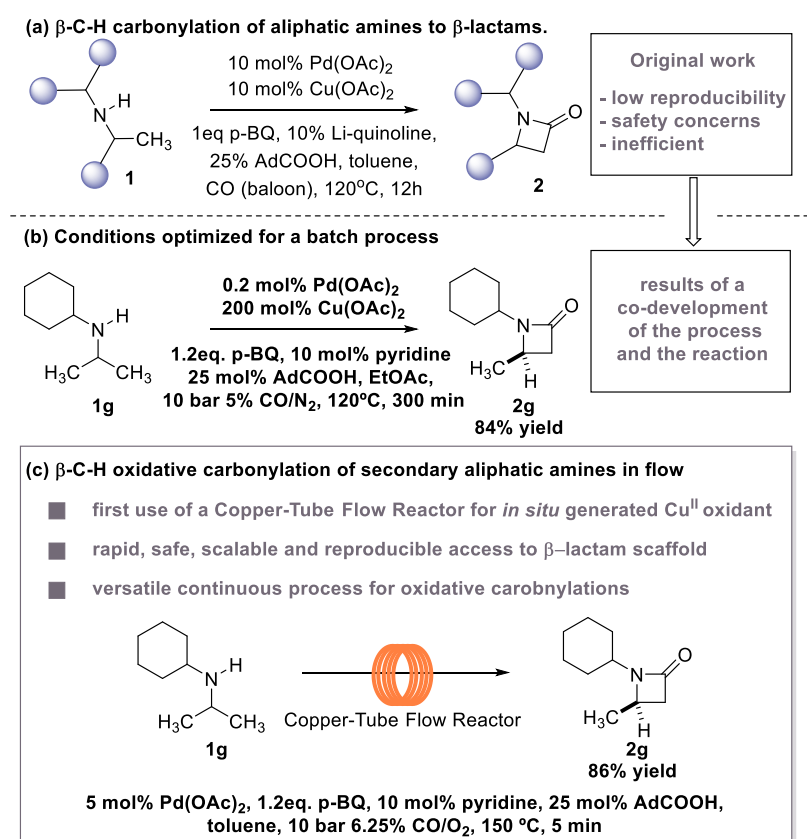


Figure 4.2-18  $\beta$ -C-H oxidative carbonylation of aliphatic amines to  $\beta$ -lactams. Yields are given for the isolated compounds.

Furthermore, the performed process optimisation allowed selection of suitable solvents, gas phase composition, ligands, temperature, pressure and concentration of reactants yielding in much higher productivity than the conditions described in the initial report.<sup>203</sup> Additionally, the much greater reproducibility and simplicity of operation were achieved. The optimisation efforts resulted in two sets of conditions, one suitable for a continuous flow setup and the second one being a batch process, see Figure 4.2-18.

The realisation of the continuous flow process was possible owing to the discovery of a suitable heterogeneous precursor of copper (II) oxidant. This is, to the best of author's knowledge, the first implementation of an oxidative carbonylation in a flow process and the first use of CTR as a precursor of an oxidant. The catalyst loading was reduced, and no dosing of Cu<sup>II</sup> salts was required to complete the reaction. Additionally, the residence times in the flow reactor were significantly shorter in comparison to the reaction times reported by Willcox and Chappell et al.<sup>203</sup> Similarly, the isolated yields were slightly higher than in the original report. For some substrates, Li-quinoline was successfully replaced with pyridine, lowering the cost of the process significantly.

For most of the tested substrates the applied conditions resulted in full consumption of the starting material, for the rest it was possible to recover and recycle the residual starting material. The inevitable ullage of the material is presumably due to thermal decomposition of starting material and losses during purification.

To prove the versatility of the developed procedure, three mechanistically different from the original reaction chemistries were tested. All resulted in highly efficient and easy in operation processes despite virtually no optimisation performed. Thus, it can be believed that the generic process for palladium/copper-catalyzed oxidative carbonylations was developed. One limitation of the protocol is exclusive use of solvents characterised by poor solubility of copper salts. This is to minimise leaching of the oxidant from the reactor. An additional benefit of the developed flow process is easy access to elevated pressures and high temperatures. This may potentially facilitate discovery of new reactivities owing to a prudent access to the conditions that are inaccessible in a standard laboratory glassware. From the safety point of view, operation in a strictly confined space, with virtually no headspace, raises fewer concerns than using balloons to deliver toxic gasses. The precisely controlled delivery of carbon monoxide can ensure that most of it is consumed in the course of the reaction and, additionally, gas phase quenches can lower the concentration of this dangerous reactant to safe levels.

The developed simple, cheap and scalable, both up and down, reactor system can give easy access to libraries of compounds with a carbonyl group added via carbonylation reactions. This may be an important invention for pharmaceutical, agrochemical and other fine chemical industries, where carbonyl groups, in the form of for example  $\beta$ -lactams, are prevalent.

The second variant of the process, i.e. the batch system, owing to the performed process optimisation, allowed further reduction of the catalyst loading down to 0.2 mol%. However, this was only possible at the cost of using a large amount of Cu<sup>II</sup> salt. The simplicity of operation and suitability to most of the commercially available reaction vessels designed to work under an elevated pressure are additional advantages of the designed protocol. Despite using remarkably low catalyst loadings, the reaction time was still shorter than the reaction time reported in the original studies; the yield remained at the same level.

To assess which design is more environmentally friendly, an analysis using simplified metrics, as well as an LCI assessment was performed. The values of the simplified metrics concluded that the flow process is environmentally superior and the batch technology generates the most of environmental burden. On the other hand, the LCI assessment revealed that the batch and the flow technology generate virtually identical environmental burden; the batch process performed marginally better for most of the considered impact categories. The LCI assessment clearly identified the original process as the least favourable form the environmental sustainability point of view.

The comparison of the simplified metrics and the LCA studies demonstrated that the broad system approach is necessary to assess the environmental aspects of developed technologies fully. Considering only the process itself without accounting for the upstream operations, one can draw unjustified conclusions.

It is worth mentioning that LCI analyses are best suited for large-scale industrial processes and for cases where a detailed description of mass and energy balances are available. In similar to the described in the thesis cases, prevalent assumptions can lead to unjustified conclusions.

Since both of the developed process options generate a comparable environmental burden, the decision which technology should be used can be based on the practicality of the developed process options. When generating small quantities in the range of milligrams or grams, the safe, robust and flexible flow process can be of great use. For larger scales, the batch protocol may be easier to implement. The commonly used equipment available in most of production facilities and research institutions is designed for operation under similar conditions, and, upon further scale-up, this could potentially become a viable process.

The role of ligands in the reaction remains unknown. However, owing to the pseudo zero order influence of ligands on the observed reaction rate a hypothesis can be drawn that they either take part in the reaction after the turnover-limiting step or does not play a direct role at all. In the second case, the increase of the maximum TON caused by the presence of amine-derived ligands may be explained by their high affinity to palladium, preventing it from forming insoluble particles that, upon aggregation, form “palladium black”. Reported by Willcox and Chappell et al. successful usage of quinuclidine as a ligand,<sup>203</sup> may advocate the latter, suggesting that the main criterion in the choice of a ligand for similar processes should be its high affinity to palladium. However, the affinity cannot be much greater than it is of used starting materials. This would result in formation of stable *bis*-amine-palladium complexes with ligands prohibiting binding of palladium to molecules of starting material, thus, precluding C–H activation events. Such behaviour was observed by Erdmann et al.,<sup>172</sup> where multiple pyridine derived ligands were tested in the oxidative coupling of *o*-xylene giving similar results. However, raising the concentration of the ligand to 2 equivalents with respect to palladium resulted in lack of reactivity in most of the presented cases. Hence, this observation may be applicable to a range of palladium-catalysed C–H activation reactions, where ligands are not directly involved in the catalytic cycle.

The conducted studies revealed that one of the main obstacles in the development of the palladium-catalyzed C–H oxidative carbonylations is a narrow range of tolerated CO concentrations. Access to elevated pressures, solvent selection and use of bespoke mixtures of gaseous phase can aid screening for accepted ranges of CO concentration and possibly can enable discovery of new reactions. The developed continuous flow protocol can further accelerate this process. Coupling it with an in-line analysis via, for example, IR spectroscopy or GC, GC/MS analysis and a semi-automated system can lead to rapid process optimisation of novel reactivities.

## Chapter 5. Conclusions

Current synthetic paths of complex fine chemical products are often long and include steps that do not generate any added value to the molecule; for example, introductions of protecting groups. These syntheses would benefit greatly in terms of economy and environmental sustainability from efficient ways allowing a reduction in the number of synthetic steps leading towards desired molecules. Recent advancements in the field of C–H activation can prove to be of great use in these efforts. However, despite their synthetic utility, the uptake of C–H activation reactions in either industrial processes or even total syntheses reported by academia is low. This may be due to the inherent difficulty of C–H activation reactions and poor mechanistic and kinetic understanding of such processes. Furthermore, when classical laboratory techniques are used, the range of available process conditions is rather limited. Thus, possibilities of intensification of C–H activation processes are severely handicapped. Therefore, the hierarchical approach can potentially be advantageous in optimisation and intensification of these processes.

This thesis has set out to develop mechanistic as well as kinetic understanding of selected C–H activation reactions and design intensified processes for them. Furthermore, the research aimed to identify inherent problems of this types of reactions and suggest possibilities to address them. The decision was taken to investigate processes involving secondary aliphatic amines owing to the fact that they are prevalent in active ingredients of, among others, pharmaceutical and agrochemical products. Moreover, C–H activation of aliphatic compounds is significantly more challenging comparing to C–H activation of aromatic substrates. It is due to the higher stability of aliphatic carbon-hydrogen bonds.

In Chapter 4.1, a C(sp<sup>3</sup>)–H activation reaction of secondary amines giving easy access to aziridines was investigated. The *ab initio* mechanistic model was developed and, based on the mechanistic understanding, a suitable method of intensification of the reaction was found. It allowed overcoming one of the prevalent causes of the inherent inefficiency of C–H activation processes of secondary aliphatic amines - formation of *bis*-amine-complexes.

Following the intensification of the process, a search for optimal conditions was performed using a multi-objective optimisation technique. The optimisation yielded a set of conditions characterised by a low catalyst loading and a short time-to-completion. The selected conditions were suitable for a continuous flow process employing a commercially available tubular reactor. The process was characterised by a very small space-time-yield.

Additionally, a suitable in-line purification method was developed. The decision was taken to harvest the possibilities of scavenging columns. The applied two-column system was designed to separate the catalyst (first column) and the product (second column) from the spent reaction mixture. The designed purification technique resulted in a high purity level of the product and high efficiency of separation of both the catalyst and the product. The developed process, as well as the purification system, should be applicable to similar reactions.

Furthermore, the utility of the process was extended by coupling the investigated C–H activation reaction with a subsequent reaction, a nucleophilic ring opening. Using a solid-supported product allowed significantly easier and, in case of using hazardous reagents such as hydrazoic acid as nucleophiles, also much safer operation. The total number of purification steps was reduced. Thus, the whole process is presumably more sustainable.

The developed flow process is, to the best of author's knowledge, the first example of a C(sp<sup>3</sup>)–H activation reaction performed in a continuous-flow system.

Finally, a black-box optimisation of the investigated reaction was performed. Employed semi-automated reactor system allowed a rapid optimisation effort. Using a very small number of experiments and virtually no labour, the implemented algorithm was able to identify a set of conditions comparable with the one established in the course of the classical kinetic studies.

In Chapter 4.2, a  $\beta$ -C–H oxidative carbonylation of aliphatic amines was investigated. The process gives convenient access to the  $\beta$ -lactam scaffold prevalent in active pharmaceutical ingredients. In the course of the project, a partial kinetic and mechanistic understanding was developed. It revealed that the reaction, even at optimal conditions, is starved of carbon monoxide. This is presumably the main reason for severe inefficiencies of oxidative carbonylation reactions.

Process optimisation and intensification were followed by feasibility studies of a

continuous process design. The 3-phasic system (solid-liquid-gas) was not suitable for a scalable continuous process. Thus, the decision was taken to reduce the number of phases. The identified opportunity of using a heterogeneous precursor of a copper-based oxidant allowed convenient operation in the gas-liquid slug flow regime. This was, to the best of author's knowledge, the first implementation of a copper-tube-flow reactor as a heterogeneous precursor of  $\text{Cu}^{2+}$  oxidant. The *in-situ* generated layer of  $\text{Cu}^{2+}$  proved to be stable for at least 8 hours on-stream. Besides its superior safety, shorter times-to-completion and scalability of the process, when compared with the originally reported procedure, the flow process gave higher yields for all tested substrates. Furthermore, the setup was tested on additional three mechanistically different reactions. All resulted in analogous or better yields compared with the original reports despite virtually no optimisation performed.

Following the design of the flow process, a suitable batch process was designed based on the available heuristics. Optimal conditions were characterised by a very low catalyst loading (0.2 mol%). However, they required a stoichiometric amount of copper (II) acetate. The yield of the batch process was slightly lower than the yield of the flow process.

To identify which designed process option is superior in terms of environmental sustainability, an assessment using simplified metrics as well as an LCI analysis was performed. The simplified metrics identified the flow technology as environmentally superior and the batch process as the one generating the most of environmental burden; the original technology scored slightly worse than the flow process. Contrary to the simplified metrics, the LCI analysis clearly showed that the original technology is the least sustainable. From the developed process options the batch technology was characterised by lower impact values. When the model was extended by a metal recovery, the LCI assessment still identified the original technology as the unfavourable choice in terms of environmental sustainability, however, now the flow and the batch process scored very similarly.

The sustainability assessment undoubtedly presented that the broad, system approach is required to assess the environmental sustainability of the available process options. The analysis using only simplified metrics can lead towards unjustified conclusions.

In summary, the research performed for the thesis resulted in a portfolio of intensified processes for novel C–H activation reactions. The reactors as well as the purification

system can be easily applied to processes characterised by similar conditions and therefore, can accelerate intensification of existing processes or even aid discovery of new reactivities. Furthermore, the developed semi-automated black-box optimisation setup can be used in a rapid search for suitable conditions.

Based on the developed process knowledge, some obstacles to intensification as well as the discovery of new C–H activation reactions were identified, and appropriate solutions were suggested. Owing to the limited number of tested processes, it is difficult to assess whether these solutions are generic. Nevertheless, they may prove to be particularly useful in the design of processes for C–H activation-type reactions of secondary amines.

## Chapter 6. Future work

The present work suggested scalable, intensified processes for two types of C–H activation reactions. Both of them, i.e., the homogeneous C–H activation process, and the oxidative carbonylation process, should be further tested on other, ideally mechanistically different C–H activation reactions. This would reveal whether the developed processes are generic and applicable to a wide range of reactions. Should reactions, that are not suitable for the developed reactor systems, be discovered, either modifications to the existing technologies could be implemented, or new reactor systems might be suggested.

The developed continuous C–H oxidative carbonylation process is currently suitable only for processes where palladium catalyst is being re-oxidised by copper salts. The modification of the process allowing the use of other commonly used oxidants such as, for example, silver salts could prove to be valuable. This might be achieved either, as in the thesis, by using heterogeneous precursors or, presumably, pack-bed reactors would be better suited for this application.

To the best of author's knowledge, there are no examples of C–H electrochemical or photochemical processes performed in continuous flow reactors. Development of intensified processes could potentially accelerate discovery and optimisation of C–H activation processes employing light and electricity to excite molecules. Such effort could be potentially achieved by utilisation of currently available commercial continuous-flow photochemical and electrochemical reactors.

Together with the development of novel continuous reactor systems, it could be valuable to implement high-throughput technologies for discovery of new C–H activation reactions. The capricious nature of such reactivities, combined with a plethora of accessible ligands, precatalyst, etc. makes it virtually impossible to test all of the available reaction conditions in a classical manner. Usage of automated systems, ideally having access to a broad range of operational conditions, such as high temperature or elevated pressure, could potentially lead to discovery of new C–H activation reactions. Perhaps it would be possible to

implement artificial intelligence in a choice of conditions tested using HTE. This could potentially increase the success rate of this technique and contribute to a faster exploration of the chemical space.

Furthermore, it would be useful to consider the development of an automated system designed for partial deconvolution of the observed behaviour using, for example, the Kinetic Motif Analysis. Automated kinetic and mechanistic studies would greatly accelerate optimisation of new processes. Furthermore, a methodology of autonomous development of detailed mechanistic models might be built. Artificial intelligence could potentially devise possible mechanistic scaffolds for a specific transformation that might be further tested in an autonomous reactor system. The process would be repeated iteratively until a satisfactory mechanistic model is built. This could not only aid optimisation efforts but also contribute to a much faster generation of chemical knowledge.

Besides development and utilisation of novel reactor systems, still much work needs to be done to develop a better mechanistic and kinetic understanding of C–H activation reactions. A broad mechanistic understanding could potentially allow formulation of generic principles of design of scalable, intensified processes for this family of reactions. This, in turn, might increase the industrial applicability of C–H activation-type reactions.

## Chapter 7. References

1. Douglas, J. M. A hierarchical decision procedure for process synthesis. *AIChE J.* **31**, 353–362 (1985).
2. Lapkin, A. A., Voutchkova, A. & Anastas, P. A conceptual framework for description of complexity in intensive chemical processes. *Chem. Eng. Process. Process Intensif.* **50**, 1027–1034 (2011).
3. Mann, F. D. System operator tutorial; 9-windows on the world. *TRIZ-journal.com* (2001).
4. Yang, A. & Marquardt, W. An ontological conceptualization of multiscale models. *Comput. Chem. Eng.* **33**, 822–837 (2009).
5. Wand, Y. & Weber, R. An Ontological Model of an Information System. *IEEE Trans. Softw. Eng.* **16**, 1282–1292 (1990).
6. Prasad, V. & Vlachos, D. G. Multiscale model and informatics-based optimal design of experiments: application to the catalytic decomposition of ammonia on Ruthenium. *Ind. Eng. Chem. Res.* **47**, 6555–6567 (2008).
7. Casola, G., Yoshikawa, S., Nakanishi, H., Hirao, M. & Sugiyama, H. Systematic retrofitting methodology for pharmaceutical drug purification processes. *Comput. Chem. Eng.* **80**, 177–188 (2015).
8. Morbach, J., Yang, A. & Marquardt, W. OntoCAPE—A large-scale ontology for chemical process engineering. *Eng. Appl. Artif. Intell.* **20**, 147–161 (2007).
9. Daichendt, M. M. & Grossmann, I. E. Integration of hierarchical decomposition and mathematical programming for the synthesis of process flowsheets. *Comput. Chem. Eng.* **22**, 147–175 (1998).
10. Krishnadasan, S., Brown, R. J. C., DeMello, a J. & DeMello, J. C. Intelligent routes to the controlled synthesis of nanoparticles. *Lab Chip* **7**, 1434–41 (2007).
11. Skilton, R. A., Parrott, A. J., George, M. W., Poliakoff, M. & Bourne, R. A. Real-time feedback control using online attenuated total reflection fourier transform infrared (atr ft-ir) spectroscopy for continuous flow optimization and process knowledge. *Appl. Spectrosc.* **67**, 1127–1131 (2013).
12. Moore, J. S. & Jensen, K. F. Automated multitrajectory method for reaction optimization in a microfluidic system using online IR analysis. *Org. Process Res. Dev.* **16**, 1409–1415 (2012).
13. Moore, J. S. & Jensen, K. F. Batch kinetics in flow: Online IR analysis and continuous control. *Angew. Chemie - Int. Ed.* **53**, 470–473 (2014).

14. Carter, C. F. *et al.* ReactIR Flow Cell: A New Analytical Tool for Continuous Flow Chemical Processing. *Org. Process Res. Dev.* **14**, 393–404 (2010).
15. Smith, C. J., Nikbin, N., Ley, S. V., Lange, H. & Baxendale, I. R. A fully automated, multistep flow synthesis of 5-amino-4-cyano-1,2,3-triazoles. *Org. Biomol. Chem.* **9**, 1938–1947 (2011).
16. Leung, S.-A., Winkle, R. F., Wootton, R. C. R. & deMello, A. J. A method for rapid reaction optimisation in continuous-flow microfluidic reactors using online Raman spectroscopic detection. *Analyst* **130**, 46–51 (2005).
17. Roberto, M. F., Dearing, T. I., Martin, S. & Marquardt, B. J. Integration of Continuous flow reactors and online raman spectroscopy for process optimization. *J. Pharm. Innov.* **7**, 69–75 (2012).
18. Bleie, O. *et al.* Moffat-Swern oxidation of alcohols: Translating a batch reaction to a continuous-flow reaction. *J. Flow Chem.* **5**, 183–189 (2015).
19. Sans, V., Porwol, L., Dragone, V. & Cronin, L. A self optimizing synthetic organic reactor system using real-time in-line NMR spectroscopy. *Chem. Sci.* **6**, 1258–1264 (2015).
20. Echtermeyer, A., Amar, Y., Zakrzewski, J. & Lapkin, A. Self-optimisation and model-based design of experiments for developing a C-H activation flow process. *Beilstein J. Org. Chem.* **13**, 150–163 (2017).
21. Parrott, A. J., Bourne, R. A., Akien, G. R., Irvine, D. J. & Poliakoff, M. Self-optimizing continuous reactions in supercritical carbon dioxide. *Angew. Chemie - Int. Ed.* **50**, 3788–3792 (2011).
22. Jumbam, D. N., Skilton, R. A., Parrott, A. J., Bourne, R. A. & Poliakoff, M. The Effect of Self-Optimisation Targets on the Methylation of Alcohols Using Dimethyl Carbonate in Supercritical CO<sub>2</sub>. *J. Flow Chem.* **2**, 24–27 (2012).
23. McMullen, J. P. & Jensen, K. F. An Automated Microfluidic System for Online Optimization in Chemical Synthesis. *Org. Process Res. Dev.* **14**, 1169–1176 (2010).
24. McMullen, J. P. & Jensen, K. F. Rapid determination of reaction kinetics with an automated microfluidic system. *Org. Process Res. Dev.* **15**, 398–407 (2011).
25. McMullen, J. P., Stone, M. T., Buchwald, S. L. & Jensen, K. F. An integrated microreactor system for self-optimization of a heck reaction: From micro-to mesoscale flow systems. *Angew. Chemie - Int. Ed.* **49**, 7076–7080 (2010).
26. Holmes, N. *et al.* Online quantitative mass spectrometry for the rapid adaptive optimisation of automated flow reactors. *React. Chem. Eng.* **1**, 96–100 (2016).
27. Holmes, N. *et al.* Self-optimisation of the final stage in the synthesis of EGFR kinase inhibitor AZD9291 using an automated flow reactor. *React. Chem. Eng.* **1**, 366–371 (2016).
28. Huyer, W. & Neumaier, A. SNOBFIT -- Stable Noisy Optimization by Branch and Fit. *ACM Trans. Math. Softw.* **35**, 1–25 (2008).
29. Peremezhney, N., Hines, E., Lapkin, A. & Connaughton, C. Combining Gaussian processes, mutual information and a genetic algorithm for multi-target optimization

- of expensive-to-evaluate functions. *Eng. Optim.* **46**, 1593–1607 (2014).
30. Reizman, B. J. & Jensen, K. F. Simultaneous solvent screening and reaction optimization in microliter slugs. *Chem. Commun.* **51**, 2–5 (2015).
  31. Schmink, J. R., Bellomo, A. & Berritt, S. Scientist-led High-Throughput Experimentation (HTE) and its utility in academia and industry. *Aldrichimica Acta* **46**, 71–80 (2013).
  32. Buitrago Santanilla, A. *et al.* Nanomole-scale high-throughput chemistry for the synthesis of complex molecules. *Science*. **347**, 49–53 (2015).
  33. Jakel, C. & Paciello, R. High-Throughput & Parallel Screening Meth for Asymmetric Hydrogenation. *Chem. Rev.* **106**, 2912–2942 (2006).
  34. Fisher, J. & Henzinger, T. A. Executable cell biology. *Nat. Biotechnol.* **25**, 1239–49 (2007).
  35. Bourne, R. A., Skilton, R. A., Parrott, A. J., Irvine, D. J. & Poliakoff, M. Adaptive Process Optimization for Continuous Methylation of Alcohols in Supercritical Carbon Dioxide. *Org. Process Res. Dev.* **15**, 932–938 (2011).
  36. Reizman, B. J. & Jensen, K. F. An Automated Continuous-Flow Platform for the Estimation of Multistep Reaction Kinetics. *Org. Process Res. Dev.* **16**, 1770–1782 (2012).
  37. Moore, J. S., Smith, C. D. & Jensen, K. F. Kinetics analysis and automated online screening of aminocarbonylation of aryl halides in flow. *React. Chem. Eng.* **1**, 272–279 (2016).
  38. Reizman, B. J., Wang, Y.-M., Buchwald, S. L. & Jensen, K. F. Suzuki–Miyaura cross-coupling optimization enabled by automated feedback. *React. Chem. Eng.* **1**, 658–666 (2016).
  39. Hone, C. A., Bourne, R. A. & Muller, F. L. Continuous-flow reactors for the rapid evolution and validation of kinetic motifs. *Chim. Oggi/Chemistry Today* **33**, 14–19 (2015).
  40. Blackmond, D. G. Reaction progress kinetic analysis: A powerful methodology for mechanistic studies of complex catalytic reactions. *Angew. Chemie - Int. Ed.* **44**, 4302–4320 (2005).
  41. Johnson, K. A. & Goody, R. S. The original Michaelis constant: Translation of the 1913 Michaelis-Menten Paper. *Biochemistry* **50**, 8264–8269 (2011).
  42. Lineweaver, H. & Burk, D. The determination of enzyme dissociation constants. *J. Am. Chem. Soc.* **56**, 658–666 (1934).
  43. Hanes, C. S. Studies on plant amylases: The effect of starch concentration upon the velocity of hydrolysis by the amylase of germinated barley. *Biochem. J.* **26**, 1406–1421 (1932).
  44. Hofstee, B. H. J. Non-Inverted Versus Inverted Plots in Enzyme Kinetics. *Nature* **184**, 1296–1298 (1959).
  45. Azadi, P. *et al.* Microkinetic Modeling of the Fischer-Tropsch Synthesis over Cobalt Catalysts. *ChemCatChem* **7**, 137–143 (2015).

46. Zakrzewski, J., Smalley, A. P., Kabeshov, M. A., Gaunt, M. J. & Lapkin, A. A. Continuous-Flow Synthesis and Derivatization of Aziridines through Palladium-Catalyzed C(sp<sup>3</sup>)-H Activation. *Angew. Chemie Int. Ed.* **55**, 8878–8883 (2016).
47. Kimoto, A., Yamauchi, K., Yoshida, M., Masaoka, S. & Sakai, K. Kinetics and DFT studies on wateroxidation by Ce<sup>4+</sup> catalyzed by [Ru(terpy)(bpy)(OH<sub>2</sub>)]<sub>2</sub><sup>+</sup>. *Chem. Commun.* **48**, 239–241 (2012).
48. Paderes, M. C. *et al.* Evidence for alkene cis-aminocupration, an aminooxygenation case study: Kinetics, EPR spectroscopy, and DFT calculations. *Chem. - A Eur. J.* **18**, 1711–1726 (2012).
49. Gernaey, K. V. & Gani, R. A model-based systems approach to pharmaceutical product-process design and analysis. *Chem. Eng. Sci.* **65**, 5757–5769 (2010).
50. Rebmann, E., Fongarland, P., Lecocq, V., Diehl, F. & Schuurman, Y. Kinetic modeling of transient Fischer–Tropsch experiments over Co/Al<sub>2</sub>O<sub>3</sub> catalysts with different microstructures. *Catal. Today* **275**, 20–26 (2016).
51. Mirwald, J. W. & Inderwildi, O. R. Unraveling the Fischer-Tropsch mechanism: a combined DFT and microkinetic investigation of C-C bond formation on Ru. *Phys. Chem. Chem. Phys.* **14**, 7028–7031 (2012).
52. Klinke, D. J. & Broadbelt, L. J. Construction of a mechanistic model of Fischer-Tropsch synthesis on Ni(1 1 1) and Co(0 0 0 1) surfaces. *Chem. Eng. Sci.* **54**, 3379–3389 (1999).
53. Franceschini, G. & Macchietto, S. Model-based design of experiments for parameter precision: State of the art. *Chem. Eng. Sci.* **63**, 4846–4872 (2008).
54. Reinhardt, H. E. Nonlinear Parameter Estimation. *SIAM Rev.* **17**, 703–704 (1975).
55. Box, G. E. P. & Lucas, H. L. Design of Experiments in Non-Linear Situations. *Biometrika* **46**, 77–90 (1959).
56. Zullo, L. C. Computer aided design of experiments: an engineering approach. (Imperial College London (University of London), 1991).
57. Atkinson, A. C. & Bogacka, B. Compound and other optimum designs for systems of nonlinear differential equations arising in chemical kinetics. **61**, 17–33 (2002).
58. Walter, E. & Pronzato, L. Qualitative and quantitative experiment design for phenomenological models-A survey. *Automatica* **26**, 195–213 (1990).
59. De Pauw, D. Optimal experimental design for calibration of bioprocess models: a validated software toolbox. (Ghent University, 2005).
60. Franceschini, G. & Macchietto, S. Validation of a model for biodiesel production through model-based experiment design. *Ind. Eng. Chem. Res.* **46**, 220–232 (2007).
61. Maheshwari, V., Rangaiah, G. P. & Samavedham, L. Multiobjective framework for model-based design of experiments to improve parameter precision and minimize parameter correlation. *Ind. Eng. Chem. Res.* **52**, 8289–8304 (2013).
62. Sidoli, F. R., Mantalaris, A. & Asprey, S. P. Modelling of Mammalian Cells and Cell Culture Processes. *Cytotechnology* **44**, 27–46 (2004).

63. Hartman, R. L., McMullen, J. P. & Jensen, K. F. Deciding Whether To Go with the Flow: Evaluating the Merits of Flow Reactors for Synthesis. *Angew. Chemie Int. Ed.* **50**, 7502–7519 (2011).
64. Hessel, V., Kralisch, D., Kockmann, N., No?l, T. & Wang, Q. Novel Process Windows for Enabling, Accelerating, and Uplifting Flow Chemistry. *ChemSusChem* **6**, 746–789 (2013).
65. Mallia, C. J. & Baxendale, I. R. The Use of Gases in Flow Synthesis. *Org. Process Res. Dev.* **20**, 327–360 (2016).
66. Movsisyan, M. *et al.* Taming hazardous chemistry by continuous flow technology. *Chem. Soc. Rev.* **45**, 4892–4928 (2016).
67. Newman, S. G. & Jensen, K. F. The role of flow in green chemistry and engineering. *Green Chem.* **15**, 1456 (2013).
68. Wegner, J., Ceylan, S. & Kirschning, A. Flow chemistry - A key enabling technology for (multistep) organic synthesis. *Adv. Synth. Catal.* **354**, 17–57 (2012).
69. Yoshida, J. I., Nagaki, A. & Yamada, T. Flash chemistry: Fast chemical synthesis by using microreactors. *Chem. - A Eur. J.* **14**, 7450–7459 (2008).
70. McQuade, D. T. & Seeberger, P. H. Applying Flow Chemistry: Methods, Materials, and Multistep Synthesis. *J. Org. Chem.* **78**, 6384–6389 (2013).
71. Plutschack, M. B., Pieber, B., Gilmore, K. & Seeberger, P. H. The Hitchhiker's Guide to Flow Chemistry. *Chem. Rev.* **117**, 11796–11893 (2017).
72. Elvira, K. S., i Solvas, X. C., Wootton, R. C. R. & deMello, A. J. The past, present and potential for microfluidic reactor technology in chemical synthesis. *Nat. Chem.* **5**, 905–915 (2013).
73. Baxendale, I. R. The integration of flow reactors into synthetic organic chemistry. *J. Chem. Technol. Biotechnol.* **88**, 519–552 (2013).
74. Malet-Sanz, L. & Susanne, F. Continuous flow synthesis. a pharma perspective. *J. Med. Chem.* **55**, 4062–4098 (2012).
75. Jensen, K. F., Reizman, B. J. & Newman, S. G. Tools for chemical synthesis in microsystems. *Lab Chip* **14**, 3206–3212 (2014).
76. Reynolds, O. An Experimental Investigation of the Circumstances Which Determine Whether the Motion of Water Shall Be Direct or Sinuous, and of the Law of Resistance in Parallel Channels. *Philos. Trans. R. Soc. London* **174**, 935–982 (1883).
77. Fick, A. On liquid diffusion. *J. Memb. Sci.* **100**, 33–38 (1995).
78. Hornung, C. H. & Mackley, M. R. The measurement and characterisation of residence time distributions for laminar liquid flow in plastic microcapillary arrays. *Chem. Eng. Sci.* **64**, 3889–3902 (2009).
79. Lohse, S. *et al.* A novel method for determining residence time distribution in intricately structured microreactors. *Lab Chip* **8**, 431 (2008).
80. Paul, E. L., Atiemo-Obeng, V. A. & Kresta, S. M. *Handbook of industrial mixing: science and practice.* (John Wiley & Sons, 2004).

81. Baldyga, J. & Bourne, J. R. *Turbulent mixing and chemical reactions*. (Wiley, 1999).
82. Alvarez, M. M., Zalc, J. M., Shinbrot, T., Arratia, P. E. & Muzzio, F. J. Mechanisms of mixing and creation of structure in laminar stirred tanks. *AIChE J.* **48**, 2135–2148 (2002).
83. Ehrfeld, W., Golbig, K., Hessel, V., Lowe, H. & Richter, T. Characterization of mixing in micromixers by a test reaction: single mixing units and mixer arrays. *Ind. Eng. Chem. Res.* **38**, 1075–1082 (1999).
84. Aoki, N. & Mae, K. Effects of channel geometry on mixing performance of micromixers using collision of fluid segments. *Chem. Eng. J.* **118**, 189–197 (2006).
85. Reckamp, J. M. *et al.* Mixing Performance Evaluation for Commercially Available Micromixers Using Villermaux-Dushman Reaction Scheme with the Interaction by Exchange with the Mean Model. *Org. Process Res. Dev.* **21**, 816–820 (2017).
86. Lee, C. Y., Chang, C. L., Wang, Y. N. & Fu, L. M. Microfluidic mixing: A review. *Int. J. Mol. Sci.* **12**, 3263–3287 (2011).
87. Damköhler, G. Einflüsse der Strömung, Diffusion und des Wärmeüberganges auf die Leistung von Reaktionsöfen.: I. Allgemeine Gesichtspunkte für die Übertragung eines chemischen Prozesses aus dem Kleinen ins Große. *Zeitschrift für Elektrochemie und Angew. Phys. Chemie* **42**, 846–862 (1936).
88. Baldyga, J., Henczka, M. & Podgórska, W. *Obliczenia w inżynierii bioreaktorów*. (Oficyna Wydawnicza Politechniki Warszawskiej, 1996).
89. Henry, W. Experiments on the Quantity of Gases Absorbed by Water, at Different Temperatures, and under Different Pressures. *Philos. Trans. R. Soc. London* **93**, 29–274 (1803).
90. Yue, J., Chen, G., Yuan, Q., Luo, L. & Gonthier, Y. Hydrodynamics and mass transfer characteristics in gas-liquid flow through a rectangular microchannel. *Chem. Eng. Sci.* **62**, 2096–2108 (2007).
91. Rebrov, E. V. Two-phase flow regimes in microchannels. *Theor. Found. Chem. Eng.* **44**, 355–367 (2010).
92. Santos, J. M. De, Melli, T. R. & Scriven, L. E. Mechanics of Gas-Liquid Flow in Packed-Bed. *Annu. Rev. Fluid Mech* **189**, 233–60 (1991).
93. Gilliland, E. R. Davidson, J. F. Fluidised particles. *AIChE J.* **10**, 783–785 (1964).
94. Deen, W. M. *Analysis of transport phenomena*. (1998).
95. Bergman, T. L. & Incropera, F. P. *Fundamentals of heat and mass transfer*. (John Wiley & Sons, 2011).
96. Odedra, A. & Seeberger, P. H. 5-(Pyrrolidin-2-yl)tetrazole-catalyzed aldol and mannich reactions: Acceleration and lower catalyst loading in a continuous-flow reactor. *Angew. Chemie - Int. Ed.* **48**, 2699–2702 (2009).
97. Valera, F. E. *et al.* The Flow's the Thing...Or Is It? Assessing the Merits of Homogeneous Reactions in Flask and Flow. *Angew. Chemie Int. Ed.* **49**, 2478–2485 (2010).

98. Usutani, H. *et al.* Generation and reactions of o-bromophenyllithium without benzyne formation using a microreader. *J. Am. Chem. Soc.* **129**, 3046–3047 (2007).
99. Loubière, K., Oelgemöller, M., Aillet, T., Dechy-Cabaret, O. & Prat, L. Continuous-flow photochemistry: A need for chemical engineering. *Chem. Eng. Process. Process Intensif.* **104**, 120–132 (2016).
100. Cambié, D., Bottecchia, C., Straathof, N. J. W., Hessel, V. & Noël, T. Applications of Continuous-Flow Photochemistry in Organic Synthesis, Material Science, and Water Treatment. *Chem. Rev.* **116**, 10276–10341 (2016).
101. Watts, K., Baker, A. & Wirth, T. Electrochemical Synthesis in Microreactors. *J. Flow Chem.* **4**, 2–11 (2015).
102. Horn, E. J., Rosen, B. R. & Baran, P. S. Synthetic organic electrochemistry: An enabling and innately sustainable method. *ACS Cent. Sci.* **2**, 302–308 (2016).
103. Green, R. A., Brown, R. C. D. & Pletcher, D. Electrosynthesis in extended channel length microfluidic electrolysis cells. *J. Flow Chem.* **6**, 191–197 (2016).
104. Kitson, P. J. *et al.* 3D printing of versatile reactionware for chemical synthesis. *Nat. Protoc.* **11**, 920–936 (2016).
105. Bao, J. & Tranmer, G. K. The utilization of copper flow reactors in organic synthesis. *Chem. Commun.* **51**, 3037–3044 (2015).
106. A. Lapkin, A., Loponov, K., Tomaiuolo, G. & Guido, S. in *Sustainable Flow Chemistry* 277–308 (Wiley-VCH Verlag GmbH & Co. KGaA, 2017).
107. Greco, R., Goessler, W., Cantillo, D. & Kappe, C. O. Benchmarking immobilized di- and triarylphosphine palladium catalysts for continuous-flow cross-coupling reactions: Efficiency, durability, and metal leaching studies. *ACS Catal.* **5**, 1303–1312 (2015).
108. Mo, Y. & Jensen, K. F. A miniature CSTR cascade for continuous flow of reactions containing solids. *React. Chem. Eng.* **1**, 501–507 (2016).
109. Chapman, M. R. *et al.* Simple and Versatile Laboratory Scale CSTR for Multiphasic Continuous-Flow Chemistry and Long Residence Times. *Org. Process Res. Dev.* **21**, 1294–1301 (2017).
110. Linstrom, P. J. & Mallard, W. G. *NIST Chemistry webBook, NIST Standard Reference Database Number 69. National Institute of Standards and Technology* (2014).
111. Gemoets, H. P. L., Laudadio, G., Verstraete, K., Hessel, V. & Noël, T. A Modular Flow Design for the meta-Selective C–H Arylation of Anilines. *Angew. Chemie - Int. Ed.* **56**, 7161–7165 (2017).
112. Dewick, P. M. *Medicinal natural products: a biosynthetic approach*. (John Wiley & Sons, 2002).
113. Webb, D. & Jamison, T. F. Continuous flow multi-step organic synthesis. *Chem. Sci.* **1**, 675 (2010).
114. Tsubogo, T., Oyamada, H. & Kobayashi, S. Multistep continuous-flow synthesis of (R)- and (S)-rolipram using heterogeneous catalysts. *Nature* **520**, 329–332 (2015).

115. Adamo, A. *et al.* On-demand continuous-flow production of pharmaceuticals in a compact, reconfigurable system. *Science*. **352**, 61–67 (2016).
116. Fitzpatrick, D. E. & Ley, S. V. Engineering chemistry: integrating batch and flow reactions on a single, automated reactor platform. *React. Chem. Eng.* **1**, 629–635 (2016).
117. Park, N. H., Senter, T. J. & Buchwald, S. L. Rapid Synthesis of Aryl Fluorides in Continuous Flow through the Balz-Schiemann Reaction. *Angew. Chemie - Int. Ed.* **55**, 11907–11911 (2016).
118. Battilocchio, C. *et al.* Iterative reactions of transient boronic acids enable sequential C–C bond formation. *Nat. Chem.* **8**, 360–367 (2016).
119. Poh, J.-S. *et al.* A multicomponent approach for the preparation of homoallylic alcohols. *Chem. Sci.* **7**, 6803–6807 (2016).
120. Roda, N. M. *et al.* Cyclopropanation using flow-generated diazo compounds. *Org. Biomol. Chem.* **13**, 2550–2554 (2015).
121. Ley, S. V. & Baxendale, I. R. New tools and concepts for modern organic synthesis. *Nat. Rev. Drug Discov.* **1**, 573–586 (2002).
122. Ley, S. V., Fitzpatrick, D. E., Ingham, R. J. & Myers, R. M. Organic Synthesis: March of the Machines. *Angew. Chemie Int. Ed.* **54**, 3449–3464 (2015).
123. Pastre, J. C., Browne, D. L. & Ley, S. V. Flow chemistry syntheses of natural products. *Chem. Soc. Rev.* **42**, 8849 (2013).
124. Sahoo, H. R., Kralj, J. G. & Jensen, K. F. Multistep Continuous-Flow Microchemical Synthesis Involving Multiple Reactions and Separations. *Angew. Chemie* **119**, 5806–5810 (2007).
125. Atherton, J. H. & Carpenter, K. J. Process Development: Physicochemical Concepts. *Oxford Chem. Prim.* **79**, 1–88 (1999).
126. Evangelista, J. J., Katz, S. & Shinnar, R. Scale-up criteria for stirred tank reactors. *AIChE J.* **15**, 843–853 (1969).
127. Koganti, V. *et al.* Application of Modeling to Scale-up Dissolution in Pharmaceutical Manufacturing. *AAPS PharmSciTech* **11**, 1541–1548 (2010).
128. Bisio, A. & Kabel, R. L. *Scaleup of chemical processes: Conversion from laboratory scale tests to successful commercial size design.* (Wiley, 1985).
129. Haswell, S. J. & Watts, P. Green chemistry: synthesis in micro reactors. *Green Chem.* **5**, 240–249 (2003).
130. Amador, C., Gavriilidis, A. & Angeli, P. Flow distribution in different microreactor scale-out geometries and the effect of manufacturing tolerances and channel blockage. *Chem. Eng. J.* **101**, 379–390 (2004).
131. Brown, D. G. & Boström, J. Analysis of Past and Present Synthetic Methodologies on Medicinal Chemistry: Where Have All the New Reactions Gone? *J. Med. Chem.* **59**, 4443–4458 (2016).
132. Stromnova, T. A., Vargaftik, M. N. & Moiseev, I. I. Mechanism of reaction of

- palladium(II) carboxylates with carbon monoxide in nonaqueous media. *J. Organomet. Chem.* **252**, 113–120 (1983).
133. Stromnova, T. A., Busygina, I. N., Kochubey, D. I. & Moiseev, I. I. Palladium carbene cluster: synthesis, structure and reactivity. *J. Organomet. Chem.* **417**, 193–204 (1991).
134. Zhang, M. *et al.* Recent advances in directed C–H functionalizations using monodentate nitrogen-based directing groups. *Org. Chem. Front.* **1**, 843 (2014).
135. Gensch, T., Hopkinson, M. N., Glorius, F. & Wencel-Delord, J. Mild metal-catalyzed C–H activation: examples and concepts. *Chem. Soc. Rev.* **110**, 1147–1169 (2016).
136. McMurray, L., O’Hara, F. & Gaunt, M. J. Recent developments in natural product synthesis using metal-catalysed C–H bond functionalisation. *Chem. Soc. Rev.* **40**, 1885–1898 (2011).
137. Chen, Z. *et al.* Transition metal-catalyzed C–H bond functionalizations by the use of diverse directing groups. *Org. Chem. Front.* **2**, 1107–1295 (2015).
138. He, J., Wasa, M., Chan, K. S. L., Shao, Q. & Yu, J.-Q. Palladium-Catalyzed Transformations of Alkyl C–H Bonds. *Chem. Rev.* **117**, 8754–8786 (2017).
139. Fairlamb, I. J. S. & Kapdi, A. R. in *Strategies for Palladium-Catalyzed Non-Directed and Directed C–H Bond Functionalization* (eds. Kapdi, A. R. & Maiti, D.) 9–48 (Elsevier, 2017).
140. Jazzar, R., Hitce, J., Renaudat, A., Sofack-Kreutzer, J. & Baudoin, O. Functionalization of organic molecules by transition-metal-catalyzed C(sp<sup>3</sup>)-H activation. *Chem. - A Eur. J.* **16**, 2654–2672 (2010).
141. Chiong, H. A., Pham, Q. N. & Daugulis, O. Two methods for direct ortho-arylation of benzoic acids. *J. Am. Chem. Soc.* **129**, 9879–9884 (2007).
142. Engle, K. M., Mei, T. S., Wasa, M. & Yu, J. Q. Weak coordination as a powerful means for developing broadly useful C–H functionalization reactions. *Acc. Chem. Res.* **45**, 788–802 (2012).
143. Stowers, K. J., Fortner, K. C. & Sanford, M. S. Aerobic Pd-catalyzed sp<sup>3</sup> C–H olefination: A route to both N-heterocyclic scaffolds and alkenes. *J. Am. Chem. Soc.* **133**, 6541–6544 (2011).
144. Simmons, E. M. & Hartwig, J. F. Catalytic functionalization of unactivated primary C–H bonds directed by an alcohol. *Nature* **483**, 70–73 (2012).
145. Chan, K. S. L. *et al.* Ligand-enabled cross-coupling of C(sp)-H bonds with arylboron reagents via Pd(II)/Pd(0) catalysis. *Nat. Chem.* **6**, 146–150 (2014).
146. Zaitsev, V. G., Shabashov, D. & Daugulis, O. Highly regioselective arylation of sp<sup>3</sup> C–H bonds catalyzed by palladium acetate. *J. Am. Chem. Soc.* **127**, 13154–13155 (2005).
147. Topczewski, J. J., Cabrera, P. J., Saper, N. I. & Sanford, M. S. Palladium-catalysed transannular C–H functionalization of alicyclic amines. *Nature* **531**, 220–224 (2016).

148. McNally, A., Haffemayer, B., Collins, B. S. L. & Gaunt, M. J. Palladium-catalysed C-H activation of aliphatic amines to give strained nitrogen heterocycles. *Nature* **512**, 338 (2014).
149. Calleja, J. *et al.* A steric tethering approach enables palladium-catalysed C-H activation of primary amino alcohols. *Nat. Chem.* **7**, 1009–1016 (2015).
150. Smalley, A. P. & Gaunt, M. J. Mechanistic Insights into the Palladium-Catalyzed Aziridination of Aliphatic Amines by C-H Activation. *J. Am. Chem. Soc.* **137**, 10632–10641 (2015).
151. He, C. & Gaunt, M. J. Ligand-Enabled Catalytic C-H Arylation of Aliphatic Amines by a Four-Membered-Ring Cyclopalladation Pathway. *Angew. Chemie - Int. Ed.* **54**, 15840–15844 (2015).
152. Gaunt, M. J., Williamson, P. & Galván, A. Cobalt-catalysed C-H carbonylative cyclisation of aliphatic amides. *Chem. Sci.* **8**, 2588–2591 (2017).
153. He, C. & Gaunt, M. J. Ligand-assisted palladium-catalyzed C-H alkenylation of aliphatic amines for the synthesis of functionalized pyrrolidines. *Chem. Sci.* **8**, 3586–3592 (2017).
154. Gabriele, B., Mancuso, R. & Salerno, G. Oxidative carbonylation as a powerful tool for the direct synthesis of carbonylated heterocycles. *European J. Org. Chem.* **2012**, 6825–6839 (2012).
155. Heck, R. F. & Breslow, D. S. Carboxyalkylation Reactions Catalyzed by Cobalt Carbonylate Ion. *J. Am. Chem. Soc.* **85**, 2779–2782 (1963).
156. Heck, R. F. & Nolley, J. P. Palladium-catalyzed vinylic hydrogen substitution reactions with aryl, benzyl, and styryl halides. *J. Org. Chem.* **37**, 2320–2322 (1972).
157. Barnard, C. F. J. Palladium-catalyzed carbonylation - A reaction come of age. *Organometallics* **27**, 5402–5422 (2008).
158. Le Berre, C., Serp, P., Kalck, P. & Torrence, G. P. in *Ullmann's Encyclopedia of Industrial Chemistry* 1–34 (Wiley-VCH Verlag GmbH & Co. KGaA, 2014).
159. Elango Varadaraj, Murphy Mark Alan, Smith Brad Lee, Davenport Kenneth G., Mott Graham N., M. G. L. Process for producing ibuprofen. (1988).
160. Davies, I. W. *et al.* A highly active catalyst for the reductive cyclization of ortho-nitrostyrenes under mild conditions. *Tetrahedron* **61**, 6425–6437 (2005).
161. Ori, M., Toda, N., Takami, K., Tago, K. & Kogen, H. Stereospecific synthesis of 2,2,3-trisubstituted tetrahydroquinolines: application to the total syntheses of benzastatin E and natural virantmycin. *Tetrahedron* **61**, 2075–2104 (2005).
162. Liu, Q., Zhang, H. & Lei, A. Oxidative Carbonylation Reactions: Organometallic Compounds (R-M) or Hydrocarbons (R-H) as Nucleophiles. *Angew. Chemie Int. Ed.* **50**, 10788–10799 (2011).
163. Wu, X.-F., Neumann, H. & Beller, M. Palladium-Catalyzed Oxidative Carbonylation Reactions. *ChemSusChem* **6**, 229–241 (2013).
164. Wu, X.-F., Neumann, H. & Beller, M. Synthesis of Heterocycles via Palladium-Catalyzed Carbonylations. *Chem. Rev.* **113**, 1–35 (2013).

165. Bertleff, W., Roeper, M. & Sava, X. in *Ullmann's Encyclopedia of Industrial Chemistry* (Wiley-VCH Verlag GmbH & Co. KGaA, 2007).
166. Alonso, N. *et al.* First Example of a Continuous-Flow Carbonylation Reaction Using Aryl Formates as CO Precursors. *J. Flow Chem.* **4**, 105–109 (2014).
167. Brancour, C., Fukuyama, T., Mukai, Y., Skrydstrup, T. & Ryu, I. Modernized low pressure carbonylation methods in batch and flow employing common acids as a CO source. *Org. Lett.* **15**, 2794–2797 (2013).
168. Orito, K. *et al.* Pd(OAc)<sub>2</sub>-Catalyzed Carbonylation of Amines. *J. Org. Chem.* **71**, 5951–5958 (2006).
169. Li, W. *et al.* Palladium-Catalyzed Oxidative Carbonylation of *N*-Allylamines for the Synthesis of  $\beta$ -Lactams. *Angew. Chemie* **126**, 2475–2478 (2014).
170. Gemoets, H. P. L., Hessel, V. & Noël, T. Aerobic C-H olefination of indoles via a cross-dehydrogenative coupling in continuous flow. *Org. Lett.* **16**, 5800–5803 (2014).
171. Moschetta, E. G. *et al.* Composite Polymer/Oxide Hollow Fiber Contactors: Versatile and Scalable Flow Reactors for Heterogeneous Catalytic Reactions in Organic Synthesis. *Angew. Chemie Int. Ed.* **54**, 6470–6474 (2015).
172. Erdmann, N., Su, Y., Bosmans, B., Hessel, V. & Noël, T. Palladium-Catalyzed Aerobic Oxidative Coupling of *o*-Xylene in Flow: A Safe and Scalable Protocol for Cross-Dehydrogenative Coupling. *Org. Process Res. Dev.* **20**, 831–835 (2016).
173. Phipps, R. J. & Gaunt, M. J. A Meta-Selective Copper-Catalyzed C – H Bond Arylation. *Science*. **323**, 1593–1598 (2009).
174. Bavykin, D. V., Lapkin, A. A., Kolaczkowski, S. T. & Plucinski, P. K. Selective oxidation of alcohols in a continuous multifunctional reactor: Ruthenium oxide catalysed oxidation of benzyl alcohol. *Appl. Catal. A Gen.* **288**, 175–184 (2005).
175. Liedtke, A. K. *et al.* Liquid-solid mass transfer for microchannel suspension catalysis in gas-liquid and liquid-liquid segmented flow. *Ind. Eng. Chem. Res.* **54**, 4699–4708 (2015).
176. Koos, P. *et al.* Teflon AF-2400 mediated gas-liquid contact in continuous flow methoxycarbonylations and in-line FTIR measurement of CO concentration. *Org. Biomol. Chem.* **9**, 6903 (2011).
177. Miller, P. W. *et al.* Rapid formation of amides via carbonylative coupling reactions using a microfluidic device. *Chem. Commun.* **5**, 546–548 (2006).
178. Miller, P. W. *et al.* Rapid multiphase carbonylation reactions by using a microtube reactor: Applications in positron emission tomography <sup>11</sup>C-radiolabeling. *Angew. Chemie - Int. Ed.* **46**, 2875–2878 (2007).
179. Rahman, M. T., Fukuyama, T., Kamata, N., Sato, M. & Ryu, I. Low pressure Pd-catalyzed carbonylation in an ionic liquid using a multiphase microflow system. *Chem. Commun. (Camb)*. **1**, 2236–8 (2006).
180. Fukuyama, T., Rahman, M. T., Kamata, N. & Ryu, I. Radical carbonylations using a continuous microflow system. *Beilstein J. Org. Chem.* **5**, 1–5 (2009).

181. Mercadante, M. a & Leadbeater, N. E. Continuous-flow, palladium-catalysed alkoxy carbonylation reactions using a prototype reactor in which it is possible to load gas and heat simultaneously. *Org. Biomol. Chem.* **9**, 6575–6578 (2011).
182. Kelly, C. B., Lee, C., Mercadante, M. A. & Leadbeater, N. E. A continuous-flow approach to palladium-catalyzed alkoxy carbonylation reactions. *Org. Process Res. Dev.* **15**, 717–720 (2011).
183. Fukuyama, T., Mukai, Y. & Ryu, I. Koch-Haaf reaction of adamantanols in an acid-tolerant hastelloy-made microreactor. *Beilstein J. Org. Chem.* **7**, 1288–1293 (2011).
184. Gross, U., Koos, P., O'brien, M., Polyzos, A. & Ley, S. V. A general continuous flow method for palladium catalysed carbonylation reactions using single and multiple tube-in-tube gas-liquid microreactors. *European J. Org. Chem.* **2014**, 6418–6430 (2014).
185. Akinaga, H., Masaoka, N., Takagi, K., Ryu, I. & Fukuyama, T. Flow Carbonylation Using Near-stoichiometric Carbon Monoxide. Application to Heck Carbonylation. *Chem. Lett.* **43**, 1456–1458 (2014).
186. Fukuyama, T., Totoki, T. & Ryu, I. Carbonylation in microflow: close encounters of CO and reactive species. *Green Chem.* **16**, 2042 (2014).
187. Anastas, P. & Eghbali, N. Green Chemistry: Principles and Practice. *Chem. Soc. Rev.* **39**, 301–312 (2010).
188. Anastas, P. T. & Warner, J. C. *Green chemistry: theory and practice*. (Oxford university press, 2000).
189. Stankiewicz, A. I., Moulijn, J. A. & Etchells, J. C. Process Intensification. *Process Saf. Environ. Prot.* **83**, 85–89 (2005).
190. Charpentier, J. C. What Kind of Modern 'green' Chemical Engineering is Required for the Design of the 'factory of Future'? *Procedia Eng.* **138**, 445–458 (2016).
191. Alder, C. M. *et al.* Updating and further expanding GSK's solvent sustainability guide. *Green Chem.* **18**, 3879–3890 (2016).
192. Sheldon, R. A. The E Factor: fifteen years on. *Green Chem.* **9**, 1273 (2007).
193. Henderson, R. K., Constable, D. J. C. & Jimnez-Gonzlez, C. in *Green Chemistry in the Pharmaceutical Industry* 21–48 (Wiley-VCH Verlag GmbH & Co. KGaA, 2010).
194. International Standard Organisation. Environmental assessment - Principles and framework. *Iso 14040* **1997**, (1997).
195. Lapkin, A. A. & Yaseneva, P. Life Cycle Assessment of Flow Chemistry Processes. *Sustain. Flow Chem. Methods Appl.* (2017).
196. Goedkoop, M. *et al.* ReCiPe 2008. *Potentials* 1–44 (2009).
197. Associates, F. & Village, P. National Council for Air and Stream Improvement an Analysis of the Methods Used To Address the Carbon Cycle in Wood and Paper Product Lca Studies. (2004).

198. Sathre, R. & O'Connor, J. Meta-analysis of greenhouse gas displacement factors of wood product substitution. *Environ. Sci. Policy* **13**, 104–114 (2010).
199. M. J. Frisch, G. W. Trucks, H. B. Schlegel, G. E. Scuseria, M. A. Robb, J. R. Cheeseman, G. Scalmani, V. Barone, G. A. Petersson, H. Nakatsuji, X. Li, M. Caricato, A. Marenich, J. Bloino, B. G. Janesko, R. Gomperts, B. Mennucci, H. P. Hratchian, J. V. Ort, and D. J. F. Gaussian 09, Revision A.02. (2017).
200. Peremezhney, N. Chemical product/process design and optimization: development of novel techniques and integration of bio-feedstocks. (University of Warwick, 2013).
201. Houben, C., Peremezhney, N., Zubov, A., Kosek, J. & Lapkin, A. A. Closed-Loop Multitarget Optimization for Discovery of New Emulsion Polymerization Recipes. *Org. Process Res. Dev.* **19**, 1049–1053 (2015).
202. Seeger, M. Gaussian Processes for Machine Learning. *Int. J. Neural Syst.* **14**, 69–106 (2004).
203. Willcox, D. *et al.* A general catalytic  $\beta$ -C–H carbonylation of aliphatic amines to  $\beta$ -lactams. *Science*. **354**, 851–857 (2016).
204. Ryabov, A. D. Mechanisms of intramolecular activation of carbon-hydrogen bonds in transition-metal complexes. *Chem. Rev.* **90**, 403–424 (1990).
205. Simmons, E. M. & Hartwig, J. F. On the Interpretation of Deuterium Kinetic Isotope Effects in C–H Bond Functionalizations by Transition-Metal Complexes. *Angew. Chemie Int. Ed.* **51**, 3066–3072 (2012).
206. Davies, D. L., Donald, S. M. A. & Macgregor, S. A. Computational study of the mechanism of cyclometalation by palladium acetate. *J. Am. Chem. Soc.* **127**, 13754–13755 (2005).
207. Lafrance, M., Rowley, C. N., Woo, T. K. & Fagnou, K. Catalytic Intermolecular Direct Arylation of Perfluorobenzenes. *J. Am. Chem. Soc.* **128**, 8754–8756 (2006).
208. Lafrance, M., Gorelsky, S. I. & Fagnou, K. High-Yielding Palladium-Catalyzed Intramolecular Alkane Arylation: Reaction Development and Mechanistic Studies. *J. Am. Chem. Soc.* **129**, 14570–14571 (2007).
209. García-Cuadrado, D., Braga, A. A. C., Maseras, F. & Echavarren, A. M. Proton abstraction mechanism for the palladium-catalyzed intramolecular arylation. *J. Am. Chem. Soc.* **128**, 1066–1067 (2006).
210. Balcells, D., Clot, E. & Eisenstein, O. C–H Bond activation in transition metal species from a computational perspective. *Chem. Rev.* **110**, 749–823 (2010).
211. Ackermann, L. Carboxylate-assisted transition-metal-catalyzed C–H bond functionalizations: Mechanism and scope. *Chemical Reviews* **111**, 1315–1345 (2011).
212. Process Systems Enterprise. gProms Model Builder.
213. Evans, M. G. & Polanyi, M. Some applications of the transition state method to the calculation of reaction velocities, especially in solution. *Trans. Faraday Soc.* **31**, 875 (1935).

214. Tano, T., Esumi, K. & Meguro, K. Preparation of organopalladium sols by thermal decomposition of palladium acetate. *J. Colloid Interface Sci.* **133**, 530–533 (1989).
215. Hu, X. E. Nucleophilic ring opening of aziridines. *Tetrahedron* **60**, 2701–2743 (2004).
216. Hsueh, N., Clarkson, G. J. & Shipman, M. Generation and Ring Opening of Aziridines in Telescoped Continuous Flow Processes. *Org. Lett.* **17**, 3632–3635 (2015).
217. Zakrzewski, J. *et al.* Continuous flow synthesis and derivatization of aziridines via C – H activation. *Angew. Chemie Int. Ed.* **55**, 8878–8883 (2016).
218. COSMOlogic GmbH & Co KG, <http://www.cosmologic.d>. COSMOtherm. (2017).
219. Porta, R., Benaglia, M. & Puglisi, A. Flow Chemistry: Recent Developments in the Synthesis of Pharmaceutical Products. *Org. Process Res. Dev.* **20**, 2–25 (2016).
220. Zhang, J., Gong, C., Zeng, X. & Xie, J. Continuous flow chemistry: New strategies for preparative inorganic chemistry. *Coord. Chem. Rev.* **324**, 39–53 (2016).
221. Fanelli, F., Parisi, G., Degennaro, L. & Luisi, R. Contribution of microreactor technology and flow chemistry to the development of green and sustainable synthesis. *Beilstein J. Org. Chem.* **13**, 520–542 (2017).
222. Wegner, J., Ceylan, S. & Kirschning, A. Ten key issues in modern flow chemistry. *Chem. Commun.* **47**, 4583 (2011).
223. Ceylan, S., Klände, T., Vogt, C., Friese, C. & Kirschning, A. Chemical synthesis with inductively heated copper flow reactors. *Synlett* **2010**, 2009–2013 (2010).
224. McQuillan, K. W. & Whalley, P. B. Flow patterns in vertical two-phase flow. *Int. J. Multiph. Flow* **11**, 161–175 (1985).
225. Giri, R. & Yu, J. Q. Synthesis of 1,2- and 1,3-dicarboxylic acids via Pd(II)-catalyzed carboxylation of aryl and vinyl C-H bonds. *J. Am. Chem. Soc.* **130**, 14082–14083 (2008).
226. Ecoinvent Centre. *Ecoinvent Data v2.2. Ecoinvent Reports No. 1-25, Swiss Centre for Life Cycle Inventories.* (2010).
227. *Ullmann's Encyclopedia of Industrial Chemistry.* (Wiley-VCH Verlag GmbH & Co. KGaA, 2009).
228. Wells, M. *Handbook of petrochemicals and processes.* (Ashgate Publishing Co., 1999).
229. Umberto v.5.6. (2010).
230. Motojima, K., Horie, M. & Torada, S. Method of recovering palladium by electrolysis and apparatus therefor. (1993).

## Chapter 8. Appendices

### 8.1. Appendix 1

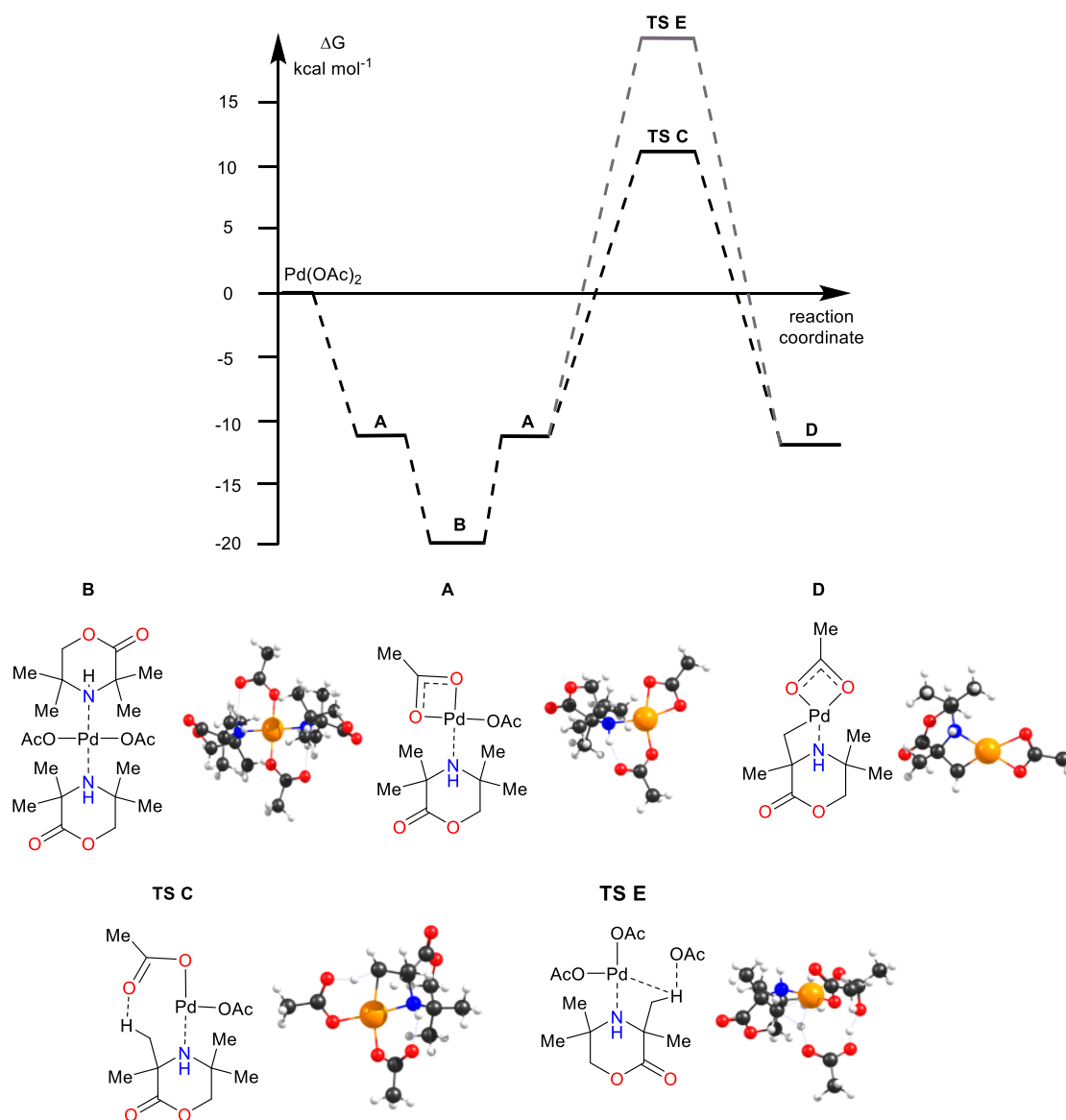


Figure 8.1-1. Energy profile of cyclopalladation proceeding through a CMD mechanism.

Cartesian coordinates and uncorrected electronic energies of the computed structures:

Complex B

Pd	-0.000047000	-0.000032000	-0.000006000
C	2.985269000	-0.508841000	-0.971197000
C	2.690679000	-0.236027000	1.573489000
C	4.211660000	-0.510547000	1.488772000
H	4.415380000	-1.577484000	1.356372000
C	-2.985305000	0.508694000	0.971072000
C	-2.690598000	0.236270000	-1.573661000
C	-4.211596000	0.510835000	-1.489043000
H	-4.415283000	1.577791000	-1.356742000
N	-2.156689000	-0.026261000	-0.180815000
N	2.156688000	0.026248000	0.180633000
C	-2.021470000	1.443435000	-2.244887000
H	-2.057819000	2.332880000	-1.614637000
H	-0.972584000	1.230415000	-2.464435000
H	-2.528701000	1.661949000	-3.191672000
C	-2.449650000	-1.029085000	-2.416034000
H	-1.389764000	-1.296844000	-2.423147000
H	-3.017102000	-1.878332000	-2.026438000
H	-2.760316000	-0.845043000	-3.449033000
C	-3.078062000	2.045263000	1.062218000
H	-2.079228000	2.462349000	1.180465000
H	-3.542719000	2.513336000	0.192955000
H	-3.688104000	2.295332000	1.934996000
C	-2.390548000	-0.029292000	2.281836000
H	-2.282866000	-1.115228000	2.248240000
H	-1.412969000	0.428050000	2.456438000
H	-3.057243000	0.221424000	3.107982000
C	2.449776000	1.029462000	2.415673000
H	3.017137000	1.878665000	2.025841000
H	1.389876000	1.297161000	2.422884000
H	2.760598000	0.845618000	3.448659000

---

C	2.021641000	-1.443117000	2.244942000
H	0.972784000	-1.230059000	2.464592000
H	2.057911000	-2.332634000	1.614782000
H	2.528983000	-1.661533000	3.191691000
C	2.390430000	0.028956000	-2.282013000
H	1.412852000	-0.428430000	-2.456505000
H	2.282702000	1.114893000	-2.248558000
H	3.057092000	-0.221853000	-3.108159000
C	3.078078000	-2.045411000	-1.062131000
H	3.542649000	-2.513358000	-0.192749000
H	2.079265000	-2.462523000	-1.180429000
H	3.688228000	-2.295583000	-1.934806000
H	-2.218857000	-1.056602000	-0.038563000
H	2.218758000	1.056565000	0.038184000
O	0.115935000	-2.036921000	-0.210871000
C	-0.791005000	-2.936214000	0.034622000
O	-1.976955000	-2.715098000	0.323320000
O	-0.115993000	2.036852000	0.211076000
C	0.790942000	2.936140000	-0.034553000
O	1.976723000	2.715009000	-0.323894000
C	-0.276257000	-4.364456000	-0.066665000
H	-1.096328000	-5.066937000	0.082747000
H	0.183384000	-4.531744000	-1.045238000
H	0.495219000	-4.535812000	0.690645000
C	0.276574000	4.364390000	0.068511000
H	-0.174131000	4.532916000	1.051073000
H	1.095132000	5.066881000	-0.088905000
H	-0.501900000	4.534419000	-0.681837000
C	-4.410225000	-0.076481000	0.817965000
O	-5.098861000	-0.413868000	1.747454000
O	-4.872856000	-0.224028000	-0.453040000
H	-4.693620000	0.197522000	-2.417353000
O	4.872754000	0.224432000	0.452721000
C	4.410198000	0.076387000	-0.818263000

O 5.098849000 0.413435000 -1.747860000  
H 4.693776000 -0.197272000 2.417046000  
E = -1623.28184932

## Complex A

Pd -1.174947000 0.035490000 -0.101614000  
O 0.376314000 2.872981000 0.590202000  
O -1.469717000 2.010215000 -0.394490000  
H 1.608166000 -1.226007000 -2.898790000  
O -1.514176000 -2.017901000 0.100775000  
O 2.916986000 -1.870140000 0.292883000  
C 1.427456000 -0.333710000 1.479939000  
C 1.810659000 -1.784664000 1.208423000  
C 2.991519000 -0.976592000 -0.718820000  
C 1.745820000 -0.117631000 -1.046034000  
N 0.903851000 0.230554000 0.177814000  
H 0.907635000 1.266789000 0.299723000  
C 2.640430000 0.502495000 1.943994000  
C 0.346059000 -0.277241000 2.568472000  
H 0.953937000 -2.341641000 0.814444000  
H 2.155192000 -2.271690000 2.123580000  
O 3.982093000 -0.939711000 -1.408482000  
C 2.189482000 1.188605000 -1.719199000  
C 0.952804000 -0.978859000 -2.058933000  
H 2.321123000 1.525535000 2.160356000  
H 3.443764000 0.546897000 1.204941000  
H 3.061221000 0.070619000 2.857277000  
H -0.041476000 0.740448000 2.663289000  
H 0.784617000 -0.563160000 3.530131000  
H -0.485602000 -0.953162000 2.355141000  
H 2.800316000 0.963305000 -2.593645000  
H 2.780385000 1.808713000 -1.040213000  
H 1.310727000 1.760346000 -2.029689000  
H 0.095711000 -0.414432000 -2.437474000

H	0.587778000	-1.908269000	-1.615874000
C	-2.772410000	-1.837964000	-0.103916000
O	-3.175424000	-0.646376000	-0.292924000
C	-3.714058000	-3.003430000	-0.148792000
C	-0.738409000	2.987383000	0.052745000
C	-1.381043000	4.351908000	-0.129933000
H	-0.653882000	5.137606000	0.077049000
H	-2.225411000	4.446470000	0.560449000
H	-1.776266000	4.453381000	-1.143635000
H	-3.712930000	-3.422439000	-1.161017000
H	-4.727601000	-2.677455000	0.090237000
H	-3.385248000	-3.782631000	0.541877000
E =-	1104.113974		

Pd(OAc)<sub>2</sub>

Pd	-0.981768000	-0.352906000	-0.220098000
H	0.402150000	-2.329058000	0.792989000
O	-2.820678000	-1.110678000	0.315085000
O	2.309249000	0.117720000	1.651569000
C	1.445108000	1.658488000	-0.087524000
C	1.491382000	1.329036000	1.397802000
C	2.385039000	-0.819285000	0.790188000
C	1.602167000	-0.897057000	-0.483937000
N	0.910152000	0.423053000	-0.757660000
H	0.895268000	0.578515000	-1.766184000
C	2.835459000	2.036363000	-0.633446000
C	0.448499000	2.806031000	-0.308767000
H	0.502218000	1.107284000	1.804276000
H	1.988075000	2.098078000	1.987320000
O	3.169136000	-1.782075000	1.166410000
C	2.463587000	-1.353563000	-1.674591000
C	0.389098000	-1.841310000	-0.185877000
H	2.784729000	2.214937000	-1.711547000
H	3.600611000	1.275580000	-0.450408000

H	3.180335000	2.961475000	-0.163899000
H	0.389274000	3.048090000	-1.374420000
H	0.790014000	3.705146000	0.211902000
H	-0.554590000	2.547703000	0.038631000
H	2.867865000	-2.360116000	-1.523760000
H	3.287993000	-0.669332000	-1.891076000
H	1.818019000	-1.421386000	-2.554843000
H	0.264040000	-2.581738000	-0.980032000
C	-3.382450000	0.044246000	0.215811000
O	-2.642783000	1.033389000	-0.099815000
C	-4.855551000	0.187207000	0.436115000
H	-5.193149000	-0.508287000	1.206982000
H	-5.377379000	-0.061339000	-0.494624000
H	-5.099105000	1.215438000	0.707189000
H	3.190482000	-2.516478000	0.529024000

E = -584.94154633

TS C

Pd	0.848132000	0.003223000	-0.208608000
O	0.102871000	2.518269000	1.470269000
O	1.472248000	1.943057000	-0.241946000
H	-0.525512000	-2.161673000	-1.047671000
O	2.323403000	-2.516759000	0.205001000
O	-3.259418000	-1.307664000	-0.889884000
C	-2.155563000	0.888864000	-0.725489000
C	-2.610744000	-0.254384000	-1.628753000
C	-2.731260000	-1.695779000	0.290842000
C	-1.377458000	-1.093941000	0.709373000
N	-1.144417000	0.322814000	0.236975000
H	-1.019096000	0.990125000	1.012583000
C	-3.332629000	1.462199000	0.086891000
C	-1.531734000	1.987961000	-1.590906000
H	-1.767468000	-0.667540000	-2.193478000
H	-3.358610000	0.099425000	-2.340306000

O	-3.283821000	-2.556226000	0.935949000
C	-1.230524000	-1.149839000	2.231495000
C	-0.270840000	-1.927237000	-0.010676000
H	-2.985923000	2.285615000	0.718577000
H	-3.807095000	0.716038000	0.730255000
H	-4.100094000	1.853483000	-0.588059000
H	-1.186489000	2.816228000	-0.969670000
H	-2.283914000	2.377371000	-2.284544000
H	-0.683199000	1.613922000	-2.169289000
H	-1.347364000	-2.177009000	2.579096000
H	-1.994334000	-0.537773000	2.720103000
H	-0.243464000	-0.784918000	2.530025000
H	-0.186559000	-2.885766000	0.515202000
H	1.081152000	-1.949999000	0.144832000
C	3.152185000	-1.665749000	-0.235754000
O	2.826239000	-0.472202000	-0.548856000
C	4.602485000	-2.052275000	-0.373838000
C	1.010482000	2.762448000	0.658386000
C	1.707004000	4.113923000	0.648734000
H	1.756581000	4.512046000	-0.368839000
H	2.737114000	3.993534000	1.000628000
H	1.184308000	4.815446000	1.300800000
H	4.688570000	-3.100696000	-0.665549000
H	5.088655000	-1.931612000	0.601025000
H	5.108976000	-1.409152000	-1.094651000

E = -1104.1139736

## Complex D

Pd	0.979391000	-0.326398000	0.157080000
H	-0.414503000	-2.120869000	-1.100767000
O	2.850752000	-1.065882000	-0.405840000
O	-2.603112000	0.187000000	-1.567069000
C	-1.478334000	1.597991000	0.108188000
C	-1.665022000	1.258437000	-1.369053000

C	-2.625345000	-0.874232000	-0.724910000
C	-1.595103000	-0.970296000	0.410709000
N	-0.913593000	0.362267000	0.736446000
H	-0.898846000	0.483002000	1.748981000
C	-2.815278000	1.979647000	0.771840000
C	-0.467076000	2.741611000	0.256534000
H	-0.701281000	0.987257000	-1.814948000
H	-2.081859000	2.109845000	-1.911170000
O	-3.430039000	-1.755500000	-0.907747000
C	-2.264597000	-1.544458000	1.660319000
C	-0.377413000	-1.795481000	-0.058160000
H	-2.667505000	2.183239000	1.837880000
H	-3.574796000	1.200705000	0.672093000
H	-3.214336000	2.889331000	0.313195000
H	-0.282801000	2.954300000	1.314839000
H	-0.862220000	3.653939000	-0.201260000
H	0.491875000	2.494767000	-0.205563000
H	-2.715196000	-2.506794000	1.413997000
H	-3.051758000	-0.885859000	2.042076000
H	-1.515365000	-1.696665000	2.444765000
H	-0.153854000	-2.639011000	0.600223000
C	3.437499000	0.055143000	-0.182432000
O	2.759055000	1.047826000	0.217278000
C	4.929486000	0.148743000	-0.373855000
H	5.235366000	-0.426307000	-1.250705000
H	5.428759000	-0.283911000	0.499878000
H	5.235356000	1.191272000	-0.472378000
E=-875.365390995			

## Amine

H	-2.895887000	-0.774746000	-1.158513000
O	-0.120523000	1.730955000	-0.246381000
C	1.488516000	-0.115158000	0.011600000
C	1.137838000	1.194004000	-0.692610000

C	-1.162252000	0.908597000	0.023393000
C	-0.991896000	-0.620870000	-0.089671000
N	0.403124000	-1.035023000	-0.345885000
H	0.564521000	-1.954777000	0.054801000
C	1.677307000	0.112624000	1.529675000
C	2.787093000	-0.671071000	-0.592780000
H	1.090639000	1.030548000	-1.775087000
H	1.872398000	1.975195000	-0.481644000
O	-2.221661000	1.396822000	0.342303000
C	-1.562898000	-1.252189000	1.199569000
C	-1.851980000	-1.067216000	-1.296097000
H	1.855237000	-0.842506000	2.035443000
H	0.803533000	0.582938000	1.987849000
H	2.539380000	0.760123000	1.724941000
H	3.042012000	-1.630003000	-0.127855000
H	3.626912000	0.010711000	-0.423214000
H	2.672267000	-0.837604000	-1.667272000
H	-2.594915000	-0.933876000	1.357243000
H	-0.978175000	-0.970179000	2.079442000
H	-1.542732000	-2.344499000	1.109705000
H	-1.795482000	-2.155822000	-1.398355000
H	-1.474471000	-0.624886000	-2.222138000

E= -519.132172674

CH<sub>3</sub>COOH

C	-0.092065000	0.125257000	0.000030000
O	-0.642950000	1.202800000	-0.000108000
O	-0.780270000	-1.045291000	0.000027000
H	-1.721156000	-0.800775000	-0.000033000
C	1.396538000	-0.111466000	0.000050000
H	1.681804000	-0.693477000	0.881188000
H	1.681790000	-0.693870000	-0.880830000
H	1.916486000	0.845303000	-0.000157000

E= -229.109365561

Amine \* CH<sub>3</sub>COOH

H	-1.240100000	-2.819418000	-1.175790000
O	-2.731261000	0.501973000	-0.749442000
C	-0.632805000	1.466807000	0.081284000
C	-1.661071000	1.415244000	-1.045354000
C	-2.445845000	-0.676432000	-0.143531000
C	-0.968714000	-1.058773000	0.090144000
N	-0.035562000	0.111087000	0.146220000
H	0.539978000	0.043186000	0.987418000
C	-1.290450000	1.885305000	1.412816000
C	0.475783000	2.465450000	-0.285178000
H	-1.177636000	1.119841000	-1.984378000
H	-2.141127000	2.385608000	-1.189528000
O	-3.350543000	-1.425108000	0.139419000
C	-0.870205000	-1.867325000	1.393381000
C	-0.576566000	-1.953187000	-1.112212000
H	-0.538093000	1.912041000	2.207638000
H	-2.084425000	1.199489000	1.719094000
H	-1.730549000	2.884879000	1.332999000
H	1.273711000	2.431364000	0.462572000
H	0.083458000	3.486774000	-0.316097000
H	0.916676000	2.229878000	-1.258084000
H	-1.517426000	-2.743854000	1.349393000
H	-1.173007000	-1.264369000	2.254646000
H	0.164380000	-2.191518000	1.545416000
H	0.453534000	-2.299840000	-0.992090000
H	-0.636587000	-1.398886000	-2.053848000
H	1.481681000	-0.105337000	-0.731385000
O	2.437099000	-0.254351000	-1.020750000
C	3.208786000	-0.239927000	0.071794000
O	2.778647000	-0.066702000	1.202973000
C	4.667192000	-0.461115000	-0.251097000
H	5.015776000	0.311534000	-0.942767000
H	5.256621000	-0.436918000	0.664641000

H 4.793908000 -1.424836000 -0.753273000  
E = -748.261587903

TS E

Pd 0.404703000 -0.081556000 -0.558819000  
O 1.842540000 1.211956000 -2.774484000  
O 2.235083000 0.813854000 -0.587806000  
H -1.045228000 2.385549000 0.145977000  
O 1.326511000 -1.917353000 -0.867292000  
O -3.400080000 0.621665000 1.213222000  
C -2.337387000 -1.448664000 0.413361000  
C -2.546067000 -0.482309000 1.574672000  
C -3.253942000 1.205049000 0.006455000  
C -2.107906000 0.751428000 -0.915830000  
N -1.621714000 -0.675527000 -0.660125000  
H -1.695327000 -1.206924000 -1.528838000  
C -3.678677000 -1.968277000 -0.137045000  
C -1.470420000 -2.622065000 0.877341000  
H -1.589445000 -0.093435000 1.938071000  
H -3.054550000 -0.980953000 2.401523000  
O -3.981525000 2.120484000 -0.301565000  
C -2.539067000 0.890815000 -2.376539000  
C -0.849135000 1.615875000 -0.604644000  
H -3.503330000 -2.666800000 -0.962373000  
H -4.331909000 -1.170460000 -0.500271000  
H -4.222402000 -2.506719000 0.645052000  
H -1.220121000 -3.274140000 0.035593000  
H -2.020755000 -3.219089000 1.611381000  
H -0.537988000 -2.281143000 1.332414000  
H -2.821510000 1.924640000 -2.579565000  
H -3.399014000 0.251518000 -2.602457000  
H -1.708294000 0.620557000 -3.035840000  
H -0.447908000 2.110623000 -1.490361000  
H 0.059713000 1.198493000 0.608780000

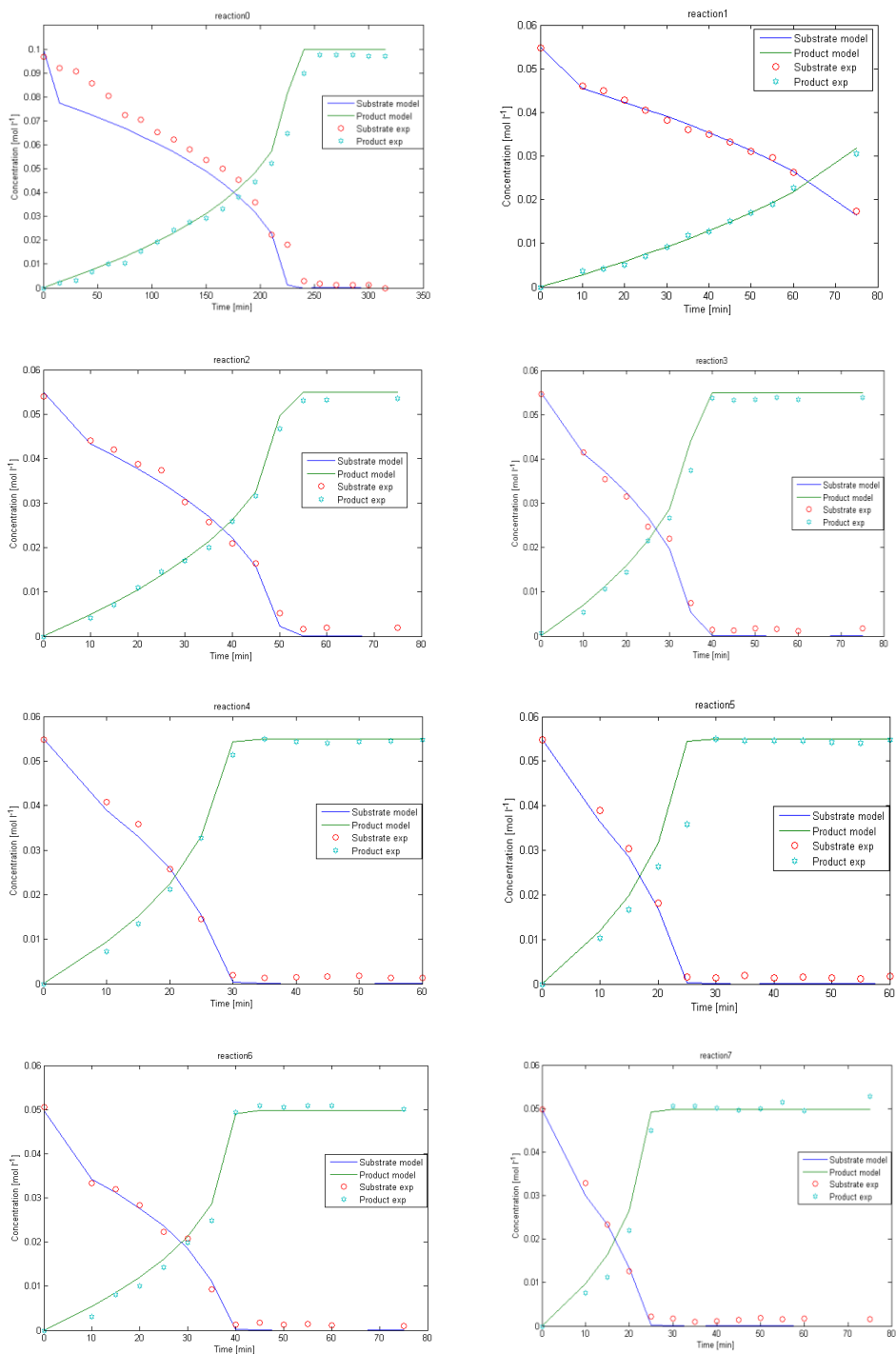
C	1.980162000	-2.372338000	0.137045000
O	2.028674000	-1.845777000	1.276683000
C	2.760850000	-3.648185000	-0.108831000
C	2.567330000	1.250225000	-1.778480000
C	3.982636000	1.805762000	-1.835628000
H	4.135378000	2.349866000	-2.769199000
H	4.698392000	0.977693000	-1.785475000
H	4.181764000	2.461325000	-0.983286000
H	2.279804000	-4.267518000	-0.868629000
H	2.882941000	-4.208193000	0.820330000
H	3.757439000	-3.377286000	-0.476624000
H	1.914015000	-0.450883000	1.822221000
O	2.113287000	0.312204000	2.500740000
C	1.383249000	1.373278000	2.564564000
O	0.373839000	1.637538000	1.864063000
C	1.823580000	2.375532000	3.595092000
H	2.372189000	1.892357000	4.404562000
H	2.491437000	3.094309000	3.105489000
H	0.962480000	2.923540000	3.980409000

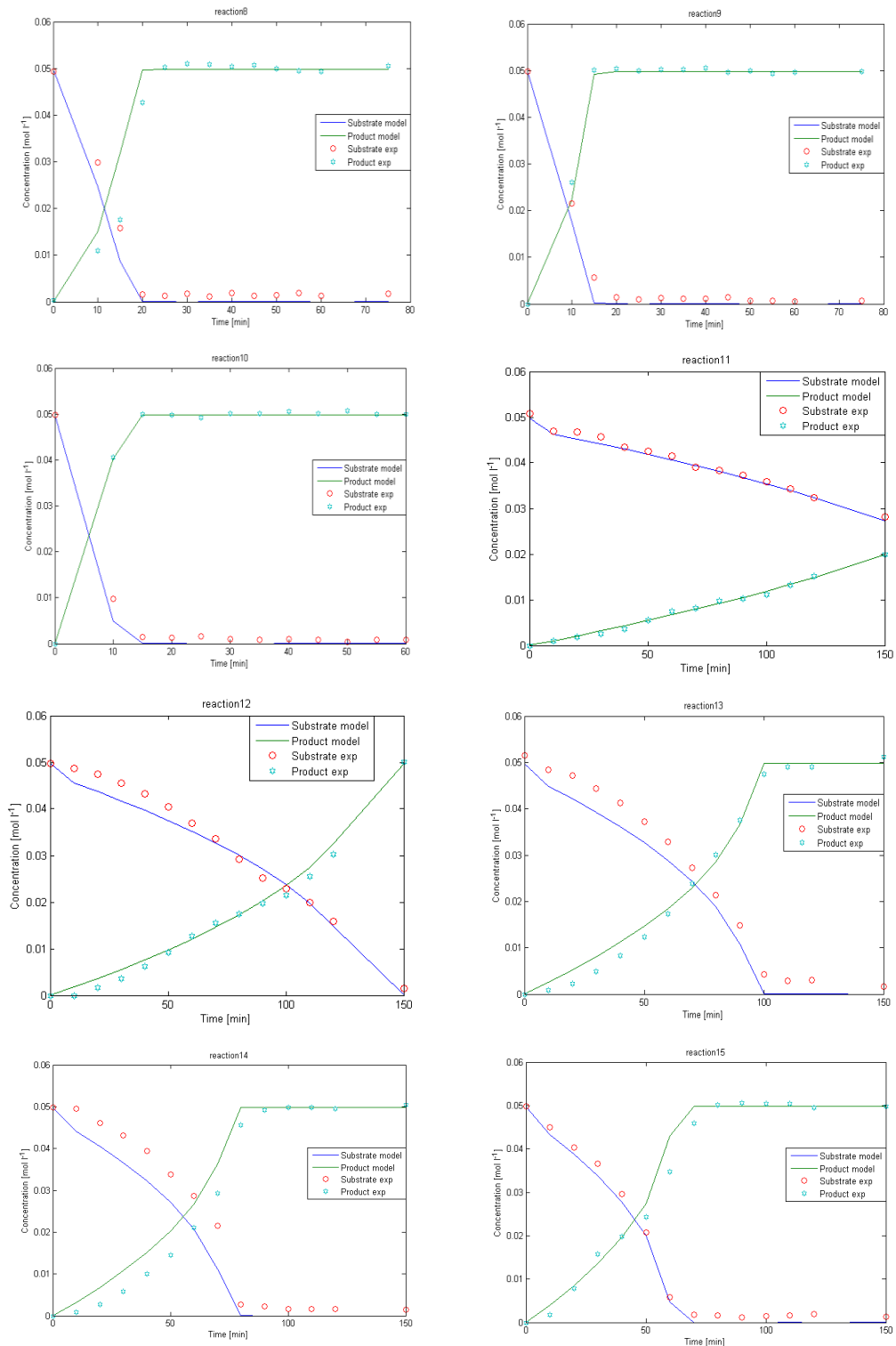
E = -1333.16923289

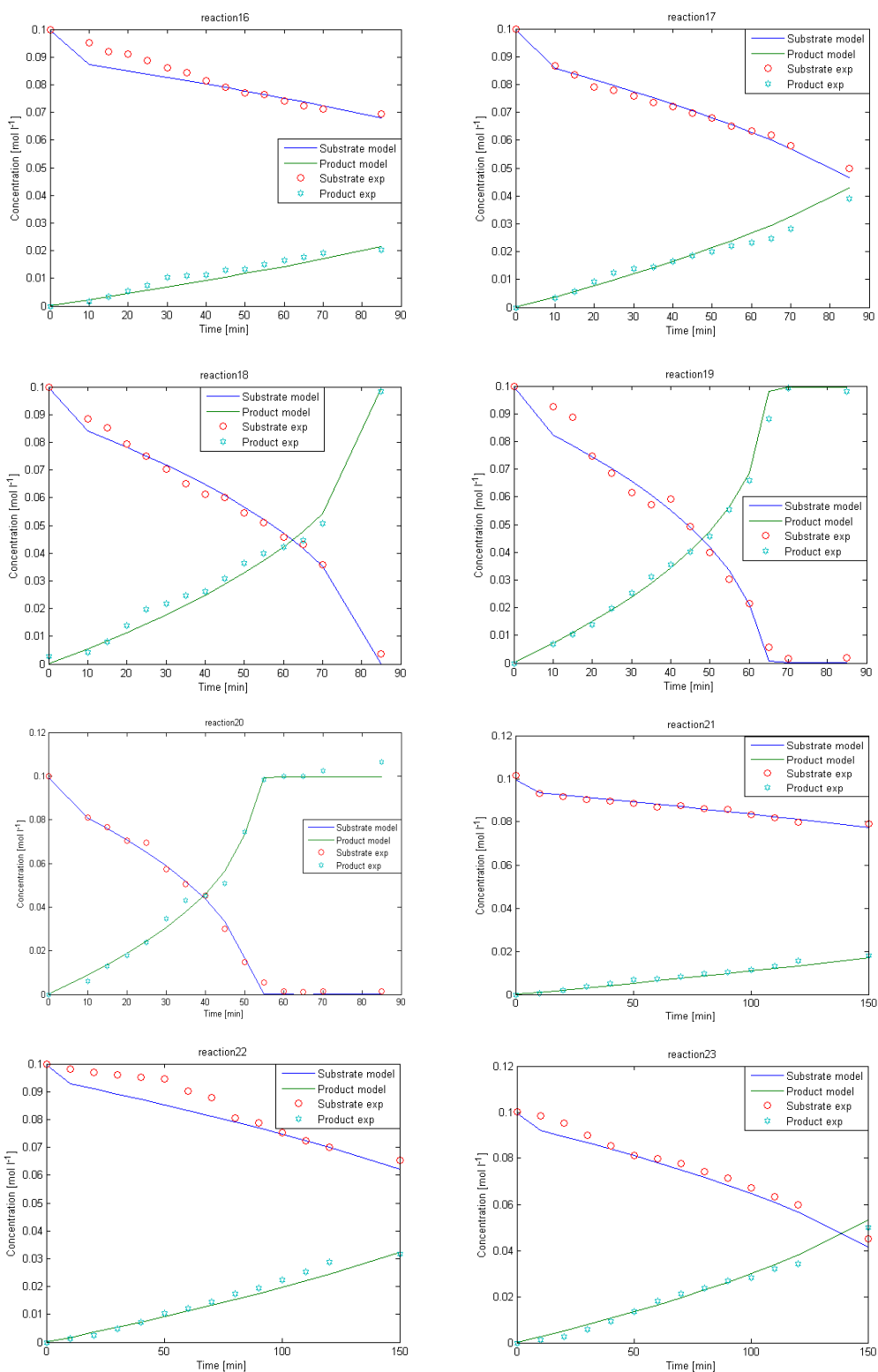
In Hartrees; calculated at  $\omega$ B97xD/cc-PVTZ (SDD on Pd) + SMD solvation (solvent = toluene)

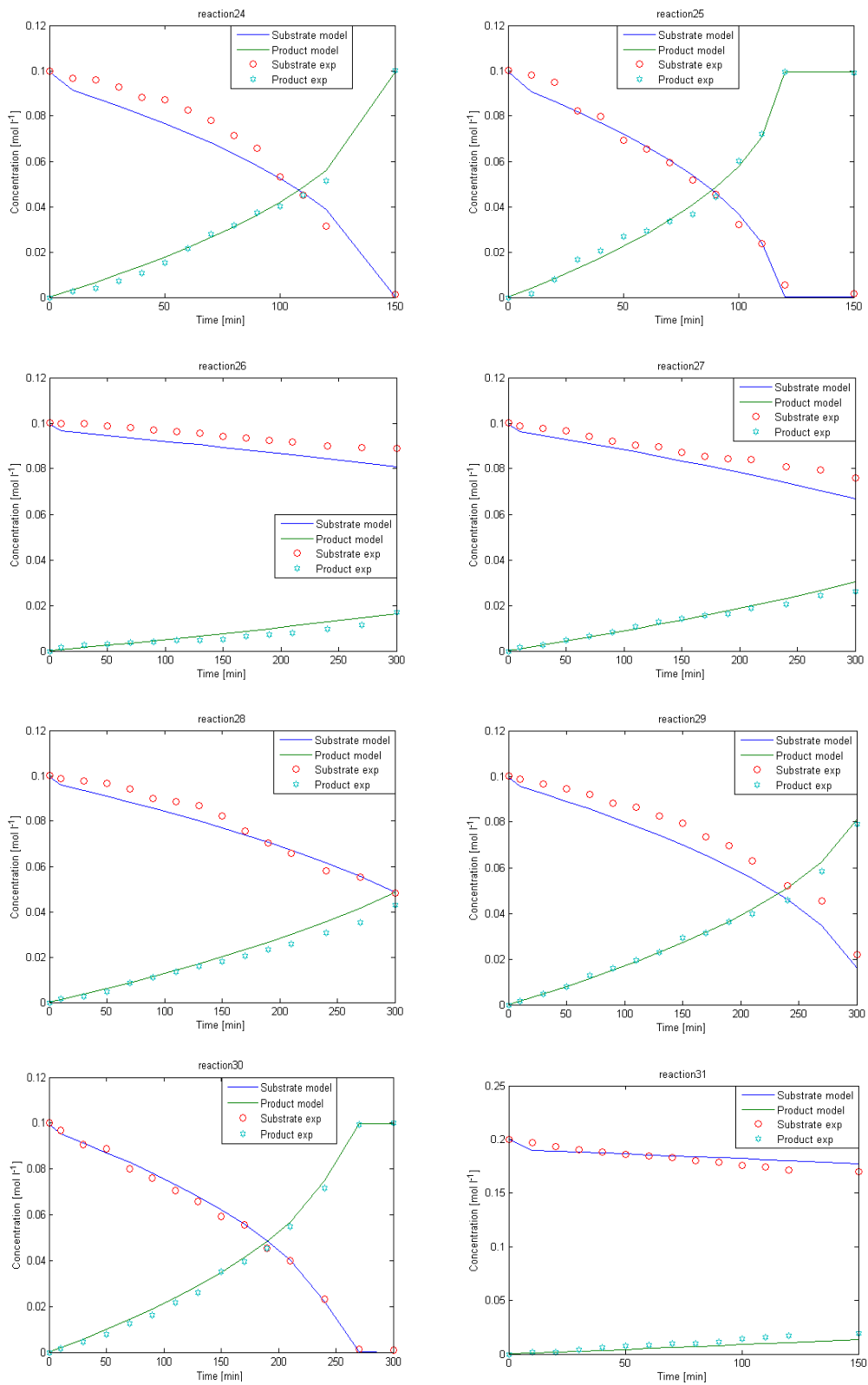
## 8.2. Appendix 2

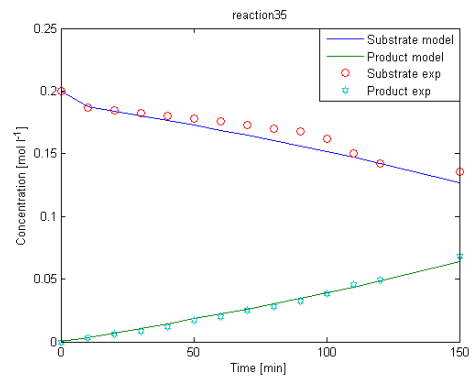
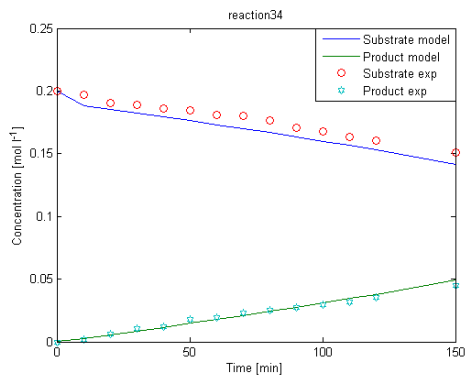
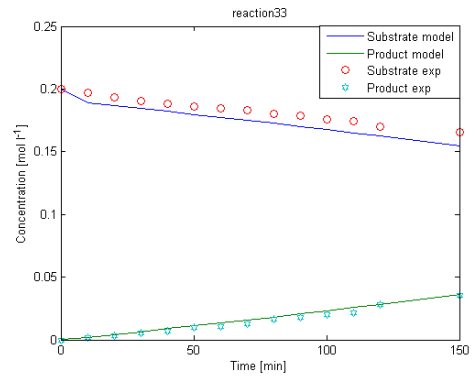
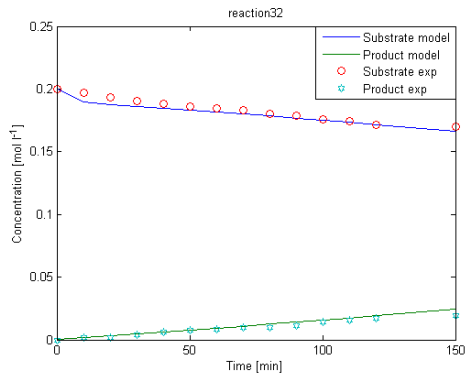
Fit between experimental data and the developed model for the aziridination reaction.







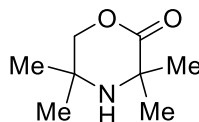




### 8.3. Appendix 3

Characterisation data for compounds isolated for the aziridination project.

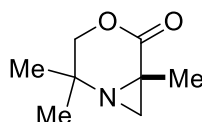
3,3,5,5-Tetramethylmorpholin-2-one; CDCl<sub>3</sub>, 400MHz (<sup>1</sup>H) 100MHz (<sup>13</sup>C)



<sup>1</sup>H NMR (400 MHz, CDCl<sub>3</sub>): δ 4.10 (s, 2H, H-1), 1.36 (s, 6H, H-6), 1.12 (s, 6H, H-3); <sup>13</sup>C NMR (100 MHz, CDCl<sub>3</sub>): δ 175.2 (C-7), 78.1 (C-1), 54.6 (C-5), 49.1 (C-2), 30.6 (C-6), 26.4 (C-3); IR  $\nu_{\max}/\text{cm}^{-1}$  (film): 3336 (N-H), 2973, 1726 (C=O), 1473, 1399, 1379, 1286, 1259, 1235, 1196, 1127, 1047, 915, 890, 806, 751

Characterisation consistent with previous literature.<sup>148</sup>

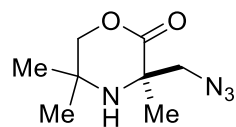
2,2,6-Trimethyl-4-oxa-1-azabicyclo[4.1.0]heptan-5-one CDCl<sub>3</sub>, 400MHz (<sup>1</sup>H) 100MHz (<sup>13</sup>C)



<sup>1</sup>H NMR (400 MHz, CDCl<sub>3</sub>): δ 3.99 (d, J = 12.1 Hz, 1H, H-1), 3.87 (d, J = 12.1 Hz, 1H, H-1), 2.45 (s, 1H, H-6), 1.90 (s, 1H, H-6), 1.45 (s, 3H, H-7), 1.29 (s, 3H, H-3/4), 1.13 (s, 3H, H-3/4); <sup>13</sup>C NMR (100 MHz, CDCl<sub>3</sub>): δ 170.8 (C-8), 71.7 (C-1), 50.0 (C-5), 36.0 (C-2), 32.9 (C-6), 25.6 (C-7), 23.7 (C-3/4), 20.9 (C-3/4); IR  $\nu_{\max}/\text{cm}^{-1}$  (film): 2973, 2934, 1721 (C=O), 1498, 1467, 1406, 1378, 1327, 1303, 1283, 1255, 1217, 1198, 1131, 1056, 1041, 981, 956, 905, 848, 768, 745, 700

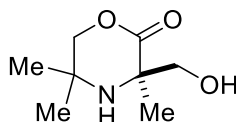
Characterisation consistent with previous literature.<sup>148</sup>

3-(Azidomethyl)-3,5,5-trimethylmorpholin-2-one; CDCl<sub>3</sub>, 400MHz (<sup>1</sup>H) 100MHz (<sup>13</sup>C)



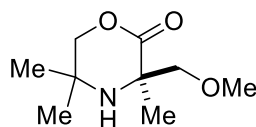
<sup>1</sup>H NMR (400 MHz, CDCl<sub>3</sub>) δ: 4.20 (d, J = 2.0 Hz, 1H, H-1), 4.13 (d, J = 2.0 Hz, 1H, H-1), 3.57 (d, J = 3.0 Hz, 1H, H-6), 3.20 (d, J = 3.0 Hz, 1H, H-6), 1.41 (s, 3H, H-7), 1.23 (s, 3H, H-3/4), 1.19 (s, 3H, H-3/4); <sup>13</sup>C NMR (100 MHz, CDCl<sub>3</sub>) δ: 172.4, 78.0, 60.6, 58.8, 48.9, 27.2, 26.2, 26.0; IR ν<sub>max</sub>/cm<sup>-1</sup>(film): 3332, 2973, 2097, 1728, 1286, 1045; m/z HRMS: (ESI) found [M+H]<sup>+</sup> 199.1186, C<sub>8</sub>H<sub>15</sub>N<sub>4</sub>O requires 199.1190

3-(Hydroxymethyl)-3,5,5-trimethylmorpholin-2-one; CDCl<sub>3</sub>, 400MHz (<sup>1</sup>H) 100MHz (<sup>13</sup>C)



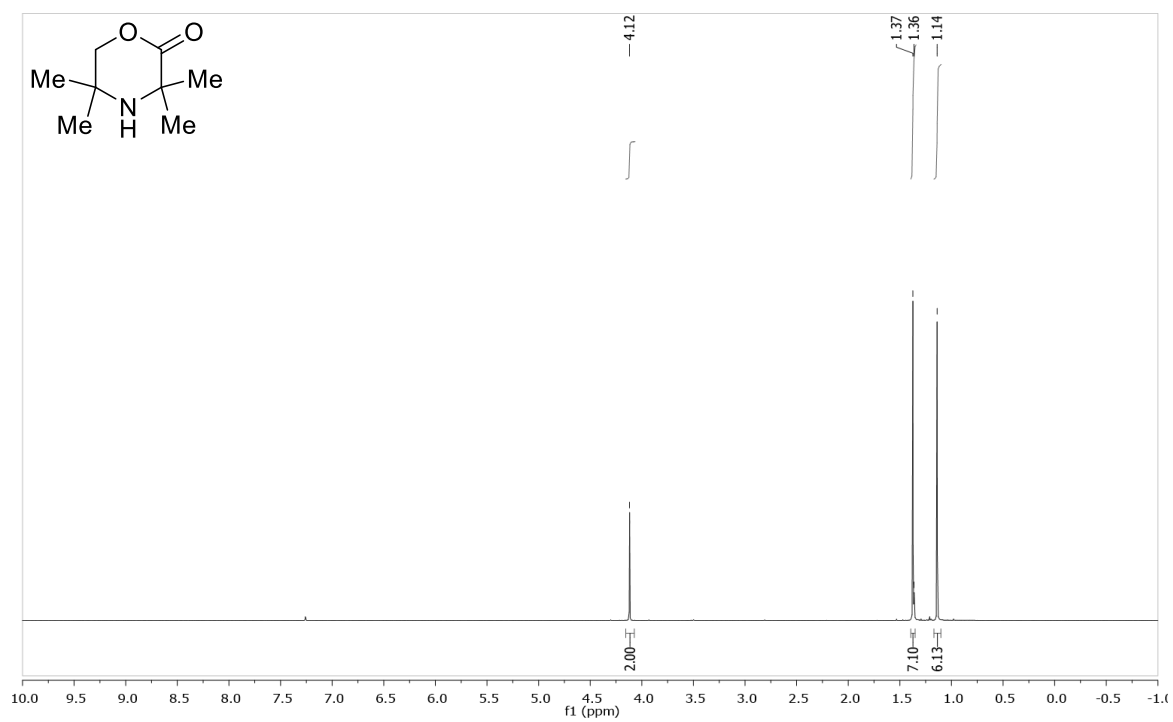
<sup>1</sup>H NMR (400 MHz, CDCl<sub>3</sub>) δ: 4.14 (d, J = 3.0 Hz, 1H, H-1), 4.13 (d, J = 3.0 Hz, 1H, H-1), 3.70 (d, J = 3.0 Hz, 1H, H-6), 3.35 (d, J = 3.0 Hz, 1H, H-6), 1.38 (s, 3H, H-7), 1.24 (s, 3H, H-3/4), 1.17 (s, 3H, H-3/4); <sup>13</sup>C NMR (100 MHz, CDCl<sub>3</sub>) δ: 173.9, 77.6, 69.2, 58.9, 48.9, 26.2, 26.1, 25.6; IR ν<sub>max</sub>/cm<sup>-1</sup>(film): 3313 (br, O-H), 2974, 1721 (C=O), 1284, 1047; m/z HRMS (ESI) found [M+H]<sup>+</sup> 174.1121, C<sub>8</sub>H<sub>16</sub>NO<sub>3</sub> requires 174.1125

3-(Methoxymethyl)-3,5,5-trimethylmorpholin-2-one; CDCl<sub>3</sub>, 400MHz (<sup>1</sup>H) 100MHz (<sup>13</sup>C)

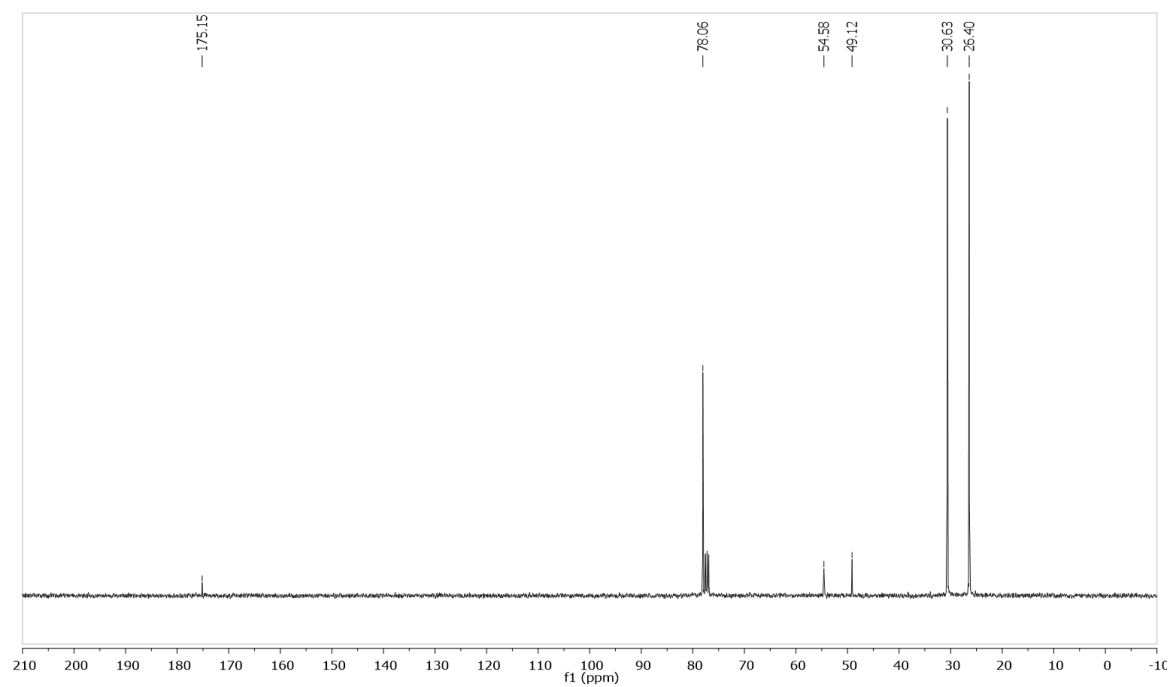


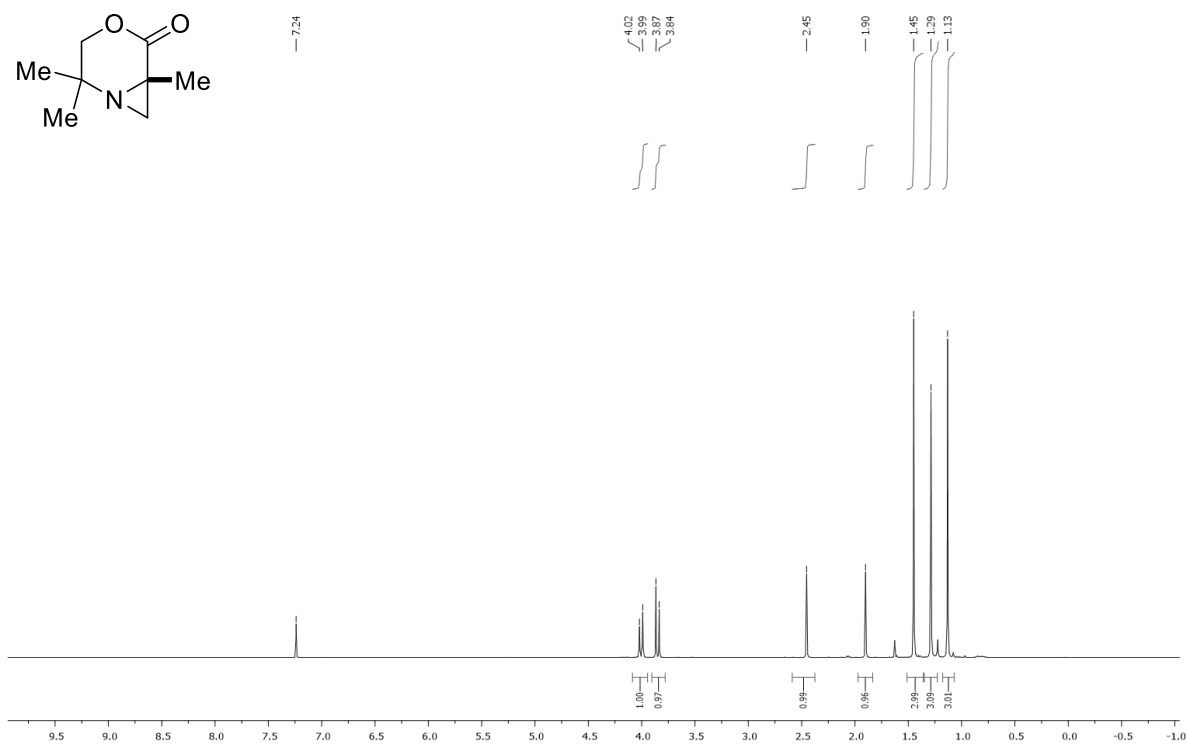
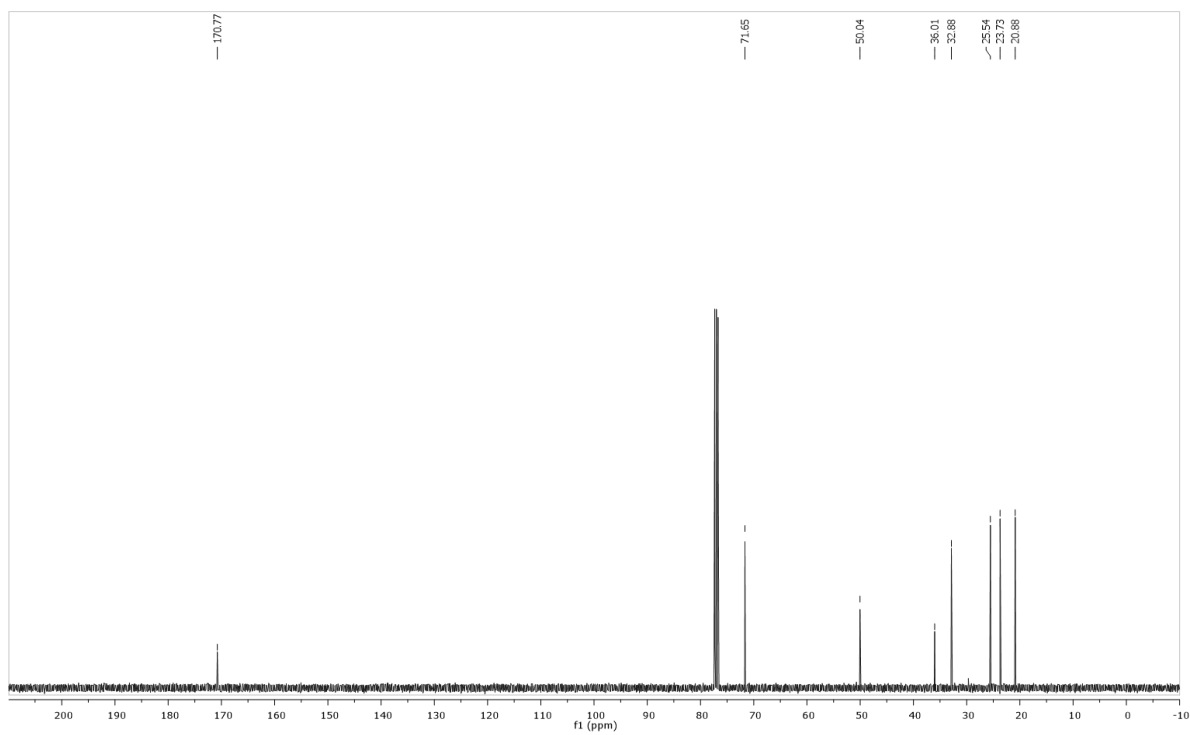
<sup>1</sup>H NMR (400 MHz, CDCl<sub>3</sub>) δ: 4.14 (d, J = 2.0 Hz, 1H, H-1), 4.12 (d, J = 2.0 Hz, 1H, H-1), 3.62 (d, J = 3.0 Hz, 1H, H-6), 3.33 (s, 3H, H-7), 3.21 (d, J = 3.0 Hz, 1H, H-6), 1.33 (s, 3H, H-8), 1.23 (s, 3H, H-3/4), 1.13 (s, 3H, H-3/4); <sup>13</sup>C NMR (100 MHz, CDCl<sub>3</sub>) δ: 173.3, 79.6, 78.5; 59.2, 58.7, 48.5, 26.6, 26.1, 25.1; IR ν<sub>max</sub>/cm<sup>-1</sup>(film): 2970, 1733 (C=O), 1284, 1104, 1049; m/z HRMS (ESI) found [M+H]<sup>+</sup> 188.1279, C<sub>8</sub>H<sub>16</sub>NO<sub>3</sub> requires 188.1281

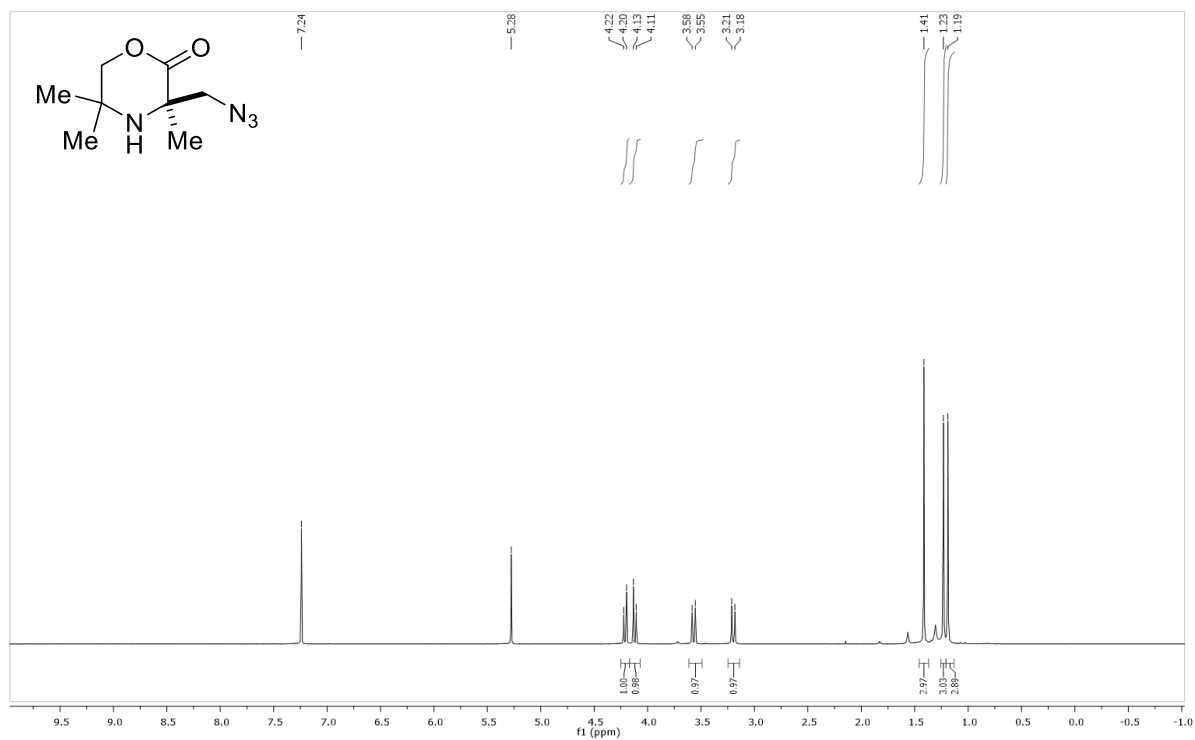
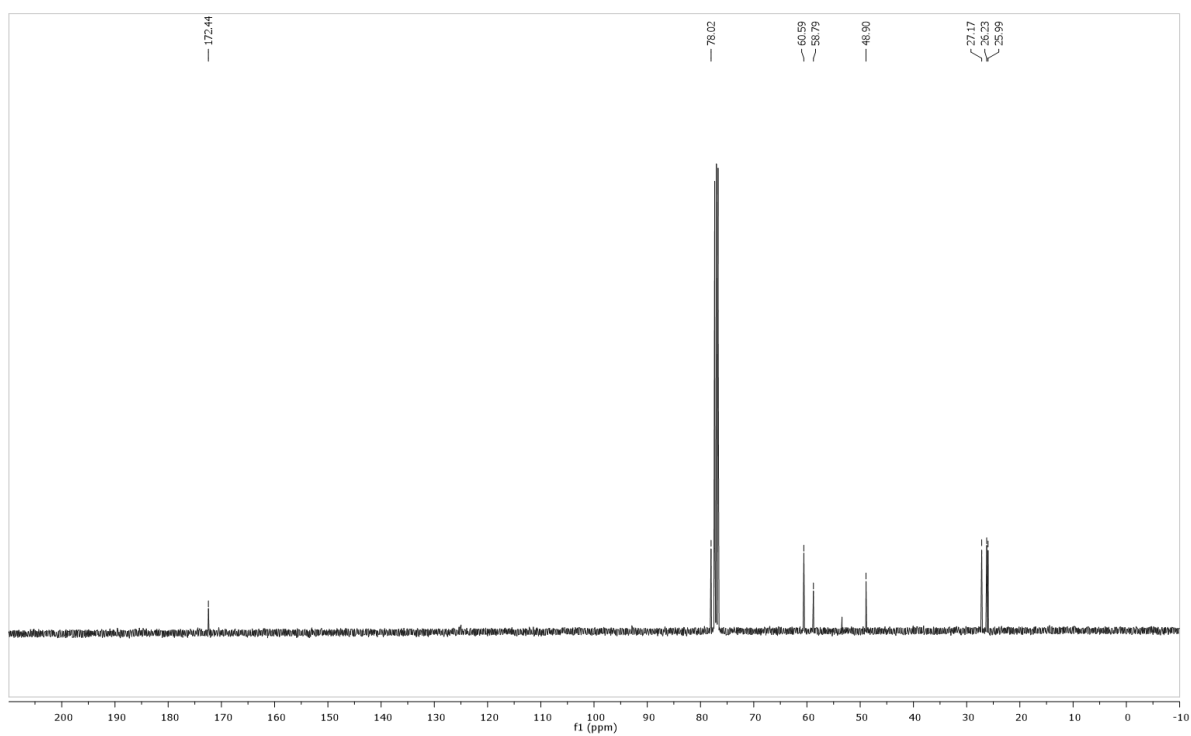
$^1\text{H}$  NMR ( $\text{CDCl}_3$ , 400 MHz)

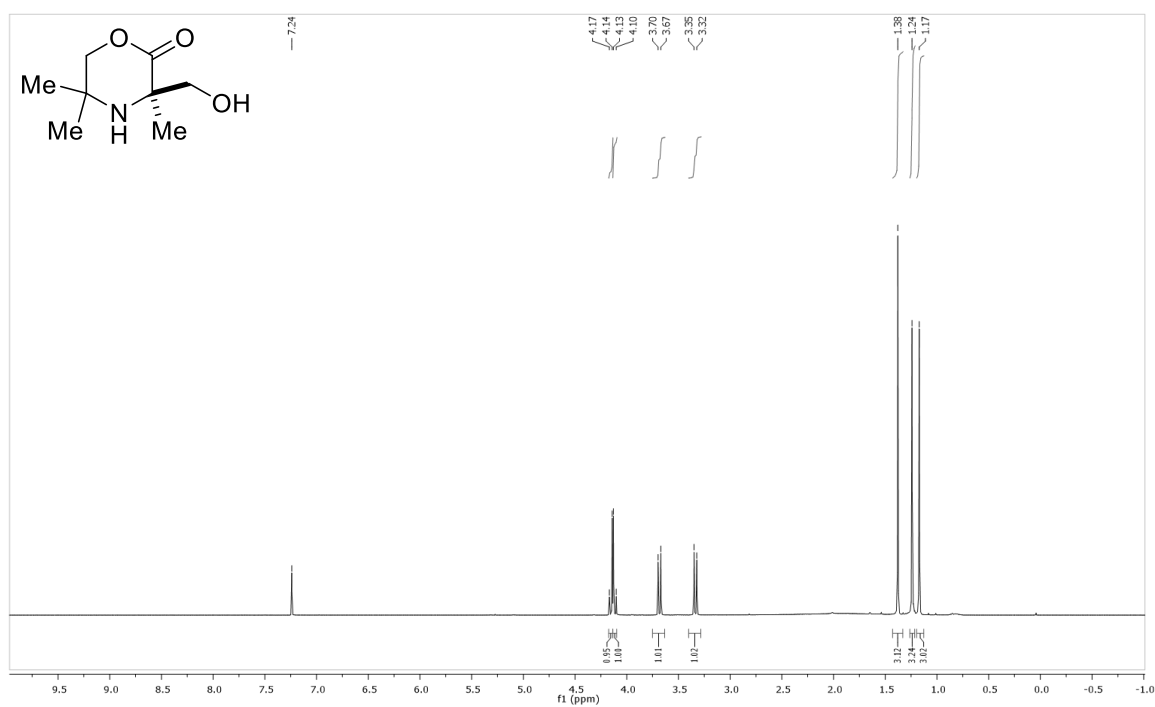
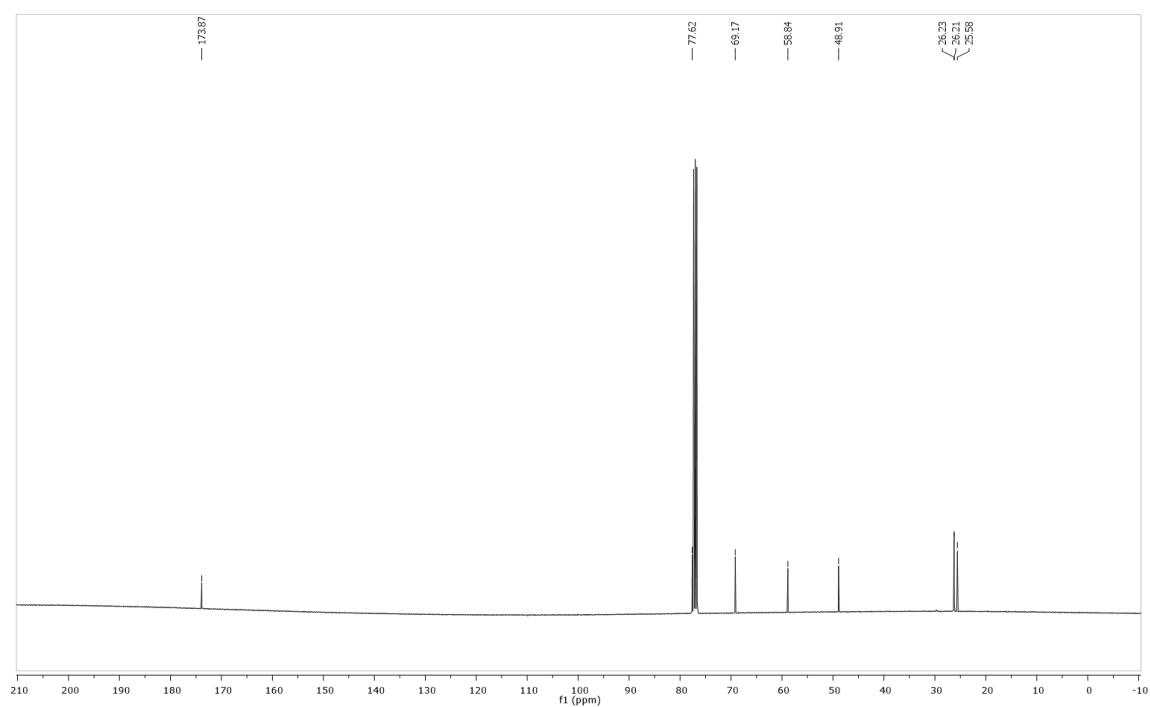


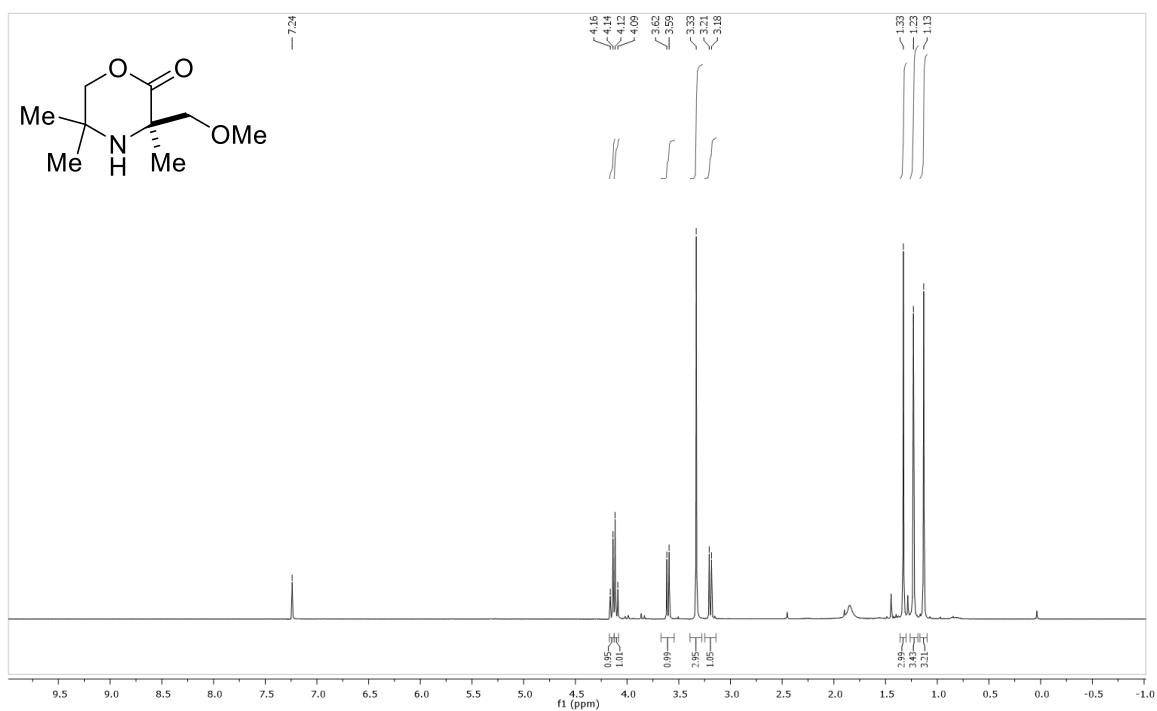
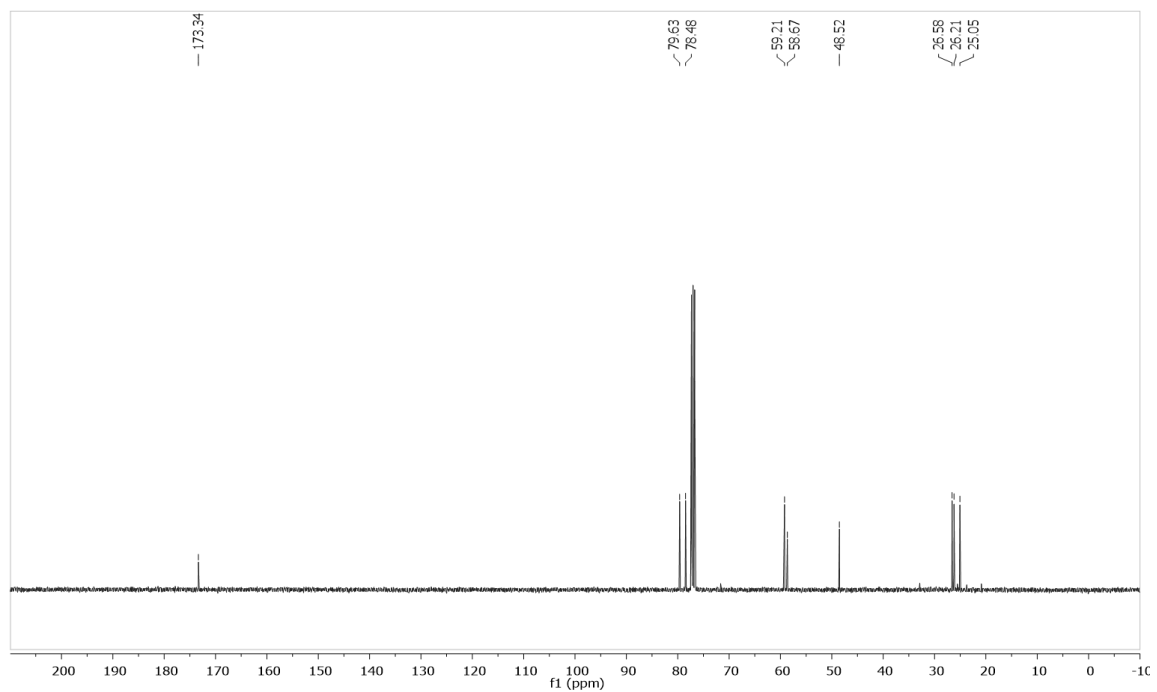
$^{13}\text{C}$  NMR ( $\text{CDCl}_3$ , 100 MHz)



$^1\text{H}$  NMR ( $\text{CDCl}_3$ , 400 MHz) $^{13}\text{C}$  NMR ( $\text{CDCl}_3$ , 100 MHz)

$^1\text{H}$  NMR ( $\text{CDCl}_3$ , 400 MHz) $^{13}\text{C}$  NMR ( $\text{CDCl}_3$ , 100 MHz)

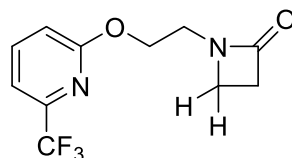
$^1\text{H}$  NMR ( $\text{CDCl}_3$ , 400 MHz) $^{13}\text{C}$  NMR ( $\text{CDCl}_3$ , 100 MHz)

$^1\text{H}$  NMR ( $\text{CDCl}_3$ , 400 MHz) $^{13}\text{C}$  NMR ( $\text{CDCl}_3$ , 100 MHz)

## 8.4. Appendix 4

Characterisation data for compounds isolated for the carbonylation project.

### 1-(2-((6-(Trifluoromethyl)pyridin-2-yl)oxy)ethyl)azetidin-2-one

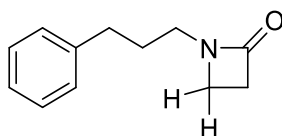


General procedure C, residence time 5 min. The residue was purified by column chromatography (silica, ethyl acetate) to afford the title compound as a light brown oil (41%);  $R_f = 0.33$  (ethyl acetate);

$^1\text{H}$  NMR (400 MHz,  $\text{CDCl}_3$ )  $\delta$ : 7.72 (1H, t,  $J = 7.9$  Hz), 7.28 (1H, d,  $J = 7.4$  Hz), 6.94 (1H, d,  $J = 8.4$  Hz), 4.51 (2H, t,  $J = 5.3$  Hz), 3.61 (2H, t,  $J = 5.3$  Hz), 3.35 (2H, t,  $J = 4.1$  Hz), 2.92 (2H, t,  $J = 4.1$  Hz);

$^{13}\text{C}$  NMR (100 MHz,  $\text{CDCl}_3$ )  $\delta$ : 167.9, 163.3, 145.5 (q,  $J = 34.9$  Hz), 139.8, 121.38 (q,  $J = 273.6$  Hz), 114.9, 113.8 (q,  $J = 3.2$  Hz), 63.9, 41.2, 39.9, 37.1;

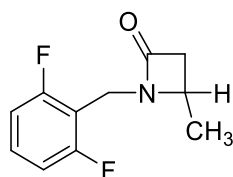
### 1-(3-Phenylpropyl)azetidin-2-one



General procedure C, residence time 5 min. The residue was purified by column chromatography (silica, ethyl acetate/hexane 4:1 (v/v)) to afford the title compound as a light brown oil (42%);  $R_f = 0.33$  (ethyl acetate/hexane 4:1 (v/v));

$^1\text{H}$  NMR (400 MHz,  $\text{CDCl}_3$ )  $\delta$ : 7.35–7.25 (2H, m), 7.21–7.17 (3H, m), 3.24 (2H, t,  $J = 7.1$  Hz), 3.19 (2H, t,  $J = 4.0$  Hz), 2.90 (2H, t,  $J = 4.0$  Hz), 2.67–2.62 (2H, m), 1.87 (2H, dt,  $J = 14.6, 7.4$  Hz);

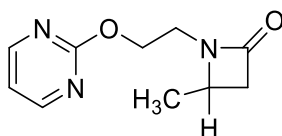
$^{13}\text{C}$  NMR (100 MHz,  $\text{CDCl}_3$ )  $\delta$ : 167.8, 141.3, 128.6, 128.5, 126.2, 41.8, 39.0, 36.7, 33.5, 29.4;

**1-(2,6-Difluorobenzyl)-4-methylazetidin-2-one**

General procedure C, residence time 5 min. The residue was purified by column chromatography (silica, ethyl acetate/hexane 1:1 (v/v)) to afford the title compound as a light brown oil (89%);  $R_f = 0.40$  (hexane/ethyl acetate 1:1 (v/v));

$^1\text{H NMR}$  (400 MHz,  $\text{CDCl}_3$ )  $\delta$ : 7.33–7.21 (1H, m), 6.91 (2H, dd,  $J = 8.3, 7.1$  Hz), 4.67 (1H, dt,  $J = 14.7, 1.5$  Hz), 4.22 (1H, d,  $J = 14.7$  Hz), 3.55 (1H, app qnd,  $J = 6.1, 2.3$  Hz), 3.02 (1H, dd,  $J = 14.5, 5.0$  Hz), 2.51 (1H, dd,  $J = 14.5, 2.3$  Hz), 1.27 (3H, d,  $J = 6.1$  Hz);

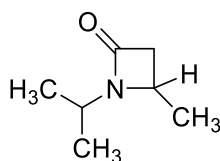
$^{13}\text{C NMR}$  (100 MHz,  $\text{CDCl}_3$ )  $\delta$ : 166.5, 161.7 (dd,  $J = 249.7, 7.8$  Hz), 130.1 (t,  $J = 10.3$  Hz), 111.8, 111.8 (dd,  $J = 18.9, 6.5$  Hz), 47.7, 44.4, 31.5 (t,  $J = 4.3$  Hz), 18.5

**4-Methyl-1-(2-(pyrimidin-2-yloxy)ethyl)azetidin-2-one**

General procedure C, residence time 30 min The residue was purified by column chromatography (silica, ethyl acetate to ethyl acetate/methanol 9:1 (v/v)) to afford the title compound as a light brown oil (89%)  $R_f = 0.27$  (ethyl acetate/methanol 9:1 (v/v));

$^1\text{H NMR}$  (400 MHz,  $\text{CDCl}_3$ )  $\delta$ : 8.55 (2H, d,  $J = 4.7$  Hz), 6.99 (1H, t,  $J = 4.8$  Hz), 4.51 (2H, t,  $J = 5.8$  Hz), 3.90–3.84 (1H, m), 3.77 (1H, dt,  $J = 14.9, 5.0$  Hz), 3.47 (1H, dt,  $J = 14.9, 6.0$  Hz), 3.10 (1H, dd,  $J = 14.5, 4.9$  Hz), 2.53 (1H, dd,  $J = 14.5, 2.1$  Hz), 1.39 (3H, d,  $J = 6.1$  Hz);

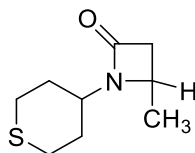
$^{13}\text{C NMR}$  (100 MHz,  $\text{CDCl}_3$ )  $\delta$ : 167.2, 164.7, 159.3, 115.3, 77.3, 77.0, 76.7, 65.6, 48.6, 44.3, 39.2, 18.7;

**1-Isopropyl-4-methylazetidin-2-one**

General procedure A, residence time 15 min at 130 °C. The residue was purified by column chromatography (silica, diethyl ether) and the combined fractions were passed through a plug of charcoal eluting with diethyl ether to afford the title compound as a colourless oil (85%). R<sub>f</sub> = 0.27 (diethyl ether);

<sup>1</sup>H NMR (400 MHz, CDCl<sub>3</sub>) δ: 3.82 (1H, sp, J = 6.8 Hz), 3.74–3.69 (1H, m), 2.96 (1H, dd, J = 14.3, 5.0 Hz), 2.41 (1H, dd, J = 14.3, 2.2 Hz), 1.35 (3H, d, J = 6.1 Hz), 1.25 (3H, d, J = 6.8 Hz), 1.21 (3H, d, J = 6.8 Hz);

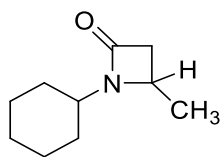
<sup>13</sup>C NMR (100 MHz, CDCl<sub>3</sub>) δ: 166.3, 46.1, 43.8, 43.3, 21.9, 20.7, 20.1;

**4-Methyl-1-(tetrahydro-2H-thiopyran-4-yl)azetidin-2-one**

General procedure B, residence time 5 min. The residue was purified by column chromatography (silica, diethyl ether/hexane 4:1 (v/v)) and the combined fractions were passed through a plug of charcoal eluting with diethyl ether to afford the title compound as a colourless oil (79%); R<sub>f</sub> = 0.21 (ethyl acetate/hexanes 80% (v/v));

<sup>1</sup>H NMR (400 MHz, CDCl<sub>3</sub>) δ: 3.76–3.71 (1H, m), 3.49 (1H, tt, J = 11.9, 3.6 Hz), 2.98 (1H, dd, J = 14.6, 5.1 Hz), 2.73–2.58 (4H, m), 2.42 (1H, dd, J = 14.6, 2.2 Hz), 2.18–2.10 (2H, m), 1.88 (1H, qd, J = 11.6, 4.2 Hz), 1.77 (1H, qd, J = 11.9, 3.8 Hz), 1.35 (3H, d, J = 6.1 Hz);

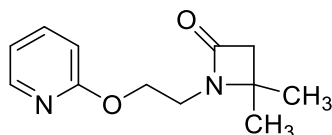
<sup>13</sup>C NMR (100 MHz, CDCl<sub>3</sub>) δ: 166.2, 50.8, 46.5, 45 43.5, 33.4, 31.8, 28.1, 28.0, 20.8;

**1-Cyclohexyl-4-methylazetidin-2-one**

General procedure A, residence time 5 min. The residue was purified by column chromatography (silica, diethyl ether/hexane 4:1 (v/v)) and the combined fractions were passed through a plug of charcoal eluting with diethyl ether to afford the title compound as a colourless oil (86%);  $R_f = 0.27$  (diethyl ether/hexane 4/1 (v/v));

$^1\text{H NMR}$  (400 MHz,  $\text{CDCl}_3$ )  $\delta$ : 3.71 (1H, qnd,  $J = 6.0, 2.0$  Hz), 3.42 (1H, tt,  $J = 11.7, 3.9$  Hz), 2.97 (1H, dd,  $J = 14.3, 5.0$  Hz), 2.41 (1H, dd,  $J = 14.4, 2.2$  Hz), 1.88 (2H, br t,  $J = 13.2$  Hz), 1.77 (2H, br t,  $J = 14.6$  Hz), 1.65–1.61 (1H, m), 1.51 (1H, qd,  $J = 12.3, 3.4$  Hz), 1.39 (1H, qd,  $J = 12.2, 3.4$  Hz), 1.34 (3H, d,  $J = 6.0$  Hz), 1.26 (2H, tt,  $J = 12.2, 3.1$  Hz), 1.14 (1H, qn,  $J = 12.5, 3.3$  Hz);

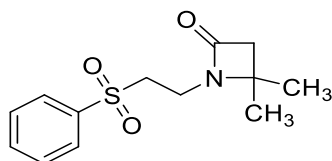
$^{13}\text{C NMR}$  (100 MHz,  $\text{CDCl}_3$ )  $\delta$ : 166.3, 51.8, 46.3, 43.3, 32.1, 30.7, 25.4, 25.3, 20.7;

**4,4-Dimethyl-1-(2-(pyridin-2-yloxy)ethyl)azetidin-2-one**

General procedure C, residence time 30 min. The residue was purified by column chromatography (silica, hexane/ethyl acetate 3:2 (v/v)) to afford the title compound as a light brown oil (90%);  $R_f = 0.08$  (hexane/ethyl acetate 7:3 (v/v));

$^1\text{H NMR}$  (400 MHz,  $\text{CDCl}_3$ )  $\delta$ : 8.13 (1H, dd,  $J = 5.0, 1.4$  Hz), 7.56 (1H, ddd,  $J = 8.5, 7.1, 2.0$  Hz), 6.87 (1H, ddd,  $J = 7.0, 5.1, 0.8$  Hz), 6.72 (1H, d,  $J = 8.3$  Hz), 4.40 (2H, t,  $J = 5.7$  Hz), 3.50 (2H, t,  $J = 5.7$  Hz), 2.73 (2H, s), 1.40 (6H, s);

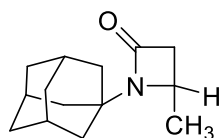
$^{13}\text{C NMR}$  (126 MHz,  $\text{CDCl}_3$ )  $\delta$ : 167.1, 163.3, 147.0, 138.8, 117.2, 111.2, 63.6, 56.0, 50.5, 38.8, 25.4;

**4,4-Dimethyl-1-(2-(phenylsulfonyl)ethyl)azetididin-2-one**

General procedure C, residence time 30 min. The residue was purified by column chromatography (silica, ethyl acetate/hexane 1:1 (v/v)) to afford the title compound as a light brown oil (81%);  $R_f = 0.08$  (ethyl acetate/hexanes 1:1 (v/v));

$^1\text{H}$  NMR (400 MHz,  $\text{CDCl}_3$ )  $\delta$ : 7.93 (2H, d,  $J = 7.3$  Hz), 7.69 (1H, t,  $J = 7.4$  Hz), 7.59 (2H, t,  $J = 7.6$  Hz), 3.45 (4H, s), 2.69 (2H, s), 1.36 (6H, s);

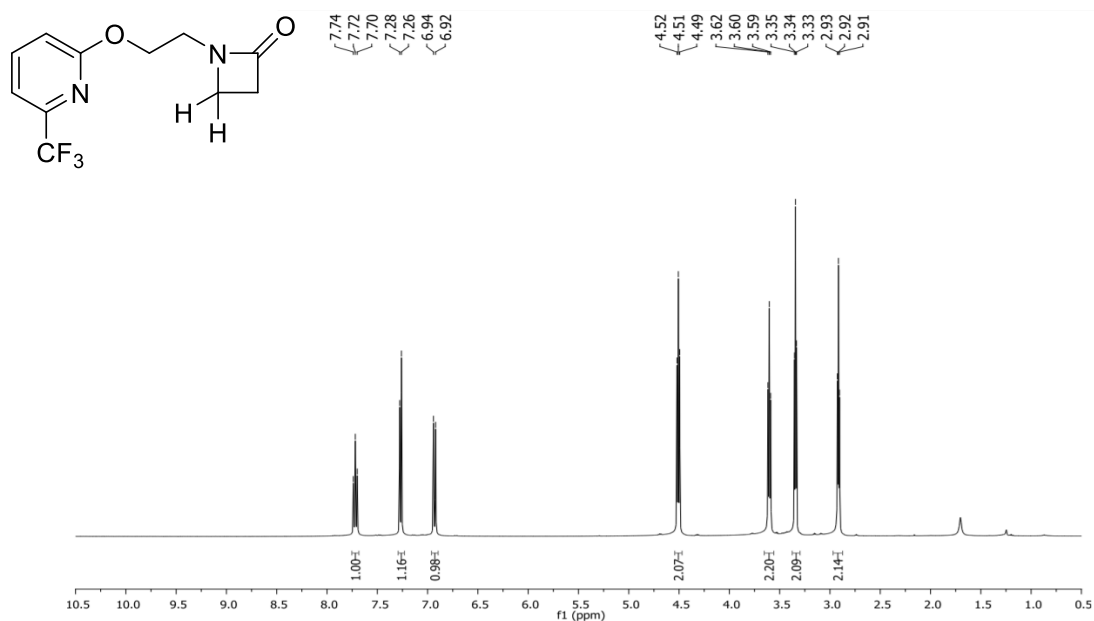
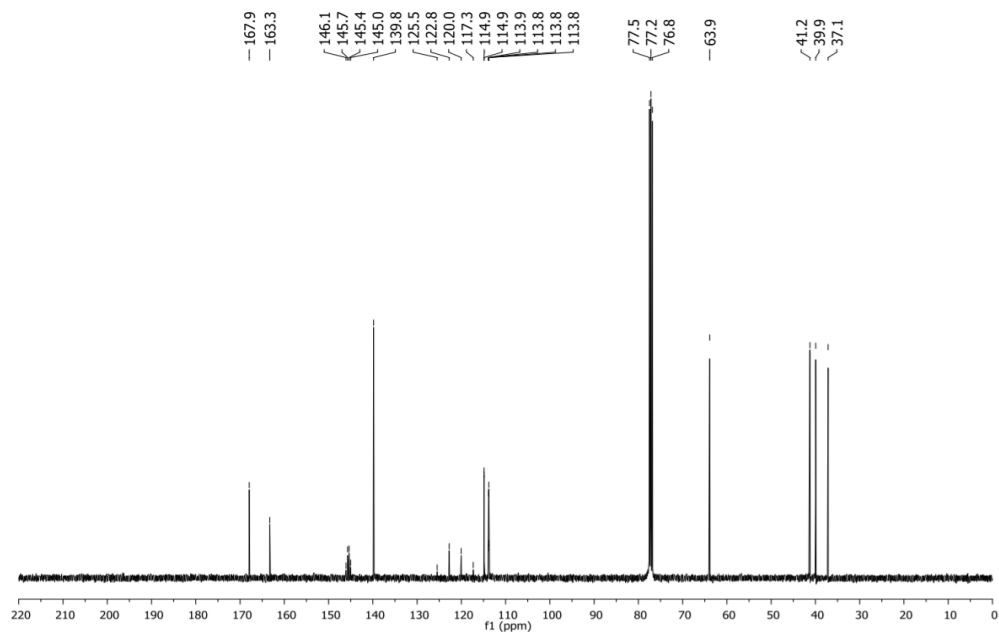
$^{13}\text{C}$  NMR (100 MHz,  $\text{CDCl}_3$ )  $\delta$ : 166.7, 138.8, 134.3, 129.6, 128.2, 56.1, 54.2, 50.6, 33.3, 25.0;

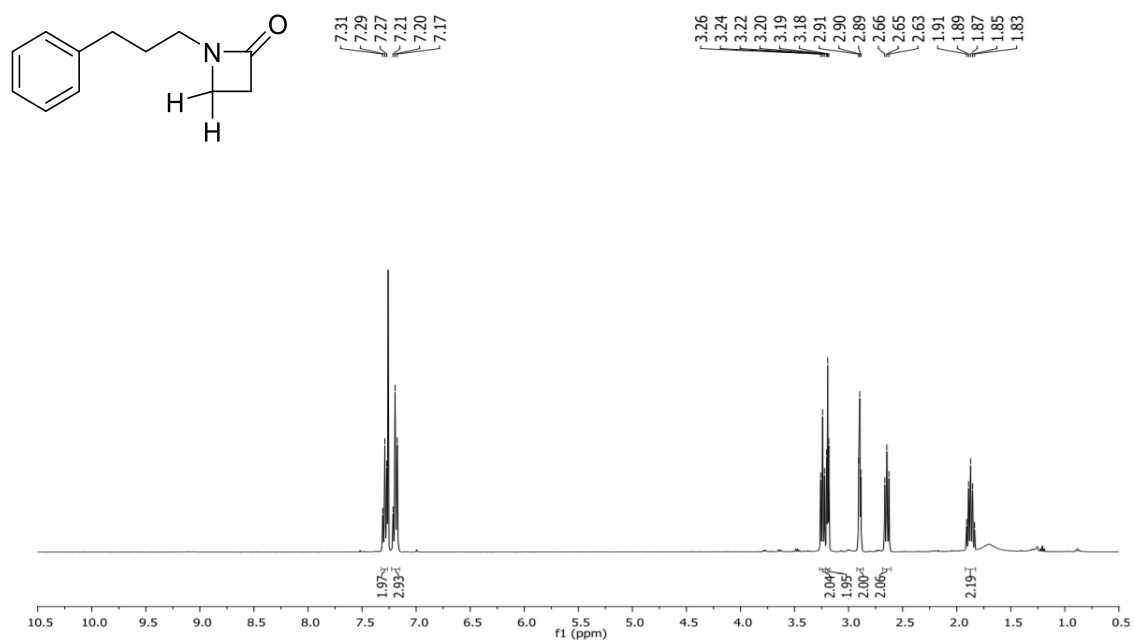
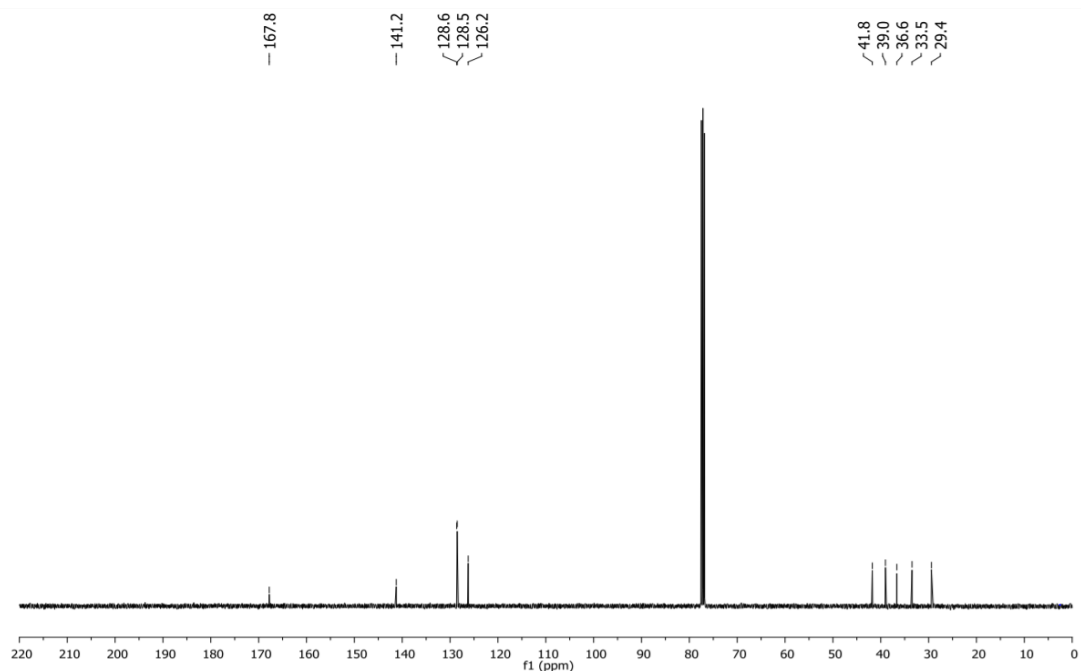
**1-Adamantan-1-yl)-4-methylazetididin-2-one**

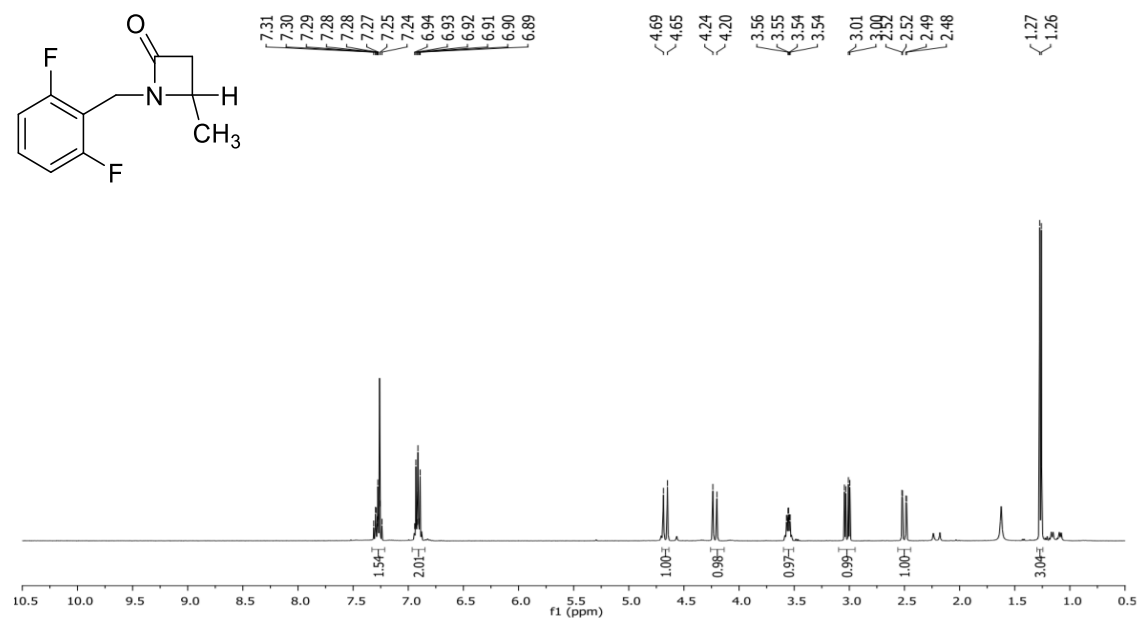
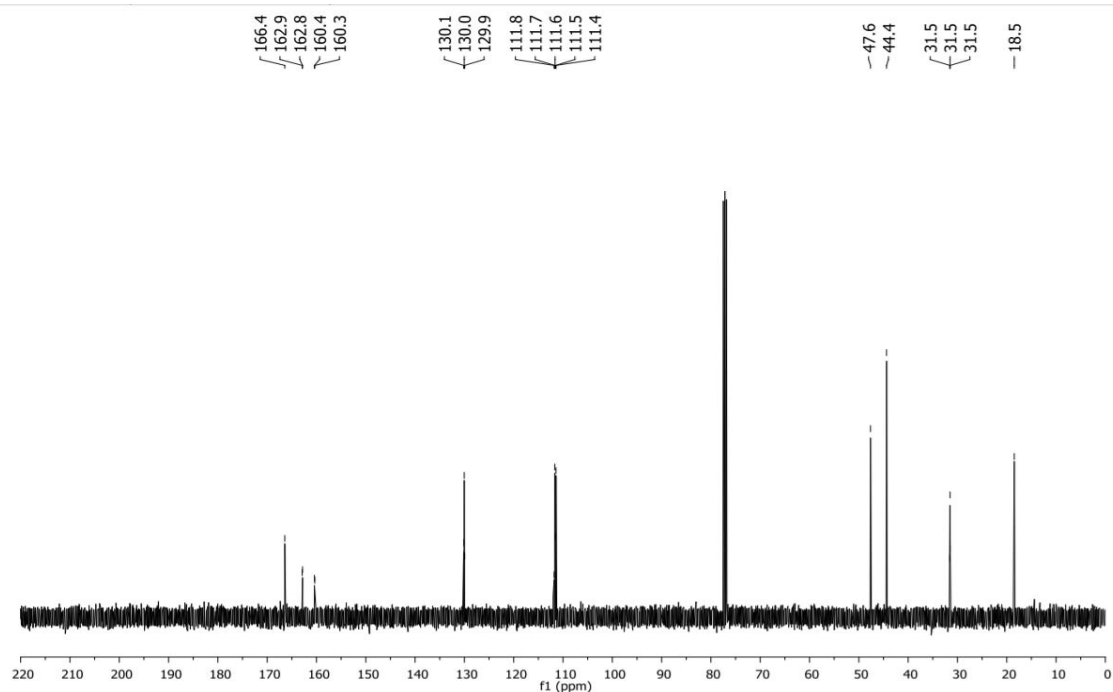
General procedure B, residence time 30 min. The crude product was purified by column chromatography (silica gel, diethyl ether/hexane 7:3 (v/v)) to afford the title compound as a brown oil (61%).  $R_f = 0.13$  (ethyl acetate/hexane 7:3 (v/v));

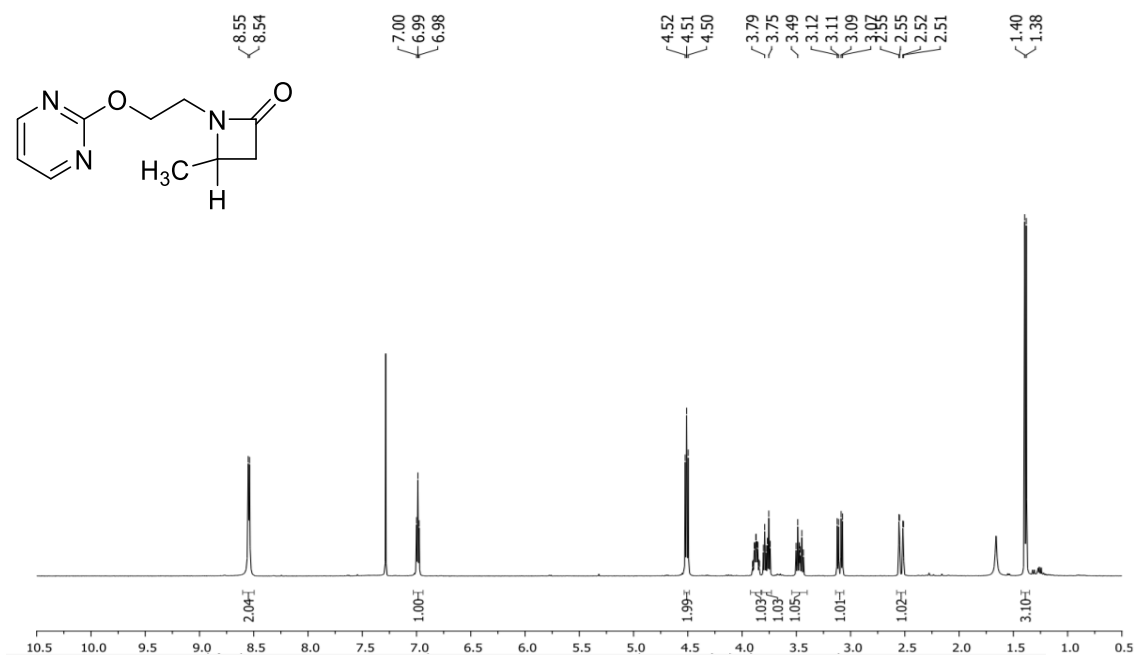
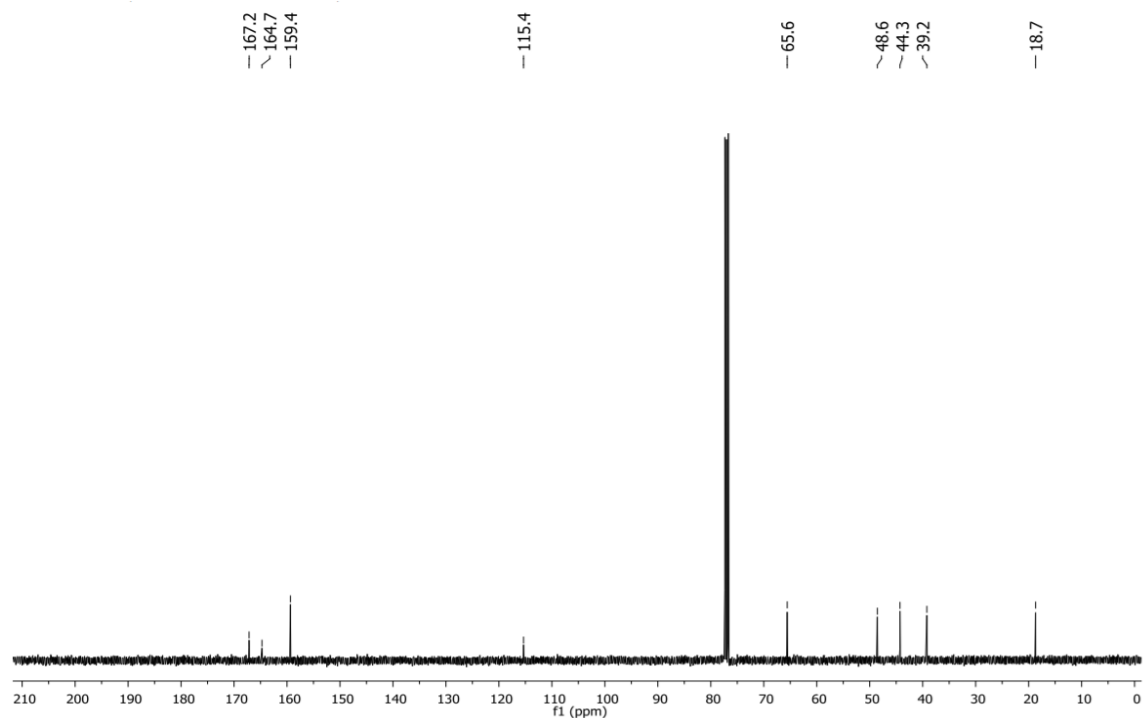
$^1\text{H}$  NMR (500 MHz,  $\text{CDCl}_3$ )  $\delta$ : 3.78–3.70 (1H, m), 2.91 (1H, dd,  $J = 14.3, 5.2$  Hz), 2.30 (1H, dd,  $J = 14.3, 2.2$  Hz), 2.11–2.04 (3H, m), 2.04–1.99 (6H, m), 1.67 (6H, t,  $J = 3.1$  Hz), 1.38 (3H, d,  $J = 6.0$  Hz);

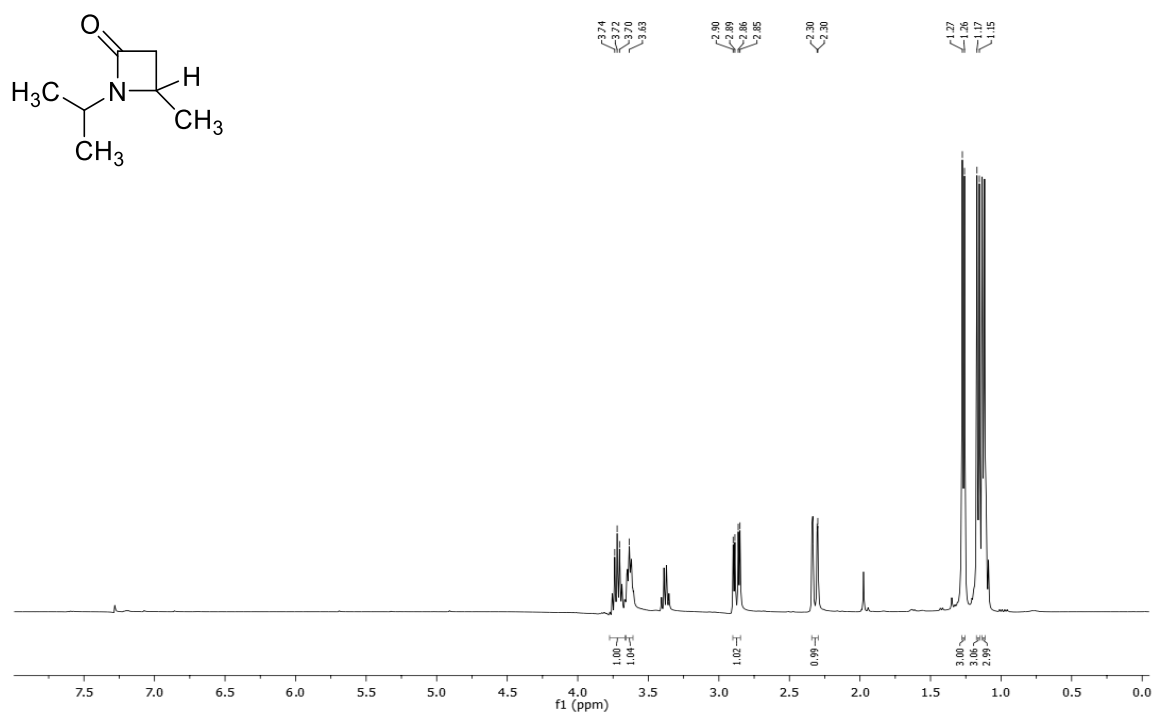
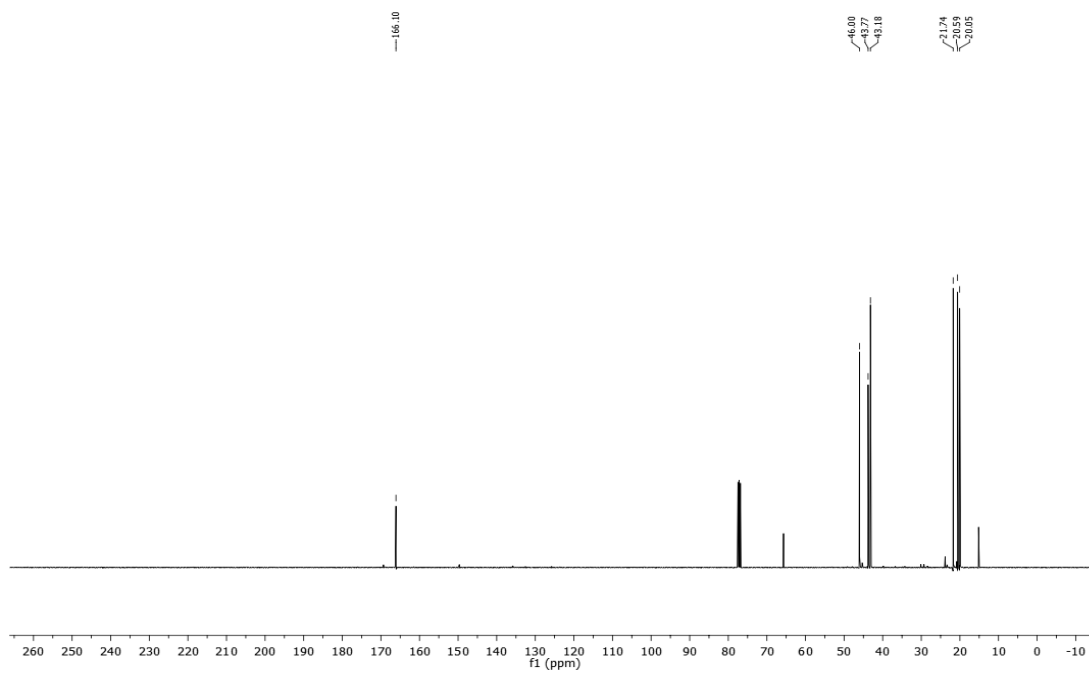
$^{13}\text{C}$  NMR (126 MHz,  $\text{CDCl}_3$ )  $\delta$ : 166.7, 55.0, 45.6, 42.9, 41.2, 36.4, 29.3, 22.5;

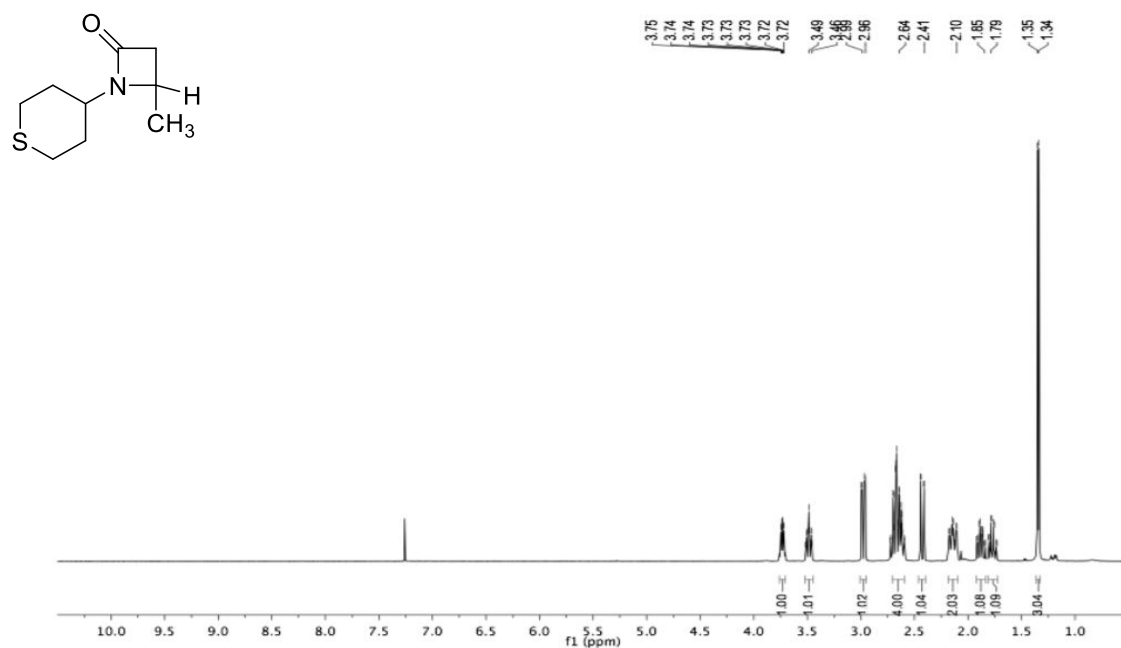
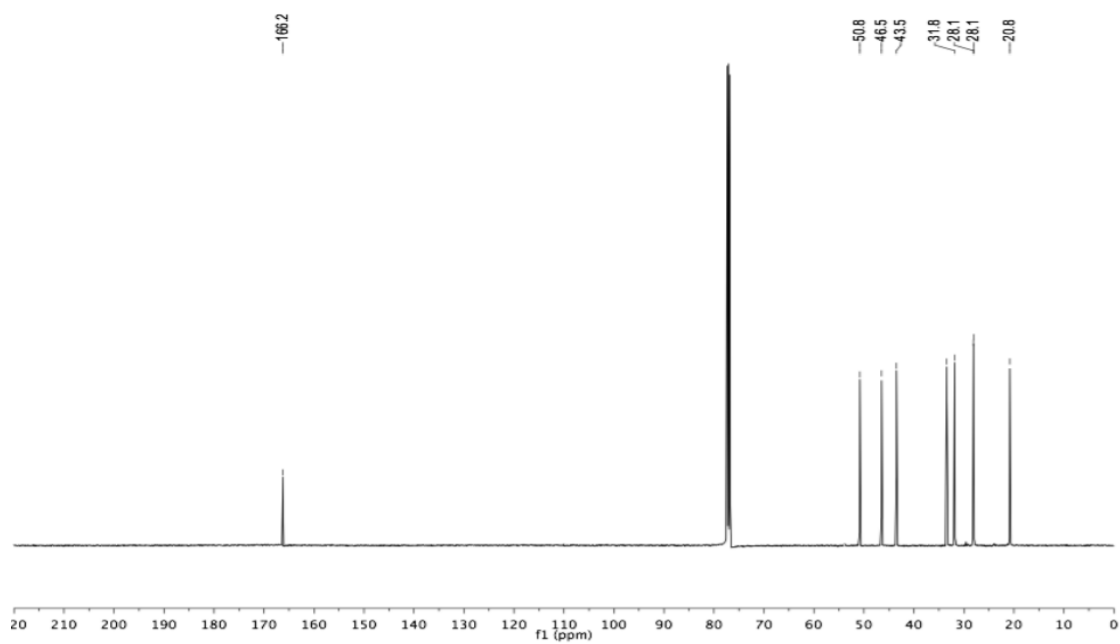
**1-(2-((6-(Trifluoromethyl)pyridin-2-yl)oxy)ethyl)azetidin-2-one** $^1\text{H}$  NMR ( $\text{CDCl}_3$ , 400 MHz) $^{13}\text{C}$  NMR ( $\text{CDCl}_3$ , 100 MHz)

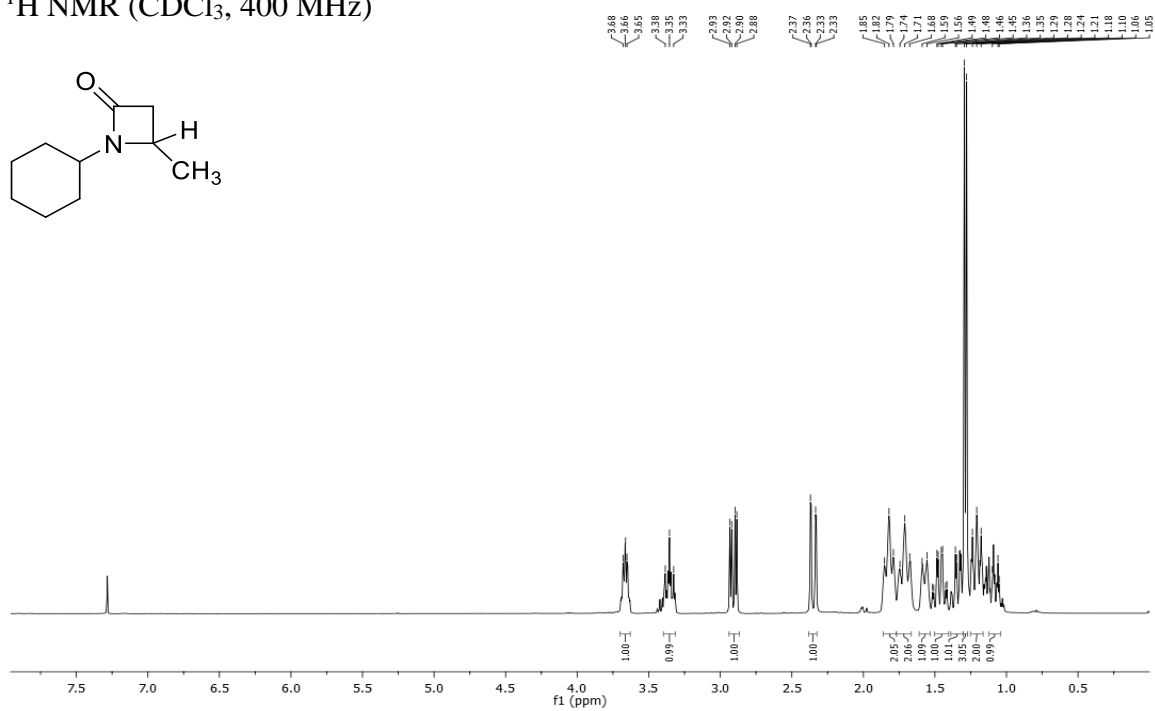
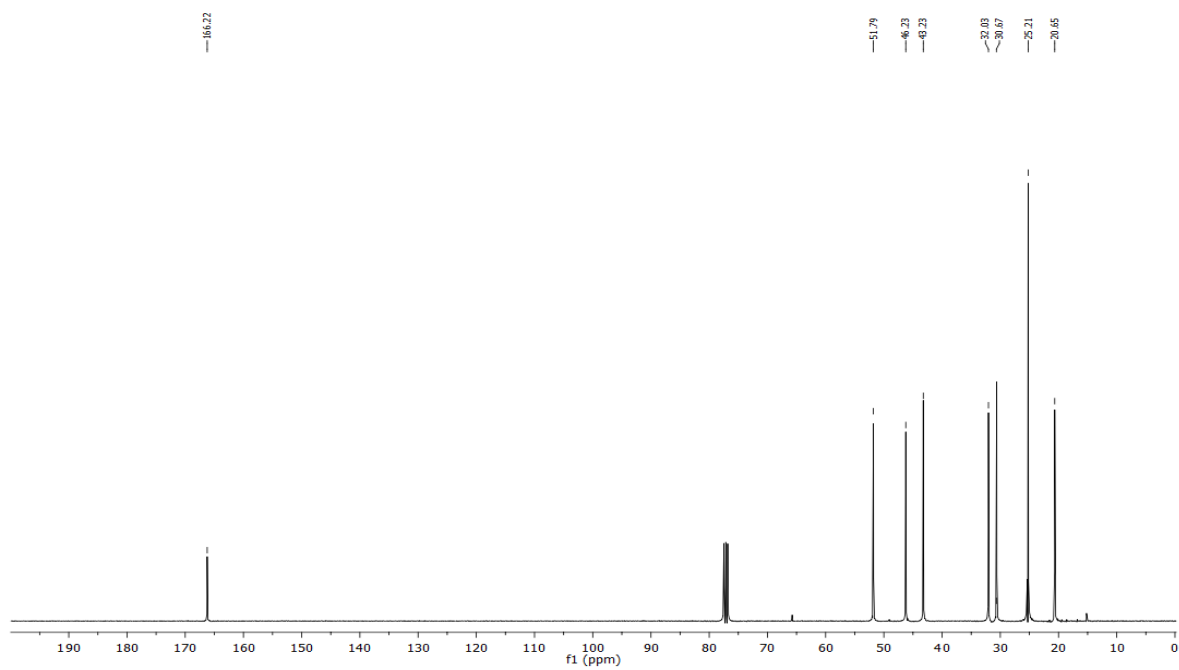
**1-(3-Phenylpropyl)azetidin-2-one** $^1\text{H}$  NMR ( $\text{CDCl}_3$ , 400 MHz) $^{13}\text{C}$  NMR ( $\text{CDCl}_3$ , 100 MHz)

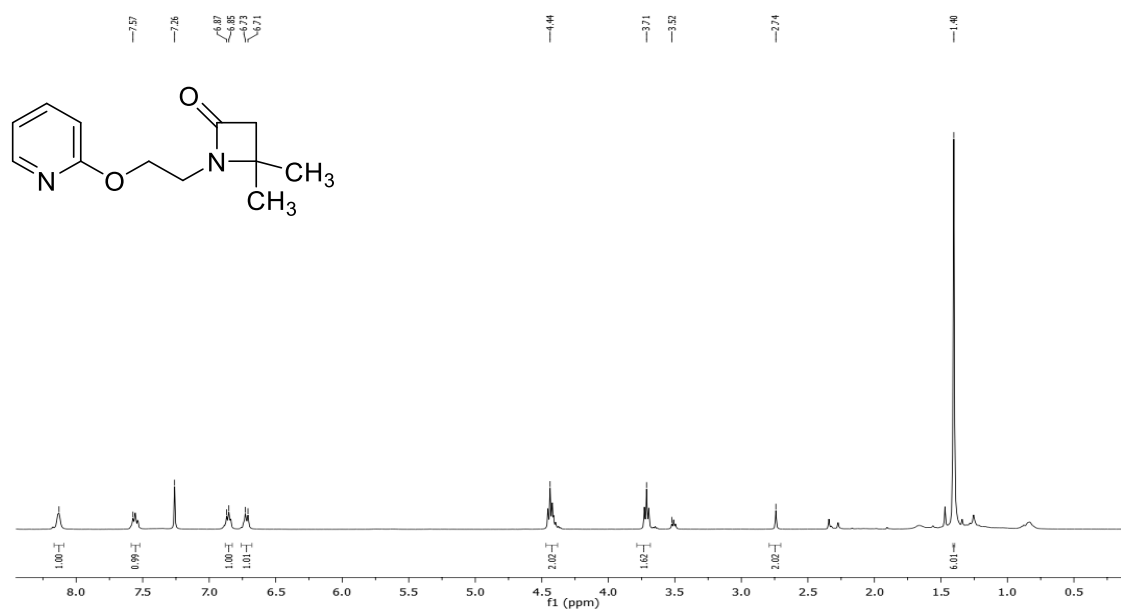
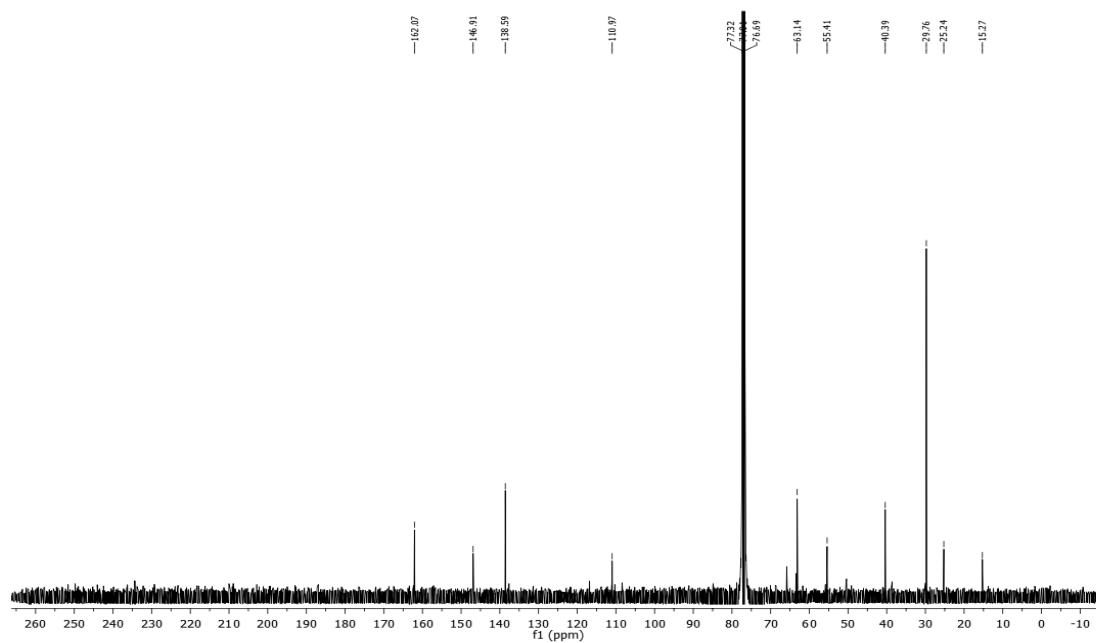
**1-(2,6-Difluorobenzyl)-4-methylazetidin-2-one** $^1\text{H}$  NMR ( $\text{CDCl}_3$ , 400 MHz) $^{13}\text{C}$  NMR ( $\text{CDCl}_3$ , 100 MHz)

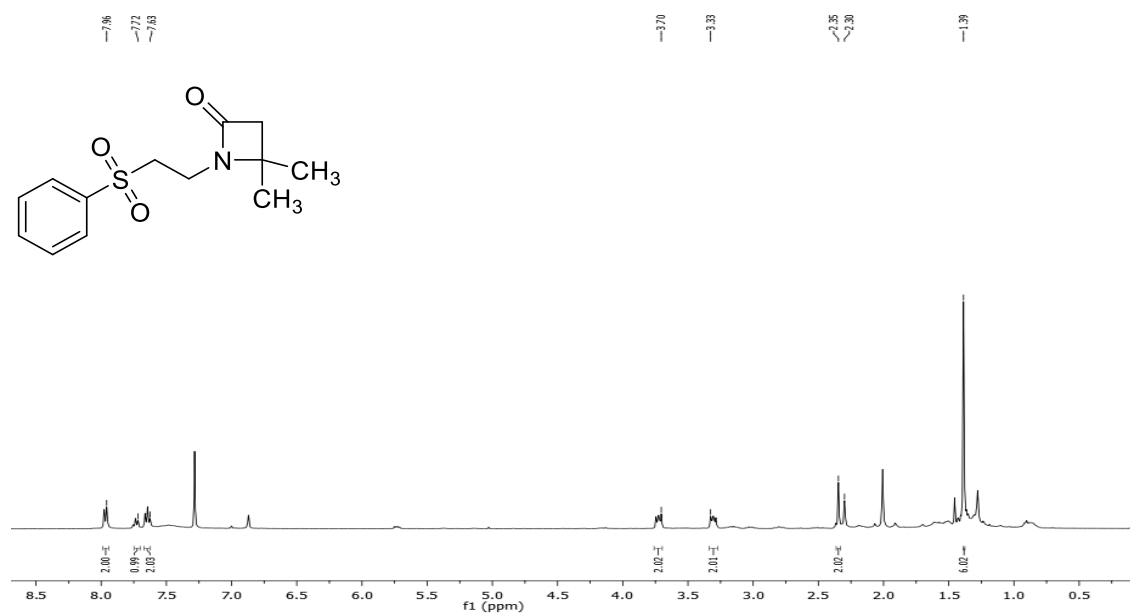
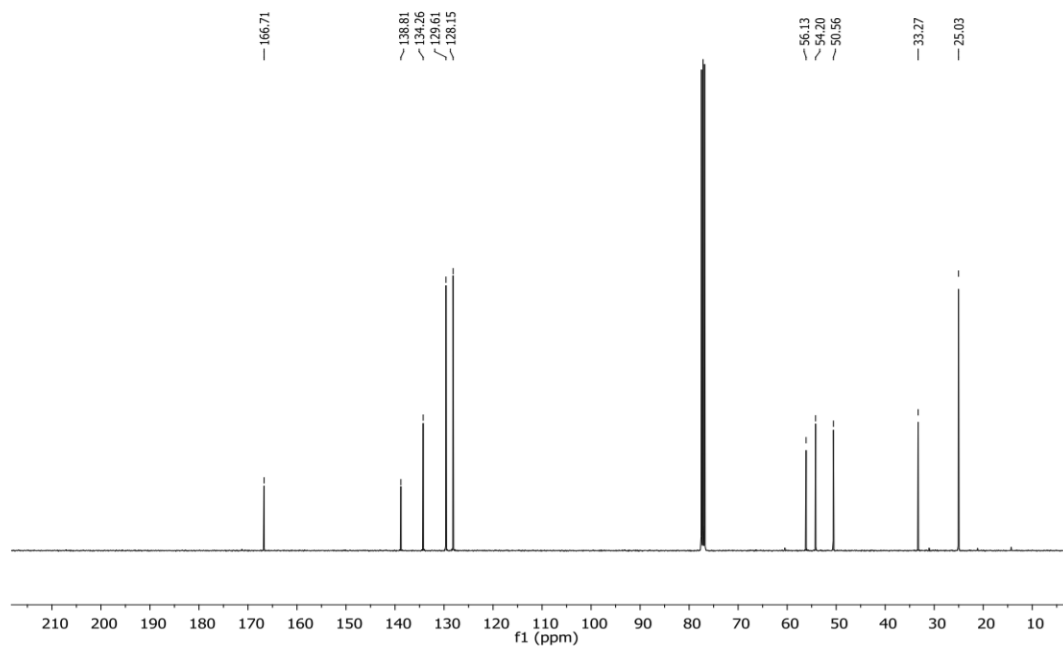
**4-Methyl-1-(2-(pyrimidin-2-yloxy)ethyl)azetidin-2-one** $^1\text{H}$  NMR ( $\text{CDCl}_3$ , 400 MHz) $^{13}\text{C}$  NMR ( $\text{CDCl}_3$ , 100 MHz)

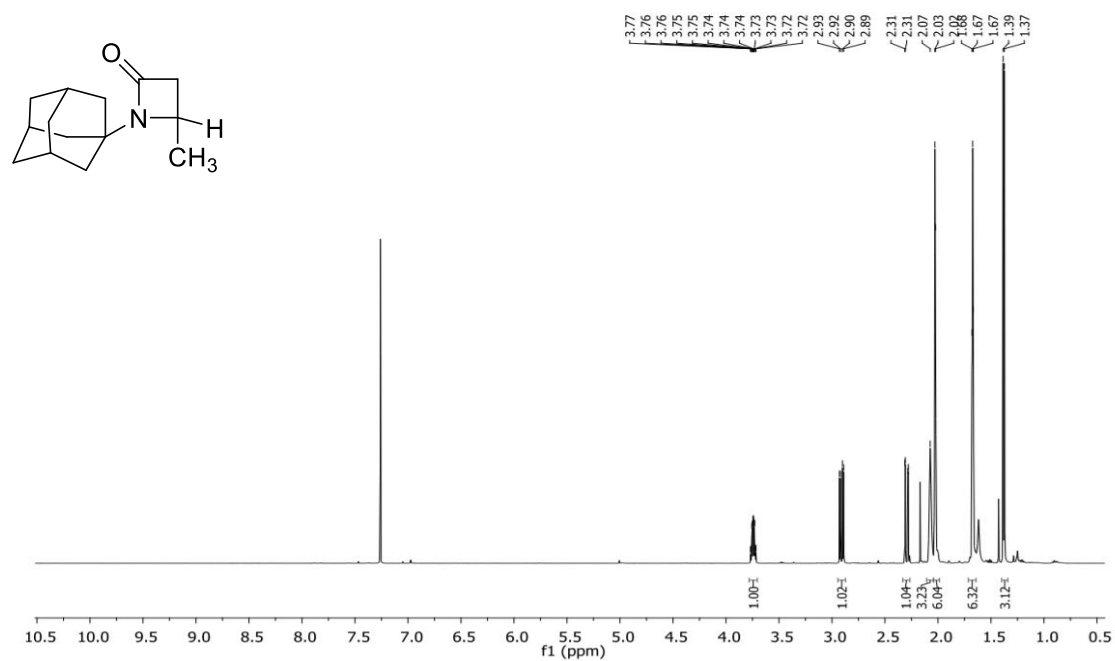
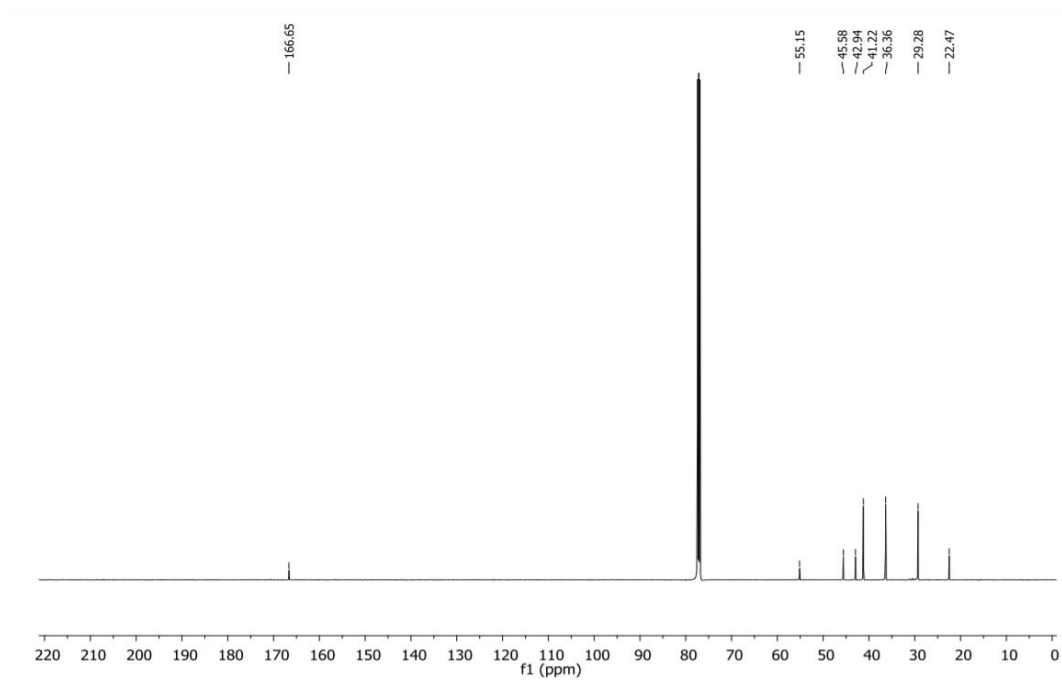
**1-Isopropyl-4-methylazetidin-2-one** $^1\text{H}$  NMR ( $\text{CDCl}_3$ , 400 MHz) $^{13}\text{C}$  NMR ( $\text{CDCl}_3$ , 100 MHz)

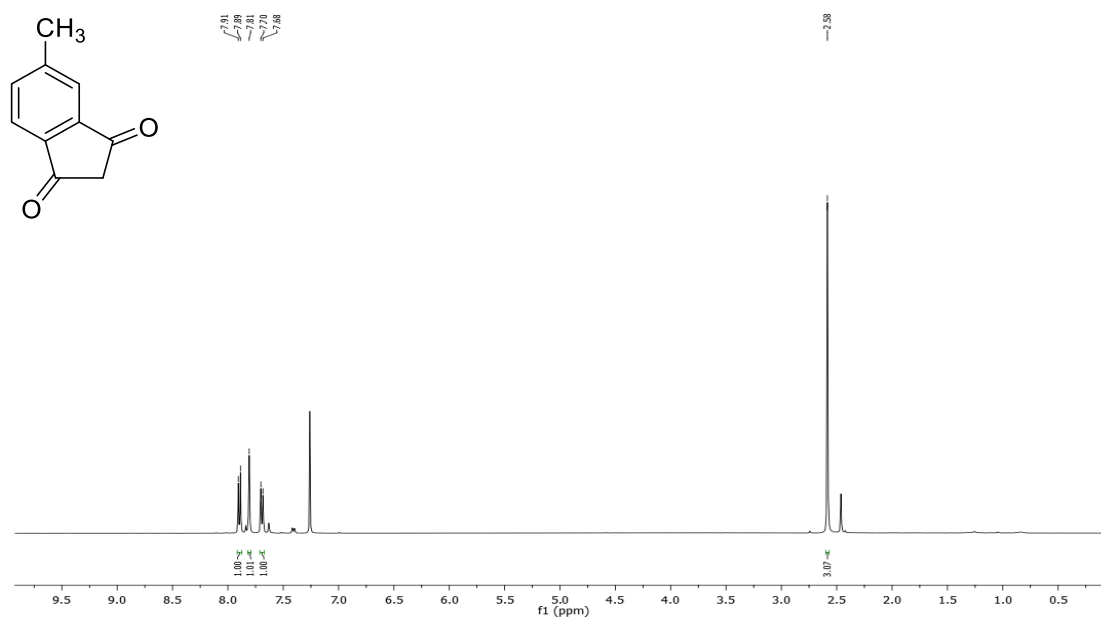
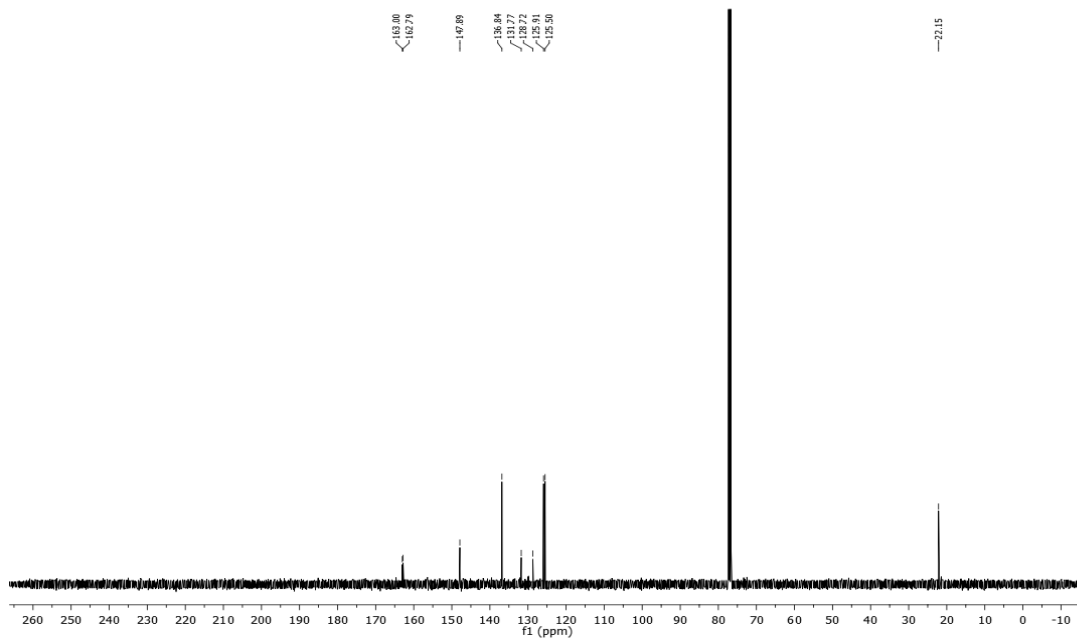
**4-Methyl-1-(tetrahydro-2H-thiopyran-4-yl)azetidin-2-one**<sup>1</sup>H NMR (CDCl<sub>3</sub>, 400 MHz)<sup>13</sup>C NMR (CDCl<sub>3</sub>, 100 MHz)

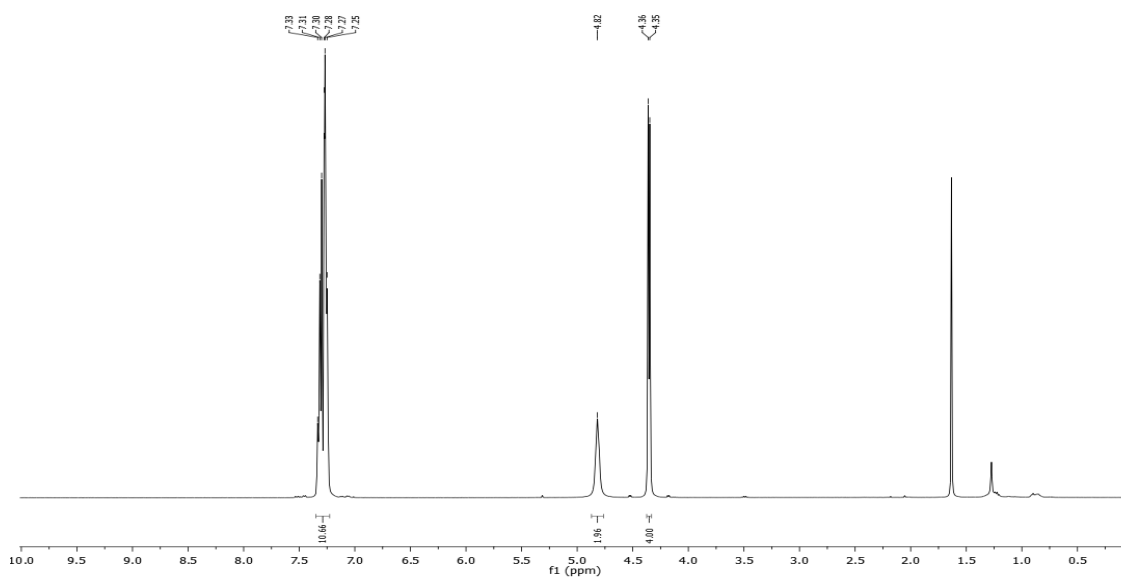
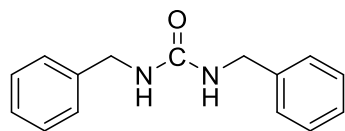
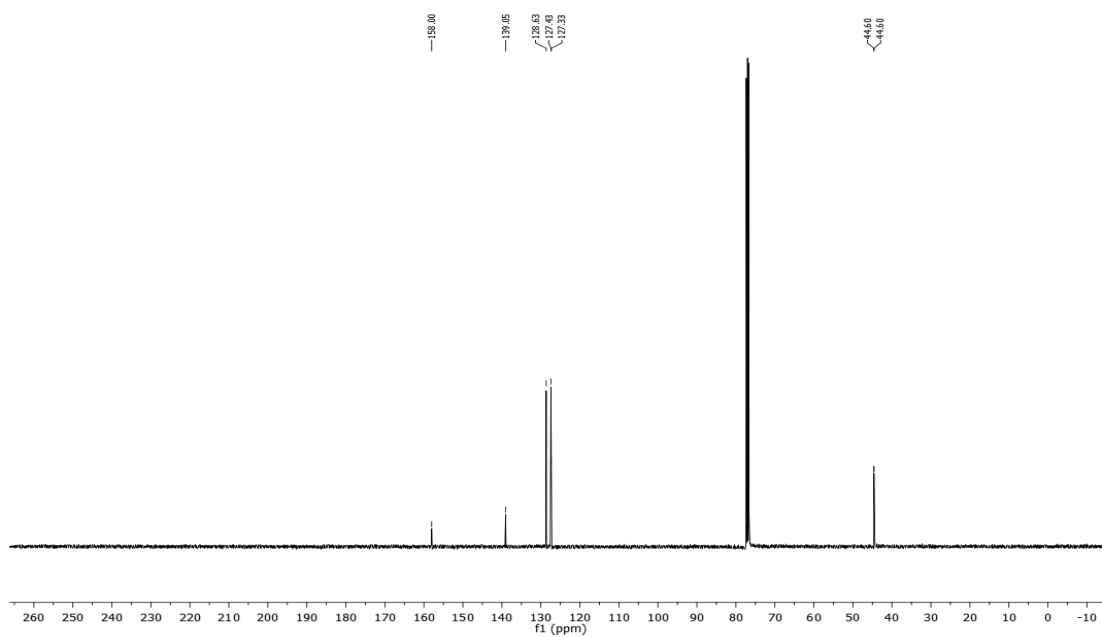
**1-Cyclohexyl-4-methylazetidin-2-one** $^1\text{H}$  NMR ( $\text{CDCl}_3$ , 400 MHz) $^{13}\text{C}$  NMR ( $\text{CDCl}_3$ , 100 MHz)

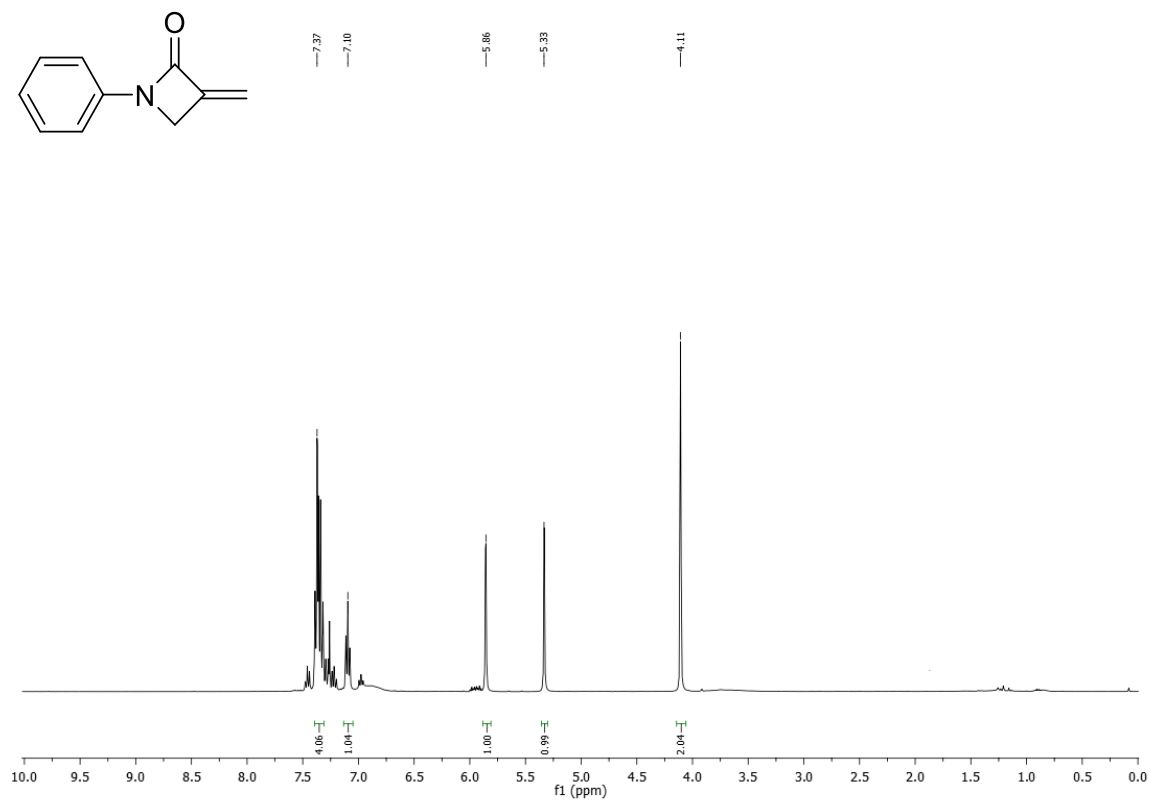
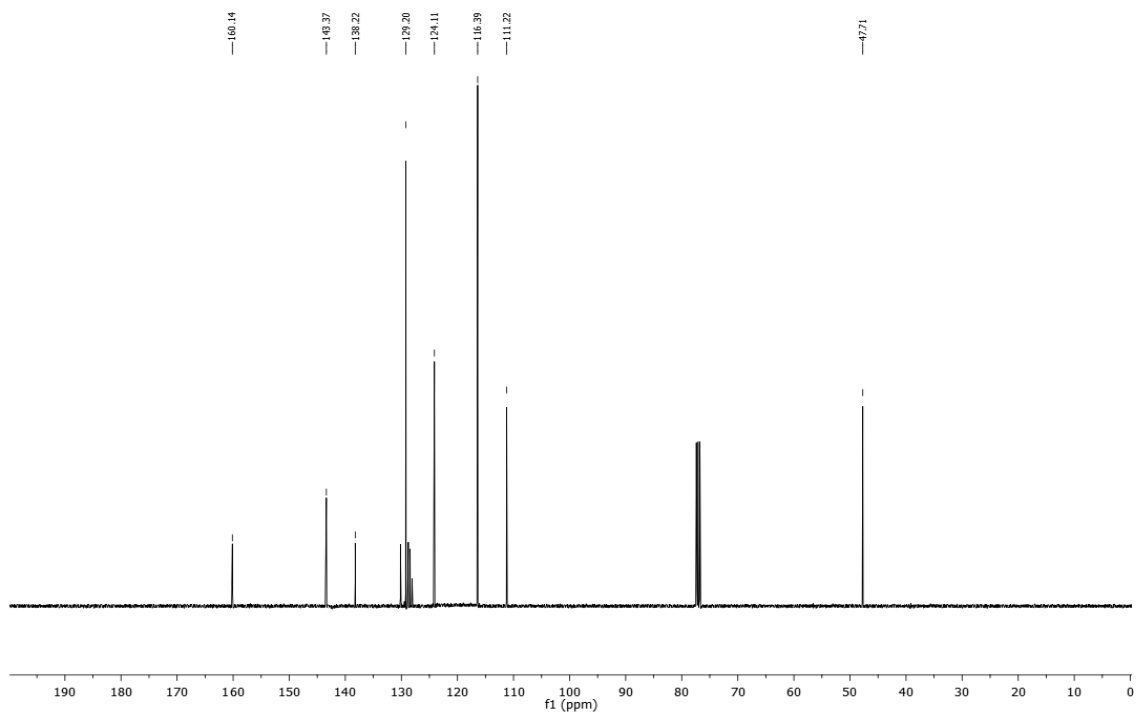
**4,4-Dimethyl-1-(2-(pyridin-2-yloxy)ethyl)azetidin-2-one** $^1\text{H}$  NMR ( $\text{CDCl}_3$ , 400 MHz) $^{13}\text{C}$  NMR ( $\text{CDCl}_3$ , 100 MHz)

**4,4-Dimethyl-1-(2-(phenylsulfonyl)ethyl)azetidin-2-one** $^1\text{H}$  NMR ( $\text{CDCl}_3$ , 400 MHz) $^{13}\text{C}$  NMR ( $\text{CDCl}_3$ , 100 MHz)

**1-Adamantan-1-yl)-4-methylazetidin-2-one** $^1\text{H}$  NMR ( $\text{CDCl}_3$ , 400 MHz) $^{13}\text{C}$  NMR ( $\text{CDCl}_3$ , 100 MHz)

**4-Methylphthalic Anhydride** $^1\text{H}$  NMR ( $\text{CDCl}_3$ , 400 MHz) $^{13}\text{C}$  NMR ( $\text{CDCl}_3$ , 100 MHz)

**1,3-Dibenzylurea** $^1\text{H}$  NMR ( $\text{CDCl}_3$ , 400 MHz) $^{13}\text{C}$  NMR ( $\text{CDCl}_3$ , 100 MHz)

**3-methylene-1-phenylazetidin-2-one** $^1\text{H}$  NMR ( $\text{CDCl}_3$ , 400 MHz) $^{13}\text{C}$  NMR ( $\text{CDCl}_3$ , 100 MHz)

## 8.5. Appendix 5

### Models built for the LCA analysis

1. Introduction .....	iv
2. Anhydrous copper (II) acetate .....	vii
2.1. Introduction .....	vii
2.2. Process description .....	viii
2.3. Process diagram .....	x
2.4. Mass balance .....	xi
2.5. Heat/energy balance .....	xii
2.6. Total energy requirement .....	xiv
3. Sodium acetate .....	xv
3.1. Process description .....	xv
3.2. Process diagram .....	xvi
3.3. Mass balance .....	xvii
3.4. Heat balance .....	xviii
3.5. Total energy requirement .....	xx
4. 1,4-benzoquinone .....	xxi
4.1. Introduction .....	xxi
4.2. Process description .....	xxii
4.3. Mass balance .....	xxiii
4.4. Heat/energy balance .....	xxiv
4.5. Total energy requirement .....	xxvii
5. 1-adamananecarboxylic acid .....	xxviii
5.1. Summary .....	xxviii
5.2. Reduction of dicyclopentadiene .....	xxviii

5.2.1.	Mass balance .....	xxix
5.2.2.	Heat/energy balance .....	xxx
5.2.3.	Total energy requirement .....	xxxi
5.3.	Synthesis of adamantane .....	xxxi
5.3.1.	Mass balance .....	xxxii
5.3.2.	Heat/energy balance .....	xxxiii
5.3.3.	Total energy requirement .....	xxxiv
5.4.	Reaction to 1-adamantanecarboxylic acid.....	xxxiv
5.4.1.	Mass balance .....	xxxv
5.4.2.	Heat/energy balance .....	xxxviii
5.4.3.	Total energy requirement .....	xxxix
6.	Li-quinoline .....	xl
6.1.	Overview of the process .....	xl
6.2.	Synthesis of 1,4-dibromobutane.....	xli
6.2.1.	Process diagram .....	xlii
6.2.2.	Mass balance .....	xliii
6.2.3.	Heat/energy balance .....	xliv
6.2.4.	Total energy requirement .....	xlvi
6.3.	Diketene .....	xlvi
6.3.1.	Introduction.....	xlvi
6.3.2.	Process description.....	xlvi
6.3.3.	Process diagram .....	xlix
6.3.4.	Mass balance .....	l
6.3.5.	Heat/energy balance .....	li
6.3.6.	Total energy requirement .....	lii
6.4.	2,2,6-Trimethyl-4H-1,3-dioxin-4-one .....	liii
6.4.1.	Mass balance .....	liv

6.4.2.	Heat/energy balance .....	lv
6.4.3.	Total energy requirement .....	lvi
6.5.	Acetoacetanilide synthesis .....	lvii
6.5.1.	Mass Balance .....	lviii
6.5.2.	Heat/energy balance .....	lix
6.5.3.	Total energy requirement .....	lix
6.6.	1-acetyl-N-phenylcyclopentanecarboxamide synthesis .....	lx
6.6.1.	Mass balance .....	lxi
6.6.2.	Heat/energy balance .....	lxii
6.6.3.	Total energy requirement .....	lxii
6.7.	Li-quinoline synthesis .....	lxiii
6.7.1.	Mass balance .....	lxiv
6.7.2.	Heat/energy balance .....	lxv
6.7.3.	Total energy requirement .....	lxvi
7.	Purification of Pd/Cu residue .....	lxvi
8.	N-Cyclohexylisopropylamine synthesis .....	lxvii
8.1.	Overview .....	lxvii
8.2.	Cyclohexylamine .....	lxviii
8.2.1.	Mass balance .....	lxix
8.2.2.	Heat/energy balance .....	lxx
8.2.3.	Total energy requirement .....	lxxi
8.3.	N-Cyclohexylisopropylamine .....	lxxii
8.3.1.	Mass balance .....	lxxiii
8.3.2.	Heat/energy balance .....	lxxiv
8.3.3.	Total energy requirement .....	lxxiv
9.	Bibliography .....	lxxv

# 1. Introduction

Synthesis routes for all compounds were selected based on available information on the best industrial practices. Sources included Ullmann's Encyclopaedia of Industrial Chemistry,<sup>1</sup> Kirk-Othmer Encyclopaedia of Chemical Technology,<sup>2</sup> patents or, in case of small-scale syntheses, scientific publications being detailed enough to reproduce the process.

Scales of the processes were selected based on the volume of available bulk orders, information from literature data or market research summaries. The same applies to the location of production plants.

Preferable technology (for example batch or continuous) was selected based on the throughput of the synthesis and available information from the literature.

All physio-chemical properties were sourced from the NIST webbook database.<sup>3</sup> For molecules not present in the database, values were simulated using appropriate models; specific models were cited in each case.

Some processes were modified to accommodate current health and safety regulations as well as green chemistry principles; for example, chlorinated solvents were replaced with appropriate alternatives.

For processes where the mass balance was not closed, an assumption was made to add a necessary amount of an unreacted substrate, which cannot be recycled, to the product side of the mass balance. Where possible, recycling of solvents and other reactants was applied.

For mass and energy balances the following assumptions were made:

1. For high-temperature differences ( $>50^{\circ}\text{C}$ ), 75% efficiency of heating/cooling was assumed.
2. For low-temperature differences ( $<30^{\circ}\text{C}$ ), 100% efficiency of heating/cooling was assumed.

3. For moderate temperature differences ( $50^{\circ}\text{C} < 30^{\circ}\text{C}$ ), 85% efficiency of heating/cooling was assumed.
4. Heating is performed using saturated steam at appropriate pressure. Heat delivered from the steam was calculated based on:

$$Q = m_s h_{fg} \quad (1)$$

where  $Q$  is the energy required (kJ);  $m_s$  is the mass of steam (kg), and  $h_{fg}$  is the specific enthalpy of evaporation of steam ( $\text{kJ kg}^{-1}$ ).

5. The energy required to heat/cool the mixture was calculated based on:

$$Q = m C_p \Delta T \quad (2)$$

where  $m$  is the mass of the mixture (kg),  $C_p$  is the heat capacity of the mixture calculated assuming that the specific heat capacity of a mixture is equal to the mass-weighted average of the components heat capacities ( $\text{kJ kg}^{-1} \text{K}^{-1}$ ), and  $\Delta T$  is the temperature difference (K). When required, latent heats of evaporation were accounted for.

6. The heat of reaction was calculated based on heats of formations of substrates and products at appropriate states (solid/liquid/gas) and heats of the phase transformation.

$$\Delta H = \sum h_{f\text{products}} - h_{f\text{substrates}} \quad (3)$$

7. Where appropriate, a heat of reaction was added/deducted from the energy required to heat/cool the mixture.
8. Specific heat capacities of mixtures were calculated based on the addition method.

$$C_{p\text{mixture}} = \sum C_{p_i} x_i \quad (4)$$

9. The energy required to pump the reactants was calculated based on ref. 4.

10. The power required for mixing was calculated based on ref. 5 assuming agitator to be a Rushton 6-blade, the scale of agitation 4 and D/T ratio 0.4
11. For other instruments, appropriate tools were used to estimate the energy required or they were neglected if their impact on the overall energy balance was small.
12. 100% efficiency of extractions was assumed.
13. Unless otherwise stated, all by-products were treated as waste streams and utilised.
14. Following industrial standards, all solvents were recycled using distillation or high-temperature incineration method.
15. All metal based, heterogeneous catalysts were recycled.

## 2. Anhydrous copper (II) acetate

### 2.1. Introduction

Copper (II) acetate is produced industrially by following chemical reactions:<sup>1</sup>

1. Reaction of copper (II) hydroxide or copper (II) carbonate with a solution of acetic acid
2. Reaction of copper (II) oxide with a solution of acetic acid at elevated temperature
3. Reaction of copper (II) sulfate solution with lead acetate
4. Reaction of metallic copper with boiling aqueous acetic acid in the presence of air or oxygen.

Copper (II) acetate occurs in two forms, anhydrous and monohydrate. Anhydrous copper(II) acetate [142-71-2],  $\text{Cu}(\text{CH}_3\text{COO})_2$ , Mr 181.63, mp 115 °C, bp 240 °C, is a dark green crystalline verdigris, neutralised verdigris. The monohydrated copper (II) acetate [6046-93-1],  $\text{Cu}(\text{CH}_3\text{COO})_2 \cdot \text{H}_2\text{O}$ , Mr 199.65, mp 115 °C, decomposition at 240 °C, forms blueish green monoclinic crystals. The commercially available copper (II) acetate is copper (II) acetate monohydrate with a density of 1.882 [g cm<sup>-3</sup>], a water solubility of 7.2 [g 100 mL<sup>-1</sup>] in cold water and 20 [g 100<sup>-1</sup>] in hot water. In addition, copper (II) acetate monohydrate is soluble in alcohols and slightly soluble in ethers and glycerol.<sup>1</sup>

Applications of copper (II) acetate:

1. As an insecticide, fungicide and mildewcide in crop protection
2. As a preservative for cellulosic materials
3. For production of Paris green
4. As a catalyst in organic chemistry
5. Others

The list of main manufacturers of copper (II) acetate includes:

1. Eastman Chemicals
2. American Elements

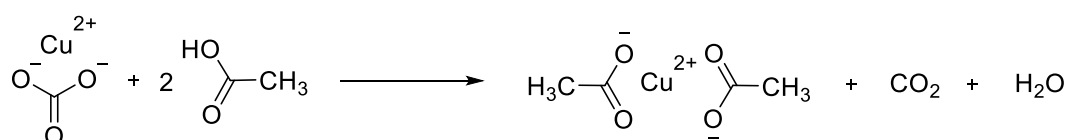
3. Kangtai Chemical
4. SRL Chemical
5. Sam Industries
6. TIB-Chemicals
7. Shepherd Chemical

Based on a market research, the maximum capacity of a single plant for copper (II) acetate was estimated to be in the range of 200 kilo-tonnes per annum.<sup>1</sup>

## 2.2. Process description

Due to lack of reliable data describing which process is currently practised in industry, the mildest option, i.e. reaction of copper (II) carbonate with acetic acid was selected. This process requires virtually no purification and occurs spontaneously under ambient conditions.

The process involves a reaction between solid copper (II) carbonate and glacial acetic acid. In the course of a slightly endothermic reaction, carbon dioxide, that is released to the environment, and water are produced. No other by-products are formed. After the reaction, a slurry of copper (II) is generated.



*Scheme 2.2-1. Formation of copper (II) acetate from copper carbonate and acetic acid.*

As reaction system, a twin-screw setup with an additional gaseous phase release is presented. A conveyer belt for solids delivery introduces crystals of copper (II) carbonate and, upon entering the twin-screw reactor, the solid phase is mixed with glacial acetic acid delivered by a pump. The formed slurry (mixture of solid copper (II) acetate and its saturated solution in water) is transported by a twin-screw along the reactor and, upon exiting, is directed into a continuous furnace (100 °C), where the liquid phase evaporates

yielding pure copper (II) acetate. Steam is supplied to the heat exchanger in the furnace. The twin-screw reactor operates at 25 °C.

In the course of the process, anhydrous copper (II) acetate is obtained, and upon exposure to moisture, a monohydrate is formed.

No heat integration is applied due to low heat of the single hot outlet stream. Water from the condenser (50 °C) is cooled down to ambient temperature in a fountain and reused.

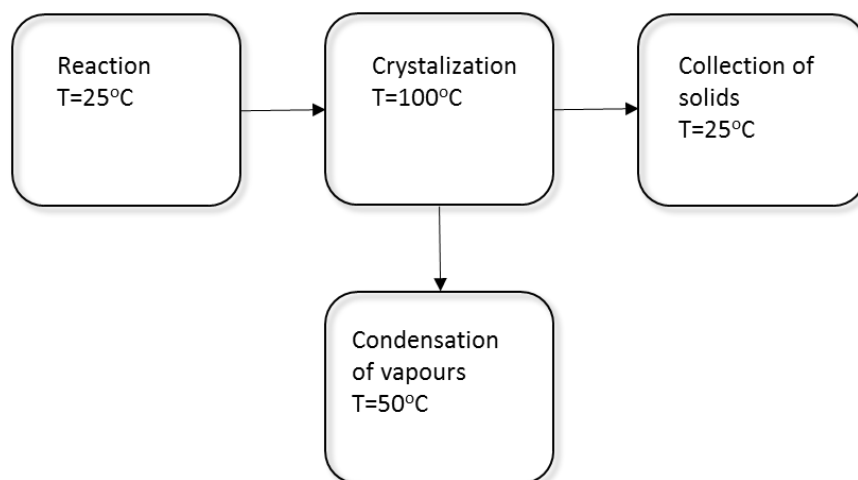


## 2.4. Mass balance

Table 2.4-1. Basis: production of 200,000,000 kg/annum copper (II) acetate product.

Stream	1	2	3	4	5	6	7
Description	AcOH in	CuCO <sub>3</sub> in	Crude out	CO <sub>2</sub> out	Cu(OAc) <sub>2</sub> out	Steam out	Water in
Pressure (bar)	1	1	1	1	1	1	1
Temperature (°C)	25	25	25	25	100	100	50
State	l	s	l/s	v	s	v	l
<b>MOLAR (mol)</b>							
AcOH	2.24E+09						
<i>mole fraction</i>	<i>0.97</i>						
CuCO <sub>3</sub>		1.10E+09					
<i>mole fraction</i>		<i>1</i>					
CO <sub>2</sub>				1.10E+09			
<i>mole fraction</i>				<i>1</i>			
H <sub>2</sub> O	6.91E+07		1.10E+09			1.10E+09	1.10E+09
<i>mole fraction</i>	<i>0.03</i>		<i>0.5</i>			<i>1</i>	<i>1</i>
Cu(OAc) <sub>2</sub>			1.10E+09		1.10E+09		
<i>mole fraction</i>			<i>0.5</i>		<i>1</i>		
<b>MASS (kg)</b>							
AcOH	1.34E+08						
CuCO <sub>3</sub>		2.43E+08					
CO <sub>2</sub>				4.85E+07			
H <sub>2</sub> O			1.98E+7			1.98E+7	1.98E+7
Cu(OAc) <sub>2</sub>			2E+08		2E+08		
TOTAL	1.34E+08	2.43E+08	2.20E+08	4.85E+07	2E+08	1.98E+7	1.98E+7

## 2.5. Heat/energy balance



*Scheme 2.5-1. Simplified scheme of the process.*

### Twin screw reactor heating

*Table 2.5-1. Enthalpies of formation.*

Compound	Enthalpy of formation [kJ mol <sup>-1</sup> ]
Copper carbonate	-595.00
Acetic acid	-484.04
Copper acetate	-836.40
Carbon dioxide	-393.52
Water	-285.83

Enthalpy of the reaction:  $\Delta H = 47.33$  [kJ mol<sup>-1</sup>]

To keep the temperature constant, the heat of reaction must be balanced by the addition of a heat stream.

Total heat required: 5.21E+10 [kJ]

Saturated steam enters the furnace at 4 bar(g) (151.9 °C);

Steam required: 2.47E+04 [t]

### Condenser

The condenser is used to recover heat from evaporated by-products of the reaction. It is assumed that the gaseous phase is 100% mole fraction water. In practice this value would be in the range of 95% - 97% and the rest would consist of acetic acid (3% - 5%). Cooling water enters the heat exchanger at 20 °C and leaves at 50 °C.

Vapour temperature in: 100 °C

Vapour temperature out: 50 °C

The latent heat of evaporation of water: 40.8 [kJ mol<sup>-1</sup>]

Heat available: 4.91E+10 [kJ]

Heat recovered: 3.68E+10 [kJ]

Cooling water required: 2.92E+05 [t]

### Furnace

It is assumed that the liquid phase is 100% mole fraction water. In practice this value would be in the range of 95% - 97% and the rest would consist of acetic acid (3% - 5%). The enthalpy of crystallisation of copper acetate is omitted due to lack of reliable data.

Due to lack of reliable data on the heat capacity of copper acetate and copper carbonate, data for copper chloride is used.

*Table 2.5-2. Heat capacities of products.*

Compound	Heat capacity [kJ mol <sup>-1</sup> K <sup>-1</sup> ]
Copper chloride	0.55
Water	4.20

The specific heat capacity of the slurry is equal to 0.88 [kJ kg<sup>-1</sup> K<sup>-1</sup>]

Energy required: 5.94E+10 [kJ]

Energy delivered: 7.43E+10 [kJ]

Saturated steam enters the furnace at 4 bar(g) (151.9 °C);

Steam required:  $3.52\text{E}+04$  [t]

### **Conveyer belt, reactor, pumps**

Conveyer belt:  $27.80$  [ $\text{t h}^{-1}$ ]

Required power:  $2.96\text{E}+07$  [kJ] (based on ref. 5)

Pump 1:  $15310.37$  [ $\text{kg h}^{-1}$ ] =  $42.53$  [ $\text{l s}^{-1}$ ]

System of 10 pumps can deliver  $44.20$  [ $\text{l s}^{-1}$ ] being at 50% efficiency.

Required power:  $10 \times 67.10$  [W] =  $2.12\text{E}+07$  [kJ]

Pump for the condenser cooling water:  $2.84$  [ $\text{t h}^{-1}$ ] =  $7.89$  [ $\text{l s}^{-1}$ ]

System of 2 pumps can deliver  $8.82$  [ $\text{l s}^{-1}$ ] being at 50% efficiency

Required power:  $2 \times 67.10$  [W] =  $4.42\text{E}+06$  [kJ]

### **Twin-screw reactor**

It is assumed that the reactor requires the same amount of power as the conveyer belt.

Required power:  $2.96\text{E}+07$  [kJ]

## **2.6. Total energy requirement**

$8.48\text{E}+7$  [kJ]

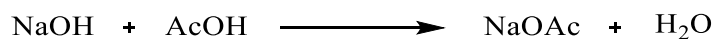
Cooling water:  $2.92\text{E}+05$  [t]

Steam (4 bar(g)):  $3.52\text{E}+04$  [t]

## 3. Sodium acetate

### 3.1. Process description

Formation of sodium acetate is a spontaneous reaction between sodium hydroxide and glacial acetic acid. Reaction proceeds at ambient temperature and pressure and is mildly exothermic.<sup>1</sup>



*Scheme 3.1-1. Formation of sodium acetate from sodium hydroxide and acetic acid.*

Sodium acetate is produced from glacial acetic acid and an aqueous solution of sodium hydroxide (50%). The spontaneous, exothermic liquid phase reaction is conducted with a slight excess of acetic acid to assure full conversion of sodium hydroxide. The purification involves evaporation of water (by-product) and remaining acetic acid (usually no more than 3 mol%). No other by-products are formed.<sup>1</sup>

The reaction occurs at ambient temperature and pressure. As reactor setup, a y-nozzle was selected due to its superior mixing properties. A solution of sodium acetate is passed into a continuous furnace where water evaporates yielding crystals of sodium acetate.

Due to the exothermic nature of the reaction, the nozzle must be cooled down using a stream of cold water. Vapours from the furnace are directed into a condenser.

### 3.2. Process diagram

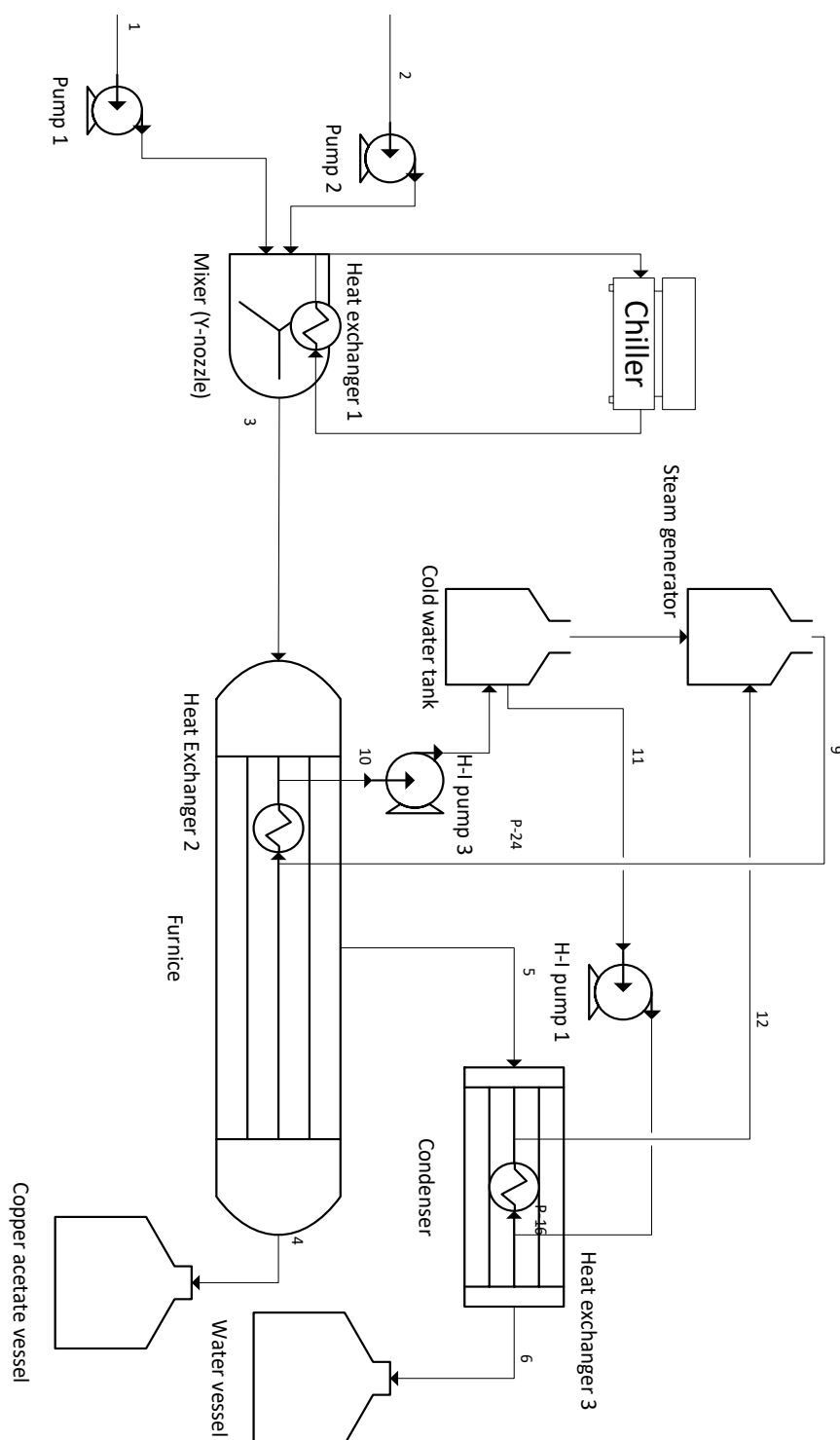


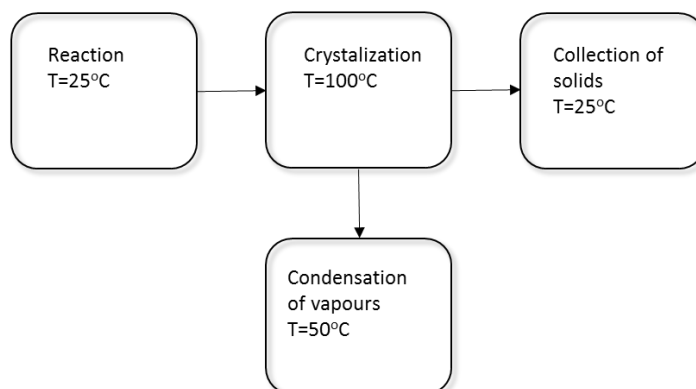
Figure 3.2-1. Process diagram for production of sodium acetate.

### 3.3. Mass balance

Table 3.3-1. Basis: production of 1 000,000,000 kg/annum sodium acetate product.

Stream	1	2	3	4	5	6
Description	AcOH in	NaOH in	Crude out	NaOAc out	steam out	H <sub>2</sub> O out
Pressure (bar)	1	1	1	1	1	1
Temperature (°C)	25	25	25	25	100	100
State	l	l	l	s	v	l
<b>MOLAR (mol)</b>						
AcOH	1.26E+10					
<i>mole fraction</i>	0.97					
NaOH		1.22E+10				
<i>mole fraction</i>		0.5				
H <sub>2</sub> O	3.89E+08	1.22E+10	2.44E+10		2.44E+10	2.44E+10
<i>mole fraction</i>	0.03	0.5	0.66		1	1
NaOAc			1.22E+10	1.22E+10		
<i>mole fraction</i>			0.33	1		
<b>MASS (kg)</b>						
AcOH	7.54E+08					
NaOH		4.88E+08				
H <sub>2</sub> O	7.00E+06		4.39E+08		4.39E+08	4.39E+08
NaOAc			1.00E+09	1.00E+09		
TOTAL	7.54E+08	4.88E+08	1.44E+09	1.00E+09	4.39E+08	4.39E+08

### 3.4. Heat balance



*Scheme 3.4-1. Simplified scheme of the process.*

#### Reactor cooling

*Table 3.4-1. Enthalpies of formation*

Compound	Enthalpy of formation [kJ mol <sup>-1</sup> ]
Sodium hydroxide	-416.88
Acetic acid	-484.04
Sodium acetate	-709.32
Water	-285.83

Enthalpy of the reaction:  $\Delta H = -94.23$  [kJ mol<sup>-1</sup>]

Total cold required:  $1.15\text{E}+12$  [kJ]

Since there is a requirement for a large amount of cooling medium, the heat integration is not sufficient to close the energy balance. Water enters the reactor at 20°C and leaves at 25°C.

Cooling water required:  $5.47\text{E}+07$  [t]

## Furnace

It is assumed that the liquid phase is 100% mole fraction water. In practice this value would be in the range of 95% - 97% and the rest would consist of acetic acid (3% - 5%).

The enthalpy of crystallisation of sodium acetate:  $h_{\text{cryst}}=17.95 \text{ [kJ mol}^{-1}\text{]}$

Saturated steam enters the furnace at 4 bar(g) (151.9 °C);

*Table 3.4-2. Heat capacities of products.*

Compound	Heat capacity [kJ mol <sup>-1</sup> K <sup>-1</sup> ]
Sodium acetate	1.22
Water	4.20

The specific heat capacity of the slurry is equal to 2.13 [kJ kg<sup>-1</sup>K<sup>-1</sup>].

Energy required: 1.44E+12 [kJ]

Energy delivered: 1.81E+12 [kJ]

Steam required: 8.57E+05 [t]

## Condenser

The condenser is used to recover heat from evaporated by-products of the reaction. It is assumed that the gaseous phase is 100% mole fraction water. In practice this value would be in the range of 95% - 97% and the rest would be acetic acid (3% - 5%).

Temperature in: 100 °C

Temperature out: 50 °C

Heat available: 1.09E+12 [kJ]

Heat recovered: 8.16E+11 [kJ]

Cooling water required: 6.48E+06 [t]

## Pumps

Pump 1: 2.24 [l s<sup>-1</sup>]

One pump can deliver 2.84 [l s<sup>-1</sup>] being at 50% efficiency

Required power: 1.41E+06 [kJ]

Pump 2: 2.39 [l s<sup>-1</sup>]

Assumed the same as Pump 1

Required power: 1.41E+06 [kJ]

### **3.5. Total energy requirement**

2.82E+06 [kJ]

Cooling water: 6.12E+07 [t]

Steam (4 bar(g)): 8.57E+05 [t]

## 4. 1,4-benzoquinone

### 4.1. Introduction

1,4-Benzoquinone,  $C_6H_4O_2$ , Mr 108.10, mp 113 °C, is soluble in most oxygenated organic solvents (ethers, alcohols, acetone), and hot ligroin, slightly soluble in petroleum ether, and insoluble in water. Crystallisation from alcohols or sublimation produces yellow monoclinic prisms.<sup>1</sup>

Applications of p-benzoquinone:<sup>6</sup>

1. Inhibition of polymerisation
2. Determination of amino acids
3. An additive in adhesive mixtures
4. Oxidative syntheses
5. Bactericidal substances

The list of main manufacturers of copper (II) acetate includes:

1. Sigma-Aldrich
2. Aladdin
3. Alfa Aesar

Based on a market research, the estimate of the maximum capacity of a single plant for p-benzoquinone is in the range of 1000 tonnes per annum.

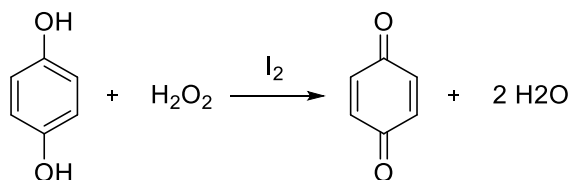
1,4-benzoquinone is produced industrially by following chemical reactions:<sup>2</sup>

1. Oxidation of aniline
2. Oxidation of phenol
3. Oxidation of glucose

The first two options include a two-step oxidation. Firstly, hydroquinone is formed, and upon a second oxidation step, p-benzoquinone is obtained. The oxidation can be performed

using hydrogen peroxide and iodine as a catalyst. The process can be performed in batch on a 1 t scale.<sup>1</sup>

## 4.2. Process description



*Scheme 4.2-1. Formation of benzoquinone upon oxidation of hydroquinone.*

In the course of the process, hydroquinone is dissolved in isopropyl alcohol, and iodine is added to the mixture. Upon vigorous stirring, an aqueous solution of hydrogen peroxide (35%) is added over 3 hours. The temperature is kept at 35 °C. Upon completion of the addition, the temperature is raised to 45 °C, and the mixture is stirred for additional 3 hours. After completion of the reaction, the mixture is transported into a crystallisation vessel and cooled down to 15 °C. The liquid phase is evaporated at 100 °C and reused for next batches; crystals of 1,4-benzoquinone are collected. The yield of the reaction is 91.6%, and the purity of the product is >99%.<sup>7</sup>

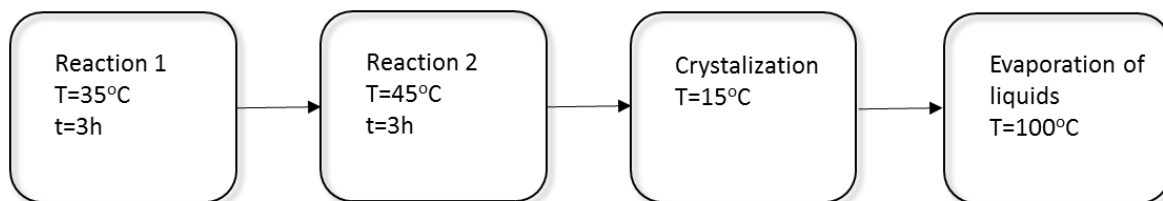
The reaction is highly exothermic and requires efficient cooling.

### 4.3. Mass balance

Table 4.3-1. Basis: production of 1000 kg *p*-benzoquinone product.

Stream	Reaction			Crystallisation		Drying		
Description	Reaction mix	H <sub>2</sub> O <sub>2</sub> in	Crude out	Liquid out	Solid out	Vapour out	Solid out	Cond.
Pressure (bar)	1	1	1	1	1	1	1	1
Temperature (°C)	35	25	45	15	15	100	100	50
State	l	l	l	v	s	v	l	l
<b>MOLAR (mol)</b>								
hydroquinone	5.49E+03							
<i>mole fraction</i>	0.3							
isopropanol	1.04E+04		1.04E+04	9.91E+03	521.47	521.47		521.47
<i>mole fraction</i>	0.66		0.28		0.07	0.33		0.33
iodine	1.65E+02		1.65E+02	1.56E+02				
<i>mole fraction</i>	0.03		0.004					
H <sub>2</sub> O		1.10E+04	2.20E+04		1097.82	1097.82		1097.82
<i>mole fraction</i>		0.35	0.58		0.16	0.67		0.67
H <sub>2</sub> O <sub>2</sub>		7.14E+03		2.09E+04				
<i>mole fraction</i>		0.65						
<i>p</i> -benzoquinone			5.03E+03		5.03E+03		5.03E+03	
<i>mole fraction</i>			0.13		0.75		1	
<b>MASS (kg)</b>								
hydroquinone	1213.73							
isopropanol	626.80		626.80	595.46	31.34	31.34		31.34
iodine	20.90		20.90	19.85				
H <sub>2</sub> O		197.61	395.22	375.46	19.76	19.76		19.76
H <sub>2</sub> O <sub>2</sub>		242.62						
<i>p</i> -benzoquinone			913.24		913.24		913.24	
TOTAL	1861.43	440.23	1956.16	990.77	964.34	51.10	913.24	51.10

## 4.4. Heat/energy balance



*Scheme 4.4-1. Simplified scheme of the process.*

### Reaction 1

#### Heating of the reaction mixture to from 20 °C to 35 °C

*Table 4.4-1. Heat capacities of substrates.*

Compound	Heat capacity [kJ mol <sup>-1</sup> K <sup>-1</sup> ]
Hydroquinone	1.20
Isopropanol	2.68

The specific heat capacity of the mixture is equal to 1.70 [kJ kg<sup>-1</sup>K<sup>-1</sup>].

Saturated steam enters the heat exchanger at 4 bar(g) (151.9 °C);

Assuming 15% heat losses per hour the heat required to maintain the temperature:

Energy required: 6.88E+4 [kJ]

Steam required: 0.032 [t]

### Reaction 2

#### Heating of the reaction mixture to from 35 °C to 45 °C

*Table 4.4-2. Heat capacities of substrates.*

Compound	Heat capacity [kJ mol <sup>-1</sup> K <sup>-1</sup> ]
Hydroquinone	1.20
Isopropanol	2.68
Hydrogen peroxide	2.63
Water	4.20

The specific heat capacity of the mixture is equal to 2.02 [kJ kg<sup>-1</sup>K<sup>-1</sup>].

Saturated steam enters the furnace at 4 bar(g) (151.9 °C);

Assuming 15% heat losses per hour, the heat required to maintain the temperature:

Energy required: 5.41E+4 [kJ]

Steam required: 0.026 [t]

### **Cooling of the reactor during reaction 2**

*Table 4.4-3. Enthalpies of formation of substrates.*

Compound	Enthalpy of formation [kJ mol <sup>-1</sup> ]
Hydroquinone	-371.10
Hydrogen peroxide	-187.34
Benzoquinone	-186.80
Water	-285.83

Enthalpy of the reaction:  $\Delta H = 200.019$  [kJ mol<sup>-1</sup>]

Heat required: -1.01E+06 [kJ]

Heat supplied: -1.26E+06 [kJ]

Cooling water required: 19.95 [t]

### **Crystallisation**

**Cooling of the reaction mixture to from 45 °C to 15 °C**

Water at 5 °C is used to cool down the reactor.

The specific heat capacity of the mixture is equal to 1.99 [kJ kg<sup>-1</sup>K<sup>-1</sup>].

Due to lack of reliable data, the enthalpy of crystallisation is omitted.

Energy required: 4.07E+04 [kJ]

Energy delivered: 5.08E+04 [kJ]

Cold water required: 1.21 [t]

### **Evaporation of liquids at 100 °C**

Saturated steam enters the furnace at 4 bar(g) (151.9 °C);

The specific heat capacity of the mixture is equal to 1.99 [kJ kg<sup>-1</sup>K<sup>-1</sup>].

Energy required: 3.31E+5 [kJ]

Energy delivered: 4.14E+5 [kJ]

Steam required: 0.20 [t]

### **Condensation at 50 °C**

Heat capacity of water: 4.20 [kJ kg<sup>-1</sup> K<sup>-1</sup>]

Heat capacity of isopropanol: 2.68 [kJ kg<sup>-1</sup> K<sup>-1</sup>]

Heat available: 1.42E+06 [kJ]

Heat recovered: 1.06E+06 [kJ]

Cold water required: 8.44 [t]

### **Reactor mixing**

Motor power: 1.18 kW

Energy required for a 6-hour batch: 2.55E+4 [kJ]

### **Crystallisation vessel mixing**

Assumed the same as reactor mixing.

Energy required for 1 batch: 2.55E+4 [kJ]

## 4.5. Total energy requirement

5.10E+4 [kJ]

Cooling water (20 °C) required: 28.38 [t]

Cooling water (5 °C) required: 1.21 [t]

Steam (4 bar(g)) required: 0.258 [t]

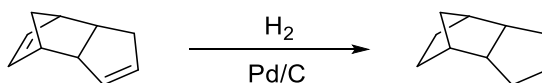
## 5. 1-adamantane carboxylic acid

### 5.1. Summary

The selected process of 1-adamantane carboxylic acid synthesis is a 3-stage reaction. The first part involves reduction of dicyclopentadiene over palladium on carbon catalyst using hydrogen.<sup>8</sup> The second part involves reaction catalyzed by aluminium chloride and yields in adamantane.<sup>9</sup> Finally, adamantane is carboxylated to 1-adamantane carboxylic acid using formic acid, sulfuric acid and t-butanol.<sup>10</sup> Alternatively, adamantane can be extracted from crude oil however, the content of adamantane in crude oil varies depending on its source between 0.03 – 0.0001% making it economically not viable to use this source.

### 5.2. Reduction of dicyclopentadiene

Dicyclopentadiene is reduced to tetrahydrodicyclopentadiene in a batch process conducted under relatively mild conditions; T=25 °C, p=10 bar(g), t=60 min. The process requires low catalyst loading 1 mass%, 2 wt% palladium/charcoal. The reaction is neat, i.e. no solvent is required, and the yield is quantitative (95% yield is assumed).<sup>8</sup> The reaction mixture is filtered to separate the catalyst and used crude in next operations. Based on a market research, the estimate of the maximum capacity of a single plant for tetrahydrodicyclopentadiene is in the range of 1 t per annum.



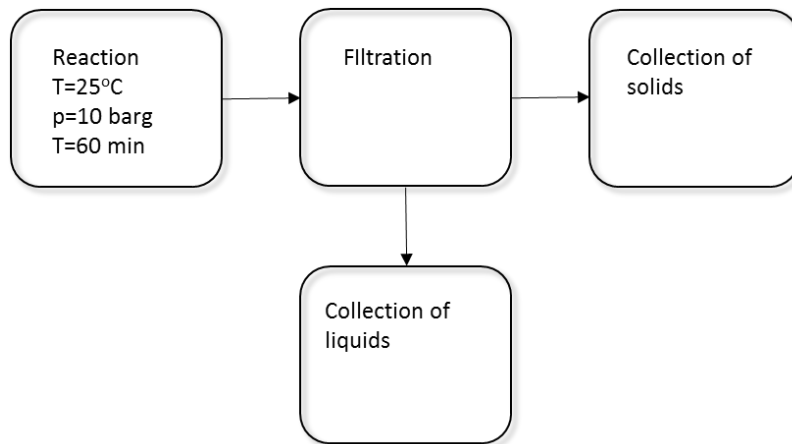
*Scheme 5.2-1. Reduction of dicyclopentadiene.*

### 5.2.1. Mass balance

Table 5.2-1. Basis: production of one batch, i.e. 1000 kg tetrahydrodicyclopentadiene product.

Stream Description	Reaction		Filtration	
	Reaction mix	Reaction out	Solid out	Liquid out
Pressure (bar)	10	1	1	1
Temperature (°C)	25	25	25	25
State	l/s	l/s	s	l
<b>MOLAR (mol)</b>				
dicyclopentadiene	7726.42	386.32		386.32
<i>mole fraction</i>	<i>0.33</i>			
Pd/C	77		77	
<i>mole fraction</i>	<i>0.01</i>		<i>1</i>	
hydrogen	15452.83			
<i>mole fraction</i>	<i>0.66</i>			
tetrahydrodicyclopentadiene		7340.096		7340.096
<i>mole fraction</i>		<i>1</i>		<i>1</i>
<b>MASS (kg)</b>				
dicyclopentadiene	1021.43	51.07		51.07
Pd/C	10	10	10	
hydrogen	30.91			
tetrahydrodicyclopentadiene		1000		1000
<b>TOTAL</b>	1062.34	1010	10	1000

### 5.2.2. Heat/energy balance



*Scheme 5.2-2. Simplified scheme of the process.*

#### Heating of the reactor during the reaction:

*Table 5.2-2. Enthalpies of formation.*

Compound	Enthalpy of formation [kJ mol <sup>-1</sup> ]
Dicyclopentadiene	-177.52
Hydrogen	0
Tetrahydrodicyclopentadiene	-113.10

Enthalpy of the reaction:  $\Delta H = 64.24$  [kJ mol<sup>-1</sup>]

Heat required:  $4.73E+05$  [kJ]

Saturated steam enters the furnace at 4 bar(g) (151.9 °C).

Steam required: 0.28 [t]

#### Compressor

Based on [http://www.engineeringtoolbox.com/horsepower-compressed-air-d\\_1363.html](http://www.engineeringtoolbox.com/horsepower-compressed-air-d_1363.html)

Compression of 30.91 kg of hydrogen from 0 bar(g) to 10 bar(g)

Energy required: 1.14E+05 kJ

**Filtration**

Neglected

**Reactor mixing**

Motor power: 0.58 kW

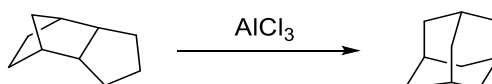
Energy required for a 1-hour batch: 2.088E+4 [kJ]**5.2.3. Total energy requirement**

1.35E+05 [kJ]

Steam (4 bar) required: 0.28[t]

**5.3. Synthesis of adamantane**

Adamantane can be prepared by refluxing (185 °C) tetrahydrodicyclopentadiene with aluminium chloride (1 mol%) over 12 hours.<sup>9</sup> The reaction is followed by distillation. The recovered from the light fraction substrate is recycled. The product (adamantane) is crystallised from the heavy fraction by lowering the temperature to 25 °C giving 10% yield of adamantane.



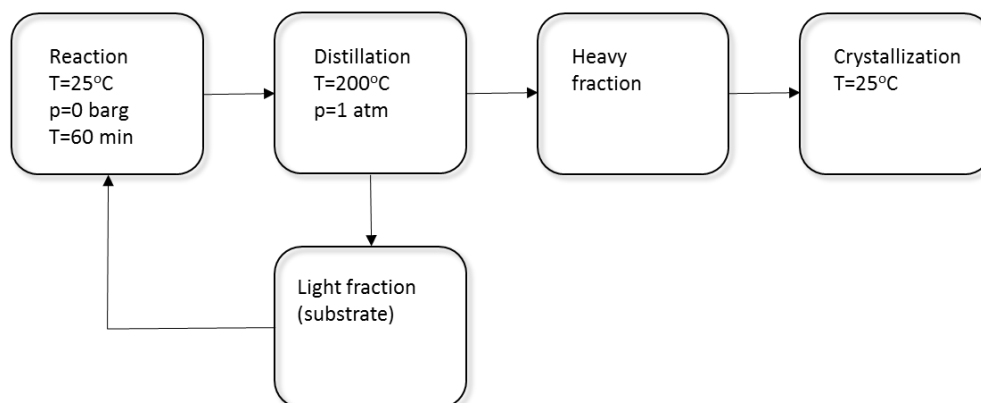
*Scheme 5.3-1. Synthesis of adamantane.*

### 5.3.1. Mass balance

Table 5.3-1. Basis: production of 8499 kg/annum tetrahydrodicyclopentadiene product.

Stream	Reaction		Distillation	
	Reaction mix	Reaction out	Liquid light	Liquid heavy
Pressure (bar)	1	1	1	1
Temperature (°C)	182	25	200	25
State	l/s	l/s	s	L
<b>MOLAR (mol)</b>				
tetrahydrodicyclopentadiene	73399.88	62389.91	62389.91	
<i>mole fraction</i>	<i>0.99</i>	<i>0.79</i>	<i>0.94</i>	
AlCl <sub>3</sub>	73.4	73.4	73.4	
<i>mole fraction</i>	<i>0.01</i>	<i>0.01</i>	<i>0.0001</i>	
adamantane		11009.97	3669.99	7339.98
<i>mole fraction</i>		<i>0.1</i>	<i>0.055</i>	<i>1</i>
<b>MASS (kg)</b>				
tetrahydrodicyclopentadiene	9999.85	8499	8499	
AlCl <sub>3</sub>	97.87	97.87	97.87	
adamantane		1500	500	1000
<b>TOTAL</b>	<b>1062.34</b>	<b>1010</b>	<b>10</b>	<b>1000</b>

### 5.3.2. Heat/energy balance



*Scheme 5.3-2. Simplified scheme of the process.*

#### Heating of the reaction mixture from 25 °C to 185 °C.

Heat capacity of the mixture is assumed to be equal to the heat capacity of the substrate, i.e. 1.26 [kJ kg<sup>-1</sup>K<sup>-1</sup>]

Enthalpy of vaporisation: 46.00 [kJ mol<sup>-1</sup>]

Heat required to preheat the mixture: 2.46E+07 [kJ]

The heat required to maintain the temperature:

Assuming 15% loss per hour.

In total: 6.88E+07 [kJ]

Saturated steam enters the furnace at 15 bar(g) (198.28 °C).

Steam required: 35.36 [t]

#### Condenser

Due to temperatures close to a boiling point of the substrate, a condenser of gaseous phase is required. Due to lack of information regarding the liquid/gas equilibrium, a mass flow rate of cold water is assumed to be 1 [t h<sup>-1</sup>].

Total cold water consumption: 12 [t].

#### Reactor mixing

Motor power: 0.58 kW

Energy required for a 12-hour batch: 2.51E+5 [kJ]

### **Flash Distillation**

The light fraction (contains substrate and by-products) is evaporated at 200 °C.

Energy required: 2.00E+06 [kJ]

Energy delivered: 4.01E+06 [kJ]

Saturated steam enters the heat exchanger at 20 bar(g) (212.37 °C).

Steam required: 2.12 [t]

The heavy fraction is cooled down to room temperature and filtered – the energy required neglected.

### **5.3.3. Total energy requirement**

2.51E+5 [kJ]

Steam required (20 bar): 2.12 [t]

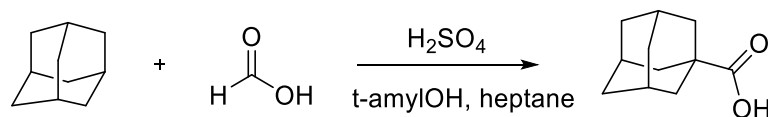
Steam required (15 bar): 35.36 [t]

Cold water: 12 [t].

### **5.4. Reaction to 1-adamantane carboxylic acid.**

1-Adamantanecarboxylic acid can be prepared by carboxylation of 1-adamantanol or 1-bromoadamantane with formic acid and 96% sulfuric acid; by carboxylation of adamantane with formic acid, t-butyl alcohol, and 96% sulfuric acid; and by carboxylation of adamantane with formic acid and oleum.<sup>10</sup>

The mildest and highest yielding reaction was chosen, i.e. the carboxylation of adamantane by formic acid, t-butyl alcohol, and 96% sulfuric acid.<sup>10</sup>



*Scheme 5.4-1. 1-adamantane carboxylic acid synthesis.*

A slight modification to the procedure was made. Instead of carbon tetrachloride, heptane was used; the change of the solvent should not change the yield.<sup>10</sup> The change was due to the high toxicity of the originally reported solvents. Additionally, ammonium bicarbonate was used instead of ammonium hydroxide.

The reaction is mildly exothermic  $\Delta H = -79.4 \text{ kJ mol}^{-1}$  and proceeds in the liquid phase. A mixture of sulfuric acid, heptane and adamantane is prepared at room temperature (20 – 25 °C) and stirred. Formic acid is added to the mixture, and tert-butyl alcohol is pumped in over 3 hours. Upon completion, the reaction mixture is stirred for 1 hour and cooled down to 0 °C. Following this, water is added. The organic phase is extracted using ethyl acetate, and combined organic fractions are mixed with ammonium bicarbonate, stirred, filtered and washed with acetone.

The obtained crystals are suspended in water, and hydrochloric acid is added to break the salt. An extraction using ethyl acetate is performed; the organic phase is dried using anhydrite (calcium sulfate).

After the solvent evaporation, crude 1-adamantane carboxylic acid is obtained in 95% purity and 70% yield.

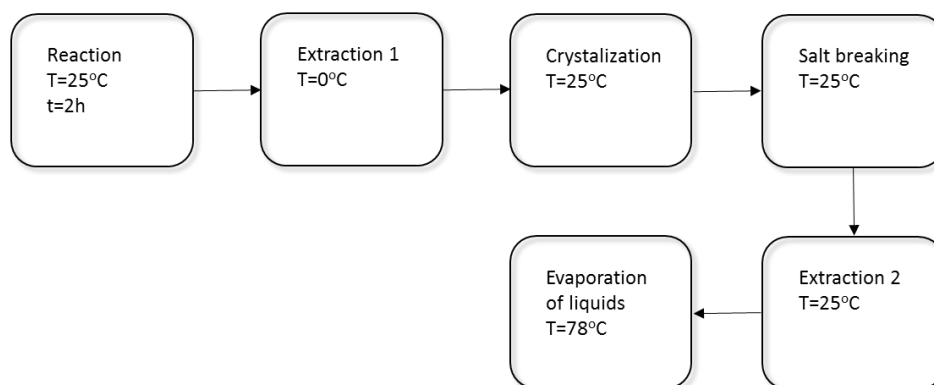
### 5.4.1. Mass balance

Table 5.4-1. Basis: production of 794 kg/annum 1-adamantanecarboxylic acid product.

Stream	Reaction		Extraction		Salt formation		Salt breaking		Extraction	
Description	Reaction mix	Reaction out	Liquid light	Liquid heavy	Liquid in	Crystals out	Crystals and liquids in	Liquids out	Liquid light	Liquid heavy
Pressure (bar)	1	1	1	1	1	1	1	1	1	1
Temperature (°C)	25	25	5	25	25	25	25	25	25	25
State	1	1	1	1	1	1				
<b>MOLAR (mol)</b>										
Adamantane	7.34E+03	2.94E+03	2.94E+03		2.94E+03					
Formic acid	8.81E+04	8.37E+04		8.37E+04						
Sulfuric acid	3.52E+05	3.52E+05		3.52E+05						
Tert-butyl alcohol	2.94E+04	2.94E+04		2.94E+04						
Heptane	4.79E+04	4.79E+04	4.79E+04		4.79E+04					
Ethyl acetate			3.00E+05		3.00E+05				3.00E+05	
Ammonium bicarbonate					4.40E+04					
Water				1.00E+05			6.66E+04	6.66E+04		6.66E+04
Hydrochloric acid (30%)							2.20E+04	1.70E+04		1.70E+04
Ammonium chloride								4.40E+03		4.40E+03
1-adamantanecarboxylic acid		4.40E+03	4.40E+03		4.40E+03			4.40E+03	4.40E+03	
Acetone					10					
1-adamantanecarboxylic acid ammonia salt						4.40E+03	4.40E+03			

Stream	Reaction		Extraction		Salt formation			Salt breaking		Extraction		
	Description	Reaction mix	Reaction out	Liquid light	Liquid heavy	Liquid in	Crystals out	Liquids out	Crystals and liquids in	Liquids out	Liquid light	Liquid heavy
Pressure (bar)	1	1	1	1	1	1	1	1	1	1	1	1
Temperature (°C)	25	25	25	5	25	25	25	25	25	25	25	25
State	1	1	1	1	1	s	1	1				
Mass (kg)												
Adamantane	1.00E+03	4.00E+02	4.00E+02		4.00E+02		4.00E+02					
Formic acid	4.05E+03	3.85E+03										
Sulfuric acid	3.46E+04	3.46E+04										
Tert-butyl alcohol	2.59E+03	2.59E+03										
Heptane	4.80E+03	4.80E+03			4.80E+03		4.80E+03					
Ethyl acetate					2.64E+04		2.64E+04				2.64E+04	
Ammonium bicarbonate					3.45E+03		3.13E+03					
Water					1.80E+02				1.00E+02	1.00E+02		1.00E+02
Hydrochloric acid (30%)									7.92E+02	6.12E+02		6.12E+02
Ammonia chloride									2.29E+02	7.94E+02		2.29E+02
1adamantane-carboxylic acid		7.94E+02		7.94E+02						7.94E+02		
Acetone					0.58			0.58				
				1							1	
1-adamantane-carboxylic acid ammonia salt						8.68E+02			8.68E+02			

### 5.4.2. Heat/energy balance



*Scheme 5.4-2. Schematic process diagram.*

Since the reaction is conducted at room temperature and is only slightly exothermic, cooling water can be neglected.

**The first extraction is conducted at 0 °C.**

*Table 5.4-2. Heat capacities.*

Compound	Heat capacity [kJ kg <sup>-1</sup> mol <sup>-1</sup> ]
Adamantane	1.29
Sulfuric acid	1.34
Tert-butanol	2.97
Formic acid	2.19
Heptane	2.24

The specific heat capacity of the mixture:

Specific heat capacity: 1.59 [kJ kg<sup>-1</sup>K<sup>-1</sup>]

Energy required: 1.87E+06 [kJ]

Assuming that an industrial chiller is used (50% efficiency)

Energy required: 3.57E+06 [kJ]

**Mixing**

Following parts of the process require efficient mixing: reaction, salt formation, salt breaking and extractions.

Assuming the same power for every part of the process, and that in total 6 hours of motor power is used.

Motor power: 0.58 kW

Energy required for 6 hours of operation: 1.26E+5 [kJ]

**Solvent evaporation.**

Saturated steam enters the heat exchanger at 4 bar(g) (151.9 °C) assuming that the specific heat capacity is equal to 1.91 [kJ kg<sup>-1</sup>K<sup>-1</sup>], i.e. the heat capacity of ethyl acetate.

Energy required: 1.71E+07 [kJ]

Steam required: 8.12 [t]

**5.4.3. Total energy requirement**

3.70E+06 [kJ]

Steam required (4 bar): 8.12 [t]

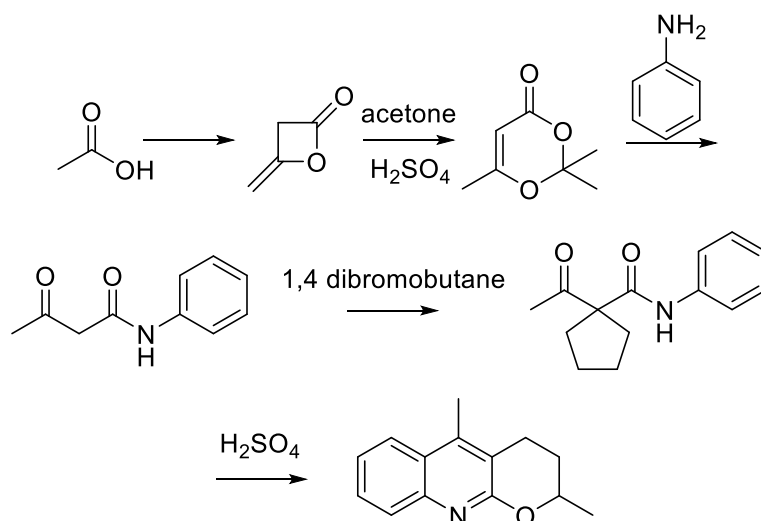
## 6. Li-quinoline

### (3,4-Dihydro-2,5-dimethyl-2H-pyrano[2,3-b]quinoline)

#### 6.1. Overview of the process

Due to the lack of reliable data on the industrial scale production of Li-quinoline and its very small scale synthesis (commercially available only on the 1g scale), production is based on laboratory scale procedures and larger scale syntheses of diketene and dioxinone.

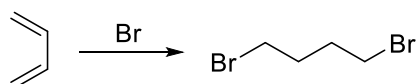
The first step involves condensation of acetic acid to diketene, which reacts with acetone to form dioxinone.<sup>11</sup> Both reactions occur at high temperatures. Following that, 3-oxo-*N*-phenylbutanamide is formed upon a reaction between dioxinone and aniline.<sup>12</sup> Next, 3-oxo-*N*-phenylbutanamide reacts with 1,4-dibromobutane giving 1-acetyl-*N*-phenylcyclopentane-1-carboxamide.<sup>13</sup> Finally, in highly acidic conditions, Li-quinoline (3,4-Dihydro-2,5-dimethyl-2H-pyrano[2,3-b]quinoline) is formed upon condensation.<sup>13</sup>



Scheme 6.1-1. Synthesis of Li-quinoline.

## 6.2. Synthesis of 1,4-dibromobutane.

The synthesis involves a reaction between butadiene and bromine and subsequent hydrogenation over palladium on charcoal 2 wt%.<sup>14</sup>



*Scheme 6.2-1. Synthesis of 1,4-dibromobutane from butadiene.*

Prior to entering the reactor, all streams, i.e. butadiene, bromine and heptane, are cooled down to -5 °C. Upon mixing the reactants enter the reactor, and the temperature is kept constant at -5 °C. After exiting the reactor, the streams are passed through a heat exchanger, where the temperature is raised to 20 °C at which the residual butadiene (approximately 12% of the initial amount) and bromine (approximately 20% of the initial amount) evaporates and is recycled back to the start of the process. The rest of the stream is passed through another heat exchanger where the solution is heated up to 95 °C, at which the isomerisation of dibromobutenes occurs. The mixture of 1,2- and 1,4-dibromobutene (assumed 1:2 ratio) is converted into a mixture consisting of 75% of 1,4 isomer and 25% 1,2 isomer and, at the same time, solvent, i.e. heptane evaporates. Isomers are separated upon crystallisation at 50 °C at which the isomer 1,4 is solid, whereas the isomer 1,2 remains in the liquid state. Separation takes place in a centrifuge.

In the second step, 1,2-dibromobutene is hydrogenated at 50 °C using platinum on carbon as a catalyst and water and ammonia as a solvent. According to the patent used, the yield is quantitative, and reaction requires only filtration and extraction using ethyl acetate as a purification procedure. Used ethyl acetate is evaporated and recycled.

### 6.2.1. Process diagram

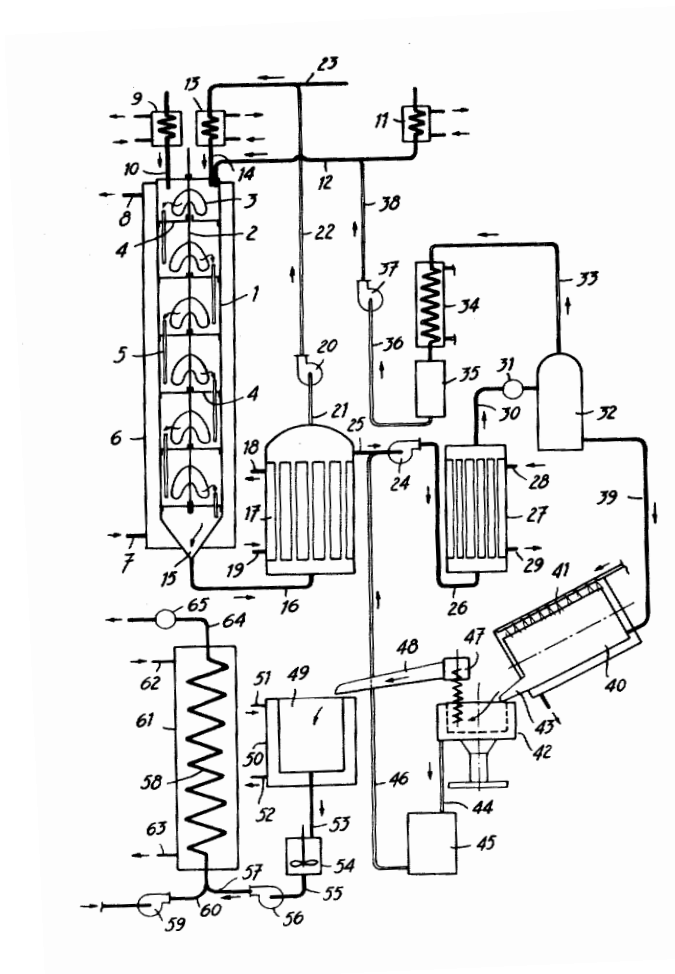


Figure 6.2-1. Synthesis of 1,4-dibromobutane from butadiene. Reproduced from ref. 14.

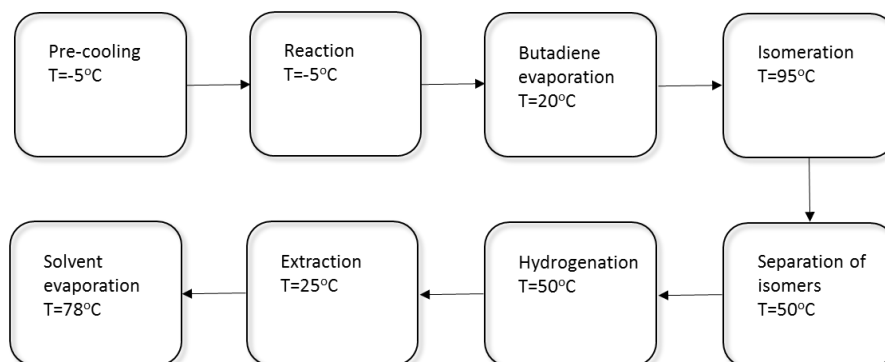
Table 6.2-1. Basis: production of 10,000,000 kg/annum 1,4-dibromobutane product.

### 6.2.2. Mass balance

Stream	Reaction		Butadiene evaporation				Isomers separation			Hydrogenation		Distillation		
	Reaction mix	Reaction out	Liquid in	Gas out	Liquid out	Liquid in	Solid out	Liquid out	Liquid in	Liquid out	Light in	Light liquid	Heavy liquid	
Pressure (bar)	1	1	1	1	25	1	1	1	1	1				
Temperature (°C)	-5	-5	25	25	25	50	50	50	50	50				
State	l	l	l	g	l	l	s	l	l	l				
<b>MOLAR (mol)</b>														
Butadiene	9.49E+07	1.16E+07	1.16E+07	1.16E+07										
Heptane	9.26E+07	9.26E+07	9.26E+07		9.26E+07	9.26E+07		9.26E+07						
Bromine	8.80E+07	1.85E+07	1.85E+07	1.85E+07										
1,4-dibromobutene		4.63E+07	4.63E+07		4.63E+07	4.63E+07	4.63E+07		4.63E+07					
1,2-dibromobutene		2.32E+07	2.32E+07		2.32E+07	2.32E+07		2.32E+07						
1,4-dibromobutane									4.63E+07	4.63E+07	4.63E+07	4.63E+07		
Ammonia									1.00E+08	1.00E+08	1.00E+08	1.00E+08		
Water									3.00E+08	3.00E+08	3.00E+08	3.00E+08		
Hydrogen									8.00E+07					
Ethyl acetate												3.00E+08		
Pv/C									4.63E+03		4.63E+03		4.63E+03	

Stream	Reaction		Butadiene evaporation				Isomers separation				Hydrogenation		Extraction	
	Description	Reaction mix	Reaction out	Liquid in	Gas out	Light in	Light in	Light in	Liquid out	Liquid /gas in	Liquid out	Light in	Light liquid	Heavy liquid
Pressure (bar)	1	1	1	1	1	1	1	1	1	1				
Temperature (°C)	-5	5	25	25	25	50	50	50	50	50				
State	1	1	1	g	1	1	s	1	1	1				
MASS (kg)														
Butadiene	4.38E+06	6.26E+05	6.26E+05	6.26E+05										
Heptane	6.96E+06	6.96E+06	6.96E+06	6.96E+06	6.96E+06	6.96E+06		6.96E+06						
Bromine	5.28E+06	1.11E+06	1.11E+06	1.11E+06	1.11E+06									
1,4-dibromobutene	9.91E+06	9.91E+06	9.91E+06	9.91E+06	9.91E+06	9.91E+06	9.91E+06	9.91E+06	9.91E+06					
1,2-dibromobutene	4.95E+06	4.95E+06	4.95E+06	4.95E+06	4.95E+06	4.95E+06	4.95E+06	4.95E+06						
1,4-dibromobutane													1.00E+07	
Ammonia										1.00E+07	1.00E+07			
Water										1.36E+06	1.36E+06	1.36E+06	1.36E+06	
Hydrogen										5.40E+06	5.40E+06	5.40E+06	5.40E+06	
Ethyl acetate										1.02E+05				2.64E+07
Pv/C										902.85	902.85	902.85	902.85	902.85

### 6.2.3. Heat/energy balance



Scheme 6.2-2. Simplified scheme of the process.

#### Cooling of the substrates to -5 °C.

Energy required to cool down butadiene: 1.79E+05[kJ]

Energy required to cool down heptane: 2.78E+05[kJ]

Energy required to cool down bromine: 2.00E+05[kJ]

Assuming an industrial chiller is used and 50% efficiency

Total energy required: 1.31E+09 [kJ]

#### Cooling of the reactor

Neglecting heat of the reaction ( $\Delta H = -7.91 \text{ kJ mol}^{-1}$ ) and assuming 15% heat loss from the reactor:

Energy required for cooling down the reactor: 1.97E+08 [kJ]

#### Heating to 20 °C to evaporate butadiene

Energy required to heat dibromobutenes: 2.32E+08 [kJ]

Energy required to heat heptane: 2.48E+08 [kJ]

Energy required to heat butadiene (accounting for the enthalpy of evaporation): 2.83E+08 [kJ]

Total: 7.63E+08 [kJ]

Total water (25 °C) consumption: 9.09E+03 [t].

**Heating to 95 °C – isomerisation**

The heat of reaction is neglected. Heptane is evaporated during the same process. Thus heat of evaporation is added.

Total energy required: 3.68E+09 [kJ]

Total energy delivered: 4.91E+09 [kJ]

Saturated steam enters the furnace at 4 bar(g) (151.9 °C)

Steam required: 2.33E+03 [t]

**Cooling down to 50 °C – separation of the isomers**

The heat of solidification is neglected.

Total energy required: 4.17E+08 [kJ]

Total energy delivered: 5.56E+08 [kJ]

Total cold water (25 °C) consumption: 5.29E+03 [t].

**Hydrogenation**

It is assumed that the reaction mixture leaves the reactor at 50 °C – i.e. heat of reaction compensates for the heat losses from the reactor.

**Evaporation of ethyl acetate after extraction**

Total energy required: 1.43E+09 [kJ]

Total energy delivered: 1.90E+09 [kJ]

Saturated steam enters the furnace at 4 bar(g) (151.9 °C)

Steam required: 9.03E+02 [t]

**Mixing**

Neglected.

**Pumps**

The process requires 7 pumps. Assuming the same energy requirement for all of them:

Power required for one pump: 1.41E+06 [kJ]

Total power requirement: 9.87E+06 [kJ]

## 6.2.4. Total energy requirement

1.51E+09 [kJ]

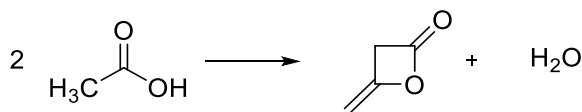
Steam required (4 bar(g)): 3.23E+03 [t]

Cold water required: 1.44E+04 [t]

## 6.3. Diketene

### 6.3.1. Introduction

Diketene can be produced upon dimerisation of ketene with yields up to 85%. The remaining 15% is made up of higher ketene oligomers and 3 – 4% acetic anhydride. Crude diketene is a mobile, dark brown liquid due to contamination with 8 – 10% of higher polymers. Diketene of >99.5 % purity can be obtained by distillation. Pure diketene (99.99 %) can be obtained by crystallisation. Diketene is generally consumed at the site of production, because of its extreme reactivity and hazardous properties.<sup>11</sup>



*Scheme 6.3-1. Synthesis of diketene*

### 6.3.2. Process description

The feed stream of acetic acid vapour is generated by passing argon through a glass bubbler maintained at approximately 40 °C filled with glacial acetic acid. The stream is then passed to the top of a vertical hollow quartz tube. At the lower part of the quartz tube (5 cm from the bottom), the removable silica foam monolith disk with 45 pores per inch, 20 mm diameter and 0.1 cm thickness is placed. The disk is supported inside of the reactor by a built-in quartz frit, and temperature of the disk is measured with an external thermocouple placed in a glass pocket located under the frit. The quartz tube is placed in a cylindrical furnace where the temperature is controlled with a PID controller and is set to 500 °C. The ketene formed in the quartz tube is passed through a condenser cooled with cold water (bearing a collector attached at the bottom receiver for liquid condensate) followed by three cylindrical gas traps connected in series filled with acetone and immersed in a dry ice/acetone baths (-72 °C). At the end of the line, the fourth glass trap filled up with acetone kept at room temperature with the outlet tube placed into the hood's exhausting vent is installed. After evaporation of acetone from traps, a yellowish liquid was obtained. It consisted of 75% diketene, 16% acetic anhydride and 5% acetic acid. Diketene was further distilled to yield 99.5% pure liquid.<sup>11</sup>

### 6.3.3. Process diagram

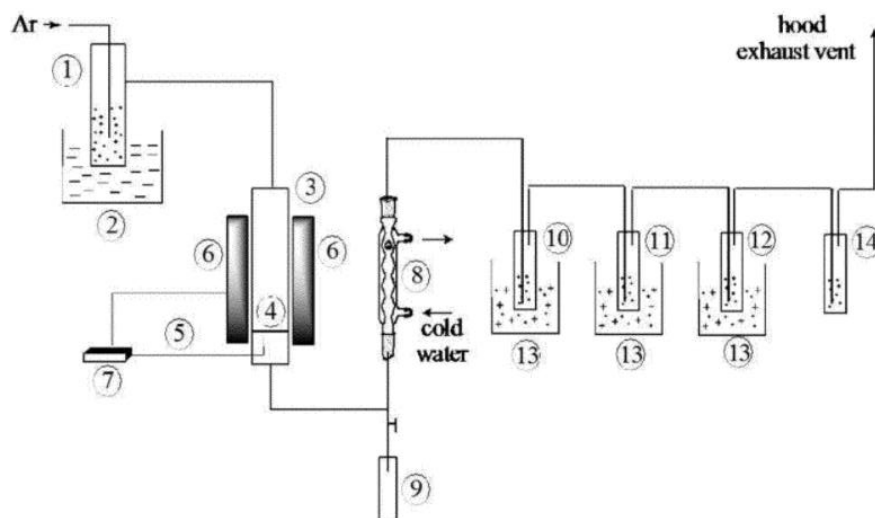


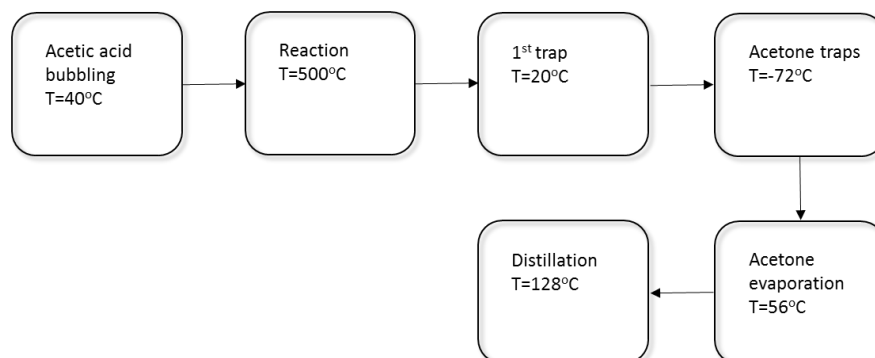
Figure 6.3-1. Process diagram of synthesis of diketene. Reproduced from ref. 11.

### 6.3.4. Mass balance

Table 6.3-1. Basis: production of 1 000,000,000 kg/annum diketene product.

Stream	1	2	3	Extraction			Distillation	
Description	AcOH in	Argon in	Crude out	Gas in	Liquid out	Gas out	Wastes	Product
Pressure (bar)	1	1	1	1	1	1	1	1
Temperature (°C)	25	25	500	500	-75	-75	56	56
State	l	g	g	g	L	g	v	v
<b>MOLAR (mol)</b>								
AcOH	3.17E+10		2.34E+09	2.34E+09				
Argon		-	-	-		-		
Diketene			1.19E+10	1.19E+10	1.19E+10			1.19E+10
Higher polymers			3.19E+09	3.19E+09	3.19E+09		3.19E+09	
Acetone					1.19E+12		1.19E+12	
Acetic anhydride			8.07E+08	8.07E+08	8.07E+08		8.07E+08	
Water			1.33E+10	1.33E+10	1.33E+10		1.33E+10	
<b>MASS (kg)</b>								
AcOH	2.55E+09							
Argon [m <sup>3</sup> ]		3.18E+12				3.18E+12		
Diketene			1.00E+09	1.00E+09	1.00E+09			1.00E+09
Higher polymers			-	-	-		-	
Acetone					6.91E+10		6.91E+10	
Acetic anhydride			8.24E+07	8.24E+07	8.24E+07		8.24E+07	
Water			2.40E+08	2.40E+08	2.40E+08		2.40E+08	
TOTAL	2.55E+09	3.18E+12	1.32E+09	1.32E+09	7.01E+10	3.18E+12		

### 6.3.5. Heat/energy balance



*Scheme 6.3-2. Simplified scheme of the process.*

#### Acetic acid bubbler

Temperature out: 40 °C

Acetic acid heat capacity: 2.05 [kJ mol<sup>-1</sup>K<sup>-1</sup>]

Total energy required: 7.84E+10 [kJ]

Assuming 75% efficiency

Total energy delivered: 9.80E+10 [kJ]

#### Furnace

The reaction is conducted at 500 °C.

Total energy required: 2.52E+12 [kJ]

Total energy delivered: 5.03E+12 [kJ]

Due to extremely high temperature, steam cannot be used to heat the reaction. An assumption is made that an electric furnace is used. 50% efficiency is assumed.

#### Cold extraction

Extraction is performed at -75 °C. Streams exiting furnace at 500 °C must be cooled down.

Combined energy for 3 acetone traps:

Total energy required: 1.94E+12 [kJ]

Total energy delivered: 2.59E+12 [kJ]

**Acetone evaporation:**

Temperature in: 25 °C

Temperature out: 58 °C

Total energy required: 4.07E+11 [kJ]

Total energy delivered: 5.09E+11 [kJ]

Saturated steam enters the furnace at 4 bar(g) (151.9 °C)

Steam required: 2.42E+05 [t]

**Distillation:**

Temperature in: 25 °C

Temperature out: 128 °C

Total energy required: 1.48E+12 [kJ]

Total energy delivered: 1.85E+12 [kJ]

Saturated steam enters the furnace at 4 bar(g) (151.9 °C)

Steam required: 8.79E+05 [t]

**Equipment**

Neglected.

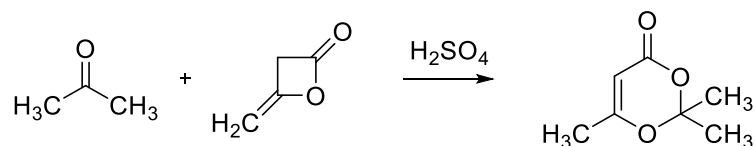
**6.3.6. Total energy requirement**

7.72E+12 [kJ]

Steam (4 bar(g)) required: 1.12E+06 [t]

## 6.4. 2,2,6-Trimethyl-4H-1,3-dioxin-4-one

Dioxinone (2,2,6-Trimethyl-4H-1,3-dioxin-4-one) can be obtained by a reaction of diketene with acetone in strongly acidic conditions. The experimental procedure was reported by Carroll.<sup>15</sup>



*Scheme 6.4-1. 2,2,6-Trimethyl-4H-1,3-dioxin-4-one synthesis*

Dioxinone is prepared by a reaction of diketene with acetone catalysed by a strong Lewis acid, in this case, p-toluenesulfonic acid. Due to lack of a detailed experimental description, it is assumed that the reaction proceeds at 50 °C, i.e. dioxinone is refluxed in acetone. Following the 12 h long reaction, the product is crystallised by lowering the temperature to 5 °C at which dioxinone is solid. 90% yield is assumed. 10 mol% of the sulfonic acid is used.

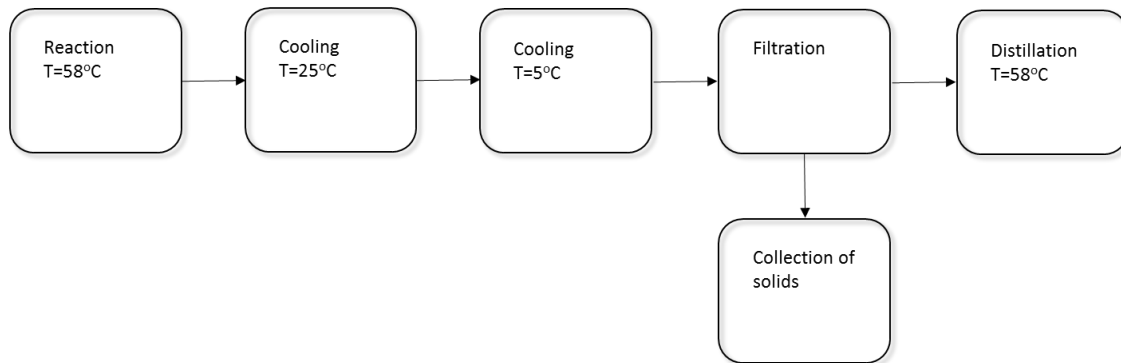
In the LCA model, p-toluenesulfonic acid was replaced with sulfuric acid.

### 6.4.1. Mass balance

Table 6.4-1. Basis: production of 154000,000,000 kg/annum 2,2,6-Trimethyl-4H-1,3-dioxin-4-one product.

Stream	1	2	Crystallisation	
Description	Reaction in	Reaction out	Liquid out	Solid out
Pressure (bar)	1	1	1	1
Temperature (°C)	25	50	0	0
State	l	l	l	s
<b>MOLAR (mol)</b>				
Diketene	1.19E+10	2.98E+09	2.98E+09	
Acetone	1.59E+10	5.03E+09	5.03E+09	
Sulfuric acid	1.19E+09	1.19E+09	1.19E+09	
Dioxinone		1.08E+10		1.08E+10
<b>MASS (kg)</b>				
Diketene	1.00E+09	2.51E+08	2.51E+08	
Acetone	9.21E+08	2.92E+08	2.92E+08	
Sulfuric acid	1.17E+08	1.17E+08	1.17E+08	
Dioxinone		1.54E+09		1.54E+09
<b>TOTAL</b>	<b>2.04E+09</b>	<b>2.20E+09</b>	<b>6.60E+08</b>	<b>1.54E+09</b>

### 6.4.2. Heat/energy balance



*Scheme 6.4-2. Simplified scheme of the process.*

#### Preheating of the reaction mixture

Assuming that the heat capacity of the mixture is equal to the heat capacity of the substrate.

The reaction is conducted at 58 °C.

Total energy required: 1.25E+11 [kJ]

Total energy delivered: 1.57E+11 [kJ]

Saturated steam enters the reactor at 4 bar(g) (151.9 °C)

Steam required: 7.43E+04 [t]

#### Heating of the reactor during the reaction (12h)

15% heat losses per hour is assumed.

Total energy required: 2.25E+11 [kJ]

Total energy delivered: 2.82E+11 [kJ]

Saturated steam enters the reactor at 4 bar(g) (151.9 °C)

Steam required: 1.34E+05 [t]

#### Cooling down to 25 °C

Cold water is used.

Total energy required: 1.25E11 [kJ]

Total energy delivered: 1.57E+11 [kJ]

Cold water required: 7E+06 [t]

### **Cooling down to 5 °C**

Industrial chiller is used.

Total energy required: 1.00E+11 [kJ]

Total energy delivered: 1.25E+11 [kJ]

### **Distillation**

Acetone is recovered at 58 °C

Accounting for heat of evaporation

Total energy required: 2.62E+11 [kJ]

Total energy delivered: 3.27E+11 [kJ]

Saturated steam enters the reactor at 4 bar(g) (151.9 °C)

Steam required: 1.55E+05 [t]

### **Mixing**

Both reaction and crystallisation require mixing.

Total process time 16 hour (12-hour reaction + 4-hour workup).

Motor power: 1.18 kW

Energy required for a 16-hour batch: 6.80E+4 [kJ]

## **6.4.3. Total energy requirement**

1.25E+11 [kJ]

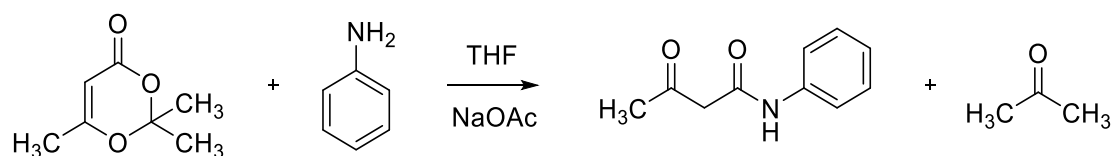
Cold water required: 7E+06 [t]

Saturated steam required (4 bar(g)): 3.63E+05 [t]

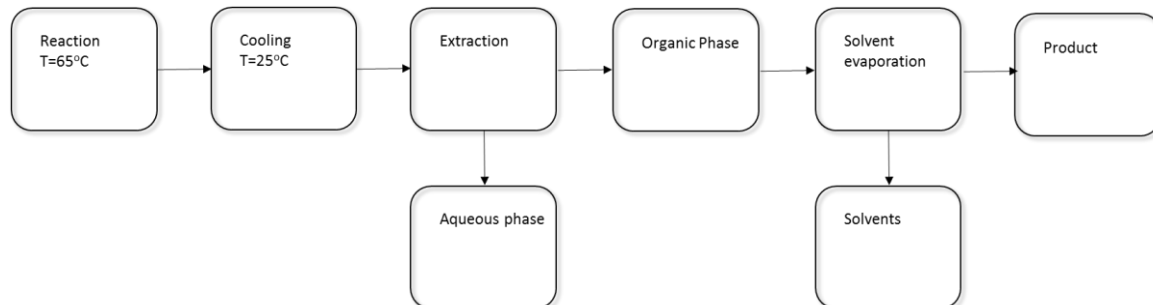
## 6.5. Acetoacetanilide synthesis

Acetoacetanilide is prepared by acetoacetylation of aniline using diketene. A practical procedure was described by Sridharan.<sup>12</sup>

A mixture of aniline, dioxinone and sodium acetate in tetrahydrofuran was heated under reflux (65 °C) for 24h. After cooling down to 25 °C the mixture was diluted with EtOAc and extracted using water. The organic phase was dried using sodium sulfate, and organic solvents were evaporated. The yield of acetoacetanilide was approximately 75%, and no additional purification was required.



*Scheme 6.5-1. Synthesis of acetoacetanilide.*



*Scheme 6.5-2. Simplified scheme of the process.*

### 6.5.1. Mass Balance

Table 6.5-1. Basis: production of 0.98 kg/annum acetoacetanilide product.

Stream	1	2	Extraction			Crystallisation	
Description	Reaction in	Reaction out	Liquid in	Aqueous out	Organic out	Liquid out	Solid out
Pressure (bar)	1	1	1	1	1	1	1
Temperature (°C)	25	65	25	25	25	0	0
State	l	l	l	l	l	l	s
<b>MOLAR (mol)</b>							
Dioxinone	7.36	1.81	1.81		1.81		1.81
Aniline	5.66	0.11	0.11		0.11	0.11	
THF	1051.43	1051.43	1051.43		1051.43	1051.43	
Sodium acetate	5.66	5.66	5.66	5.66			
Acetoacetanilide		5.55	5.55		5.55	5.55	
Acetone		5.55	5.55	5.55			
Water			5.55E+04	5.55E+04			
Ethyl acetate			3.41E+04		3.41E+04	3.41E+04	
<b>MASS (kg)</b>							
Dioxinone	1.05	0.26	0.26		0.26		0.26
Aniline	0.53	0.01	0.01		0.01	0.01	
THF	75.82	75.82	75.82		75.82	75.82	
Sodium acetate	0.46	0.46	0.46	0.46			
Acetoacetanilide		0.98	0.98		0.98	0.98	
Acetone		0.33	0.33	0.33			
Water			1000	1000			
Ethyl acetate			3000		3000	3000	
NaSO <sub>4</sub>					1		
<b>TOTAL</b>	<b>77.86</b>	<b>77.86</b>	<b>4077.86</b>	<b>1000.79</b>	<b>3077.07</b>	<b>76.81</b>	<b>0.26</b>

## 6.5.2. Heat/energy balance

### Preheating of the reaction mixture

The reaction is conducted at 65 °C.

Total energy required: 3.94E+04 [kJ]

Total energy delivered: 7.89E+04 [kJ]

Due to the small scale synthesis, the reactor is heated using electricity; 50% efficiency is assumed.

### Heating of the reactor during the reaction

Due to the small scale synthesis, 25% heat losses per hour is assumed.

Total energy required: 4.73E+05 [kJ]

### Mixing

Both reaction and crystallisation require mixing.

A large laboratory scale overhead stirrer is used.

Total process time 30 hour (24-hour reaction + 6-hour workup).

Motor power: 0.032 kW

Energy required for a 30-hour batch: 3456 [kJ]

### Solvent evaporation after extraction

Total energy required: 2.80E+05 [kJ]

Total energy delivered: 3.51E+05 [kJ]

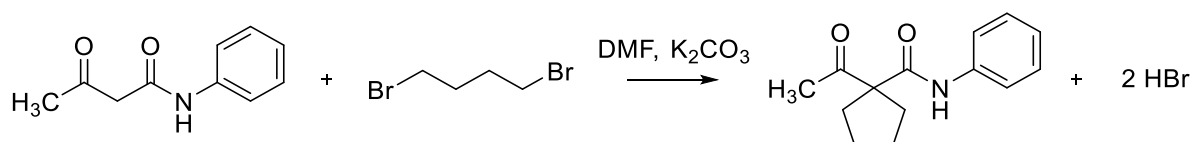
Due to the small scale synthesis, the reactor is heated using electricity.

## 6.5.3. Total energy requirement

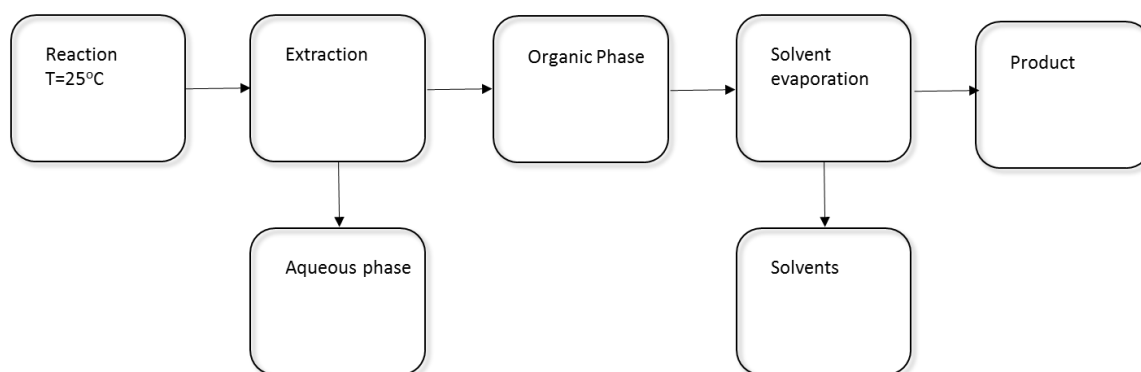
9.064E+5 [kJ]

## 6.6. 1-acetyl-N-phenylcyclopentanecarboxamide synthesis

Acetoacetanilide and potassium carbonate were added to DMF and stirred for 1h. After this time, 1,4-dibromobutane was added, and the mixture was stirred for another 12h. All operations were conducted at room temperature. Following this, water was added to the reaction mixture and extraction using EtOAc was performed. Combined organic fractions were washed with hydrochloric acid (3M), and after phase separation, the organic phase was dried using sodium sulfate. After solvent evaporation, the product was used without any further purification. The yield of the reaction was approximately 92%.<sup>13</sup>



*Scheme 6.6-1. Synthesis of 1-acetyl-N-phenylcyclopentanecarboxamide*



*Scheme 6.6-2. Simplified scheme of the process.*

### 6.6.1. Mass balance

Table 6.6-1. Basis: production of 1.18 kg/annum 1-acetyl-N-phenylcyclopentane-carboxamide product.

Stream	1	2	Crystallisation	
Description	Reaction in	Reaction out	Liquid out	Solid out
Pressure (bar)	1	1	1	1
Temperature (°C)	25	25	0	0
State	l	l	l	s
<b>MOLAR (mol)</b>				
Acetoacetanilide	5.55	0.45	0.45	
1,4-dibromobutane	6.11	1	1	
K <sub>2</sub> CO <sub>3</sub>	12.76	12.76	12.76	
DMF	179.89	179.89	179.89	
Product		5.11		5.11
HBr		10.2	10.2	
Water			-	
<b>MASS (kg)</b>				
Acetoacetanilide	0.98	0.08	0.08	
1,4-dibromobutane	1.31	0.21	0.21	
K <sub>2</sub> CO <sub>3</sub>	1.76	1.76	1.76	
DMF	13.15	13.15	13.15	
Product		1.18		1.18
HBr		0.90	0.90	
Water			200	
<b>TOTAL</b>	<b>17.2</b>	<b>17.28</b>	<b>216.098</b>	<b>1.18</b>

## 6.6.2. Heat/energy balance

### Heating of the reaction mixture

Reaction at room temperature.

### Mixing

Both reaction and crystallisation require mixing.

A large laboratory scale overhead stirrer is used.

Total process time 15 hour (13-hour reaction + 2-hour workup).

Motor power: 0.032 kW

Energy required for a 10-hour batch: 1728 [kJ]

Filtration and drying are neglected.

### Solvent evaporation after extraction

Total energy required: 2.50E+05 [kJ]

Total energy delivered: 3.13E+05 [kJ]

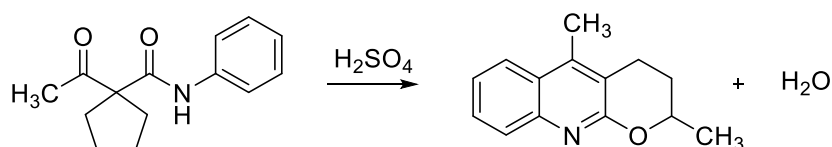
Due to the small scale synthesis, the reactor is heated using electricity.

## 6.6.3. Total energy requirement

3.13E+05 [kJ]

## 6.7. Li-quinoline synthesis

Li quinoline can be produced by condensation of 1-acetyl-*N*-phenylcyclopentanecarboxamide. Due to lack of available industrial procedures and small-scale synthesis (1 kg per annum), a laboratory scale synthesis is reproduced. Detailed procedure was described by Yu and Wang.<sup>13</sup>



*Scheme 6.7-1. Li-quinoline synthesis*

1-acetyl-*N*-phenylcyclopentanecarboxamide was mixed with concentrated sulfuric acid, and the mixture was stirred at 50 °C for 1.5 h. After this time, the mixture was mixed with an aqueous solution of ammonia and extracted using EtOAc. Combined organic phases were dried using magnesium sulfate, the solvent was evaporated, and the residue was purified using flash column chromatography. It was assumed that flash chromatography requires 1 kg of solvent per 1 g of the compound.

### 6.7.1. Mass balance

Table 6.7-1. Basis: production of 0.95 kg/annum Li-quinoline product.

Stream	1	2	Extraction			Chromatography	
Description	Reaction in	Reaction out	Liquid in	Aqueous out	Organic out	Fraction 1	Fraction 2
Pressure (bar)	1	1	1	1	1		
Temperature (°C)	25	50	0	0	0		
State	1	1	1	1	1		
<b>MOLAR (mol)</b>							
1-acetyl-N-phenylcyclopentanecarboxamide	5.11	0.67	0.67		0.67	0.67	
sulfuric acid	76.47	76.47	76.47	76.47			
Li-quinoline		4.44	4.44		4.44		4.44
Ethyl acetate			170.24		170.24	510.72	2156.37
Heptane						1197.49	7983.24
Ammonia			349.22	349.22			
Water		4.44	1504.44	1504.44			
<b>MASS (kg)</b>							
1-acetyl-N-phenylcyclopentanecarboxamide	1.18	0.15	0.15		0.15	0.15	
sulfuric acid	7.5	7.5	7.5	7.5			
Li-quinoline		0.95	0.95		0.95		0.95
Ethyl acetate			15		15	45	190
Heptane						120	800
Ammonia			12.24	12.24			
Water		0.079	27.079	27.079			
<b>TOTAL</b>	<b>8.68</b>	<b>8.68</b>	<b>62.919</b>	<b>46.819</b>	<b>16.1</b>	<b>165.15</b>	<b>990.95</b>

## 6.7.2. Heat/energy balance

### Heating of the reaction mixture

Reaction at room temperature.

### Heating to 50 °C

Due to the small scale, electric heater is used (50% efficiency is assumed)

Energy required: 191.17 [kJ]

Energy delivered: 382.34 [kJ]

Heat losses: 15% per hour.

Energy required for 2 h reaction: 114.7 [kJ]

Total energy delivered: 497.04 [kJ]

### Cooling down to 0 °C

Due to the small scale industrial chiller is used (50% efficiency assumed)

Energy required: 382.34[kJ]

Energy delivered: 764.69 [kJ]

### Mixing

Both reaction and crystallisation require mixing.

A large laboratory scale overhead stirrer is used.

Total process time 4 hour (2-hour reaction + 2-hour workup).

Motor power: 0.032 kW

Energy required for a 4-hour batch: 460.80 [kJ]

### Flash chromatography and extraction

Solvent evaporation:

Due to the small scale, electric heater is used (50% efficiency is assumed)

Energy required: 5.92E+05 [kJ]

Energy delivered: 2.65E+06 [kJ]

### **6.7.3. Total energy requirement**

2.65E+06 [kJ]

## **7. Purification of Pd/Cu residue**

The solid waste formed after purification of the reaction mixture from the carbonylation reaction contains a large amount of palladium and copper species that should be recycled. It is performed via electrolysis.<sup>16</sup>

The residue is dissolved in 3N nitric acid and metals are recovered using electrolysis. In the first step, copper is plated on the electrode at 0.5 V potential. In the second step, palladium is recovered by applying 2V potential. According to the patent, 95% of metal is recovered.

Accounting for the conductivity of a 3N aqueous solution of nitric acid:

Energy required: 255 [kWh]

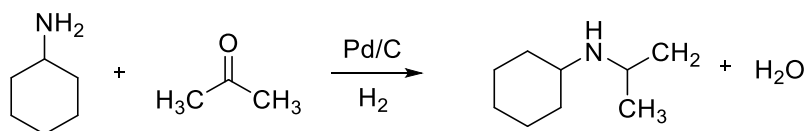
## 8. *N*-Cyclohexylisopropylamine synthesis

### 8.1. Overview

*N*-Cyclohexylisopropylamine can be synthesised using classical methods of secondary amines synthesis, i.e.:<sup>2</sup>

1. Reductive amination using hydrogen
2. Reductive amination using sodium triacetoxyborohydride
3. Reductive amination using sodium borohydride and titanium isopropoxide
4. Michael addition

In this case, option 1 was used, i.e. reductive amination of cyclohexylamine and acetone catalysed by palladium on carbon.

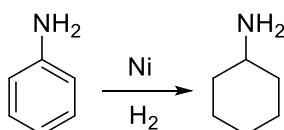


*Scheme 8.1-1. N-Cyclohexylisopropylamine synthesis*

## 8.2. Cyclohexylamine

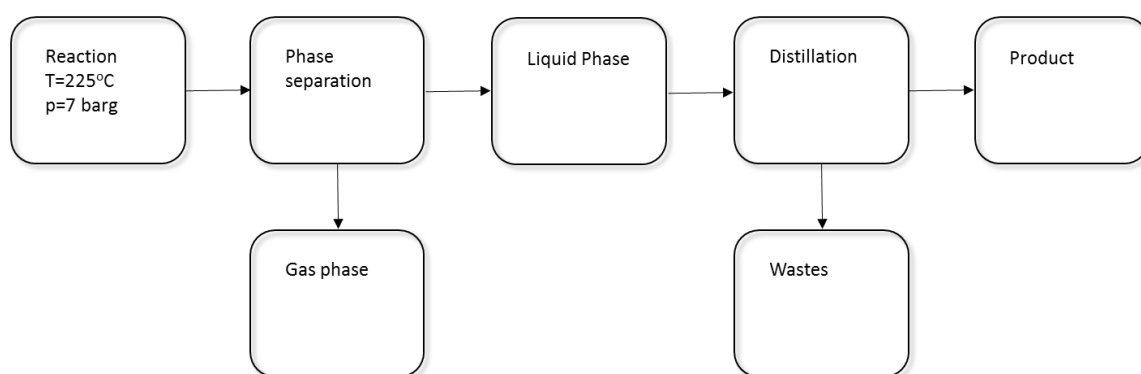
Cyclohexylamine can be produced by catalytic hydrogenation of aniline or by reaction between cyclohexanol and ammonia over cobalt catalyst.

The first option, i.e. hydrogenation of aniline was selected due to high yields and relatively mild conditions.



*Scheme 8.2-1. Hydrogenation of aniline*

A packed-bed reactor filled with nickel catalyst was used. From the bottom, streams of hydrogen, ammonia and aniline were fed. The temperature of the reaction was maintained at 225 °C, and the back pressure was set at 7 bar(g). The outlet stream was cooled down to 60 °C and the liquid phase was collected containing 75% cyclohexylamine, 15% Dicyclohexylamine, 9% aniline and no more than 1% of hydrocarbons. The pure product was obtained by distillation.<sup>17</sup> An assumption was made that the catalyst is fully recycled.



*Scheme 8.2-2. Simplified scheme of the process.*

### 8.2.1. Mass balance

Table 8.2-1. Basis: production of 50000 kg/annum cyclohexylamine product.

Stream	1	2	Distillation		
Description	Reaction in	Reaction out	Liquid in	Heavy out	Light out
Pressure (bar)	7	7	1	1	1
Temperature (°C)	25	225	60	0	0
State	l/g	l/g	1	1	1
<b>MOLAR (mol)</b>					
Aniline	6.72E+05	6.05E+04	6.05E+04	6.05E+04	
Hydrogen	6.72E+05				
Ammonia	1.34E+05	1.34E+05			
Cyclohexylamine		5.04E+05	5.04E+05		5.04E+05
N-cyclohexylaniline		6.72E+03	6.72E+03	6.72E+03	
Di-Cyclohexylamine		1.01E+05	1.01E+05	1.01E+05	
<b>MASS (kg)</b>					
Aniline	6.26E+04	5.63E+03	5.63E+03	5.63E+03	
Hydrogen	1.34E+03				
Ammonia	2.29E+03	2.29E+03			
Cyclohexylamine		5.00E+04	5.00E+04		5.00E+04
N-cyclohexylaniline		5.79E+02	5.79E+02	5.79E+02	
Di-Cyclohexylamine		1.83E+04	1.83E+04	1.83E+04	
<b>TOTAL</b>	<b>6.62E+04</b>	<b>7.45E+04</b>	<b>7.45E+04</b>	<b>2.39E+04</b>	<b>5.00E+04</b>

## 8.2.2. Heat/energy balance

### Heating to 225 °C

Energy required: 5.77E+07 [kJ]

Energy delivered: 7.69E+07 [kJ]

Heat losses are compensated by the heat of the reaction.

Saturated steam enters the furnace at 30 bar(g) (233.84 °C)

Steam required: 4.29 [t]

### Compressor

Based on [http://www.engineeringtoolbox.com/horsepower-compressed-air-d\\_1363.html](http://www.engineeringtoolbox.com/horsepower-compressed-air-d_1363.html)

Compression of 1340 kg of hydrogen from 0 bar(g) to 7 bar(g)

Energy required: 4.31E+06 kJ

### Cooling down to 60 °C

Energy required: 4.06E+07 [kJ]

Energy delivered: 5.41E+07 [kJ]

Cold water required: 322.30 [t]

### Distillation

Pressure: 1 [atm]

Temperature: 135 [°C]

Energy required: 2.68E+07 [kJ]

Energy delivered: 3.58E+07 [kJ]

Saturated steam enters the furnace at 4 bar(g) (151.9 °C).

Steam required: 1.70 [t]

Cold water for condensation: 1 [t]

Energy for pumps neglected.

### **8.2.3. Total energy requirement**

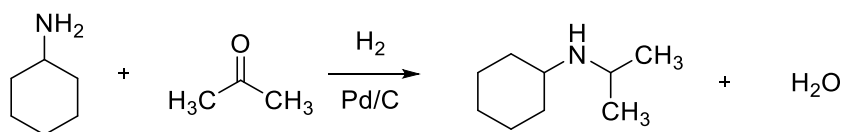
Cold water required: 323.30 [t]

Steam (30 bar) required: 4.29 [t]

Steam (4 bar) required: 1.70 [t]

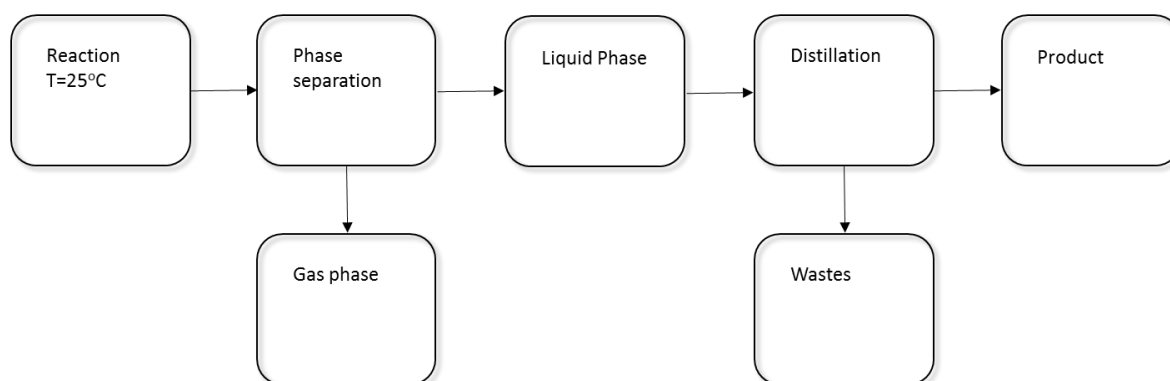
Energy required: 4.31E+06 kJ

### 8.3. *N*-Cyclohexylisopropylamine



*Scheme 8.3-1. Synthesis of N-cyclohexylisopropylamine.*

The substrates and the catalyst, i.e. cyclohexylamine, acetone and palladium on carbon were charged into a reactor and pressurised with hydrogen (1 bar(g)). After 3 hours, the reactor was unloaded, and the reaction mixture was filtered to recover the catalyst. The liquid phase was distilled yielding approximately 85% of the pure product.<sup>18</sup> An assumption was made that the catalyst is fully recycled.



*Scheme 8.3-2. Simplified scheme of the process.*

### 8.3.1. Mass balance

Table 8.3-1. Basis: production of 60500 kg/annum N-Cyclohexylisopropylamine product.

Stream	1	2	Distillation		
Description	Reaction in	Reaction out	Liquid in	Waste	Product
Pressure (bar)	1	1	1	1	1
Temperature (°C)	25	25	25	-	-
State	l/g	1	1	1	1
<b>MOLAR (mol)</b>					
Cyclohexylamine	5.04E+05	7.50E+04	7.50E+04	7.50E+04	
Acetone	7.56E+05	3.28E+05	3.28E+05	3.28E+05	
Pd/C					
Hydrogen	1.01E+06	5.81E+05			
N-Cyclohexyl- isopropylamine		4.29E+05	4.29E+05		4.29E+05
Water		4.29E+05	4.29E+05	4.29E+05	
<b>MASS (kg)</b>					
Cyclohexylamine	5.00E+04	7.44E+03	7.44E+03	7.44E+03	
Acetone	4.39E+04	1.90E+04	1.90E+04	1.90E+04	
Pd/C					
Hydrogen	5.04E+02	2.90E+02			
N-Cyclohexyl- isopropylamine		6.05E+04	6.05E+04		6.05E+04
Water		7.71E+03	7.71E+03	7.71E+03	
<b>TOTAL</b>	<b>9.44E+04</b>	<b>9.47E+04</b>	<b>9.46E+04</b>	<b>3.42E+04</b>	<b>6.05E+04</b>

### 8.3.2. Heat/energy balance

#### Heating of the reaction mixture

Reaction at room temperature. The heat of the reaction is balanced by heat losses from the reactor.

#### Vacuum Distillation

Pressure: 0.016 [bar(g)]

Temperature: 62.55 [°C]

Energy required: 5.00E+07 [kJ]

Energy delivered: 6.67E+07 [kJ]

Saturated steam enters the furnace at 4 bar(g) (151.9 °C).

Steam required: 3.16 [t]

Cold water for condensation: 1 [t]

Energy for pumps neglected.

### 8.3.3. Total energy requirement

Steam required: 3.16 [t]

Cold water: 1 [t]

## 9. Bibliography

1. *Ullmann's Encyclopedia of Industrial Chemistry*. (Wiley-VCH Verlag GmbH & Co. KGaA, 2009).
2. Stolka, M. & Mort, J. *Kirk-Othmer Encyclopedia of Chemical Technology*. Wiley, New York 245 (1994).
3. Linstrom, P. J. & Mallard, W. G. *NIST Chemistry webBook, NIST Standard Reference Database Number 69*. National Institute of Standards and Technology (2014).
4. [http://www.engineeringtoolbox.com/pumping-water-horsepower-d\\_753.html](http://www.engineeringtoolbox.com/pumping-water-horsepower-d_753.html). (Accessed: 29th November 2017)
5. <http://www.solidsprocessing.nl/applic/jh/bandtransporteur/berekening.php>. (Accessed: 29th November 2017)
6. Finley, K. T. in *Ullmann's Encyclopedia of Industrial Chemistry* (Wiley-VCH Verlag GmbH & Co. KGaA, 2000).
7. Saito, T., Ikemoto, K., Tsunomachi, H., Sakaguchi, K. & Toranosuke Osaka, Kenichi Kumamoto, Hiroki Osaka, K. F. Process for the preparation of p-benzoquinone. (1990).
8. Skala, D. & Hanika, J. Kinetics of dicyclopentadiene hydrogenation using Pd/C catalyst. *Pet. Coal* **45**, 105–108 (2003).
9. von Schleyer, R. P. A simple preparation of adamantane. *J. Am. Chem. Soc.* **79**, 3292 (1957).
10. H. Koch, W. H. 1-Adamantanecarboxylic Acid. *Org. Synth.* **44**, 1 (1964).
11. Henri, J. T., Zygmunt, J., Bergren, M. & Zubrin, R. Synthesis of High Caloric Fuels and Chemicals. (2013).
12. Sridharan, V., Ruiz, M. & Menendez, J. Mild and High-Yielding Synthesis of Keto Esters and Ketoamides. *Synthesis (Stuttg)*. **2010**, 1053–1057 (2010).
13. Zhang, Q., Zhang, Z., Yan, Z., Liu, Q. & Wang, T. A New Efficient Synthesis of Pyranoquinolines from 1-Acetyl N -Aryl Cyclopentanecarboxamides. *Org. Lett.* **9**, 3651–3653 (2007).
14. John, E. & Marcel, L. Process for the preparation of 1, 4-dibromobutane. (1959).
15. Carroll, M. F. & Bader, A. R. the Reaction of Diketene With Ketones. *J. Am. Chem. Soc.* **74**, 6305–6305 (1952).
16. Motojima, K., Horie, M. & Torada, S. Method of recovering palladium by electrolysis and apparatus therefor. (1993).
17. Kiyuma, T. & Naramoto, I. Method for production of cyclohexylamines. (1990).
18. Fallstad, H. T. & Rheineck, A. E. Process for producing tertiary amines. (1965).